



**MONASH** University

**Fabrication and evaluation of biodegradable inorganic-organic hybrid nanoparticles as potential tools for targeted delivery of genes and small interfering RNAs into breast cancer cells.**

**Md Emranul Karim**

**Bachelor of Pharmacy (Hons.)**

A thesis submitted for the degree of **Master of Biomedical Science**

Jeffrey Cheah School of Medicine and Health Sciences,

Monash University

May, 2019.

**Fabrication and evaluation of biodegradable inorganic-organic hybrid nanoparticles as potential tools for targeted delivery of genes and small interfering RNAs into breast cancer cells.**

**Md Emranul Karim**

**Master of Biomedical Science  
2019**

## **Copyright Notice**

### **Notice 1**

© Md Emranul Karim (2019)

Under the Copyright Act 1968, this thesis must be used only under the normal conditions of scholarly fair dealing. In particular no results or conclusions should be extracted from it, nor should it be copied or closely paraphrased in whole or in part without the written consent of the author. Proper written acknowledgement should be made for any assistance obtained from this thesis.

### **Notice 2**

© Md Emranul Karim (2019)

I certify that I have made all reasonable efforts to secure copyright permissions for third-party content included in this thesis and have not knowingly added copyright content to my work without the owner's permission.

# Table of Contents

<b>Abstract.....</b>	<b>1</b>
<b>Declaration.....</b>	<b>2</b>
<b>Acknowledgements.....</b>	<b>8</b>
<b>Publications and awards.....</b>	<b>10</b>
<b>List of abbreviations.....</b>	<b>11</b>
 <b>Chapter 1: Literature Review</b>	
<b>1.2. Introduction.....</b>	<b>16</b>
<b>1.3. Challenges and Breakthrough of siRNA delivery: from concept to clinical trial.....</b>	<b>18</b>
<b>1.4. In-Vivo delivery of siRNAs and shRNAs directed against different Cancer- causing Genes in various cancer models</b>	
1.4.1. Silencing of Bcl-2 Gene.....	23
1.4.2. Silencing of VEGF Gene.....	26
1.4.3. Silencing of EGF Receptors Gene.....	29
1.4.4. Silencing of Survivin Gene.....	29
1.4.5. Silencing of Cyclin-B1 Gene.....	37
1.4.6. Silencing of RhoA and RhoC Gene.....	38
1.4.7. Silencing of $\beta$ -Catenin Gene.....	41
1.4.8. Silencing of EphA2 Gene.....	43
1.4.9. Silencing of MDM-2 Gene.....	45
1.4.10. Silencing of IGF-1R Gene.....	46
1.4.11. Silencing of Livin Gene.....	48

1.4.12. Silencing of WT1 Gene.....	49
1.4.13. Miscellaneous.....	51
<b>1.5. Future Directions.....</b>	<b>52</b>
<b>1.6. Conclusions.....</b>	<b>54</b>
<b>Chapter 2: Research gap, Hypothesis, Objectives and Overview of Inorganic salt nanoparticles.</b>	
<b>2.1. Research gap. ....</b>	<b>92</b>
<b>2.2. Hypothesis. ....</b>	<b>92</b>
<b>2.3. Objectives. ....</b>	<b>92</b>
<b>2.4. Overview of Inorganic salt nanoparticles. ....</b>	<b>93</b>
<b>Chapter 3: Strontium Sulfite: A New pH-Responsive Inorganic Nanocarrier to Deliver Therapeutic siRNAs to Cancer Cells</b>	
<b>3.1. Introduction.....</b>	<b>98</b>
<b>3.2. Materials and Methods</b>	
3.2.1. Materials .....	99
3.2.2. Cell Culture and Seeding.....	100
3.2.3. Synthesis of SSNs and Na-Glc-SSNs.....	100
3.2.4. Particle Size, Zeta Potential Measurements and Observation of SSNs and Na-Glc-SSNs.....	100
3.2.5. Characterization of Particles by a Field Emission Scanning Electron Microscope (FE-SEM) and an Energy Dispersive X-ray (EDX) Analyzer.....	100
3.2.6. Characterization of NPs by Fourier Transform Infrared Spectroscopy (FT-IR) and X-Ray Diffraction (XRD) .....	101
3.2.7. Acid Dissolution Study of SSNs and Na-Glc-SSNs.....	101
3.2.8. Assessment of siRNA Binding Affinity to Particles.....	101

3.2.9. Cellular Uptake of siRNA-Loaded NPs.....	102
3.2.10. Cell Viability Assay with MTT (3-(4,5-Dimethylthiazol-2-yl)-2,5-Diphenyltetrazolium Bromide).....	102
3.2.11. In-Solution Digestion of SSN and Na-Glc-SSN Protein Corona for Mass Spectrometric Analysis.....	103
3.2.12. Sample Preparation for Mass Spectrometry-Based Proteomics.....	103
3.2.13. High Efficiency Nanoflow Liquid Chromatography Electrospray-Ionization Coupled with Mass Spectrometry.....	104
3.2.14. Protein Identification and Quantification by Automated De Novo Sequencing (PEAKS Studio 8.0).....	104
3.2.15. In Vivo Biodistribution Study of SSNs and Na-Glc-SSNs.....	105
3.2.16. 4T1.-Induced Mouse Model of Breast Cancer and Anti-Tumor Activity of siRNA-Loaded NPs.....	105
3.2.17. Statistical Analysis .....	106
<b>3.3. Results and Discussion</b>	
3.3.1. Generation of SSNs and Evaluating Effects of NaCl and Glucose on Regulation of Particle Growth.....	106
3.3.2. Characterization of SSNs and Na-Glc-SSNs by Zeta Sizer.....	109
3.3.3. Characterization of Differently Formulated Particles by FE-SEM.....	111
3.3.4. Elemental Analysis of Nanoparticles by EDX.....	112
3.3.5. Characterization of SSNs and Na-Glc-SSNs by FT-IR and XRD.....	113
3.3.6. Acid Dissolution Profiles of SSNs and Na-Glc-SSNs.....	115
3.3.7. Assessment of Binding Affinity of siRNA to SSNs and Na-Glc-SSNs.....	116
3.3.8. Cellular Uptake of Fluorescence-Labeled siRNA Carried by Differently Formulated Strontium Sulfite Nanoparticles.....	116
3.3.9. Cell Viability Assessment with MTT Assay.....	119

3.3.10. Intracellular Delivery of EGFR and ROS1 siRNA using SSNs and Na-Glc-SSNs.....	120
3.3.11. Analysis of Protein Corona Formed onto SSNs and Na-Glc-SSNs.....	121
3.3.12. In Vivo Biodistribution Study of SSNs and Na-Glc-SSNs.....	125
3.3.13. In Vivo Anti-Tumor Effect of ROS1 siRNA-Loaded SSNs and Na-Glc-SSNs....	127
<b>3.4. Conclusion.....</b>	<b>128</b>
<b>Chapter 4: PEGylated Strontium sulfite for improving antitumor efficacy of EGFR siRNA against the breast cancer cell.</b>	
<b>4.1. Introduction .....</b>	<b>135</b>
<b>4.2. Materials and methods</b>	
4.2.1. Materials .....	136
4.2.2. Synthesis of SSNs and PEG-SSNs .....	137
4.2.3. Turbidity and Optical images of PEG-SSNs .....	137
4.2.4. Characterizations of PEG-SSNs .....	137
4.2.5. Energy Dispersive X-ray (EDX) assay of PEG-SSNs .....	137
4.2.6. Stability of PEG-SSNs in mice plasma .....	138
4.2.7. siRNA encapsulation efficiency of PEG-SSNs .....	138
4.2.8. Cytotoxicity and hemolysis assay of PEG-SSNs .....	139
4.2.9. In vitro cytotoxicity assay of SSNs and PEG-SSNs coupled EGFR siRNA by MTT .....	139
4.2.10. Animals and xenograft tumors: .....	140
4.2.11. In vivo antitumor efficacy of SSNs and PEG-SSNs conjugated EGFR .....	140
4.2.12. Blood Chemistry and Histology (H&E) study .....	140
4.2.13. Statistical analysis .....	141

### **4.3. Results**

4.3.1. Turbidity and optical images of PEG-SSNs .....	141
4.3.2. Size and Zeta potential of free SSN and PEG-SSNs complex .....	142
4.3.3. Characterization SSNs and PEG-SSNs by Dynamic Light Scattering (DLS) .....	144
4.3.4. Elemental analysis of PEG-SSNs by EDX .....	146
4.3.5. Stability of PEG-SSNs in mice plasma by DLS: .....	147
4.3.6. siRNA encapsulation efficiency of PEG-SSNs: .....	147
4.3.7. Cytotoxicity and hemolysis assay .....	148
4.3.8. In vitro antitumor activity assay of EGFR siRNA coupled SSNs and PEG-SSNs.....	149
4.3.9. Tumor regression study of PEG-SSNs conjugated EGFR siRNA in mouse model: .....	153
4.3.10. Blood Chemistry and Histology (H&E) study: .....	153
<b>4.4. Discussion</b> .....	154
<b>4.5. Conclusion</b> .....	157

## **Chapter 5: Effects of PEGylated SSNs on protein corona formation and off-target distribution of siRNA.**

<b>5.1. Introduction</b> .....	163
<b>5.2. Materials and methods:</b>	
5.2.1. Materials.....	164
5.2.2. Synthesis of PEG-SSNs.....	165
5.2.3. Field Emission Scanning Electron Microscope (FE-SEM) of PEG-SSNs.....	165
5.2.4. In-Solution Digestion of SSNs and PEG-SSNs Protein Corona for Mass Spectrometric Analysis.....	165
5.2.5. Sample Preparation for Mass Spectrometry-Based Proteomics.....	166



5.2.6. High Efficiency Nanoflow Liquid Chromatography Electrospray-Ionization Coupled with Mass Spectrometry.....	166
--	-----

5.2.7. Protein Identification and Quantification by Automated De Novo Sequencing (PEAKS Studio 8.5).....	166
---	-----

5.2.8. Biodistribution study of SSNs and PEG-SSNs conjugated siRNA complex.....	167
---	-----

### **5.3.Results**

5.3.1. FESEM of SSNs and PEG-SSNs.....	168
--	-----

5.3.2. Protein corona profiling of SSNs and PEG-SSNs by LC-MS/MS.....	170
---	-----

5.3.3. Bio-distribution of SSNs and PEG-SSNs.....	173
---	-----

<b>5.4. Discussion.....</b>	<b>174</b>
-----------------------------	------------

<b>5.5. Conclusion.....</b>	<b>176</b>
-----------------------------	------------

## **Chapter 6: Conclusion and Future directions:**

<b>6.1. Conclusion.....</b>	<b>182</b>
-----------------------------	------------

<b>6.2. Future directions.....</b>	<b>183</b>
------------------------------------	------------

## Abstract

Cancer is the result of uncontrolled proliferation of cells as a result of genetic mutations in proto-oncogenes, tumor suppressor genes and DNA repair genes. Due to the imbalance between cell adhesion receptors and cell motility enhancing receptors, and activation of membrane metalloproteinase, tumor cells achieve metastatic properties, spreading to various organs of the body. Genetic manipulation through delivery of a functional gene or a gene silencing element is an attractive strategy to treat cancer effectively. Rigorous research on cancers pathophysiology revealed many cardinal genes as possible targets for cancer gene therapy. To facilitate cell or tissue-directed delivery of a functional gene a lot of viral and non-viral carriers have emerged via genetic and chemical engineering processes. But the existing vectors are not considered to be ideal in terms of safety and efficacy. Development of salt crystals with nano-size diameters having the capacity of adsorbing negatively charged plasmid DNA or siRNA, carrying them across the plasma membrane and efficiently inducing transgene expression or facilitating targeted gene knockdown in cancerous cells could be a promising platform for therapeutic intervention. We have developed for the first time strontium sulfite nanoparticles (SSNs) and additionally modulated the fabrication process with NaCl and glucose to stabilize the particle size within 200 nm. We found a strong binding affinity of SSNs towards the negatively charged siRNA as well as significant cellular uptake. In addition, SSNs with ROS1 and EGFR siRNAs demonstrated enhancement of cytotoxicity compared to free SSNs in breast cancer cell lines. The LC-MS analysis and bio-distribution study revealed stability in systemic circulation, significant tumor accumulation and clearance of SSNs after 24 hour of administration. Finally, the tumor regression study with ROS1 siRNA-loaded SSNs showed remarkable antitumor effects in a syngeneic mouse model of breast cancer compared with free SSNs without any visible toxicity. Furthermore, for the first time, we have modified the SSNs via a hydrophilic coating material, PEG to improve the tumor targetability and reduce systemic toxicity. We have found excellent size reduction capacity of biotin PEG, significant affinity towards siRNA and improved cytotoxicity of siRNA-loaded PEGylated NPs against various cancer cell lines. The LCMS study revealed that PEG provides a steric hindrance against protein opsonization in blood through reducing protein adsorption on the surface of NPs. The bio-distribution and tumor regression study of PEGylated SSNs demonstrated reduced off target drug distribution, extended blood circulation time, improved tumor accumulation and augmented anti-tumor efficacy without systemic toxicity. Thus SSNs, NaCl-Glu-SSNs and PEG-SSNs emerged as potential tools for targeted delivery of genes and siRNAs into breast cancer cells.

## **Declaration**

I hereby declare that this thesis contains no material which has been accepted for the award of any other degree or diploma, except where due reference is made in the text of the thesis.

To the best of my knowledge, this thesis contains no material previously published or written by another person except where due reference is made in the text of the thesis.

Signed: Md Emranul Karim

Date: 28.04.2019

## **Monash University**

Declaration for thesis based or partially based on conjointly published or unpublished work

### **General Declaration**

In accordance with Monash University Doctorate Regulation 17.2 Doctor of Philosophy and Research Master's regulations the following declarations are made:

I hereby declare that this thesis contains no material which has been accepted for the award of any other degree or diploma at any university or equivalent institution and that, to the best of my knowledge and belief, this thesis contains no material previously published or written by another person, except where due reference is made in the text of the thesis.

This thesis includes **1** review article, **1** original paper published in peer reviewed journals and **2** unpublished manuscripts (submitted). The main theme of the thesis is fabrication and evaluation of biodegradable inorganic-organic hybrid nanoparticles as potential tools for targeted delivery of genes and small interfering RNAs into breast cancer cells. The ideas, development and writing up of all the papers in the thesis were the principal responsibility of myself, the candidate, working within the Jeffrey Cheah School of Medicine and Health Sciences under the supervision of Associate Professor Dr Ezharul Hoque Chowdhury.

The inclusion of co-authors reflects the fact that the work came from active collaboration between researchers and acknowledges input into team-based research.

In the case of chapters 1 to 6 my contribution to the work involved the following:

<b>Thesis chapter</b>	<b>Publication Title</b>	<b>Publication status</b>	<b>Nature and extent of candidate's contribution</b>
1	Therapeutic Potency of Nanoformulations of siRNAs and shRNAs in Animal Models of Cancers	Published	Concept, data collection, data analysis and interpretation, manuscript preparation
3	Strontium Sulfite: A New pH-Responsive Inorganic Nanocarrier to Deliver Therapeutic siRNAs to Cancer Cells	Published	Experimental design and conduct, data collection, data analysis and interpretation, statistical analysis, manuscript preparation
4	PEGylated Strontium sulfite for improving antitumor efficacy of EGFR siRNA against the breast cancer cell.	Submitted	Experimental design and conduct, data collection, data analysis and interpretation, statistical analysis, manuscript preparation
5	Effects of PEGylated SSNs on protein corona formation and off-target distribution of siRNA.	Submitted	Experimental design and conduct, data collection, data analysis and interpretation, statistical analysis, manuscript preparation

I have renumbered sections of the submitted or published papers in order to generate a consistent presentation within the thesis.

Signed: Md Emranul Karim

## Thesis including published works declaration

I hereby declare that this thesis contains no material which has been accepted for the award of any other degree or diploma at any university or equivalent institution and that, to the best of my knowledge and belief, this thesis contains no material previously published or written by another person, except where due reference is made in the text of the thesis.

This thesis includes **1** review article, **1** original article published in peer reviewed journals and **2** unpublished manuscripts (submitted). The main theme of the thesis is fabrication and evaluation of biodegradable inorganic-organic hybrid nanoparticles as potential tools for targeted delivery of genes and small interfering RNAs into breast cancer cells. The ideas, development and writing up of all the papers in the thesis were the principal responsibility of myself, the candidate, working within the Jeffrey Cheah School of Medicine and Health Sciences under the supervision of Associate Professor Dr Ezharul Hoque Chowdhury.

The inclusion of co-authors reflects the fact that the work came from active collaboration between researchers and acknowledges input into team-based research.

In the case of Chapter 1, 3, 4, and 5 my contribution to the work involved the following:

Thesis Chapter	Publication Title	Status (published, in press, accepted or returned for revision)	Nature and % of student contribution	Co-author name(s) Nature and % of Co-author's contribution*	Co-author(s), Monash student Y/N*
1	Therapeutic Potency of Nanoformulations of siRNAs and shRNAs in Animal Models of Cancers	Published	80% Concept, data collection, data analysis and interpretation, manuscript preparation	1)Kyi Kyi Tha helped to edit the manuscript 5% 2) Iekhsan Othman helped to edit the manuscript 5%, 3)Mohammad Borhan Uddin helped to edit the manuscript 5% 4)Ezharul hoque Chowdhury helped to prepare the initial draft of the manuscript 5%	No  No  Yes  No

3	Strontium Sulfite: A New pH-Responsive Inorganic Nanocarrier to Deliver Therapeutic siRNAs to Cancer Cells	Published	75% Experimental design and conduct, data collection, data analysis and interpretation, statistical analysis, manuscript preparation	1)Jayalaxmi Shetty helped in vivo work 5% 2)Rowshan Ara Islam helped in cell work 5% 3)Ahsanul Kaiser helped to measure the particle size 5% 4)Athirah Bakhtiar helped to develop project 5% 5)Ezharul Hoque Chowdhury did research proposal and experimental design and manuscript editing 5%	Yes  Yes  Yes  No  No
4	PEGylated Strontium sulfite for improving antitumor efficacy of EGFR siRNA against the breast cancer cell.	Submitted	80% Experimental design and conduct, data collection, data analysis and interpretation, statistical analysis, manuscript preparation	Ezharul Hoque Chowdhury did research proposal and experimental design and manuscript editing 20%	No
5	Effects of PEGylated SSNs on protein corona formation and off-target distribution of siRNA.	Submitted	80% Experimental design and conduct, data collection, data analysis and interpretation, statistical analysis, manuscript preparation	Ezharul Hoque Chowdhury did research proposal and experimental design and manuscript editing 20%	No

I have renumbered sections of submitted or published papers in order to generate a consistent presentation within the thesis.

**Student signature:** Md Emranul Karim

**Date:** 28.04.2019

The undersigned hereby certify that the above declaration correctly reflects the nature and extent of the student's and co-authors' contributions to this work. In instances where I am not the responsible author I have consulted with the responsible author to agree on the respective contributions of the authors.

**Main Supervisor signature:** Md Ezharul Haque Chowdhury

**Date:** 28.04.2019



## ACKNOWLEDGEMENTS

First and foremost, praises and thanks to the Allah, the Almighty, the most merciful, for His showers of blessings throughout my research work to complete the research successfully.

I would like to acknowledge my indebtedness and render my warmest thanks to my supervisor, Associate Professor Dr. Md. Ezharul Hoque Chowdhury who made this work possible. His dynamism, vision, sincerity and motivation have deeply inspired me. He has taught me the methodology to carry out the research and to present the research works as clearly as possible. It was a great privilege and honor to work and study under his guidance. I am extremely grateful for what he has offered me. I would also like to thank him for his friendship, empathy and great sense of humor. I am extending my heartfelt thanks to his wife, family for their acceptance and patience during the discussion I had with him on research work and thesis preparation. I am also indebted to my co-supervisors, Professor Dr. Iekhsan Othman, Dr. Kyi Kyi Tha and Dr. Athirah Baktiar for their excellent encouragements, advices and supports throughout my research journey. Their work ethics, professionalism, intellectual knowledge, excellent encouragement has inspired me to become a better researcher and critical thinker.

I would like to say thanks to my research colleagues, Mr. Borhan Uddin, Rowshan Ara Islam, Ahsanul Kaiser, Sheikh Tanzina Hoque, Rahela Zaman, Nabila Ibnat, Sultana Mehbuba Hossain, Maeirah Afzal Ashaei and Alexis Chung. I am grateful to all of colleagues with whom I have had the pleasure to work during this and other related projects. . I would also like to thank to Syafiq Asnawi Zainal Abidin from LC-MS unit and particularly grateful for the expert assistance given by Mr. Andrew Leong and Mr. Zulkhaili Zainal from the Animal Facility Unit especially during the animal handling and experiments. My appreciation to all the administrative staffs from School of Medicine and Health Sciences for their excellent work for ensuring the smoothness of my Monash journey.

Nobody has been more important to me in the pursuit of this project than the members of my family. It's my honor to show my deepest gratitude to my beloved Grandparents. I would like to thank my parents, Mr. Shah Farid Ahmad & Nargis Akhter whose love, prayers, caring and guidance are with me in whatever I pursue. They are the ultimate role models. I am also grateful to have a wonderful and continuous support from my siblings Shamima Akhtar, Mr. Rezaul Karim, Jasmin Akhtar, Mr. Nijamul Karim, Mr. ABM Siddiqullah, sister in laws and brother in laws.

Most importantly, I wish to thank my loving and supportive wife, Sulltana Jahan Romana, who provides unending inspiration and made my life meaningful and worthwhile. Thank you for standing together in every step and especially I can't thank you enough for encouraging me throughout this experience.

Finally I thank my God, my good Father, for letting me through all the difficulties. I have experienced Your guidance day by day. You are the one who let me finish my degree. I will keep on trusting You for my future. Thank you, Lord.

**Md Emranul Karim**

## Publications and Awards

### Publications included in this thesis:

01. **Md. Emranul Karim**, Kyi Kyi Tha, Iekhsan Othman, Mohammad Borhan Uddin and Ezharul Hoque Chowdhury. Therapeutic Potency of Nanoformulations of siRNAs and shRNAs in Animal Models of Cancers. *Pharmaceutics* 2018, 10(2), 65; doi.org/10.3390.
02. **Md. Emranul Karim**, Jayalaxmi Shetty, Rowshan Ara Islam, Ahsanul Kaiser, Athirah Bakhtiar and Ezharul Hoque Chowdhury. Strontium Sulfite: A New pH-Responsive Inorganic Nanocarrier to Deliver Therapeutic siRNAs to Cancer Cells. *Pharmaceutics* 2019, 11(2), 89; doi: 10.3390.
03. **Md. Emranul Karim** and Ezharul Hoque Chowdhury. PEGylated Strontium sulfite for improving antitumor efficacy of EGFR siRNA against the breast cancer cell. *Molecular Therapy* (submitted).
04. **Md. Emranul Karim** and Ezharul Hoque Chowdhury. Effects of PEGylated SSNs on protein corona formation and off-target distribution of siRNA. *Biochemical and Biophysical Research Communications* (submitted).

### Publications not included in the thesis:

01. Mohammad Borhan Uddin, Balakavitha Balaravi Pillai, Kyi Kyi Tha, Maeirah Ashaie, **Md. Emranul Karim** and Ezharul Hoque Chowdhury. Carbonate Apatite Nanoparticles-Facilitated Intracellular Delivery of siRNA(s) Targeting Calcium Ion Channels Efficiently Kills Breast Cancer Cells. *Toxics* 2018, 6(3), 34; doi.org/10.3390.
02. Hamed Al-Busaidi, **Md. Emranul Karim**, Syafiq Asnawi Zainal Abidin, Kyi Kyi Tha and Ezharul Hoque Chowdhury. Magnesium Fluoride Forms Unique Protein Corona for Efficient Delivery of Doxorubicin into Breast Cancer Cells. *Toxics* 2019, 7(1), 10; doi.org/10.3390.

### Awards

1. Full Tuition Fee Waiver, 2017 – 2019
2. Monash University Merit Scholarship, 2018 – 2019

## List of abbreviations

RNA	Ribonucleic acid
RNAi	RNA interference
dsRNA	double stranded RNA
siRNA	small interfering RNA
RISC	RNA-induced silencing complex
mRNA	Messenger RNA
shRNA	short hairpin RNA
DNA	Deoxyribonucleic acid
pDNA	plasmid DNA
AONs	anti-sense oligonucleotides
ECM	Extracellular matrix
IFP	interstitial fluid pressure
AAV	adeno associated virus
LNPs	lipid nanoparticles
PEG	Polyethylene glycol
RES	reticuloendothelial system
CPP	cell-penetrating peptides
VEGF	vascular endothelial growth factor
NRP-2	Neuropilin-2
EGF	Epidermal growth factor
ROCK	Rho-associated coiled coil-containing protein kinase
RhoA	Ras homologous A
RhoC	Ras homologous C

PEI	polyethylenimine
PIHCA	polyisohexylcyanoacrylate
IBC	Inflammatory breast cancer
Eph	Erythropoietin-producing hepatocellular
DOPC	1, 2-dioleoyl-sn-glycero-3-phosphatidyl choline
MMPs	matrix metalloproteinases
IGF-1R	Type 1 insulin-like growth factor receptor
NSCLC	Non-small cell lung cancer
SPIONS	Super-paramagnetic iron oxide nanoparticles
WT1	Wilms' tumor gene 1
Bag-1	Bcl-2-associated athanogene-1
CRC	colorectal cancer
PTTG1	pituitary tumor transforming gene 1
RTKs	receptor tyrosin kinases
EGFR	epidermal growth factor receptor
TNBC	triple-negative breast cancer
SSNs	strontium sulfite NPs
HEPES	4-(2-hydroxyethyl)-1-piperazineethanesulfonic acid
DMEM	Dulbecco's modified eagle medium
DMSO	dimethyl sulphoxide
MTT	thiazolyl blue tetrazolium bromide
EDTA	ethylene diamine tetra acetic acid
FBS	fetal bovine serum
FE-SEM	Field Emission Scanning Electron Microscope
EDX	Energy Dispersive X-ray

FT-IR	Fourier Transform Infrared Spectroscopy
XRD	X-Ray Diffraction
FDR	False discovery rate
PDI	poly dispersing index
PC	protein corona
NP-PC'' complex	Nanoparticle-protein corona complex
MPS	mononuclear phagocyte system
IgG	immunoglobulin



# **Chapter 1**

## **Literature Review**

Work that is presented in this chapter is published in *Pharmaceutics* **2018**, 10(2), 65 with minor adjustments in Figure/Table number to fit into the current thesis format. A snapshot of the research paper is included in page 15.

Review

# Therapeutic Potency of Nanoformulations of siRNAs and shRNAs in Animal Models of Cancers

Md. Emranul Karim , Kyi Kyi Tha, Iekhsan Othman, Mohammad Borhan Uddin   
and Ezharul Hoque Chowdhury \*

Jeffrey Cheah School of Medicine and Health Sciences, Monash University Malaysia, Jalan Lagoon Selatan, Bandar Sunway, Petaling Jaya 47500, Selangor, Malaysia; karim604306@gmail.com (M.E.K.); tha.kyi.kyi@monash.edu (K.K.T.); iekhsan.othman@monash.edu (I.O.); mohammad.uddin@monash.edu (M.B.U.)

\* Correspondence: md.ezharul.hoque@monash.edu; Tel.: +603-5514-4978; Fax: +603-5514-6323

Received: 6 April 2018; Accepted: 22 May 2018; Published: 26 May 2018



**Abstract:** RNA Interference (RNAi) has brought revolutionary transformations in cancer management in the past two decades. RNAi-based therapeutics including siRNA and shRNA have immense scope to silence the expression of mutant cancer genes specifically in a therapeutic context. Although tremendous progress has been made to establish catalytic RNA as a new class of biologics for cancer management, a lot of extracellular and intracellular barriers still pose a long-lasting challenge on the way to clinical approval. A series of chemically suitable, safe and effective viral and non-viral carriers have emerged to overcome physiological barriers and ensure targeted delivery of RNAi. The newly invented carriers, delivery techniques and gene editing technology made current treatment protocols stronger to fight cancer. This review has provided a platform about the chronicle of siRNA development and challenges of RNAi therapeutics for laboratory to bedside translation focusing on recent advancement in siRNA delivery vehicles with their limitations. Furthermore, an overview of several animal model studies of siRNA- or shRNA-based cancer gene therapy over the past 15 years has been presented, highlighting the roles of genes in multiple cancers, pharmacokinetic parameters and critical evaluation. The review concludes with a future direction for the development of catalytic RNA vehicles and design strategies to make RNAi-based cancer gene therapy more promising to surmount cancer gene delivery challenges.

**Keywords:** RNA interference; small interfering RNA (siRNA); short hairpin RNA (shRNA); viral and non-viral carriers; cancer; gene therapy

## 1. Introduction

Gene therapy is the delivery of functional genes into the cell to modulate gene expression and the extent of their expression. Specificity and stability in biological media should be adequate to carry the corrected genetic information to their progeny for consistent effects. Since the discovery of gene sequencing technology, the journey from concept to clinical trial has faced a lot of hurdles to attain clinical reliability [1]. The era of catalytic RNA added a new dimension to the management of a broad range of critical human disorders like cancers and Alzheimer's disease. The formal appearance of RNAi techniques based on a double stranded RNA (dsRNA) came into sight at the end of the nineteenth century to silence genes in nematodes [2,3]. The long dsRNA is able to silence gene expression in both nematodes and mammalian cells, but its non-specificity, sequence-independent pathways and activation of innate immune response make it incompatible in gene silencing technology [4,5]. At the beginning of the twentieth century, vigorous research on minimizing the shortcomings of dsRNA concluded that long dsRNAs can be processed into less than 30 base pair sequences, inducing the sequence-specific silencing of targeted genes in mammals [6]. This finding unfolded synthetic



## **1. Literature Review**

### **1.1. Therapeutic Potency of Nanoformulations of siRNAs and shRNAs in Animal Models of Cancers**

#### **1.2. Introduction**

Gene therapy is the delivery of functional genes into the cell to modulate gene expression and the extent of their expression, specificity and stability in biological media should be adequate to carry the corrected genetic information to their progeny for consistent effects. Since the discovery of gene sequencing technology, the journey from concept to clinical trial has faced a lot of hurdles to attain clinical reliability (1). The era of catalytic RNA added a new dimension to the management of a broad range of critical human disorders like cancers, Alzheimer's disease. The formal appearance of RNAi techniques based on a double stranded RNA (dsRNA) came into sight at the end of the nineteenth century to silence genes in nematodes (2, 3). The long dsRNA is able to silence gene expression in both nematodes and mammalian cells, but its non-specificity, sequence-independent pathways and activation of innate immune response make it incompatible in gene silencing technology (4, 5). At the beginning of the twentieth century, vigorous research on minimizing the shortcomings of dsRNA concluded that long dsRNAs can be processed into less than 30 base pair sequences, inducing the sequence-specific silencing of targeted genes in mammals (6). This finding unfolded synthetic siRNA (small interfering RNA) as a new biological tool for silencing the genes in mammalian cell specifically. The smaller fragments of siRNA (21 to 23 nucleotides) are processed from long pieces of dsRNA by the enzyme dicer (7, 8). The siRNA can be produced synthetically and delivered into mammalian cells via multiple transfection methods. After reaching the cytoplasm of the target mammalian cell, siRNA is incorporated with RNA-induced silencing complex (RISC) (9). Argonaute 2, a multi protein of Argonaute family is the catalytic core of RISC that unwinds the siRNA double strand and degrades sense strand (passenger strand). The activated guide strand (anti-sense strand) containing RISC identifies and guides the sequence-specific cleavage at a position of nucleotides 10-11 of target mRNA by post-transcriptional gene silencing mechanisms, preventing translation and silencing specific gene expression(10, 11)(Figure 1). The activated RISC then heads to other mRNA targets until their degradation. The degradation of activated RISC requires 3 to 7 days for fast growing cells and several weeks for slowly dividing cells (12, 13). On the other hand, short hairpin RNA (shRNA) are synthesized in nucleus of cells, transported into cytoplasm and processed into siRNA for silencing target mRNA via binding with RISC. The shRNA expression vectors therefore need to be transported into the nucleus of a cell for transcription (14-16). The

precisely designed siRNA can specifically silence any gene in the body and therefore appears to be therapeutically more potent than conventional small molecular drugs.

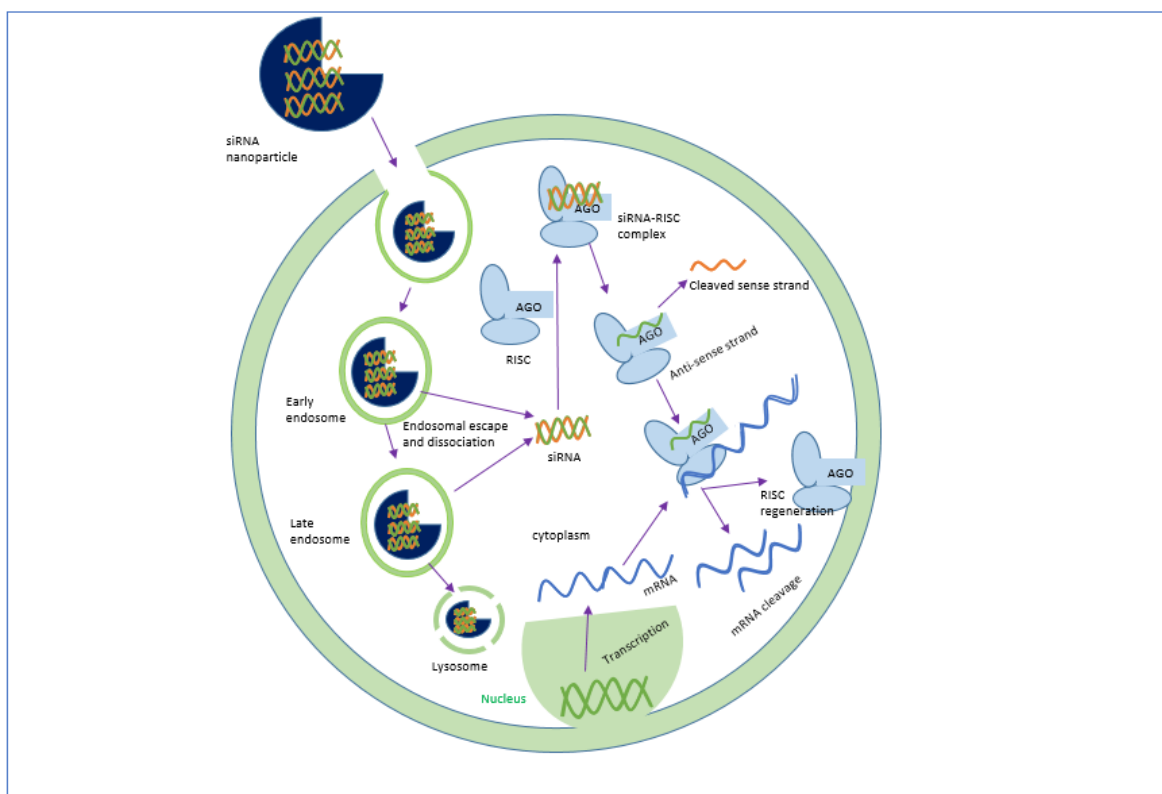
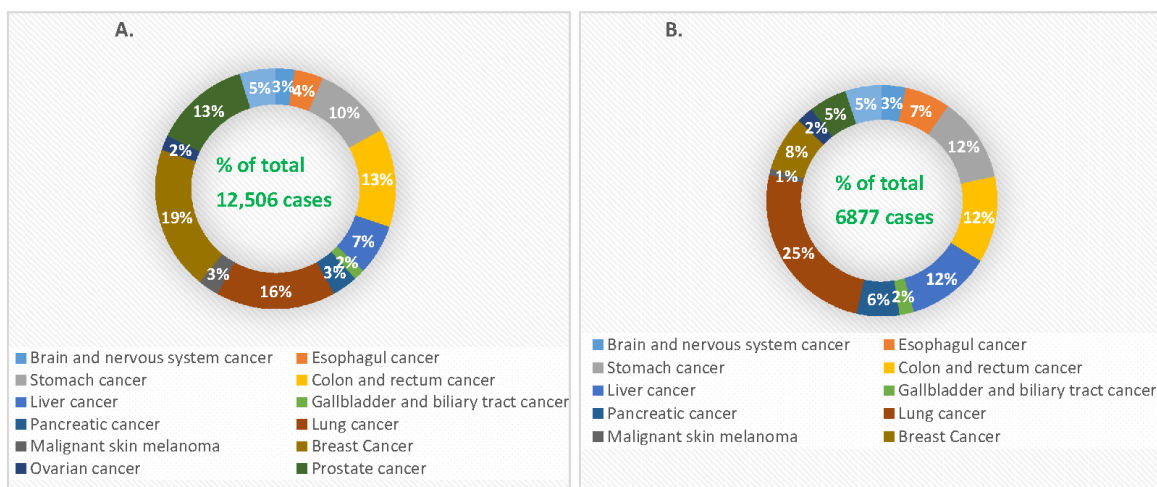


Figure 1: RNAi-mediated gene silencing mechanism. Cellular internalization of siRNA-nanoparticle complex via endocytosis is followed by siRNA release from both the particle and the endosome. In cytoplasm, the released siRNA is loaded into RISC, degrades passenger strand and activates anti-sense strand. The activated anti-sense strand subsequently cleaves target mRNA. The catalytic RNAs that are unable to escape endosome are subjected to lysosomal degradation.

Cancer is generally characterized by genetically abnormal signal transduction pathways that lead to heterogeneous cellular proliferation because of mutation and heritable alteration in an oncogene or tumor suppressor gene [17]. Cancer gene therapy includes gene amplification or deletion, suicide gene therapy, inactivation of oncogene by epigenetic silencing, mutation correction, chromosomal translocation, tumor suppressor activation and blocking of angiogenesis via the delivery of nucleic acids like plasmid DNA (pDNA), mRNA, short interfering or silencing RNA (siRNA), micro RNA (miRNA), short hairpin RNA (shRNA), anti-sense oligonucleotides (AONs) and DNA enzymes into the target cells [18–21]. Since the emergence of gene therapy, approximately 1300 clinical trials in different cancers have been taken place [22,23]. Cancer management still poses a major challenge with high incidence and mortality rates (Figure 2) due to the detrimental effects of conventional treatment modalities, despite the fact that the number

of cancer survivors in the USA is increasing because of advancement in early cancer diagnosis and treatment [24].



**Figure 2.** The 2015 global incidence and deaths for different type of cancers, (A) represents the incident rate (thousand) per 100,000 person-years; (B) represents the death rate (thousand) per 100,000 person-years [25].

Here, we review the current advancement of siRNA-based cancer therapy, emphasizing the challenges and breakthroughs of siRNA delivery especially in preclinical studies and the development of various delivery vehicles from viral vectors to inorganic nanoparticles in overcoming the biological barriers. The roles of genes in multiple cancers and the knockdown effects of those genes in tumor regression will be discussed, highlighting the pharmacokinetic parameters of the delivery vehicles in different animal models of cancers.

### 1.3. Challenges and Breakthrough of siRNA Delivery: From Concept to Clinical Trial:

Gene sequencing technology has gained significant attention owing to its ability to unmask genomic data for treating disease at the genetic level. The effective and controlled intracellular delivery of siRNAs into cancer cells and cancer stem cells both in vitro and in vivo has remained a long-standing challenge, hampering siRNA-based therapeutics to move into the clinical setting. The amount of siRNA should be optimized for maximum potency. Although naked siRNA without and with chemical modification demonstrated silencing and therapeutic efficacy in the lung [26] and brain [27], respectively, following local administration, systemic administration of unmodified siRNA is subjected to nuclease degradation, phagocytic uptake, aggregation with serum protein and rapid renal clearance before reaching the cytoplasm of the target cell [28–31] (Figure 3). Once the siRNA extravasates, it faces the barriers of the dense structure of Extracellular matrix (ECM) [32], higher interstitial fluid pressure [33] and negatively charged cellular membrane. After endocytosis-facilitated entry into the cell, siRNA should escape from

the endosome; otherwise, it would be subjected to lysosomal degradation [34]. Besides, naked siRNA exerts innate immune responses and off-target effects and demands repeated dosing for consistent effects [35–37]. To overcome these hurdles, an effective delivery vehicle is required for the delivery of siRNA to the target site by preventing the naked or modified siRNA from biological degradation and enabling it to cross the intended cellular membrane and release from the endosome [9, 38, 39].

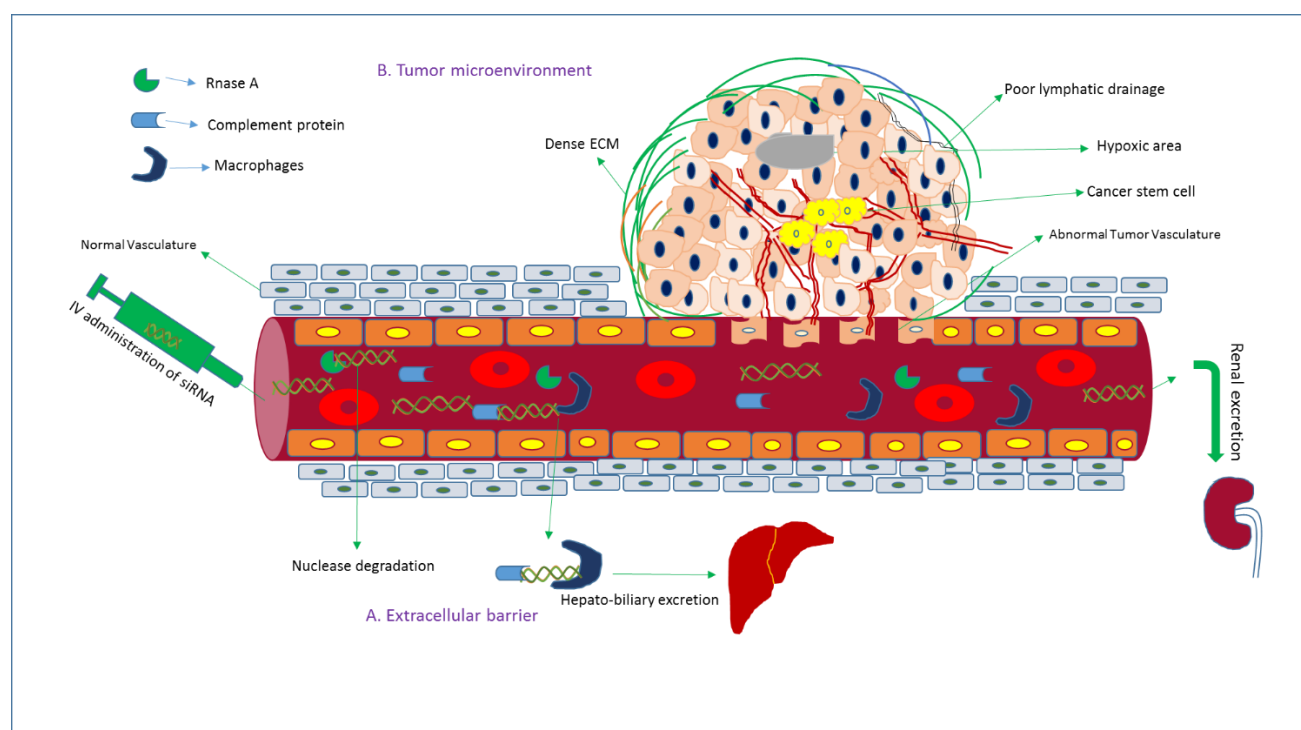


Figure 3: Extracellular and cellular barriers faced by unmodified siRNA to reach target site after intravenous (IV) administration. A. after IV administration, naked siRNA is subjected to extracellular barriers like nuclease degradation, macrophage-facilitated hepato-biliary excretion and rapid renal clearance. B. To enter into cancer cell, naked siRNA is to fight with cellular barriers like abnormal tumor vasculature, dense and irregular structure of extracellular matrix (ECM), high interstitial fluid pressure (IFP), hypoxia and poor lymphatic drainage, and intracellular barriers like negatively charged cell membrane and lysosomal lysis.

Delivery vehicles are categorized into two main subclasses: viral vectors and non-viral vectors (Figure 4). The viral vectors like retroviruses, adeno viruses, and adeno associated virus (AAV) have been successfully used to carry genes in both preclinical and clinical trials (69% of total human trials are viral-assisted cancer gene therapy)

[23]. The engineered viral vectors possess high specificity, unassisted entry to the cell membrane, lack of replication and pathogenicity and higher gene expression efficiency [40, 41]. The activation of innate immune response, carcinogenicity and higher treatment cost of viral vectors limit their use in the clinic [20,40,42–44], thus motivating to develop non-viral vehicles for specific delivery of nucleic acids to the target cancer cells. The non-viral vectors are non- immunogenic, biologically compatible, higher specificity, higher packing capacity and less manufacturing cost in contrast to viral counterparts [23,45]. They are mainly subdivided into two categories depending on their composition: organic and inorganic carriers. The organic nanoparticles are widely used and are categorized into three classes based on their constituents, namely cationic lipids, cationic polymers and hybrids of both lipids and polymers. Several preclinical studies using lipid nanoparticles (LNPs), dendrimers, carbon nanotubes, graphene oxide and micelles, etc. as carriers have been accomplished for silencing mutant genes in multiple animal models of cancer. Among them, a number of organic nanocarriers are in clinical trials. The poor delivery efficiency, low rate of endosomal escape (1%) and retarded release of siRNA from the carriers and associated toxicity have slowed down the success rate of organic carrier-based RNAi therapy for cancers management [46–48]. On the other hand, inorganic nanoparticles, the newly introduced nanocarriers, have been widely explored to suppress the shortcomings of organic carriers in a gene silencing platform. Inorganic nanoparticles possess unique physicochemical properties, biocompatibility, flexibility to be functionalized with different ligands and surface-coating materials, such as Polyethylene glycol (PEG), controlled release pattern and compatibility with other existing therapeutic agents [49]. The inorganic nanoparticles that are frequently used in both in vitro and in vivo studies to repress multiple overexpressed cancer genes are gold NPs, magnetic NPs, up conversion NPs, mesoporous silica NPs, pH sensitive carbonate apatite NPs and other multifunctional NPs. Both organic and inorganic carriers have undergone several modifications like PEGylation for escaping RES (reticuloendothelial system) and renal clearance, attachment of targeting moiety like ligands and antibodies for specific delivery as part of active targeting, cell-penetrating peptides (CPP) for improving the cellular uptake and stimuli-responsive linker to improve the therapeutic index of antisense cancer gene therapy [50].

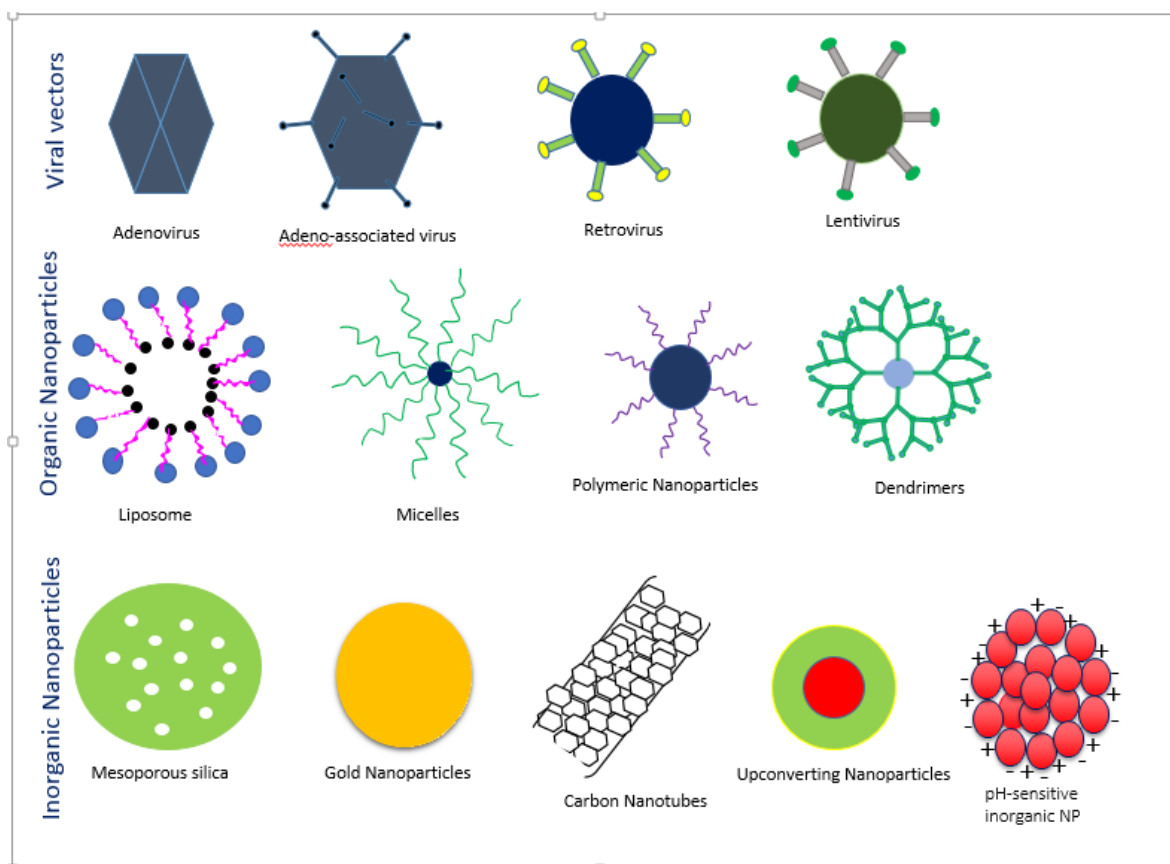


Figure 4: Various viral and non-viral vectors used for the delivery of genetic materials such as DNA, RNA, siRNA and shRNA.

The emergence of multifunctional NPs and comprehensive investigation of RNAi against oncogenes led to potential NP-based cancer gene therapies and more than 40,000 (based on active targeting strategy) studies have been reported in the last decades [51]. However, the issues of biological stability and delivery of siRNA in the presence of multiple physiological barriers have yet to be fully resolved. Tumor microenvironment is another prominent barrier for successful intracellular delivery of RNAi therapeutics. Although the immature blood vessel with heterogeneous hyper permeability and the irregular lymphatic vasculature cause abnormal blood circulation and poor lymphatic drainage [52], respectively, resulting in enhanced permeability and retention of NPs in tumor tissues, higher interstitial pressure, synthesis of heterogeneous extracellular matrix molecules (e.g., glycoprotein) and excessive matrix metalloproteinase pose hindrance to insufficient delivery of the particles [53–55]. Poor cellular uptake by RNAi therapeutics is another hurdle arising as a result of repulsion between the negatively charged siRNA and the anionic cell membrane, and could be improved via chemical modification, e.g., by coating with cell-penetrating peptide [56] or stably complexing or conjugating with NPs. After entering a cell,

Drug formulation	Target Gene	NPs	Treatment	Diseases	Phase	Status	Identifier trial number( <a href="https://clinicaltrials.gov">https://clinicaltrials.gov</a> )
DCR-MYC	MYC	Lipid	siRNAs	Hepatocellular carcinoma	1/2	Ongoing, not recruiting 2014-present	NCT02314052
DCR-MYC	MYC	Lipid	siRNAs	Solid tumors, multiple myeloma, non-Hodgkin lymphoma, or pancreatic neuroendocrine tumors	1	Ongoing, not recruiting 2014-present	NCT02110563
ALN-VSP02	KSP and VEGF	Lipid	siRNAs	Solid tumors	1	Completed	NCT00882180
Atu 027	PKN3	Lipid Nanoparticles	siRNAs	Advanced cancers	1	Completed	NCT00938574
TKM-080301	PLK1	Lipid	siRNAs	Primary and secondary liver cancer	1	completed	NCT01437007
	PLK1	Lipid	siRNAs	Neuroendocrine tumors	1/2	completed	NCT01262235
	PLK1	Lipid	siRNAs	Advanced hepatocellular carcinoma	1/2	completed	NCT02191878
siRNA-EphA2-DOPC	EphA2	Lipid	siRNAs	Advanced solid tumors	1	Recruiting	NCT01591356
siG12D-LODER	KRAS	LODER polymer	siRNAs	Ductal adenocarcinoma or pancreatic cancer	1	completed	NCT01188785
siG12D-LODER	KRAS	LODER polymer	siRNAs	pancreatic cancer	2	Not yet recruiting	NCT01676259
SNS01-T	eIF5A	polyethyleneimine	siRNAs plasmids	Multiple myeloma	1/2	unknown	NCT01435720

Table 1. siRNAs-based clinical trials for cancer therapy.

the siRNA is usually transported from early endosome to late endosomes for degradation. To get better silencing outcome, siRNA could be released in the cytosol from endosomes at an early stage, for instance, by complexing with pH-sensitive nanoparticles (e.g., carbonate apatite). Exocytosis or cellular recycling of internalized siRNA via recycling routes e.g., non-secretory exosome might reduce the silencing efficiency of siRNAs, and could be prevented by using an exocytosis inhibitor [57,58]. Despite the successes in cell culture and preclinical studies, a small number of NPs-based siRNA formulations have successfully entered clinical trials (Table 1). Toxicity of vectors, immunogenicity and off-target effects of siRNA are the remaining hurdles in the clinic. Moreover, a difference between the physiology of humans and

experimental animals, extracellular physiological barrier, technological barrier and inability to target metastases limit the success in clinical trials.

## **1.4. In-Vivo Delivery of siRNAs and shRNAs Directed against Different Cancer-Causing Genes in Various Cancer Models**

### **1.4.1. Silencing of Bcl-2 Gene**

Bcl-2 (a mitochondrial protein of 239 amino acids), is a crucial factor for promoting cell growth and survival by inhibiting apoptosis pathways of cells (Figure 5). It plays critical roles in the growth, development and metastasis of various cancers, including breast, lung, liver and gastric cancers [59–62]. Bcl-2 expression was found in 37% (10 out of 27) of biliary tract invasive cancers and the frequency of expression was observed in 90% of small cell lung cancers [63,64]. The role in cancer development and the frequency of expression make Bcl-2 as a potential target for cancer gene therapy.

The DNA vector-based Bcl-2 siRNA was synthesized under the control of H1 RNA polymerase III (pol III) promoter and mixed with liposome-protamine for evaluating anti-tumor activity of liposome-protamine-psilencer3.1 H1-Bcl-2 complexes (at a ratio of 10:3:1) in a liver cancer mouse model generated via subcutaneous injection of and H22 (liver tumor) cells into male Balb/C mice of  $26 \pm 2$  gm. Intravenous injections of 0.4 mL of liposome-protamine-psilencer3.1 H1-Bcl-2, 0.4 mL of liposome-protamine-psilencer3.1 H1 and liposome-protamine(0.4 mL) as a control were given daily over a seven days period. There was a 66.5% decrease in tumor weight in the group of mice treated with liposome-protamine-psilencer3.1 H1-Bcl-2 in contrast to control group. Moreover, it was found that treatment with Bcl-2-silencing plasmid efficiently down regulated the expression of Bcl-2 gene in tumor cells and induced their apoptosis ratio remarkably [65]. Other researchers who used Bcl-2-targeted siRNA also observed consistent anti-cancer effects upon Bcl-2 gene silencing, indicating that the Bcl-2 antisense therapy is one of the most fruitful strategies to induce apoptosis in cancer cells [66, 67]



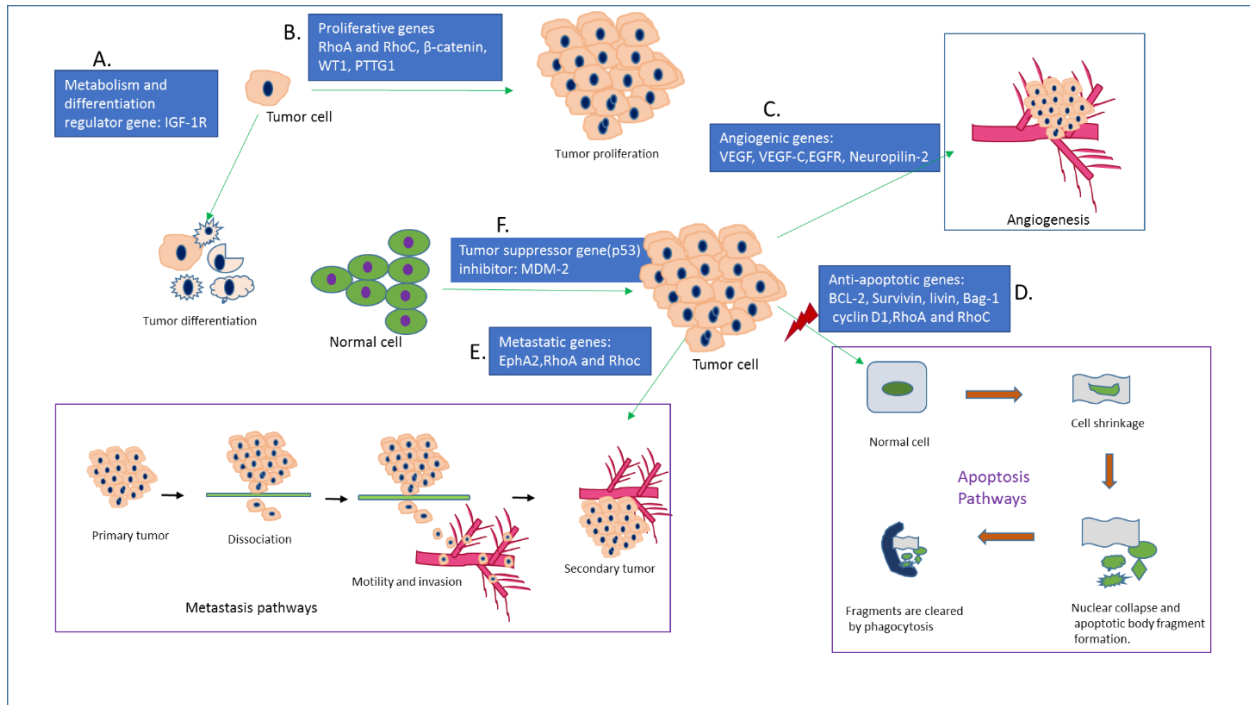


Figure 5: Roles of various genes in cancer development; A. Genes that regulate differentiation and metabolism of a cancer cell e.g., IGF-1R, B. Proliferative genes like RhoA and RhoC,  $\beta$ -catenin, WT1, PTTG1 via activating cellular process like mitosis, C. Angiogenic genes like VEGF, VEGF-C, EGFR, Neuropilin-2 that regulate tumor-induced angiogenesis, D. Anti-apoptotic genes including BCL-2, Survivin, livin, Bag-1, cyclin D1, RhoA and RhoC which block the normal apoptosis pathways of a cell, E. Metastasis regulating genes like EphA2, RhoA and RhoC which trigger cellular motility and invasion for metastasis of tumor cell, F. Tumor suppressor gene (p53) inhibitor e.g. MDM-2, deactivates the p53 pathways.

In gallbladder carcinoma, antisense-Bcl-2-siRNA against aberrantly expressed Bcl-2 gene (positive expression rate is ~23.4–51.7%) exerted significant tumor regression effect in a mouse model study [68–71]. In an in vivo tumorigenicity study, Balb/c nude mice (4–6 weeks) of 18–22 gm were subjected to subcutaneous injection of Bcl-2-siRNA transfected human gallbladder carcinoma cells (GBC-SD) suspensions of  $6 \times 10^6$  cells in 0.2 mL for experimental group and GBC-SD suspensions of  $6 \times 10^6$  cells in 0.2 mL alone for control group into the left flank of the mice. After 39 days of treatment, it was found that the volumes of tumor for both Bcl-2-siRNA transfected group and the control group were  $629 \pm 78.9$  mm<sup>3</sup> and  $1914 \pm 125.0$  mm<sup>3</sup> respectively. The average weights of tumors were  $0.77 \pm 0.12$  gm and  $2.24 \pm 0.33$  gm for experimental and control groups, respectively, and the rate of tumor growth with Bcl-2-siRNA treatment was 14.99% compared to 45.58% in the control group. Thus, Bcl-2-siRNA treating mice group had three-fold reduction of tumor volume and weight in comparison to control group and significant lower tumor growth rate relative to control group [72]. For gene therapy evaluation studies, the antisense Bcl-2 sequences were mixed with recombinant plasmid vector and

formed pSilencer<sup>TM</sup> EGFP sh515 (experimental group) and pSilencer<sup>TM</sup>-EGFP shCon (negative control group) for comparative study. Subsequent to the establishment of a human gallbladder carcinoma model by implanting  $6 \times 10^6$  of GBC-SD cells (human gallbladder carcinoma cells) into the Balb/C mice of 4–6 weeks, 10  $\mu$ g of pSilencer<sup>TM</sup> EGFP sh515 with 30  $\mu$ L of lipofectamine-2000 liposome (Invitrogen, Carlsbad, CA, USA) (experimental group) and 10  $\mu$ g of pSilencer<sup>TM</sup>-EGFP shCon with 30  $\mu$ L of lipofectamine-2000 liposome (Invitrogen) (negative control group) were administered into multiple sites of peritumoral tissue for five times with a two-days. After 39 days of injection, the average tumor volume for pSilencer<sup>TM</sup> EGFP sh515 containing group was approximately 700 mm<sup>3</sup> (experimental group) relative to negative control group, psilencer-EGFP shcon (1400 mm<sup>3</sup>) and control group (1400 mm<sup>3</sup>), demonstrating 50% reduction of tumor volume in recombinant DNA plasmid psilencer-EGFP sh515-treated mice [72].

In addition, cationic liposome LIC-101 and B717, a sequence-specific synthetic Bcl-2-siRNA was mixed to form B717/LIC-101 for exploring tumor inhibitory effect in a prostate cancer mouse model, developed by given  $5 \times 10^6$  of PC-3 cells (prostate cancer cell) subcutaneously into 5 weeks old male Balb/C mice. Intravenous injections of 0.1 mg of B717/LIC-101 and 10% (w/v) maltose solution as a control were given for five times in a week from day 7 to day 18 after the tumor volume became palpable. The tumor volumes were measured by using Dunnett's test at a regular time interval for 36 days of treatment. The group of mice receiving B717/LIC-101 was found to have smaller tumor volume (487 mm<sup>3</sup>) than the control group (1300 mm<sup>3</sup>), showing 63% reduction of tumor volume at the end of experiment [73].

Similarly, antitumor activity and pharmacokinetics parameter of sequence-specific Bcl-2 antisense siRNA (B043) and liposome complex could be improved through attachment of PEG into the surface of liposomal-siRNA complex by enhancing blood retention time, reducing the plasma clearance by the liver and thus, increasing accumulation of siRNA in the tumor region. In a study, male Balb/c nude mice (5 weeks) were allowed to inoculate prostate tumor by injecting  $3.0 \times 10^6$  of PC-3 cells (human prostate cancer cells) in 100  $\mu$ L of the nutrient mixture, resulting in growth of tumor size approximately 50–80 mm<sup>3</sup> after 10 days of subcutaneous injection. PEGylated B043/PEG-LIC (antisense Bcl-2/PEG-LIC) was given intravenously at three different doses of 1 mg/kg, 3 mg/kg, and 10 mg/kg in two five-day consecutive courses of injections and 10% maltose solution for control groups. After 24 days of post injection, the average tumor volumes for treatments with 1 mg/kg, 3 mg/kg, and 10 mg/kg of B043/PEG-LIC were 310 mm<sup>3</sup>, 220 mm<sup>3</sup> and 160 mm<sup>3</sup>, respectively, whereas for the control group it was 450 mm<sup>3</sup>, demonstrating the tumor inhibitory effects (65% at a dose 10 mg/kg of B043/PEG-LIC) in a dose-dependent manner. Accumulation of siRNA in S.C. tumor was also improved three-fold more than non-PEGylated liposome, resulting in superior targeted antitumor action of PEGylated siRNA-LIC complex [74].

### 1.4.2. Silencing of VEGF Gene

Angiogenesis is a developmental and adult physiological process of the formation of new blood vessels from preexisting micro vessels that regulate growth and metastasis of solid tumor [75–78]. Several pathological conditions like hypoxia, ischemia and inflammation result in imbalance between proangiogenic and antiangiogenic factors, leading to interactions among endothelial cells, tumor cells and a variety of growth factors. This imbalance leads to extracellular matrix remodeling, endothelial cell migration and proliferation, and capillary differentiation of tumor cells [79]. VEGF (vascular endothelial growth factor) also known as vascular permeability factor is an endothelial cell specific mitogen that plays a vital role in stimulating angiogenesis and vascular permeability through binding with VEGF tyrosine kinase receptors VEGFR1 (Flt-1), VEGFR2 (KDR, Flk-1) and VEGFR3 [80–83]. There are six subtypes of VEGF protein including VEGF-A, VEGF-B, VEGF-C, VEGF-D, VEGF-E and placental growth factor that regulate tumor-induced angiogenesis, vascular permeability and cell migration for the survival of cancer cells [84–86]. Over expression of VEGF and vascular density have been found to be higher in many human tumors including breast cancer and renal carcinoma, relative to normal cells [87–91]. Therefore, to stop metastasis of various cancer cells, VEGF gene silencing could be one of the most efficient therapeutic modalities [92–94].

A replication-deficient recombinant adenoviral vector-based antisense-VEGF-cDNA (Ad5CMV- $\alpha$ VEGF) was developed [95] and applied in an in vivo study for exploring the antitumor efficacy against a breast tumor induced by subcutaneous injection of  $5 \times 10^6$  of human breast cancer cells (MDA251-MB) into the mammary fat pads of athymic female nude mice (4–6 weeks of age). E1-deleted adenovirus type-5 without the gene (Ad5 (d1312) [96] and Ad5CMV- $\alpha$ VEGF were given intratumorally with  $5 \times 10^8$  plaque-forming units (PFU) into the mice bearing breast tumor after 4 days of inoculation. The mean tumor sizes for the Ad5CMV- $\alpha$ VEGF and Ad5 (d1312) were, respectively,  $67.85 \pm 34.65 \text{ mm}^3$  and  $335.23 \pm 83.98 \text{ mm}^3$ , with 80% reduction in tumor size by the former (Ad5CMV- $\alpha$ VEGF) [97].

A non-viral polyplex-based delivery vehicle, composed of PEG-b-poly (L-lysine) di block co-polymer and PEG-grafted PEI was synthesized to deliver therapeutic genes with improved biological stability, reduced virus-associated toxicity and increased anti-tumor effects [98–102]. Antisense-VEGF-siRNA was encapsulated with polyplex (VEGF-siRNA-PEG) and polyethyleneimine (PEI) to form VEGF-siRNA-PEG/PEI PEC micelles to assess the tumor inhibitory effects for both intratumoral and intravenous administration in a prostate tumor model generated by subcutaneous injection of  $1.5 \times 10^6$  PC-3 cells (human prostate cancer cells) into the flank of the mouse. 500 pmol of VEGF-siRNA formulation at 0, 6 and 15 days was given intratumorally after tumor size grew to  $50 \text{ mm}^3$ . Tumor regression result showed 79% reduction of tumor volume in

VEGF-siRNA-PEG/PEI PEC micelles-treated mice (120 mm<sup>3</sup>) compared to the untreated group (590 mm<sup>3</sup>). For systemic delivery, 1.5 nmol of VEGF-siRNA-PEG/PEI PEC was given intravenously into the tail vein of mice at 0, 4, 10, 18 and 28 days, exerting drastic tumor inhibitory effects (86%) (tumor volume, 196 mm<sup>3</sup>) relative to the control group (tumor volume, 1400 mm<sup>3</sup>) [103].

VEGF-C, a subtype of the VEGF family is an essential lymphangiogenic factor which promotes lymphogenesis, tumorigenesis and metastasis of cancer cells [104–107]. The autocrine effect of upregulated VEGF-C initiates several intracellular signaling pathways that mediate tumor progression in various cancers like ovarian cancer, breast cancer, bladder cancer and non-small cell lung cancer (NSCLC) [105–119]. Hifectin was employed to deliver VEGF-C-targeted siRNA (siV2) and assess potency of the delivered siRNA against the breast tumors developed by subcutaneous administration of  $5 \times 10^4$  of 4T1 cells (mouse breast cancer cells) in the right-front dorsum of a Balb/C female mouse (4 weeks old) of 18–20 gm each. When the size of tumors reached at  $\sim 0.1$  cm<sup>3</sup>, the mice were treated with siV2 (1  $\mu$ g/gm body weight), scrambled siRNA (SCR) (1  $\mu$ g/gm body weight) as a negative control and PBS (Blank control) intratumorally for every 2 days. After 3 days of post injection, the mean tumor weights for siV2, SCR and controls were 2.272 g, 3.242 g and 3.185 g, respectively, and the tumor volume for either control or SCR was approximately 2.5 cm<sup>3</sup>, whereas that for the siV2-treated group was 1.8 cm<sup>3</sup>, thus demonstrating 28% reduction of tumor volume in comparison to the control group [120].

In addition, to increase the antitumor efficacy VEGF-C-directed siRNA was mixed with lentivirus (Lv-VEGF-C-siRNA) for specific delivery to the target gene. The knockdown efficacy of virus-associated VEGF-siRNA (Lv-VEGF-C-siRNA) was assayed in a lung cancer mouse model generated via subcutaneous injection of  $1 \times 10^7$  A549 cells into the left flank of a Balb/c nude mouse at 6 weeks of age. Lv-VEGF-C-siRNA, Lv-siRNA negative control and PBS at a dose of 250  $\mu$ L in 24 h intervals for 3 weeks into the tail vein of the mice were given after 15 days of subcutaneous injection. The average volumes of tumors for Lv-VEGF-C-siRNA-treated group and untreated group were  $87.36 \pm 10.93$  and  $241.88 \pm 34.03$ , respectively. The weights of tumor for untreated and Lv-VEGF-C-siRNA-treated groups were  $1079 \pm 168.47$  mg and  $565.57 \pm 89.33$  mg, respectively, thus showing reduced tumor weight (64%) and volume (48%) in Lv-VEGF-C-siRNA-treated group relative to the untreated group. Protein and mRNA expression analysis confirmed that the silencing of VEGF-C gene expression lowered the expression of VEGFR-2, VEGFR-3, CXCR4 and CXCR7 significantly in NSCLC and suppressed the effects of AKT, ERK and p38 signaling pathways, thereby regressing the tumor growth [121].

Neuropilin-2 (NRP-2), a non-kinase cell surface receptor binds with VEGF and regulates vascularization and lymphogenesis of various tumors. Despite its expression in normal tissues, over expression of NPR-2 is found in colorectal cancer cells and important for the development and metastasis of colorectal cancer cells [122–124]. Liposomal complexes of NRP-2-targeted siRNA (NPR-2-siRNA-DOPC) could be used to slow down

the tumor growth. Following administration of  $1 \times 10^6$  cells of HTC-116 cells (lenti-luc-transfected colorectal cancer cell) into the male athymic nude mice (6–8 weeks old), NPR-2-siRNA/liposomal complexes (NPR-2-siRNA-DOPC) and siRNA-DOPC (without NPR-2) as a negative control were given intraperitoneally at a dose of 5  $\mu\text{g}$  of siRNA on every 5 days. The tumor volumes were measured 36  $\text{mm}^3$  and 420  $\text{mm}^3$  for both NPR-2-siRNA-DOPC- and control siRNA-DOPC-treated mice. Tumor growth was clearly slowed down by NPR-2-siRNA-DOPC (91.43%) compared to control siRNA-DOPC [125].

Although targeted therapeutic gene delivery has been successfully used to inhibit tumor growth by silencing specific genes, toxicity has not been diminished completely due to non-specific immune reactions and poor intracellular uptake [126–130]. To overcome this hurdle, self-assembled siRNA layered nanoparticles (nanoplexes) comprising PEI and PEGylated Ar3-Gly-Asp (RGD) peptide ligand were synthesized to target the tumor neovasculature expressing integrin to attenuate the VEGFR2 expression and tumor angiogenesis [131–139]. VEGF-R2 sequence-specific siRNA encapsulated with RGD-PEG-PEI (RPP) was subjected to an *in vivo* study for assessing the antitumor activity against a neuroblastoma tumor developed by administering  $1 \times 10^6$  of N2A cells (mouse neuroblastoma cells) into the flank of the female nude mice (6–8 weeks old). After 7 days of inoculation, when the mice had tumor size of 20  $\text{mm}^3$ , the mice were treated with RPP-nanoplexes-siLacZ (nonspecific siRNA) and RPP-nanoplexes-siVEGFR-2 at a dose of 40  $\mu\text{g}$  into the tail vein at every 3 days. The average tumor volume measured for VEGFR-2 sequence-specific siRNA-treated group was approximately 100  $\text{mm}^3$ , whereas in siLacZ-treated and control groups, the mean volumes were 1700  $\text{mm}^3$  and 1200  $\text{mm}^3$  respectively, demonstrating that RPP-VEGFR-2 siRNA reduced 91.67% of tumor volume in comparison to the control groups [100].

Taken together, VEGF and its subtype VEGF-C, VEGF receptors (VEGFR) and their signaling pathways NRP-2 play vital roles in developing tumor and lymphangiogenesis. The adenoviral vector-mediated siRNA reduced 80% of tumor volume in breast cancer. However, non-viral carrier, PEC loaded siRNA was shown to lower 86% of tumor volume with a minimal toxicity in prostate cancer mouse model. In case of VEGF-C, naked anti-VEGF-C-siRNA reduced only 28% of tumor volume, but when it was mixed with lentivector the inhibition rate was increased up to 48%. NRP-2 along with liposomal complex also inhibited 91.43% of tumor volume in colorectal cancer. VEGFR 2 with nanoplexes-ligand reduced 91.67% of tumor volume without any notable toxicity in neuroblastoma. The anti-tumor effects following nanoparticle-assisted delivery of tailored siRNAs directed against VEGF, NRP-2, VEGFR 2 and EGFR genes warrant further clinical investigation like toxicity to establish VEGF targeted gene therapy either alone or in combination as successful modalities for different cancer treatments. The tissue-targeted siRNA therapy allows huge improvement in silencing technology and identification of genes as the most selective targets for cancer gene therapy.

### 1.4.3. Silencing of EGF Receptor Genes

Epidermal growth factor (EGF) receptors, EGFR-1 and EGFR-2 are cell surface proteins that initiate growth signals in a normal cell. EGF receptors stimulate tyrosine kinase activity and activate downstream signaling pathways, playing key roles in cell division and proliferation [140]. EGFR triggers the expression of VEGF gene. Overexpression of EGFR-1 and EGFR-2 has been found in many breast cancers (30%) [141]. To improve the silencing efficacy of EGFR-1 and EGFR-2, siRNAs targeting EGFR-1 and EGFR-2 were electrostatically complexed with pH-sensitive carbonate apatite (CA) nanoparticles [142] and the anti-cancer effects of the complexes were assessed in a murine syngeneic breast cancer model. Breast tumors were inoculated with subcutaneous injection of  $1 \times 10^5$  4T1 cells into the mammary pads of female Balb/c mice (15–20 g) with ages of 6–8 weeks. When the tumor volume reached  $13.20 \pm 2.51 \text{ mm}^3$ , CA-siRNA(s) against EGFR-1(50 nM) or EGFR-2 (50 nM) were given intravenously into the tail vein of mice at 3 days with a total of two injections. CA-siRNA(s) directed EGFR-1(50 nM) or EGFR-2 (50 nM) showed no robust tumor regression after 29 days of treatment. On the other hand, concurrent delivery of EGFR-1 and EGFR-2 siRNAs with carbonate apatite exerted significant tumor volume reduction (61%) in contrast to control groups. These results suggested that combined delivery of multiple siRNAs with pH-sensitive CA is a very promising strategy in treating cancer, highlighting a huge potential of pH-responsive drug delivery to the tumor microenvironment [143].

### 1.4.4. Silencing of Survivin Gene

Survivin is a human gene that encodes a 16.5-kD wild-type protein of 142 amino acids, which is extensively expressed at G2/M phase and declines rapidly in G1 phase of the cell cycle [144,145]. Survivin is one of the subtypes of apoptosis protein inhibitor family (IAP) including X-linked inhibitor of apoptosis (XIAP), cIAP1, cIAP2, NAIP (NLR family, apoptosis inhibitory protein), Livin, ILP2 (IAP-like protein) and BRUCE [146–148]. It suppresses apoptosis by blocking both intrinsic and extrinsic pathways of apoptosis [149]. Survivin can be co-immune precipitated with caspases-3, caspases-7 and caspases-9 processing and blocks apoptosis [150]. It also mediates cellular division by increasing escape from G1 checkpoint arrest and facilitates to enter into S phase subsequently and influences tumor aggressiveness in cancer patients [145,151–153]. Survivin helps to develop chemo-resistance against various chemotherapeutics, thereby increasing tumor recurrence rate [154–157]. Survivin expression in normal tissue is low, but an aberrant expression of Survivin is found in various types of cancers, including esophageal, lung, ovarian, central nervous system, breast, colorectal, bladder, gastric, prostate, pancreatic, laryngeal, uterine, hepatocellular, renal cancers as well as sarcoma,

melanoma and hematologic malignancies [158]. This abnormal expression of Survivin makes it a potential biomolecular target for different therapeutic strategies of cancer management. Several RNAi studies targeting Survivin gene in vitro and in vivo were performed by using different carriers to deliver specifically and explore the roles of Survivin in cancer development and metastasis as well as the antitumor activity of anti-Survivin-siRNA in various cancer cell lines (Table 2).

Table 2. Summary of animal studies of siRNA- and shRNA- based cancer gene therapy.

Target Genes	Role of Genes	Delivery vehicle	Treatment	Preclinical studies application	Preclinical studies outcome	Refs
Bcl-2	Inhibits apoptosis pathways and promote cellular growth and survival in breast, lung, liver and gastric cancer	Liposome-protamine	siRNA	Balb/c mouse model inoculated with H22 liver tumor cells	66.5% reduction of tumor growth by suppressing Bcl-2 gene expression	65
Bcl-2		pSilencer <sup>TM</sup> -EGFP sh515	shRNA	Balb/C mouse model inoculated with GBC-SD, gallbladder carcinoma cells	50% reduction of tumor volume and decreased tumor growth rate	72
Bcl-2		Cationic liposome, LIC-101	siRNA	Balb/C nu <sup>++</sup> mouse model inoculated with PC-3 prostate cancer cells	63% reduction of tumor volume	73
Bcl-2		PEG-LIC complex	siRNA	Balb/C mouse model inoculated with PC-3 human prostate cancer cells	Increased siRNA uptake, 65% tumor reduction without any systemic toxicity	74
VEGF	Stimulates angiogenesis and vascular permeability	Adenoviral vector (Ad5CMV)	siRNA	Athymic female mouse model inoculated with MDA251-MB, human breast cancer cells	Reduced 80% of tumor through anti-angiogenesis mechanism	97
VEGF		Polyelectrolyte complex (PEG/PEI PEC micelles)	siRNA	Female nude mice (nu/nu) model inoculated with PC-3 human prostate cancer cells	Intratumoral injection caused 79% tumor inhibition; Intravenous administration reduced 86% of tumor volume	103
VEGF-C	Promotes lymphogenesis, tumorigenesis and initiates metastasis	Hifectin-mediated transfection	siRNA	Balb/C mouse model inoculated with 4T1 cells, mouse breast cancer cells	Reduced 28% of tumor volume.	120

VEGF-C		Lentivirus vector (Lv)	siRNA	Balb/C mouse model inoculated with A549, human NSCLC cells	64% tumor inhibition and 48% reduction of tumor volume by decreasing VEGF-C expression	121
NRP-2	Binds with VEGF and regulates vascularization and lymphogenesis of various tumors	DOPC(neutral lipid 1, 2-dioleoyl-sn-glycero-3-phosphatidyl choline)	siRNA	Male athymic nude mouse model inoculated with HTC-116, human colorectal carcinoma cell lines	Reduced 91.3% of tumor volume via increasing anti-angiogenic mechanism	125
VEGF R2	Regulates angiogenesis and tumor growth	RGD(Ar3-Gly-Asp peptides)-PEG-PEI nanoplexes	siRNA	Female nude mouse model inoculated with N2A, mouse neuroblastoma cells	Enabled tissue-specific delivery and inhibited more than 90% of tumor volume	100
EGFR 1 & ERBB2	Activate downstream signaling pathways and play key role in cell division and proliferation	Carbonate apatite Nano-particle	siRNA	Female Balb/C mouse model inoculated with 4T1 cells, mouse breast cancer cells	61% reduction of tumor volume without any toxicity	143
Survivin	Suppresses apoptosis by inhibiting both intrinsic and extrinsic pathways of apoptosis, as well as improves chemo-resistance to various chemotherapeutics and increases tumor recurrence rate	PEGylated chitosan (PEG-CS)	siRNA	Female Balb/C mouse model inoculated with 4T1 cells, mouse breast cancer cells	Increased biological stability and targeted gene delivery, reduced 55% of tumor volume	165
Survivin		Chiosan-6-poly arginine and histidine (H6R6-CS)	siRNA	Female Balb/C mouse model inoculated with 4T1 cells, mouse breast cancer cells	Improved cellular uptake and endosomal escape with 63% tumor inhibition	176
Survivin		Cationic linear polyethyleneimine (PEI)	Sticky siRNA (ssiRNA)	NMRI nude female mouse model inoculated with B16-F10 cells, murine melanoma cell lines	Reduced 50% of tumor volume through silencing of Survivin gene	181
Survivin		PCPP(mPEG-CPB-PEI) nano-particle	siRNA	Balb/C mouse model inoculated with 4T1 cells, mouse breast cancer cells	Increased tumor accumulation and improved cellular uptake with 66% reduction of tumor volume	185
Cyclin-B1	As a mitosis promoting factor triggers uncontrolled cell	MPG-8 (Primary amphipathic	siRNA	Swiss nude mouse model inoculated with	90% tumor size inhibition for maximum dose,	



	proliferation and hampers the stability of chromosomes	peptide carrier)-cholesterol (MPG-8/choI)		PC-3 cells, human prostate cancer cells	60-80% reduction of Cyclin B1 expression and extended survival rate	206
Cyclin-B1		Cationic linear polyethyleneimine (PEI)	Sticky siRNA (ssiRNA)	NMRI nude female mouse model inoculated with B16-F10 cells, Murine melanoma cell lines	Reduced 44% of tumor volume via down regulating Cyclin B1 expression	181
RhoA & RhoC	Triggers signal transduction and drives a series of pathologies of cancer including cell motility, proliferation, apoptosis inhibition, cell cycle progression, invasion, metastasis and inflammation	Adenoviral vector	shRNA	Male Balb/C mouse model inoculated with HTC-116, human colorectal carcinoma cell lines	Slowed tumor growth (2.38 fold) and reduced 37% of tumor volume	225
RhoA & RhoC		Cytfectin-mediated transfection	siRNA	Athymic female mouse model inoculated with MDA251-MB, human breast cancer cells	Reduced tumor volume 85% (anti-RhoA) and 53% (anti-RhoC), lowered angiogenesis index	227
RhoA		Chitosan-PIHCA(polyisohexylcyanoacrylate)	siRNA	Athymic female mouse model inoculated with MDA251-MB, human breast cancer cells	At higher dose the tumor were completely removed	228
RhoC		Lipofectamine-mediated transfection	siRNA	Balb/C-nu mouse model inoculated with SUM149, human IBC cells	Reduced tumor volume by 35%, increased survival rate to 85%, up-regulated metastasis suppressor gene KAI1	234
$\beta$ -Catenin	Regulates cell-cell adhesion and gene transcription, ultimately controlling cellular proliferation	Oligofectamine-mediated transfection	siRNA	Female nude/nu mouse model inoculated with HTC-116, human colorectal carcinoma cell lines	Three-fold smaller in size of tumor in comparison to control with extended survival rate	253
$\beta$ -Catenin		Lentivirus vector	shRNA	Male athymic nude mouse model inoculated with AGS cells, human gastric cancer cells	75% reduction of tumor volume by inhibiting CCAR1 gene expression	259
EphA2	Enhances cell-extracellular matrix (ECM) adhesion,	DOPC (neutral lipid 1, 2-dioleoyl-	siRNA	Female athymic nude (Ncr-nu) mouse model	Reduced 35-50% of tumor size	

	anchorage-dependent growth and metastasis	sn-glycero-3-phosphatidyl choline)		inoculated with SkOV3ip1 cells, ovarian cancer cell lines	275
EphA2 and FAK		DOPC (neutral lipid 1, 2-dioleoyl-sn-glycero-3-phosphatidyl choline)	siRNA	Female athymic nude (Ncr-nu) mouse model inoculated with SkOV3ip1 cells, ovarian cancer cell lines	Reduced 62-82% of tumor metastasis and slowed down tumor growth rate 283
EphA2		Liposome	siRNA	Balb/C mouse model inoculated with SGC 7901, human gastric adenocarcinoma cells	43.1% inhibition of tumor growth, with reduction in expression of metastatic gene MMP-9 285
MDM-2	Inhibits the regulation of p53 tumor suppressor gene	PMPC-b-PDPA (di-block copolymer of poly (methacryloyl oxy ethyl phosphorylcholine)-b-poly (diisopropano lamine ethyl methacrylate)	siRNA	Athymic mouse model inoculated with H2009 cells, NSCLC cells	67% reduction of tumor growth via down regulation of MDM-2 gene expression without any systemic toxicity 290
MDM-2, c-myc and VEGF		cationic lipid-PEG	siRNA	Female C57B216 mouse model inoculated with B16-F10 cells, murine melanoma cell lines	20-30 % reduction of tumor load with extended survival rate 291
IGF-1R	Promotes cellular metabolism, differentiation, apoptosis, chemo resistance and angiogenesis as well as protecting cells from UV irradiation, cytokine and gamma radiation-induced apoptosis	Plasmids-PEI	siRNA	Male nude mouse model inoculated with A549 cells, human lung adenocarcinoma cell lines	60% of reduction of tumor volume, Increasing apoptotic cells 305
IGF-1R		Magnetic lipoplexes	shRNA	Male Balb/C AnNcrj-nu mouse model inoculated with A549 cells (NSCLC cells line with overexpression of IGF-1R)	Improved site specificity and cellular uptake, and reduced 85.1±3% of IGF-1R gene expression 306
Livin	Thwarts both extrinsic and intrinsic apoptosis pathways by interacting with specific cysteine proteases or caspases, while playing a significant role in tumor	Single chain antibody	siRNA	Nude mouse model inoculated with LiBr cells, malignant melanoma cell lines.	Reduces approximately 64% of tumor size. 324
Livin		Plasmid vector	siRNA	Balb/C nu/nu mouse model	73% reduction of mean tumor size,

	progression and chemo resistance development			inoculated with SPCA-1 cells, human lung cancer cell lines.	with increased apoptotic fraction and improved survival rate	325
WT1	The key drivers that control cell proliferation and apoptosis via regulation of the expression of proliferative genes	Plasmid vector	shRNA	Balb/C <sup>nu/nu</sup> mouse model inoculated with A549, H1299 and H1650 cells	69-76% reduction of tumor volume without any systemic toxicity	348
WT1		Liposome-PEG	shRNA	Female C57BL/6 mouse model inoculated with B16F10 cell, murine melanoma cell lines	Reduced 34% of tumor weight and extended survival rate (62.5%)	353
Bag-1	Regulates Bcl-2 gene expression and mimics the anti-apoptotic activities via bridging between the growth factor and anti-apoptotic mechanisms	Magnetic gold nanoparticles	siRNA	Balb/C nude mouse model inoculated with LoVo cell, human colon cancer cell lines	69% of tumor inhibition without toxicity	360
PTTG1	Plays a vital role in several cellular processes like mitosis, DNA repair, apoptosis and gene regulation and causes aneuploidy.	Adenoviral vector	siRNA	Balb/C nude mouse model inoculated with SH-J1 cells, hepatoma cell lines	Significant tumor inhibition efficacy (84%)	375
CD-47	Causes the tumor cells escape from immunosurveillance with the result of tumor progression	Liposome-protamine-hyaluronic acid	siRNA	C57B2/6 mouse model inoculated with B16F10 cell, murine melanoma cell lines	Above 90% tumor inhibition without toxicity	382

Chitosan, a non-viral vector for gene delivery, has been widely used due to their nontoxic, non-immunogenic, biodegradable and biocompatible properties [159]. The siRNA targeted to the Survivin was electrostatically binds chitosan (CS-siRNA) for improving siRNA stabilization against nuclease-mediated degradation and avoids renal clearance [160,161]. However, a poor water-soluble CS-siRNA complex is attacked by blood proteins and attributed to protonation effects in biological media. To overcome this hurdle, the CS-siRNA complex was grafted with PEG by an ionic gelation method for increasing stability and solubility in biological media [162]. The PEG provides steric stabilization effect of CS-siRNA complex against blood proteins and cells [163,164]. Mouse breast cancer cell lines (4T1) were inoculated into female Balb/C mice at the age of 4–6 weeks, and PEG-CS-siRNA (0.3 mg siRNA/Kg), free siRNA (negative control group) and saline (blank) were administered for total five times at every 2 days after the mice had a tumor volume of 100 mm<sup>3</sup>. At 28 days of post-injection, the tumor volume of PEG-CS-siRNA-treated mice was found to be approximately 500 mm<sup>3</sup>, whereas for saline and naked siRNA treatments the volumes were approximately 1500 mm<sup>3</sup> and 1100 mm<sup>3</sup>,

respectively. PEGylated-CS-siRNA demonstrated increased biological stability and selective tumor accumulation, thereby reducing tumor growth (55%) more significantly than the non-PEGylated ones [165].

Although chitosan nanoparticles (CS-NPs) are stable in biological media, the use of CS-NPs is limited due to poor cell penetrating capability and buffering capacity. Cell penetrating peptides (CPPs), 6-poly arginine and histidine (H6R6) were combined with CS-siRNA for improvising cellular internalization and mediating early endosomal escape of antisense siRNA into the cytoplasm [166–168]; 6-poly arginine has strong positive charge which helps to transport of nucleic acids into tumor more easily, whereas poly-histidine increases the buffering capacity of chitosan nanoparticles and thereby destabilizes endosomal membrane in the acidic environment for rapid endosomal escape [169–173]. The H6R6-CS and siRNA directed to Survivin (H6R6-CS-siRNA nanoparticles) was combined by complex coacervation method [174,175] before being investigated for the activity against tumor growth and metastasis. Breast tumors were induced into 4–6-week-old Balb/C female mice via subcutaneous injection of 4T1 cells prior to the evaluation of antitumor efficacy of H6R6-CS-siRNA at a concentration of 0.3 mg/kg through injections of the formulation for five times at a two days after the tumor size became 130–140 mm<sup>3</sup>.

Naked siRNA, as well as saline, were also given as controls. After 28 days of treatment, the tumor volume for H6R6-CS-siRNA was approximately 600 mm<sup>3</sup>, whereas in blank and naked siRNA-treated group the volumes were, respectively, 1600 mm<sup>3</sup> and 1200 mm<sup>3</sup>, thus demonstrating significant antitumor efficacy for H6R6-CS-siRNA complexes (63% reduction of tumor volume) compared to the control group. The improved cellular internalization and early endosomal escape capability of H6R6-CS-siRNA complexes resulted in more transfection efficiency with higher capability of silencing Survivin gene [176].

Melanoma is one of the most common malignancies characterized by strong metastasis and chemo-resistance properties, leading to higher mortality rate relative to other cancers [177–179]. The combined action of anti-apoptotic factors, pro-apoptotic effectors and stringent survival signal contributes to the development of chemo-resistance. The anti-apoptotic protein Survivin has a strong correlation with melanoma metastasis and is found to be expressed at a higher level in melanoma which makes Survivin a potential therapeutic target for melanoma treatment [151–153]. Sticky siRNA (ssiRNA) with cationic linear polyethyleneimine (PEI) was shown to promote gene silencing by improving stability and reducing conventional toxicity [180]. Murine melanoma tumors

were implanted in NMRI nude female mice (5 weeks old) by subcutaneous injection of  $1 \times 10^6$  B16-F10 cells into the right flank of mice. When the tumor volume grew to  $50 \text{ mm}^3$ , the mice were treated with glucose (control), negative control ssiRNA and antisense Survivin-siRNA/PEI at a dose of 1 mg/kg. At 10 days of post injection, the tumor volumes for both ssiRNA-Survivin/PEI and control groups were approximately  $1000 \text{ mm}^3$  and  $2000 \text{ mm}^3$ , respectively. The ssiRNA-Survivin/PEI reduced 50% of the tumor volume in comparison to the control group, via attenuating the Survivin gene expression [181].

Sialic acid (SA) is found to be overexpressed on cell surfaces of most cancer cells and aids in tumor metastasis by avoiding immune recognition of cancer cells [182–184]. Phenylboronic acid (PBA) grafted with polyethyleneimine (PBA-PEI) for targeting SA, and shielded with PEG (polyethylene glycol) to increase stability in systemic circulation, was shown to reduce off-target effects and carry anti-Survivin siRNA into targeted tumor cells. The PEG shell which could be detached from NP-siRNA complexes at extracellular pH of tumor enabled internalization of the NP-siRNA complexes into cancer cell. After internalization, the PBA-ribose ester bond was completely disrupted at the acidic pH of tumor microenvironment, releasing the siRNA into the cytoplasm. Tumor growth inhibition of the dual pH-responsive nanoparticle complex (PEG-CPB-PEI (PCPP)/siRNA) was studied in a breast tumor mouse model generated by subcutaneous injection of  $1 \times 10^5$  of 4T1 cells in mammary fat pad of Balb/C mice. When the mice had a tumor of  $80 \text{ mm}^3$ , the tumor-bearing mice were treated 6 times in every 3 days with saline, naked siSUR, PEI1.8ksiSUR, PCPPsiN.C (siRNA of nonsense sequences), and PCPPsiSUR (siRNA of anti-Survivin gene) at a dose of 1 mg/kg (siRNA). The tumor volumes of the mice treated with PCPPsiSUR and control groups were approximately  $500 \text{ mm}^3$  and  $1300\text{--}1500 \text{ mm}^3$ , respectively, revealing notable tumor volume reduction (66%) in comparison to the control groups [185].

The rigorous study on Survivin demonstrated that Survivin is one of the key players to drive cancer formation by mediating apoptosis in various tumors. The issue of effective, non-toxic delivery and cellular internalization is a key challenge for successful siRNA delivery. To address this challenge, researchers are trying to establish a safe and secure carrier for the successful delivery of Survivin into target cancer cells. Sticky siRNA (ssiRNA) with Polyethyleneimine (PEI) reduced 50% of tumor volume in malignant melanoma. Additionally, when the siRNA was given with polyethylene grafted chitosan (PEG-CS), the tumor reduction rate increased to 55% along with reduction of side effects. Recently, to improve cellular internalization, cellular peptide proteins (CPPs) with chitosan were used to carry Survivin-siRNA which improved the antitumor efficacy

(63%). Moreover, dual pH-responsive PCPP exerted significant tumor regression effects (66%) without hampering normal physiology of mice.

#### 1.4.5. Silencing of Cyclin-B1 Gene

Cyclin-B1 is a regulatory protein, involved in mitosis. Cyclin B1, along with Ser/Thr kinase Cdc2 (cyclin-dependent kinase1, cdk1), forms the “mitosis promoting factor” and this complex triggers the cell from G2 phase to mitosis [186–188]. Overexpression of cyclin-B1 resulted in uncontrolled cell proliferation and hampered the stability of chromosomes [189–193]. Deregulated Cyclin-B1 expression has been observed in various cancers like esophageal squamous cell carcinoma, laryngeal squamous cell carcinoma, and colorectal cell carcinoma and induces resistance against radiotherapy in different tumors [194–196]. The silencing of the cyclin-B1 gene caused induction of growth arrest at G2 phase and stopped cancer cell division [197,198]. The inevitable role of cyclin-B1 in abnormal cellular growth makes it a striking therapeutic target for cancer management. Several studies with the siRNA targeting cyclin-B1 were accomplished in the mouse model for evaluating its role in tumorigenesis (Table 2).

Non-covalent bonding between carrier and siRNAs is a very promising technique for complexing and delivering siRNA into tumor cells as well as embryonic stem cells [199–203] more efficiently. Cell-penetrating peptide, MPG-8 (Primary amphipathic peptide carrier) binds with siRNA non-covalently to form stable complexes with a siRNA which can be further functionalized for improving intracellular delivery [204,205]. The MPG-siRNA complex was tailored with cholesterol for improving stability in biological fluid and overall potency. The higher stability in biological fluid and slow release pattern of MPG-siRNA to the target tumor cells make them more advantageous over the other existing strategies. A prostate cancer mouse model was developed by injecting 106 PC-3 cells into Swiss nude mice. When the mice had a tumor size of 100 mm<sup>3</sup>, they were treated with 0.1 mL of PBS (as a control), free cyclin-B1 siRNA (100 µg), control siRNA Cyc-B3 (50 µg), cyclin-B1-siRNA (5 µg and 10 µg) complexes with MPG-8/chol-MPG-8 at a 1/20 molar ratio and cyclin-B1 siRNA with MPG-8(10 µg) in every 3 days. After 50 days of treatment, it was found that the Cyc-B1 siRNA-MPG-8/chol-MPG-8 (5 µg) reduced 60% of tumor size while for 10 µg of Cyc-B1 siRNA-MPG-8/chol-MPG-8 it was 92% in contrast to control groups. Cyclin-B1 protein expression was also reduced to 60% and 80% for both 5 µg and 10 µg of Cyc-B1 siRNA-chol-MPG-8 containing group at the end of 48 days. There was dose dependent tumor growth inhibition were seen for Cyclin-B1 siRNA treating group. The survival rate for 10 µg of Cyc-B1 siRNA-MPG-8/chol-MPG-8 was 70% at day 40 while in cholesterol free group it was only 20% [206]. On the other hand,

intratumoral injection of cyclin-B1-siRNA (1  $\mu$ g and 5  $\mu$ g) complexes with MPG-8/cholesterol-MPG-8 at a 1/20 molar ratio and cyclin-B1 siRNA with MPG (5  $\mu$ g) caused 75% reduction of tumor volume for 1  $\mu$ g and complete disappearance of tumor for 5  $\mu$ g of Cyclin-B1-directed siRNA. The notable antitumor efficacy of Cyclin-B1-siRNA for both intravenous and Intratumoral administration and their prolonged survival rate confer new prospective for tumor management modality [206].

In addition, a sticky siRNA (ssiRNA) with cyclin-B1-antisense was encapsulated with cationic linear polyethylenimine (PEI) for improving target ability and biological stability. The murine melanoma tumor was inoculated into the NMR1 (5 weeks) nude mice via subcutaneous injection of  $1 \times 10^6$  cells of B-16-F10 into the right flank of mice. When the mice had a tumor volume of 50 mm<sup>3</sup>, the mice were treated with glucose (as a control), negative control ssiRNA and cyclin-B1-ssiRNA at a dose of 1 mg/kg intravenously every alternative day. After 20 days of treatment, massive enlargement of tumor volume for both control groups (1300 mm<sup>3</sup> and 1100 mm<sup>3</sup>) were seen in contrast to cyclin-B1-ssiRNA/PEI group (700 mm<sup>3</sup>). The ssiRNA cyclin-B1-PEI complex delivered the cyclin-B1-ssiRNA to the targeted tumor cell and down regulated the Cyclin-B1 expression which resulted in significant inhibition of tumor growth [181].

In conclusion, Cyclin-B1 has a prominent role in tumor cell proliferation and is found to be heterogeneously expressed in multiple cancers. Sticky siRNA (ssiRNA) targeting Cyclin-B1 exerted 44% reduction in tumor volume and improved biological safety profile in malignant melanoma. However, Cyclin-B1 targeted siRNA loaded with cholesterol-layered MPG-8-CPP reduced more than 90% of the tumor volume in a dose-dependent manner. The prolonged survival rate and null immune responses rendered it a promising tool for cancer treatment in a therapeutic context for the future.

#### **1.4.6. Silencing of RhoA and RhoC Gene**

Ras homologous A (RhoA) and Ras homologous C (RhoC) are the members of GTP/GDP-binding GTPase of the Ras superfamily [207,208]. They are low molecular weight compounds and act as molecular switches to promote cellular processes like actin and microtubule cytoskeleton organization, cell division, motility, cell adhesion, vesicular trafficking, phagocytosis, transcriptional regulation, matrix remodeling and cell mobility [209–211]. RhoA and RhoC are the key drivers for a series of pathologies of cancer, including cell motility, proliferation, apoptosis inhibition, cell cycle progression, invasion, metastasis and inflammation of tumor cells [212–217]. RhoA activation triggers signal transduction pathways; Rho-associated coiled coil-containing protein kinase (ROCK) activation pathway and the phosphatidylinositol-3-phosphokinase/protein B (PI3-

K/AKT) pathways. These activated pathways resulted cell locomotion, cell survival and expression of cell proliferative genes [218]. On the other hand, the active RhoC drives cell invasion and metastasis by increasing focal adhesion, contact information and angiogenesis [219,220]. Moreover, excessive expression of RhoA and RhoC are found to be more than 30% of all cancers which make them a vulnerable molecular target for cancer therapy.

Colorectal carcinoma is one of the fastest growing cancers all over the world [221–223]. There is a remarkable percentage of deaths from colorectal cancer owing to its tumor metastasis and recurrence properties [224]. Several mutant genes are responsible for proliferation, invasion and metastasis of colorectal cancer. Among them, RhoA and RhoC genes are found to be overexpressed in colorectal cancer and are considered to be potential targets for the management of colorectal cancer. Recombinant adenovirus-based shRNA-targeted RhoA and RhoC (Ad-RhoA-RhoC) were synthesized and subjected to animal studies for evaluating anti-tumor efficacy.  $1.0 \times 10^7$  of HCT116 (human colon carcinoma cell line) were implanted subcutaneously into the right flank of the athymic nude male Balb/C mice (15–18 g) of 4–5 weeks old. When the tumor nodules grew to 5–7 mm, the mice were assigned to treatment. Each group of mice ( $n = 7$ ) was treated with normal saline as a control group (30  $\mu$ L/mouse), Ad-Hk (negative control group) at a dose of  $4 \times 10^8$  pfu (30  $\mu$ L/mouse) and Ad-RhoA-RhoC at a dose of  $4 \times 10^8$  plaque-forming unit (pfu) (30  $\mu$ L/mouse) intratumorally 4 times daily at a 1-day interval of total accumulated dose of  $1.6 \times 10^9$  pfu (plaque-forming unit). After 17 days of treatment, the tumor volume for Ad-RhoA-RhoC was  $(444.38 \pm 63.03)$  mm<sup>3</sup> whereas for the control and Ad-HK groups it was  $(699.62 \pm 190.56)$  mm<sup>3</sup> and  $(678.81 \pm 155.39)$  mm<sup>3</sup>, respectively. The tumor volume for control and Ad-Hk was almost five-fold higher than the starting volume. On the other hand, the Ad-RhoA-RhoC-containing group exerted a relatively slow tumor growth (2.38-fold) and reduced approximately 37% of tumor volume in comparison to the control group [225].

Aggressiveness of breast cancers is the most lethal condition that leads to death in most breast cancer patients. RhoA and RhoC are the key drivers for cancer aggressiveness e.g., increased cellular proliferation and metastasis by activating several pathways that catalyze cell survival and proliferation [207,226]. RNAi therapy targeted to RhoA and RhoC genes is supposed to be more effective to suppress tumor growth than conventional therapy. The anti-tumor effect following cytofectin-mediated delivery of anti-RhoA and anti-RhoC siRNAs was evaluated in a breast cancer mouse model, developed by employing  $4 \times 10^6$  of MDA-MB-231 cells (human breast carcinoma cells) into female athymic nude mice of 6 weeks of age. After 2 weeks of implantation, when the mice had



a tumor volume of 20 mm<sup>3</sup>, the mice were treated with 100 µL of anti-RhoA (85 nM), anti-RhoC (85 nM) siRNA and cytofectin containing excipient as a control intratumorally at a 3-day interval over a period of 20 days. Mice treated with anti-RhoA siRNA (tumor volume, 200 mm<sup>3</sup>) and anti-RhoC siRNA (tumor volume, 600 mm<sup>3</sup>) showed less tumor growth than in the control group (1300 mm<sup>3</sup>). The angiogenesis index values of anti-RhoA and anti-RhoC siRNA were  $8.75 \pm 3.30$  and  $22.5 \pm 3.32$  relative to  $30.5 \pm 4.12$  for the control group. The above findings demonstrated that anti-RhoA and anti-RhoC siRNA reduced tumor volume by 85% and 53%, respectively, in contrast to the control by down regulating RhoA and RhoC gene expression. The remarkable gene silencing effect and antitumor effects of anti-RhoA in intratumoral delivery revealed that there is a strong correlation between RhoA, and tumorigenesis. To furnish this approach for further investigation, intravenous administration of anti-RhoA siRNA is required for assessing its efficacy and safety in the systemic circulation [227].

Chitosan, a mucopolysaccharides was combined with polyisohexylcyanoacrylate (PIHCA) to deliver siRNA to the target site as well as to protect it from enzymatic degradation. The efficacy and safety profile of chitosan-polyisohexylcyanoacrylate-antiRhoA were assayed in a mouse model study. Human breast cancer (MDA-MB-231) cells ( $5 \times 10^6$  cells in a volume of 250 µL) were injected subcutaneously into the right hind limb of the female athymic nude (nu/nu) mice aged 6 weeks to let the cells grow into a tumor of 20 mm<sup>3</sup>, and the mice were treated with 150 µg of siRNA/kg body weight in the low dose group and 1500 µg of siRNA/kg body weight in the high dose group, while empty chitosan nanoparticles at a 300 µg/mL were also injected as a control at every 3 days to 30 days. The anti-RhoA siRNA inhibited tumor growth in a dose-dependent manner. There was >90% decrease in mean tumor volume for 150 µg (low dose group) siRNA containing group, whereas for 1500 µg (high dose group) siRNA containing group it completely disappeared in comparison to control group [228].

Inflammatory breast cancer (IBC) is characterized by fast proliferation, metastasis, lower survival rate and local recurrences [219,229–232]. It was found that 90% of IBCs contain over-expressed RhoC GTPase gene [233] which might be involved in growth and metastasis of cancer cells. Cellular uptake and bioavailability of the anti-RhoC siRNA were increased by mixing with lipofectamine. SUM149 cells ( $1 \times 10^7$ ) were injected into each female BALB/c-nu mice (47 weeks old) subcutaneously to allow them to grow into a tumor volume of 50–70 mm<sup>3</sup>. Intratumoral injections of saline (control), control siRNA, and anti-RhoC-siRNA (0–1 mL, 80 nM) were given at 2-day-intervals for a total of 14 days. The relative tumor volume for anti-RhoC siRNA was 3.4, whereas it was approximately 5.2 for both control and untreated siRNA, demonstrating 35% reduction of tumor volume

in contrast to the control group. The survival rate after 30 days of treatment was approximately 85% for anti-RhoC siRNA-treated group, indicating that lipofectamine mediated anti RhoC siRNA had a significant effect on tumor growth reduction as well as survival rate enhancement. The down regulation of RhoC gene expression results in up-regulation of metastasis suppressor gene KAll expression as well as reducing the expression of CXCR4 and MMP cardinal regulator of breast metastasis [234].

The amazing results of pre-clinical studies (Table 2) indicate that RhoA and RhoC have different clinical roles in regulating transcriptional factors, invasion and metastasis of cancer cells in multiple cancers and are overexpressed in various solid tumors. Despite the technique's novelty, the roles of RhoA and RhoC are being searched for successful management of cancer for further advancement in the future. Adenoviral-mediated combined delivery of RhoA and RhoC in colorectal carcinoma reduced 37% of tumor volume. RhoA-directed siRNA exerted extraordinary tumor volume inhibitory effects (85% of tumor volume) in breast cancer, whereas when it was given with chitosan-polyisohexylcyanoacrylate (PIHCA) complex the tumor volume reduction was increased to 90% (to completely abolishing) for the higher dose. On the other hand, RhoC with lipofactamine in inflammatory breast cancer reduced only 35% of tumor volume and 53% in aggressive breast cancer. Although RhoC is extensively expressed in almost all cancers, its clinical role and efficient treatment modality should be investigated for using it in the clinical setting.

#### **1.4.7. Silencing of $\beta$ -Catenin Gene**

$\beta$ -Catenin is a protein that is encoded by the CTNNB1 gene in humans and a subunit of cadherin protein, which are the key drivers for the WNT pathway [235,236]. It regulates the intracellular signal of WNT pathway and exerts a dual function, like cell adhesion and gene transcription which ultimately control the cellular proliferation [237–239].  $\beta$ -Catenin undergoes ubiquitination and proteasome degradation without WNT pathways. However, in the presence of WNT pathways, WNT ligands prevent the  $\beta$ -catenin degradation by knocking down the destruction complex of  $\beta$ -catenin [240,241]. The activated  $\beta$ -catenin binds to the Tcf/Let family and initiates transcription of cyclin D1, C-myc, MMP-7, Lgr5+ and CD-44 in nucleus continuously without any external stimulation [242,243]. It also acts as a proto-oncogene and accumulation of  $\beta$ -catenin in nucleus serves as a tumor marker for diagnosis. Mutations of  $\beta$ -catenin have been found in a variety of solid tumors like primary hepatocellular carcinoma, colorectal cancer, breast cancer, lung cancer, cervical cancer, skin cancer, liver cancer and glioblastoma [244]. The involvement

of  $\beta$ -catenin in the cancer development makes  $\beta$ -catenin as a potential molecular target for cancer gene therapy.

Overexpression of  $\beta$ -catenin and APC (adenomatous polyposis coli) genes are seen in colorectal carcinoma, mediating uncontrolled cell proliferation and development of colon cancer [245–251]. The elevated  $\beta$ -catenin levels are supposed to be lowered by introducing sequence-specific post-transcriptional silencing siRNA directed against  $\beta$ -catenin [252]. HCT 116 cells (colon cancer adenocarcinoma cell lines) were inoculated into female nude/nu mice (4–6 weeks old) for tumor inoculation. Oligofectamine-associated siRNA (250 pmol) targeting  $\beta$ -catenin and tax-siRNA (control) was given, and tumor volume and survival rates were monitored. Mice treated with antisense- $\beta$ -catenin siRNA showed higher tumor inhibitory effects (three-fold smaller in tumor size) than the control group. The survival rate for the  $\beta$ -catenin-directed group was more significant and the expression of  $\beta$ -catenin was also down remarkably regulated relative to the control group [253].

The stem cells of the gastric gland ( $Lgr5^+$ ) are responsible for the development of stomach and intestines [254,255]. Mutation and dysregulation of signaling pathways of  $Lgr5^+$  stem cells result in intestinal cancer and gastric cancer. Cell cycle and apoptosis regulators 1 (CCAR1/CARP-1) has cell growth inhibition and apoptosis promoting effects in human breast Cancer cells [256,257]. Co-delivery of CCAR1-shRNA with  $\beta$ -catenin-shRNA improved the transcriptional activation of  $\beta$ -catenin in colon cancer cells [258]. Besides CCAR1, a coactivator of  $\beta$ -catenin is considered to have a vital role in the tumorigenesis and metastasis of gastric cancer. Lentivirus based Sh-CCAR1 for targeting CCAR 1 and scrambled shRNA as a negative control were prepared to explore the tumor regression capability. Male athymic nude mice of 8 weeks were taken and subjected to subcutaneous injection of  $5 \times 10^6$  AGS cells into the posterior leg of mice at a regular time period. After a certain time period the mice were divided into two groups ( $n = 3$ ) and assigned to the treatment of shRNA-CCRA1 and scramble shRNA (shNuIT) as a control. Tumor volume and width were measured found that, control group has a fast growing tumor size of 800 mm<sup>3</sup> whereas CCAR1-shRNA groups has a relatively slow growing and smaller tumor size of 200 mm<sup>3</sup>, exerting 75% reduction of tumor size in CCAR 1-shRNA group in comparison control group [259].

In summary, the proto-oncogene  $\beta$ -catenin along with WNT pathway controls cellular proliferation by regulating transcriptional processes in various tumors. Overexpression of  $\beta$ -catenin is observed in a wide variety of cancers.  $\beta$ -catenin-targeted siRNA reduced 62% of tumor volume with a significant survival rate of colon cancer.

Another most amazing finding was that the siRNA directed against  $\beta$ -catenin suppressed the  $\beta$ -catenin expression for a long period of time (6 h) even at a small dose, which is very promising for drug safety profile. On the other hand, for gastric cancer, shRNA directed against CCAR1 co-activator of  $\beta$ -catenin reduced 75% of tumor volume and lowered the growth rate. So  $\beta$ -catenin targeted siRNA and shRNA are very promising for further study to make it feasible to the clinical trial.

#### **1.4.8. Silencing of EphA2 Gene**

Erythropoietin-producing hepatocellular (Eph) receptors are the tyrosine kinase receptors of the Ephrin family that play a vital role in the development of malignancy [260,261]. The Ephrin family is divided into two subclasses such as Ephrin A and Ephrin B based on their attachment to the membrane [262]. The EphA2 is located on human chromosome 1p36 [263] and contribute to develop Central nervous system (CNS) in the embryonic stage. In adult tissue, EphA2 is found to be expressed smaller amount in epithelial cells, but excessive expression almost ten-fold higher is seen in various tumors, including GBM patient tumor (61%), ovarian cancer (76%), prostate adenocarcinoma (85%), gastric cancer (77%), hepatocellular carcinoma, colorectal carcinoma and endometrial cancer [264–273]. Overexpressed EphA2 elicits oncogenic effects by enhancing cell-extracellular matrix (ECM) adhesion, anchorage-dependent growth and metastasis [274]. The expression rate, localization and significant clinical role in developing tumors make it an ideal target for cancer treatment.

The pharmacokinetic profile and specific delivery of the anti-EphA2 siRNA could be improved via inclusion of neutral lipid 1,2-dioleoyl-sn-glycero-3-phosphatidyl choline (DOPC) in liposome. Ovarian cancer cell lines, HeyA8 cells ( $2.5 \times 10^5$ ) and SkOV3ip1 cells ( $1.0 \times 10^6$ ) were given through intraperitoneal injection into female athymic nude mice (Ncr-nu). Empty DOPC liposomes, control siRNA in DOPC liposomes, EphA2-targeting siRNA in DOPC liposomes, paclitaxel (100  $\mu$ g) + control EphA2 Pharmaceuticals 2018, 10, 65 20 of 44 siRNA in DOPC liposomes and paclitaxel+EphA2 siRNA in DOPC liposomes were administered after the mice had a tumor size of to 0.5 to 1.0 cm<sup>3</sup>. The siRNA-liposomes at a dose of 150  $\mu$ g/kg siRNA were given twice in a week and paclitaxel was given once in a week. In HeyA8 cell line, the size of the tumor for EphA2 targeted siRNA group was 0.98 g relative to control siRNA 1.51 g. On the other hand, in the SkOV3ip1 cell line, the tumor volume for EphA2-targeted siRNA and control siRNA were 0.35 gm and 0.70 gm, respectively. Liposomal anti-EphA2-siRNA reduced 35–50% of tumor size, but when it was co-delivered with paclitaxel, tumor size reduction went up to 82% relative to the control group [275].

In addition, to improve the antitumor activity of EphA2-targeted siRNA in ovarian cancer, combinatorial targeting of EphA2, Src and FAK (focal adhesion kinase) genes were made to downregulate the expression of FAK and Src (non-receptor tyrosine kinase) involved in tumor growth and aggressiveness in ovarian cancer [276–282]. The siRNAs-loaded DOPC liposomes were employed in ovarian cancer mouse model generated by treating female athymic nude mice with  $5 \times 10^5$  of HeyA8 cells and  $1.0 \times 10^6$  of SKOVip1 cells. The tumor-bearing mice were treated with control siRNA-DOPC, EphA2-siRNA-DOPC, EphA2+FAK-siRNA-DOPC and EphA2+Src-siRNA-DOPC intraperitoneally twice in a week at a dose of 5  $\mu$ g siRNA/200  $\mu$ L suspensions. EphA2-FAK-siRNA-DOPC exerted significant tumor growth reduction (90%) in comparison to EphA2-siRNA-DOPC (67%) and FAK-siRNA-DOPC (62%) in HeyA8 model. While in SkOVi31 model, there was also notable reduction of tumor growth in EphA2-FAK-siRNA-DOPC (76%)-treated group compared to the EphA2- (50%) and FAK- (61%) treated group. Combined delivery of EphA2 and FAK siRNAs decreased 67–70% of tumor weight compared to EphA2 and FAK (single) treated group. The EphA2-Src-siRNA DOPC had a less reduction rate of tumor growth than EphA2-FAK-siRNA DOPC-treated group. Besides, EphA2-FAK-siRNA-DOPC reduced 62–82% more tumor metastasis than a single group [283].

In gastric carcinoma, erythropoietin producing hepatocellular (EphA2), a receptor tyrosine kinase (RTK) is found to be over expressed in 77.3% of gastric cancer patients [260,264,266,284] and plays a vital role in metastasis via regulation of MMP-9 gene expression. MMP-9 (gelatinase-B), member of matrix metalloproteinase (MMPs) increased cancer cell metastasis by degrading denatured collagens (gelatins) and type iv collagen which are the structural components of ECM(extra cellular matrix). The MMP-9 mediated degradation of collagen is one of the most important steps in the development of cancer cell. SGC 7901 (human gastric adenocarcinoma) cells were injected into the axillary fossa region of 3–4 weeks old Balb/C mice (18–22 g), and when the tumor size grew to  $52.2 \pm 6.9 \text{ mm}^3$ , intratumoral injections of 0.9% sodium chloride as a blank control group, non-silencing siRNA with liposomes and EphA2-siRNA with liposome were given twice in a week. After 21 days of treatment it was found that EphA2-targeted siRNA inhibited the tumor growth by 43.1% compared to the negative control group. Immunocytochemistry analysis of tumor xenograft demonstrated less expression of MMP-9 in the mouse treated with EphA2-siRNA, suggesting that silencing of EphA2 gene down regulated the MMP-9 gene expression and exerted tumor inhibitory effects [285].

Briefly, EphA2 is functionally vital to tumor growth and development. It is highly expressed in a variety of cancers. In ovarian cancers, anti-EphA2-siRNA with DOPC

reduced the 35–50% of tumor volume and its antitumor activity was increased when it has given with anticancer drug paclitaxel (67–82%). After couple years later, dual therapy of anti-FAK-siRNA along with anti-EphA2 in DOPC exerted significant tumor reduction (90%). The tumor metastasis rate also decreased to (62–82%) which is very promising. On the other hand, intratumoral injection of liposomal anti-EphA2 reduces 43.1% of tumor volume in gastric cancer cell which is need to be further analyzed in systemic administration to make it feasible for use in human.

#### 1.4.9. Silencing of MDM-2 Gene

p53, a tumor suppressor gene that is involved in cell cycle arrest, apoptosis and tumor growth inhibition. Oncoprotein mouse model minute 2 (MDM-2) inhibits the regulation of p53 tumor suppressor gene. It interacts with p53 and deactivates the p53 pathway. MDM-2 is over expressed in a various number of human tumors, including lung and prostate carcinoma [286]. Activation of p53 Pharmaceuticals 2018, 10, 65 21 of 44 pathway by blocking the MDM-2 gene is considered to be an effective treatment modality of human cancers [287,288]. To attenuate the expression of MDM-2 in the tumor cell, anti-sense-MDM-2 were employed for specific tumor growth inhibition. But the delivery of siRNA in vivo is limited due to nonspecific tissue distribution, less blood circulation retention time and self-aggregation by biological salt [289]. To overcome this hurdle, pH-responsive di-block copolymer of poly (methacryloyloxy ethyl phosphorylcholine)-b-poly (diisopropanolamine ethyl methacrylate) PMPC-b-PDPA were synthesized for the delivery of siRNA for improving biological stability, tumor specific delivery and cellular uptake. The PMPC-b-PDPA/siRNA complex were prepared by precipitation method. Athymic mice (25 g) of 6–8 weeks old were taken and  $5 \times 10^6$  of H2009 cells (NSCLC cells) were injected subcutaneously. After ten days of injection, when the tumor size reached at 100 mm<sup>3</sup>, the mice were treated with; siRNA-MDM-2 loaded nanoparticles (0.32 mg/kg) and siRNA-Scr with NPS as a negative control (6.4 mg/kg) into the tail veins at 2 days for total 12 days. The volume of tumor was measured for both groups, with 67% reduction of tumor growth observed for siRNA-MDM-2-loaded nanoparticles in comparison to Scr-siRNA. The down regulation of MDM-2 might induce apoptosis by activating p53 gene, exerting a remarkable tumor inhibitory effect [290].

A mixture of siRNA(s) targeting MDM-2 gene along with other oncogenes, c-myc and VEGF that initiate and flourish the metastatic behavior of a cancer, were encapsulated with nanoparticles formulated by protamine, cationic lipid and PEG. The constructed combo siRNA-NP complex showed superior anti-tumor effects over the control. In a study, female C57B216 mice of 16–18 g (6–7 weeks old) were inoculated with

$2 \times 10^5$  of B16F10 cells, combo siRNA (MDM-2, c-myc and VEGF at a ratio of 1:1:1), the non-targeted NP, free siRNA and control siRNA at a dose of 0.45 mg/kg of total two consecutive doses were given. After 7 days of treatment, the mice were killed and lung of mice were collected for analysis. It was found that the control group had no notable tumor regression, whereas the combo siRNA with targeted NP exerted 20–30% reduction of tumor load. The survival rate of combo siRNA-containing group was found to be extended in comparison to control group of mice [291].

So, MDM-2 gene has a driving role in development and regulation of tumors via inhibiting expression of p53 tumor suppressor gene. MDM-2 targeted siRNA along with pH-responsive di-block copolymer of poly (methacryloyloxy ethyl phosphorylcholine)-b-poly (diisopropanolamine ethyl methacrylate) PMPC-b-PDPA reduced 67% of tumor volume in NSLSC animal model. On the other hand, combination of MDM-2, c-myc and VEGF siRNAs also reduced tumor load in lungs (20–30%) and extended survival rate were found in comparison to control group. The excellent tumor regression rate of MDM-2-siRNA and reduced lung tumor load warrant more preclinical studies (Table 2) focusing on pharmacokinetics profile and survival study to make it more reliable for clinicians.

#### **1.4.10. Silencing of IGF-1R Gene**

IGF-1R (Type 1 insulin-like growth factor receptor) is a tyrosine kinase receptor which is the members of the insulin receptor family including IR (a homodimer), IGF-1R (homodimer), IGF-1R/R (hybrid, heterodimeric receptors) and mannose 6-phosphate receptor (IGF-2R) [292]. The insulin receptor (IR) has two subtypes IR- $\alpha$  and IR- $\beta$ . The ligands of IGF-1R, IGF-1 and IGF-2 interact with IR receptors, resulting in receptor oligomerization, PTK activation and other pathways. The activation of these pathways mediate gene activation, DNA synthesis and cell proliferation [293–295]. The IGF-1R also plays a vital role in cell metabolism, differentiation, apoptosis, chemo resistance and angiogenesis as well as protecting cells from UV irradiation, cytokine and gamma radiation-induced apoptosis [296]. It is ubiquitously expressed in normal tissues for growth and multiple physiological activities, but heterogeneous expression has been found in many solid tumors like breast cancer, prostate cancer, colorectal cancer, lung cancer and hematological malignancies [297–300]. The excessive expression in tumors and their role in tumor development makes IGF-1R is an auspicious bio molecular target for cancer treatment.

Non-small cell lung cancer (NSCLC) comprises more than 80% of the total lung cancer, which is the leading cause of death all over the world with a minimal survival time [301–

303]. Insulin like growth factor 1 receptor (IGF-1R) is expressed abnormally in lung cancer and mediates malignant transformation of lung tumor cell. Overexpressed IGF-1R gene hampered UV irradiation-, cytokine- and gamma radiation-induced cell apoptosis and play a critical role in the development of tumors [304]. Among the other treatment options, Anti-sense-siRNA targeting IGF-1R is considered due to its high specificity. Polyethyleneimine (PEI) coated anti-sense-IGF1R-siRNA were examined for assessing antitumor efficacy in human adenocarcinoma mouse model, developed by injecting  $2 \times 10^7$  of A549 into the male nude mice of 4–5 weeks of age. IGF-1R specific siRNA ( $0.125 \mu\text{g}/\text{mm}^3$  of tumor volume) expressing plasmids with polyethyleneimine (PEI)  $3 \mu\text{L}/\mu\text{g}$  and negative control siRNA at a same dose were injected intratumorally 4 times every 5 days. After 40 days of treatment, the tumor volume for IGF-1R siRNA was found approximately  $200 \text{ mm}^3$ , whereas for the control group it was approximately  $490 \text{ mm}^3$ . The IGF-1R siRNA inhibit 60% of tumor growth in comparison to control group. The apoptotic cells were also increased remarkably in IGF-1R siRNA groups ( $117.6 \pm 8.07$ ) than control group ( $40 \pm 9.11$ ) [305].

Magnetofection is a process of delivery of nucleic acid-magnetic nanoparticles complexes to the target cells through applying magnetic field. The IGF-1R-targeted catalytic RNA was given through magnetofection for improving antitumor effects in an NSCLC animal model. Super-paramagnetic iron oxide nanoparticles (SPIONS) were complexed with cationic lipids (lipofectamine 2000) and plasmid DNA to form self-assembling magnetic lipoplexes for the targeted delivery of IGF-1R gene and evaluated the anti-cancer potential in a non-small cell lung cancer mouse model. Male Balb/CAnNcrj-nu mice of 4 weeks old were implanted with  $5 \times 10^6$  of A549 cells (NSCLC cells line with overexpression of IGF-1R) in  $100 \mu\text{L}$  medium and allowed to grow tumor size about  $400 \text{ mm}^3$ . The group of mice was treated with;  $200 \mu\text{L}$  PBS as a control, pGFPshIGF-1R ( $50 \mu\text{g}/\text{mouse}$ ):Lp2000 ( $125 \mu\text{L}/\text{mouse}$ ) as a lipofection group and a pGFPshIGF-1R ( $50 \mu\text{g}/\text{mouse}$ ) combined with MAG ( $50 \mu\text{g}/\text{mouse}$ ):Lp2000 ( $125 \mu\text{L}/\text{mouse}$ ) under the influence of a magnetic field ( $400 \text{ mT}$ ), which was holding onto the subcutaneous tumor surface for 1 min to additional 14 min following the injection. The IGF-1R-shRNA of liposomal magnetofection silenced the expression of IGF-1R  $85.1 \pm 3\%$  than lipofection group  $56.1 \pm 6\%$ , suggesting liposomal magnetofection improve site specificity and cellular uptake which significantly down regulated the IGF-1R gene expression [306].

Taken together, IGF-1R plays a vital role in cellular proliferation and tumor growth and aberrantly expressed in multiple cancers. The anti-sense siRNA targeting IGF-1R along with PEI reduced 60% of tumor volume and increased apoptotic cell expression more than 60% in lung adenocarcinoma. After a couple of years of this experiment, IGF-1R



targeted shRNA with super-paramagnetic iron-oxide nanoparticles (SPIONs) under the influence of magnetic field silenced 86% of IGF-1R gene expression in the same lung cancer model. These exciting results provide us a novel delivery method for siRNA in different cancer cell lines.

#### **1.4.11. Silencing of Livin Gene**

Human IAP (inhibitors of apoptosis protein) are the endogenous proteins that are thwarted both extrinsic and intrinsic apoptosis pathways by interacting with specific cysteine proteases or caspases [307–310]. There are eight members of human IAP have been reported, including NAIP, c-IAP-1 (MIHB, HIAP-2), c-IAP-2 (MIHC, HIAP-1), XIAP (hILP, MIHA, ILP-1), Survivin, Apollon (Bruce), ILP-2 and Livin (ML-IAP, KIAP) [311]. Among them Livin, a 39 kDa protein is a novel family of Human IAP and it has two analogs like Livin- $\alpha$  (298 amino acids) and Livin- $\beta$  (280 amino acids) which protect the cells of heart, placenta, lung, spleen and ovary from tumor necrosis factor (TNF) and anti-CD95-induced apoptosis [312,313]. Livin expression is limited in most of the normal tissues, but found to be overexpressed in a variety of human malignancies such as colon cancer, gastric cancer, breast carcinomas, melanomas and lung cancer [312,314–316]. It plays a significant role in tumor progression, chemo resistance development and anti-apoptotic activity which makes Livin a potential therapeutic target for cancer treatment. Several siRNAs targeted to Livin gene were investigated both in vitro and in vivo (Table 2) to evaluate pharmacodynamics and pharmacokinetics properties of antisense-Livin.

Transformation of non-metastatic human melanoma to metastatic melanoma and their resistance to the current chemotherapeutics account for a huge number of deaths in both male and female in U.S.A. [317–320]. The anti-Livin-siRNA was combined with single chain antibody (anti-MM scFC-tp-siRNA) for targeted delivery in order to reduce potential side effects and enhance therapeutic efficacy in vivo [321–323]. LiBr, malignant melanoma (MM) cells ( $1 \times 10^7$ ) were given subcutaneously into right side of the flank region of a nude mouse to induce the tumor. PBS (200  $\mu$ L) as a control, anti-MM scFv-tp-siRNA NC (Mock group) and anti-MM-ScFV-tp-siRNA (20  $\mu$ g of siRNA) were given at 2 days through the tail vein. Anti-MM scFv-tp-Livin-siRNA (400 mm<sup>3</sup>) reduced 64% of the tumor volume compared to the control group (1100 mm<sup>3</sup>) [324].

Similarly, RNAi targeting Livin gene coated with lipofectamine were generated for improving apoptosis and chemo-sensitivity to chemotherapeutics and comparing the antitumor effects between treatment and control groups. In a human lung cancer mouse model generated by injecting  $1 \times 10^6$  SPCA-1 (human lung cancer cell lines), plasmid vector pS-L1, PS-NS (a non-specific sequence as a control) and pS-CMV neo plasmids

(250 µg each) were injected through the intratumoral route after 7 and 14 days of post tumor implantation. The mean tumor size for control groups (Mock, pS-CMV neo or pS-NS treated) was approximately 690 mm<sup>3</sup>, whereas for the group treated with siRNA targeting Livin it was approximately 190 mm<sup>3</sup> with 73% reduction of mean tumor size. The apoptotic fraction of siRNA-Livin group (30%) was also increased significantly compared to the control groups (5%), along with extended survival rate [325].

The above data exposed that, there was a strong correlation between Livin and tumor development. Abnormal expression of Livin is found in many solid tumors. Recently intravenous administration of antibody conjugated siRNA in Livin reduces 64% of tumor volume in malignant melanoma. But in lung cancer cells, Intratumoral administration of Livin-siRNA along with lipofectamine reduces 73% of tumor volume and increased 30% of apoptotic fraction. It should be extended to systemic administration for testing pharmacokinetics parameter for further advancement.

#### **1.4.12. Silencing of WT1 Gene**

Wilms' tumor gene 1 (WT1) is a 52–54 kDa protein, encodes four zinc finger transcriptional factors located at chromosome 11p13q and arises due to inactivation of the WT1 alleles gene [326,327]. It is the key drivers that control cell proliferation and apoptosis via attenuation of the expression of proliferative gene [328]. WT1 was defined as a tumor suppressor gene but recent evidence claimed that, it acts as an oncogene in leukemogenesis and tumorigenesis [329–334]. It is highly expressed in most of the acute myeloid leukemia (AML) and acute lymphoid leukemia (ALL) [335–337], lung, breast, thyroid and melanomas [338–341]. High rate of expression of WT1 and their significant role as a prognostic factor makes WT1 mRNA an ideal tumor marker for leukemic blast cells as well as a potential target for RNAi mediated gene therapy for various cancer treatments (Table 2).

Signal transducers and activators of transcription 3 (STAT-3) enhances the expression of anti-apoptotic gene MCI-1 and BCL-XL as well as other gene like cyclin D1/D2 and c-Myc which ultimately mediates cancer development and progression [342–346]. Over expression of WT1 increased transcriptional activity of phosphorylated STAT 3 (P-STAT 3) that upregulated anti-apoptotic gene and regulate the growth and differentiation of lung tumor cells [338,347]. To identify the relationship between over expressed WT1 and NSCLC (non-small cell lung cancer) development as well as to reveal the antitumor activity of WT1-targeted shRNA in vivo, NSCLC model was generated by subcutaneously injecting  $5 \times 10^6$  cells into Balb/C nu/nu mice. When the tumor size reached at palpable size, the three groups of mice were subcutaneously treated with pLV-

GEP-WT1, pLL3.7-WT1-shRNA (plasmid expressing WT1-shRNA) with wild type WT1 and empty plasmid (as a control). After 31 days of treatment, remarkable reduction of tumor volume was found for pLL3.7-WT1-shRNA (76%, 74% and 69%), whereas tumor growth curves for pLV-GEP-WT1 and the control group were found to be increased [348].

Transferrin (Tf), a glycoprotein over expressed on the surface of the cancer cells was used as a ligand to carry WT1-shRNA to tumor [349–352]. The WT1 shRNA-Tf was complexed with liposomes and polyethylene glycol (PEG) for improving biological stability of the shRNA in the systemic circulation. To explore the antitumor activity, B16F10 cell ( $5 \times 10^5$  cells) were subcutaneously injected into the female C57BL/6 mice (20–25 g) of 7–8 weeks aged, prior to intravenous administration of 50  $\mu$ L of Lip-RNAi-Tf, lip-RNAi against WT1 (50  $\mu$ L), 50  $\mu$ L of lip-GFP-Tf (PEGFP-N3 vector, liposome and Tf complex) and 50  $\mu$ L of saline solution at a 5 days until 29 days. The mean tumor weight for Lip-RNAi-Tf was 5.5 g whereas it was 8.8 g for untreated group. The mice of the other two groups were not counted because of all of the mice were dead after day 30. The liposome-WT1-shRNA-Tf reduced 34% of tumor weight in comparison to control group. Survival rate was also prolonged in liposome-WT1 shRNA-Tf containing group (62.5%) than control group (22.2%) [353].

In summary, WT1 plays key role in leukemogenesis and tumorigenesis as an oncogene but it was originally known as a tumor suppressor gene. Overexpression of WT1 has been detected in many solid tumors. In different lung cancer cell lines (A549, H1299 and H1650), anti-WT1 shRNA exerted notable tumor reduction 76%, 74% and 69% for lung cancer cell lines. On the other hand, ligand conjugated WT1-shRNA reduces 34% of tumor weight with prolonged survival rate. So this variation arises more questions about the role of WT1 and their targeting efficacy for the management of different tumors. To go for clinical setting more investigation is required to establish WT1 as a potential target for cancer management. Although clinical role of WT1 is obscured, liposome and ligand mediated delivery reduced the secondary effects and increased site specific delivery, which is very promising for the delivery of catalytic RNA.

#### **1.4.13. Miscellaneous**

The human Bcl-2-associated athanogene-1 (Bag-1) encodes the three major isoforms, including Bag-1S (p36), Bag-1M (p46) and Bag-1L (p50) that are located on chromosome 9 and involved in differentiation, cell cycle and apoptosis. It regulates Bcl-2 gene expression and mimics the anti-apoptotic activities via bridging between the growth factor and anti-apoptotic mechanism. The aberrant expression of Bag-1 has been found in breast, lung, cervix, esophagus and colorectal cancers [354–356]. Colorectal cancer has

the second largest morbidity and mortality rate all over the world [357,358] and human Bcl-2 associated athanogene-1(bag-1) anti-apoptotic gene is found to be involved in the tumor genesis of colorectal cancer (CRC) by mediating progression and metastasis and acts as a positive regulator of Bcl-2 gene in CRC [359]. The anti-Bag-1-siRNA plasmid was combined with magnetic gold nanoparticles and evaluated its tumor inhibitory effects in colon cancer mouse model, developed by giving  $1 \times 10^6$  of LoVo cell (human colon cancer cell lines) into the right flank of the Balb/C nude mice (14–16 g) of 4–5 weeks old. The tumor-bearing mice were divided into five groups and treated with; normal saline, nanoparticles (25  $\mu$ g), plasmid (5  $\mu$ g), nano-plasmid complexes (nano-plasmid-1; 5  $\mu$ g plasmid/25  $\mu$ g nanoparticles) and nano-plasmid complexes (nano-plasmid 2; 5  $\mu$ g plasmid/25  $\mu$ g nanoparticles) intratumorally. Nano-plasmid 2 was given to mice under the influence of about 5000 gauss magnetic fields. The 5 doses were given at a 3 day intervals. The tumor volume was measured after every 3 days, 28 days later of treatment, the tumor volume for nano-plasmid complex-1 was found to be approximately 200 mm<sup>3</sup>, whereas it was 700 mm<sup>3</sup> and 650 mm<sup>3</sup> for nanoparticle alone and control group and it was 69% reduction of tumor volume. The nano-plasmid-2 under the influence of magnetic field reduced the tumor volume at a same rate of nano-plasmid-1 without any significant reduction. Silencing of Bag-1 gene was supposed to down-regulate the expression of C-MYC protein that is clinically important for colorectal cancer. The potent anti-tumor effect makes anti-Bag-1-siRNA as a potential therapeutic for colorectal cancer management [360].

The pituitary tumor transforming gene 1 (PTTG1) is the member of PTTG family, including PTTG2 and PTTG3, that plays a vital role in several cellular processes like mitosis, DNA repair, apoptosis and gene regulation. Abnormal expression of PTTG-1 interferes in cellular processes and causes aneuploidy which is the necessary events in the tumorigenesis [361–365]. PTTG1 is over-expressed in various cancers and promotes tumor development and angiogenesis via triggering the expression of the fibroblast growth factor 2 and VEGF [366–371]. Tuning of PTTG1 gene expression by using anti-sense siRNA is considered to be an effective modality to reduce cancer aggressiveness. Hepatocellular carcinoma (HCC) is the most prominent tumor in humans all over the world having a higher alarming rate of incidence rate [372,373]. Over expression of PTTG-1 hampered the expression and function of intact p53, which ultimately promotes hepatocellular carcinogenesis [374].

Adenovirus vector assisted delivery of siRNA targeting PTTG-1 would be more efficient in down-regulation of PTTG-1 expression for hepatocellular carcinoma management. Five weeks old Balb/C nude mice were given with SH-J1 cells ( $10^7$ ) in 100  $\mu$ L of PBS

subcutaneously into the right flank of the mice and allowed to grow to a tumor volume of 3–5 mm in diameter. Following intratumoral administration of  $1 \times 10^9$  plaque-forming units (pfu) of Ad-PTTG-1-siRNA into the mice, tumor regression study demonstrated that Ad-PTTG-1-siRNA-treated groups regressed 84% of tumor volume in comparison to the control groups, suggesting that Ad-PTTG1-siRNA may serve a new paradigm for treating human cancers [375].

CD-47 is a membrane receptor of the immunoglobulin (Ig) superfamily that induces the phagocytic process of macrophages via binding with signal regulatory proteins  $\alpha$  (SiRP  $\alpha$ ). Overexpression of CD-47 causes the tumor cells escape from immunosurveillance and results in tumor progression [376,377]. The expression level of CD-47 was reported to be higher in leukemic cell lines, bladder-tumor-initiating cells and lymphomas [378–381]. The LPH-NPs (liposome-protamine-hyaluronic acid) were constructed to carry CD-47-targeted siRNA for evaluating pharmacodynamic properties against melanoma tumors. C57B2/6 mice of 6–8 weeks were harvested with subcutaneous injection of B16F10 cells at a concentration of  $2 \times 10^5$  cells/50  $\mu$ L into the hind legs of mice. The mice were treated with 12  $\mu$ g of CD-47 or control siRNA (0.6 mg/kg) along with LPH-NPs intravenously after the mice had a tumor volume of 50 mm<sup>3</sup>. The doses were given at a one-day interval to a total of six injections from the 8th day of tumor implantation. The tumor volume for CD-47-siRNA-LPH-NPs was found to be smaller than the control group, with approximately 93% reduction of tumor volume in comparison to the untreated group [382].

### 1.5. Future Directions

In preclinical studies, catalytic RNAs are mixed with several viral and non-viral vectors for safe, effective and targeted delivery to the cytoplasm of cancer cells. As exemplified in this review through various in vivo studies, siRNAs or shRNAs targeted to oncogenes, tumor suppressor genes and anti-angiogenic genes have been used with the help of various carriers over the past two decades for improving anticancer efficacy (Table 2). Among them, only few are translated into human trials and the others are in the pipeline. Although tremendous progress has been made, limitations still remain in the systemic applications of RNAi-based cancer nanotherapeutics. These hurdles should be addressed and resolved for the rational design of delivery vehicles for the targeted drug delivery to cancer cells in the future. Firstly, the issues of manufacturing hurdles like small size distribution, homogeneity, uniform functionalization, reproducibility at a large scale and manufacturing cost. Secondly, the poor understanding of mechanistic behavior of RNAi therapy with a view to their penetration and deposition in tumor tissue are not

still clear. Thirdly, the poor cellular uptake and lower silencing effects which are the key parameters of therapeutic index along with less tumor accumulation (0.7%). These obstacles have hampered the progress of RNAi-based cancer therapy to get clinical approval.

To minimize the hurdles mentioned above, extensive research on molecular events of cancer pathogenesis and mechanisms of siRNA delivery including cellular attachment, target binding, biological interactions, intracellular trafficking and nuclease attack should be further studied to understand absolute biological phenomena. This new RNAi-based therapeutic entity should overcome the physiological barriers and differentiate between cancer and normal cells for a broader therapeutic index. From a clinical standpoint, biological readouts, bio distribution and kinetics should be analyzed to ensure safety and efficacious therapies. Future studies should, therefore, be emphasized for development of SMART nano carrier (Figure 6) and computer assisted drug delivery for evaluating pharmacokinetics and pharmacodynamics profiles before heading to clinical trials.

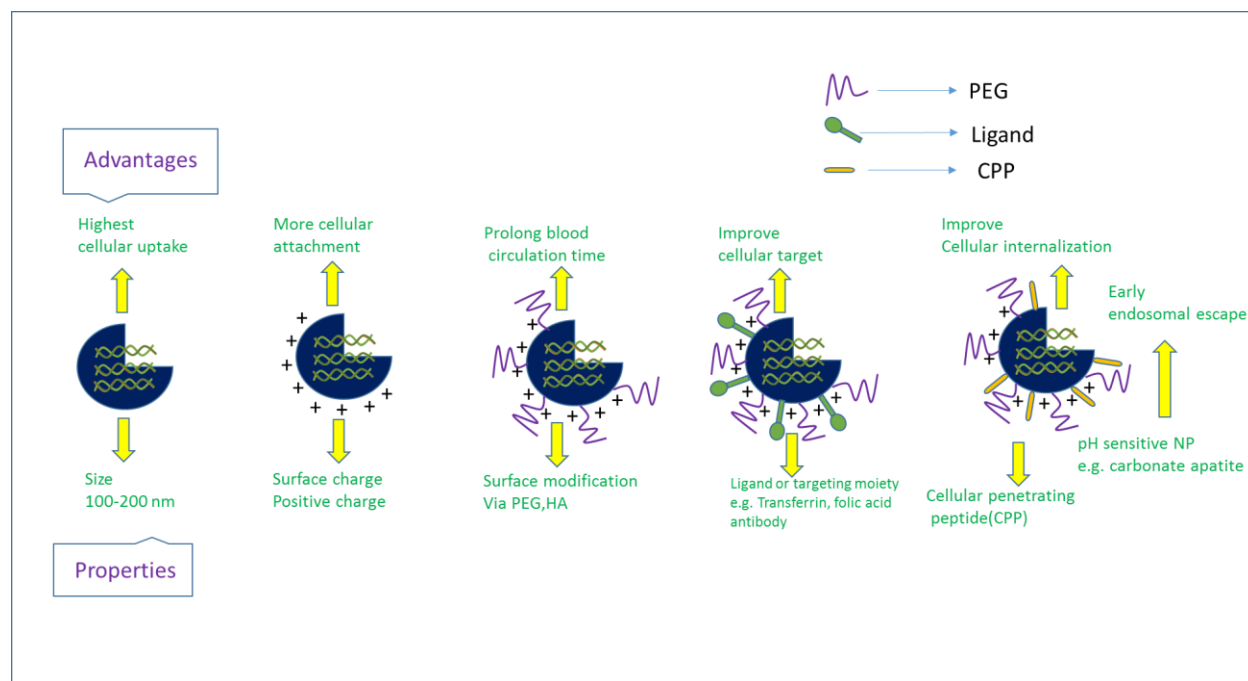


Figure 6: A proposal of a tailored made SMART nanocarrier (S=specific size; M=modified surface chemistry; A=accelerated cellular internalization; R=rapid endosomal escape T=targetted tumor cells).

## 1.6. Conclusions

Although RNAi technology has advanced rapidly and become a clinical reality as this technology has the capability to reach and treat cancer at the molecular level, cancer target discovery and validation, gene editing system and cancer stem cell targeting demand further research for improved RNAi-based cancer therapy. The RNAi-based cancer therapy would, therefore, lead the next wave of cancer nanomedicine.

## References

1. Naldini, L. Gene therapy returns to centre stage. *Nature* 2015, 526, 351–360. [CrossRef] [PubMed]
2. Fire, A.; Xu, S.; Montgomery, M.K.; Kostas, S.A.; Driver, S.E.; Mello, C.C. Potent and specific genetic interference by double-stranded RNA in *Caenorhabditis elegans*. *Nature* 1998, 391, 806–811. [CrossRef] [PubMed]
3. Zamore, P.D. RNA interference: Big applause for silencing in Stockholm. *Cell* 2006, 127, 1083–1086. [CrossRef] [PubMed]
4. Hannon, G.J. RNA interference. *Nature* 2002, 418, 244–251. [CrossRef] [PubMed]
5. Williams, B. Role of the Double-Stranded RNA-Activated Protein Kinase (PKR) in Cell Regulation; Portland Press Limited: London, UK, 1997.
6. Elbashir, S.M.; Harborth, J.; Lendeckel, W.; Yalcin, A.; Weber, K.; Tuschl, T. Duplexes of 21-nucleotide RNAs mediate RNA interference in cultured mammalian cells. *Nature* 2001, 411, 494–498. [CrossRef] [PubMed]
7. Hannon, G.J.; Rossi, J.J. Unlocking the potential of the human genome with RNA interference. *Nature* 2004, 431, 371–378. [CrossRef] [PubMed]
8. Meister, G.; Tuschl, T. Mechanisms of gene silencing by double-stranded RNA. *Nature* 2004, 431, 343–349. [CrossRef] [PubMed]
9. Whitehead, K.A.; Langer, R.; Anderson, D.G. Knocking down barriers: Advances in siRNA delivery. *Nat. Rev. Drug Discov.* 2009, 8, 129–138. [CrossRef] [PubMed]
10. Matranga, C.; Tomari, Y.; Shin, C.; Bartel, D.P.; Zamore, P.D. Passenger-strand cleavage facilitates assembly of siRNA into Ago2-containing RNAi enzyme complexes. *Cell* 2005, 123, 607–620. [CrossRef] [PubMed]

11. Rand, T.A.; Petersen, S.; Du, F.; Wang, X. Argonaute2 cleaves the anti-guide strand of siRNA during RISC activation. *Cell* 2005, 123, 621–629. [CrossRef] [PubMed]
12. Hutvagner, G.; Zamore, P.D. A microRNA in a multiple-turnover RNAi enzyme complex. *Science* 2002, 297, 2056–2060. [CrossRef] [PubMed]
13. Bartlett, D.W.; Davis, M.E. Insights into the kinetics of siRNA-mediated gene silencing from live-cell and live-animal bioluminescent imaging. *Nucl. Acids Res.* 2006, 34, 322–333. [CrossRef] [PubMed]
14. Silva, J.M.; Li, M.Z.; Chang, K.; Ge, W.; Golding, M.C.; Rickles, R.J.; Siolas, D.; Hu, G.; Paddison, P.J.; Schlabach, M.R.; et al. Second-generation shRNA libraries covering the mouse and human genomes. *Nat. Genet.* 2005, 37, 1281. [CrossRef] [PubMed]
15. Rao, D.D.; Vorhies, J.S.; Senzer, N.; Nemunaitis, J. siRNA vs. shRNA: Similarities and differences. *Adv. Drug Deliv. Rev.* 2009, 61, 746–759. [CrossRef] [PubMed]
16. Cullen, B.R. RNAi the natural way. *Nat. Genet.* 2005, 37, 1163. [CrossRef] [PubMed]
17. Karim, E.; Rosli, R.; Chowdhury, E.H. Systemic Delivery of Nanoformulations of Anti-cancer Drugs with Therapeutic Potency in Animal Models of Cancer. *Curr. Cancer Ther. Rev.* 2016, 12, 204–220. [CrossRef]
18. Davis, M.E. Non-viral gene delivery systems. *Curr. Opin. Biotechnol.* 2002, 13, 128–131. [CrossRef]
19. Kim, H.J.; Kim, A.; Miyata, K.; Kataoka, K. Recent progress in development of siRNA delivery vehicles for cancer therapy. *Adv. Drug Deliv. Rev.* 2016, 104, 61–77. [CrossRef] [PubMed]
20. Pahle, J.; Walther, W. Vectors and strategies for nonviral cancer gene therapy. *Expert Opin. Biol. Ther.* 2016, 16, 443–461. [CrossRef] [PubMed]
21. Wirth, T.; Parker, N.; Ylä-Herttuala, S. History of gene therapy. *Gene* 2013, 525, 162–169. [CrossRef] [PubMed]
22. Bertrand, N.; Wu, J.; Xu, X.; Kamaly, N.; Farokhzad, O.C. Cancer nanotechnology: The impact of passive and active targeting in the era of modern cancer biology. *Adv. Drug Deliv. Rev.* 2014, 66, 2–25. [CrossRef] [PubMed]



23. Zhou, Z.; Liu, X.; Zhu, D.; Wang, Y.; Zhang, Z.; Zhou, X.; Qiu, N.; Chen, X.; Shen, Y. Nonviral cancer gene therapy: Delivery cascade and vector nanoproperty integration. *Adv. Drug Deliv. Rev.* 2017, 115, 115–154. [CrossRef] [PubMed]
24. Miller, K.D.; Siegel, R.L.; Lin, C.C.; Mariotto, A.B.; Kramer, J.L.; Rowland, J.H.; Stein, K.D.; Alteri, R.; Jemal, A. Cancer treatment and survivorship statistics, 2016. *CA Cancer J. Clin.* 2016, 66, 271–289. [CrossRef] [PubMed]
25. Fitzmaurice, C.; Allen, C.; Barber, R.M.; Barregard, L.; Bhutta, Z.A.; Brenner, H.; Dicker, D.J.; Chimed-Orchir, O.; Dandona, R.; Dandona, L. Global, regional, and national cancer incidence, mortality, years of life lost, years lived with disability, and disability-adjusted life-years for 32 cancer groups, 1990 to 2015: A systematic analysis for the global burden of disease study. *JAMA Oncol.* 2017, 3, 524–548. [PubMed]
26. Bitko, V.; Musiyenko, A.; Shulyayeva, O.; Barik, S. Inhibition of respiratory viruses by nasally administered siRNA. *Nat. Med.* 2005, 11, 50–55. [CrossRef] [PubMed]
27. DiFiglia, M.; Sena-Esteves, M.; Chase, K.; Sapp, E.; Pfister, E.; Sass, M.; Yoder, J.; Reeves, P.; Pandey, R.K.; Rajeev, K.G. Therapeutic silencing of mutant huntingtin with siRNA attenuates striatal and cortical neuropathology and behavioral deficits. *Proc. Natl. Acad. Sci. USA* 2007, 104, 17204–17209. [CrossRef] [PubMed]
28. Pecot, C.V.; Calin, G.A.; Coleman, R.L.; Lopez-Berestein, G.; Sood, A.K. RNA interference in the clinic: Challenges and future directions. *Nat. Rev. Cancer* 2011, 11, 59–67. [CrossRef] [PubMed]
29. Bumcrot, D.; Manoharan, M.; Koteliensky, V.; Sah, D.W. RNAi therapeutics: A potential new class of pharmaceutical drugs. *Nat. Chem. Biol.* 2006, 2, 711–719. [CrossRef] [PubMed]
30. Alexis, F.; Pridgen, E.; Molnar, L.K.; Farokhzad, O.C. Factors affecting the clearance and biodistribution of polymeric nanoparticles. *Mol. Pharm.* 2008, 5, 505–515. [CrossRef] [PubMed]
31. Scherphof, G. In vivo behavior of liposomes: Interactions with the mononuclear phagocyte system and implications for drug targeting. In *Targeted Drug Delivery*; Springer: Berlin, Germany, 1991; pp. 285–327.
32. Zamecnik, J.; Vargova, L.; Homola, A.; Kodet, R.; Sykova, E. Extracellular matrix glycoproteins and diffusion barriers in human astrocytic tumours. *Neuropathol. Appl. Neurobiol.* 2004, 30, 338–350. [CrossRef] [PubMed]

33. Decuzzi, P.; Causa, F.; Ferrari, M.; Netti, P. The effective dispersion of nanovectors within the tumor microvasculature. *Ann. Biomed. Eng.* 2006, 34, 633–641. [CrossRef] [PubMed]
34. Dominska, M.; Dykxhoorn, D.M. Breaking down the barriers: siRNA delivery and endosome escape. *J. Cell Sci.* 2010, 123, 1183–1189. [CrossRef] [PubMed]
35. Kim, D.H.; Rossi, J.J. Strategies for silencing human disease using RNA interference. *Nat. Rev. Genet.* 2007, 8, 173–184. [CrossRef] [PubMed]
36. Jackson, A.L.; Bartz, S.R.; Schelter, J.; Kobayashi, S.V.; Burchard, J.; Mao, M.; Li, B.; Cavet, G.; Linsley, P.S. Expression profiling reveals off-target gene regulation by RNAi. *Nat. Biotechnol.* 2003, 21, 635–637. [CrossRef] [PubMed] *Pharmaceutics* 2018, 10, 65 28 of 44
37. Jackson, A.L.; Burchard, J.; Schelter, J.; Chau, B.N.; Cleary, M.; Lim, L.; Linsley, P.S. Widespread siRNA “off-target” transcript silencing mediated by seed region sequence complementarity. *RNA* 2006, 12, 1179–1187. [CrossRef] [PubMed]
38. Petros, R.A.; DeSimone, J.M. Strategies in the design of nanoparticles for therapeutic applications. *Nat. Rev. Drug Discov.* 2010, 9, 615–627. [CrossRef] [PubMed]
39. Kanasty, R.L.; Whitehead, K.A.; Vegas, A.J.; Anderson, D.G. Action and reaction: The biological response to siRNA and its delivery vehicles. *Mol. Ther.* 2012, 20, 513–524. [CrossRef] [PubMed]
40. Thomas, C.E.; Ehrhardt, A.; Kay, M.A. Progress and problems with the use of viral vectors for gene therapy. *Nat. Rev. Genet.* 2003, 4, 346–358. [CrossRef] [PubMed]
41. Castanotto, D.; Rossi, J.J. The promises and pitfalls of RNA-interference-based therapeutics. *Nature* 2009, 457, 426–433. [CrossRef] [PubMed]
42. Walter, W.; Stein, U. Viral vectors for gene transfer a review of their use in the treatment of human disease. *Drugs* 2000, 60, 249–271. [CrossRef]
43. Ylä-Herttuala, S. Glybera’s second act: The curtain rises on the high cost of therapy. *Mol. Ther.* 2015, 23, 217–218. [CrossRef] [PubMed]
44. Kay, M.A. State-of-the-art gene-based therapies: The road ahead. *Nat. Rev. Genet.* 2011, 12, 316–328. [CrossRef] [PubMed]

45. Mintzer, M.A.; Simanek, E.E. Nonviral vectors for gene delivery. *Chem. Rev.* 2008, 109, 259–302. [CrossRef] [PubMed]
46. Gilleron, J.; Querbes, W.; Zeigerer, A.; Borodovsky, A.; Marsico, G.; Schubert, U.; Manygoats, K.; Seifert, S.; Andree, C.; Stöter, M. Image-based analysis of lipid nanoparticle-mediated siRNA delivery, intracellular trafficking and endosomal escape. *Nat. Biotechnol.* 2013, 31, 638–646. [CrossRef] [PubMed]
47. Schaffer, D.V.; Fidelman, N.A.; Dan, N.; Lauffenburger, D.A. Vector unpacking as a potential barrier for receptor-mediated polyplex gene delivery. *Biotechnol. Bioeng.* 2000, 67, 598–606. [CrossRef]
48. Lv, H.; Zhang, S.; Wang, B.; Cui, S.; Yan, J. Toxicity of cationic lipids and cationic polymers in gene delivery. *J. Control. Release* 2006, 114, 100–109. [CrossRef] [PubMed]
49. Loh, X.J.; Lee, T.-C.; Dou, Q.; Deen, G.R. Utilising inorganic nanocarriers for gene delivery. *Biomater. Sci.* 2016, 4, 70–86. [CrossRef] [PubMed]
50. Shim, M.S.; Kwon, Y.J. Efficient and targeted delivery of siRNA in vivo. *FEBS J.* 2010, 277, 4814–4827 [CrossRef] [PubMed]
51. Rosenblum, D.; Joshi, N.; Tao, W.; Karp, J.M.; Peer, D. Progress and challenges towards targeted delivery of cancer therapeutics. *Nat. Commun.* 2018, 9, 1410. [CrossRef] [PubMed]
52. Stacker, S.A.; Williams, S.P.; Karnezis, T.; Shayan, R.; Fox, S.B.; Achen, M.G. Lymphangiogenesis and lymphatic vessel remodelling in cancer. *Nat. Rev. Cancer* 2014, 14, 159. [CrossRef] [PubMed]
53. Jain, R.K.; Stylianopoulos, T. Delivering nanomedicine to solid tumors. *Nat. Rev. Clin. Oncol.* 2010, 7, 653. [CrossRef] [PubMed]
54. Danquah, M.K.; Zhang, X.A.; Mahato, R.I. Extravasation of polymeric nanomedicines across tumor vasculature. *Adv. Drug Deliv. Rev.* 2011, 63, 623–639. [CrossRef] [PubMed]
55. Chen, X.; Mangala, L.S.; Rodriguez-Aguayo, C.; Kong, X.; Lopez-Berestein, G.; Sood, A.K. RNA interference-based therapy and its delivery systems. *Cancer Metastasis Rev.* 2018, 37, 107–124. [CrossRef] [PubMed]
56. Layek, B.; Lipp, L.; Singh, J. Cell penetrating peptide conjugated chitosan for enhanced delivery of nucleic acid. *Int. J. Mol. Sci.* 2015, 16, 28912–28930. [CrossRef] [PubMed]

57. Shukla, R.S.; Jain, A.; Zhao, Z.; Cheng, K. Intracellular trafficking and exocytosis of a multi-component siRNA nanocomplex. *Nanomed. Nanotechnol. Biol. Med.* 2016, 12, 1323–1334. [CrossRef] [PubMed]
58. Sahay, G.; Querbes, W.; Alabi, C.; Eltoukhy, A.; Sarkar, S.; Zurenko, C.; Karagiannis, E.; Love, K.; Chen, D.; Zoncu, R. Efficiency of siRNA delivery by lipid nanoparticles is limited by endocytic recycling. *Nat. Biotechnol.* 2013, 31, 653. [CrossRef] [PubMed]
59. Pezzella, F.; Turley, H.; Kuzu, I.; Tungekar, M.F.; Dunnill, M.S.; Pierce, C.B.; Harris, A.; Gatter, K.C.; Mason, D.Y. bcl-2 protein in non-small-cell lung carcinoma. *N. Engl. J. Med.* 1993, 329, 690–694. [CrossRef] [PubMed]
60. Yang, J.; Zhang, Y. Antisense bcl-2 oligodeoxynucleotide enhancing 5-fluorouracil induced apoptosis in human gastric cancer cell line SGC 7901. *Tumor* 2002, 5, 15.
61. Joensuu, H.; Pylkkänen, L.; Toikkanen, S. Bcl-2 protein expression and long-term survival in breast cancer. *Am. J. Pathol.* 1994, 145, 1191. [PubMed] *Pharmaceutics* 2018, 10, 65 29 of 44
62. Sinicrope, F.A.; Hart, J.; Michelassi, F.; Lee, J.J. Prognostic value of bcl-2 oncoprotein expression in stage II colon carcinoma. *Clin. Cancer Res.* 1995, 1, 1103–1110. [PubMed]
63. Li, S.-M.; Yao, S.-K.; Yamamura, N.; Nakamura, T. Expression of Bcl-2 and Bax in extrahepatic biliary tract carcinoma and dysplasia. *World J. Gastroenterol.* 2003, 9, 2579. [CrossRef] [PubMed]
64. Jiang, S.X.; Sato, Y.; Kuwao, S.; Kameya, T. Expression of bcl-2 oncogene protein is prevalent in small cell lung carcinomas. *J. Pathol.* 1995, 177, 135–138. [CrossRef] [PubMed]
65. Fu, G.-F.; Lin, X.-H.; Han, Q.-W.; Xu, Y.-F.; Guo, D.; Xu, G.-X.; Hou, Y.-Y. RNA interference remarkably suppresses bcl-2 gene expression in cancer cells in vitro and in vivo. *Cancer Biol. Ther.* 2005, 4, 822–829. [CrossRef] [PubMed]
66. Koty, P.P.; Zhang, H.; Levitt, M.L. Antisense bcl-2 treatment increases programmed cell death in non-small cell lung cancer cell lines. *Lung Cancer* 1999, 23, 115–127. [CrossRef]
67. Lima, R.T.; Martins, L.M.; Guimaraes, J.E.; Sambade, C.; Vasconcelos, M.H. Specific downregulation of bcl-2 and xIAP by RNAi enhances the effects of chemotherapeutic agents in MCF-7 human breast cancer cells. *Cancer Gene ther.* 2004, 11, 309–316. [CrossRef] [PubMed]

68. Weyhenmeyer, B.; Murphy, A.; Prehn, J.; Murphy, B. Targeting the anti-apoptotic Bcl-2 family members for the treatment of cancer. *Exp. Oncol.* 2012, 34, 192–199. [PubMed]
69. Garcia-Saez, A. The secrets of the Bcl-2 family. *Cell Death Differ.* 2012, 19, 1733–1740. [CrossRef] [PubMed]
70. Sasatomi, E.; Tokunaga, O.; Miyazaki, K. Spontaneous apoptosis in gallbladder carcinoma: Relationships with clinicopathologic factors, expression of E-cadherin, bcl-2 protooncogene, and p53 oncosuppressor gene. *Cancer* 1996, 78, 2101–2110. [CrossRef]
71. Mikami, T.; Yanagisawa, N.; Baba, H.; Koike, M.; Okayasu, I. Association of Bcl-2 protein expression with gallbladder carcinoma differentiation and progression and its relation to apoptosis. *Cancer* 1999, 85, 318–325. [CrossRef]
72. Geng, Z.-M.; Zhang, M.; Pan, X.-T.; Wang, L. Bcl-2 gene silencing by RNA interference inhibits the growth of the human gallbladder carcinoma cell line GBC-SD in vitro and in vivo. *Oncol. Rep.* 2013, 30, 793–800. [CrossRef] [PubMed]
73. Yano, J.; Hirabayashi, K.; Nakagawa, S.-I.; Yamaguchi, T.; Nogawa, M.; Kashimori, I.; Naito, H.; Kitagawa, H.; Ishiyama, K.; Ohgi, T. Antitumor activity of small interfering RNA/cationic liposome complex in mouse models of cancer. *Clin. Cancer Res.* 2004, 10, 7721–7726. [CrossRef] [PubMed]
74. Sonoike, S.; Ueda, T.; Fujiwara, K.; Sato, Y.; Takagaki, K.; Hirabayashi, K.; Ohgi, T.; Yano, J. Tumor regression in mice by delivery of Bcl-2 small interfering RNA with pegylated cationic liposomes. *Cancer Res.* 2008, 68, 8843–8851. [CrossRef] [PubMed]
75. Grunewald, M.; Avraham, I.; Dor, Y.; Bachar-Lustig, E.; Itin, A.; Yung, S.; Chimenti, S.; Landsman, L.; Abramovitch, R.; Keshet, E. VEGF-induced adult neovascularization: Recruitment, retention, and role of accessory cells. *Cell* 2006, 124, 175–189. [CrossRef] [PubMed]
76. Saint-Geniez, M.; D'Amore, P.A. Development and pathology of the hyaloid, choroidal and retinal vasculature. *Int. J. Dev. Biol.* 2004, 48, 1045–1058. [CrossRef] [PubMed]
77. Stefater, J.A., III; Lewkowich, I.; Rao, S.; Mariggi, G.; Carpenter, A.C.; Burr, A.R.; Fan, J.; Ajima, R.; Molkentin, J.D.; Williams, B.O. Regulation of angiogenesis by a non-canonical Wnt-Flt1 pathway in myeloid cells. *Nature* 2011, 474, 511–515. [CrossRef] [PubMed]
78. Folkman, J. Angiogenesis and breast cancer. *J. Clin. Oncol.* 1994, 12, 441–443. [CrossRef] [PubMed]

79. Blood, C.H.; Zetter, B.R. Tumor interactions with the vasculature: Angiogenesis and tumor metastasis. *Biochim. Biophys. Acta Rev. Cancer* 1990, 1032, 89–118. [CrossRef]
80. Ferrara, N.; Gerber, H.-P.; LeCouter, J. The biology of VEGF and its receptors. *Nat. Med.* 2003, 9, 669–676. [CrossRef] [PubMed]
81. Dvorak, H.F.; Detmar, M.; Claffey, K.P.; Nagy, J.A.; van de Water, L.; Senger, D.R. Vascular permeability factor/vascular endothelial growth factor: An important mediator of angiogenesis in malignancy and inflammation. *Int. Arch. Allergy Immunol.* 1995, 107, 233–235. [CrossRef] [PubMed]
82. Ferrara, N.; Kerbel, R.S. Angiogenesis as a therapeutic target. *Nature* 2005, 438, 967–974. [CrossRef] [PubMed]
83. Ferrara, N. VEGF and the quest for tumour angiogenesis factors. *Nat. Rev. Cancer* 2002, 2, 795–803. [CrossRef] [PubMed]
84. Tsai, J.H.; Lee, W.M. Modeling antiangiogenesis gene therapy. *Cancer Biol. Ther.* 2002, 1, 554–555. [CrossRef] [PubMed] *Pharmaceutics* 2018, 10, 65 30 of 44
85. Wu, H.-P.; Feng, G.-S.; Liang, H.-M.; Zheng, C.-S.; Li, X. Vascular endothelial growth factor antisense oligodeoxynucleotides with lipiodol in arterial embolization of liver cancer in rats. *World J. Gastroenterol.* 2004, 10, 813. [CrossRef] [PubMed]
86. Namiecińska, M.; Marciniak, K.; Nowak, J.Z. VEGF jako czynnik angiogeny, neurotroficzny i neuroprotekcyny\* VEGF as an angiogenic, neurotrophic, and neuroprotective factor. *Postep. Hig. Med. Dosw.* 2005, 59, 573–583.
87. Takahashi, Y.; Kitadai, Y.; Bucana, C.D.; Cleary, K.R.; Ellis, L.M. Expression of vascular endothelial growth factor and its receptor, KDR, correlates with vascularity, metastasis, and proliferation of human colon cancer. *Cancer Res.* 1995, 55, 3964–3968. [PubMed]
88. Toi, M.; Inada, K.; Suzuki, H.; Tominaga, T. Tumor angiogenesis in breast cancer: Its importance as a prognostic indicator and the association with vascular endothelial growth factor expression. *Breast Cancer Res. Treat.* 1995, 36, 193–204. [CrossRef] [PubMed]
89. Weidner, N.; Folkman, J.; Pozza, F.; Bevilacqua, P.; Allred, E.N.; Moore, D.H.; Meli, S.; Gasparini, G. Tumor angiogenesis: A new significant and independent prognostic indicator in early-stage breast carcinoma. *JNCI J. Natl. Cancer Inst.* 1992, 84, 1875–1887. [CrossRef] [PubMed]

90. Maeda, K.; Chung, Y.; Takatsuka, S.; Ogawa, Y.; Sawada, T.; Yamashita, Y.; Onoda, N.; Kato, Y.; Nitta, A.; Arimoto, Y. Tumor angiogenesis as a predictor of recurrence in gastric carcinoma. *J. Clin. Oncol.* 1995, 13, 477–481. [CrossRef] [PubMed]
91. Algire, G.H.; Chalkley, H.W.; Legallais, F.Y.; Park, H.D. Vasculae reactions of normal and malignant tissues in vivo. I. vascular reactions of mice to wounds and to normal and neoplastic transplants. *JNCI J. Natl. Cancer Inst.* 1945, 6, 73–85. [CrossRef]
92. Rhee, J.; Hoff, P.M. Angiogenesis inhibitors in the treatment of cancer. *Expert Opin. Pharmacother.* 2005, 6, 1701–1711. [CrossRef] [PubMed]
93. Takei, Y.; Kadomatsu, K.; Matsuo, S.; Itoh, H.; Nakazawa, K.; Kubota, S.; Muramatsu, T. Antisense oligodeoxynucleotide targeted to Midkine, a heparin-binding growth factor, suppresses tumorigenicity of mouse rectal carcinoma cells. *Cancer Res.* 2001, 61, 8486–8491. [PubMed]
94. Lu, P.Y.; Xie, F.Y.; Woodle, M.C. Modulation of angiogenesis with siRNA inhibitors for novel therapeutics. *Trends Mol. Med.* 2005, 11, 104–113. [CrossRef] [PubMed]
95. Zhang, W.; Fang, X.; Branch, C.; Mazur, W.; French, B.; Roth, J. Generation and identification of recombinant adenovirus by liposome-mediated transfection and PCR analysis. *Biotechniques* 1993, 15, 868–872. [PubMed]
96. Jones, N.; Shenk, T. An adenovirus type 5 early gene function regulates expression of other early viral genes. *Proc. Natl. Acad. Sci. USA* 1979, 76, 3665–3669. [CrossRef] [PubMed]
97. Im, S.; Kim, J.; Gomez-Manzano, C.; Fueyo, J.; Liu, T.; Cho, M.; Seong, C.; Lee, S.; Hong, Y.; Yung, W.
- Inhibition of breast cancer growth in vivo by antiangiogenesis gene therapy with adenovirus-mediated antisense-VEGF. *Br. J. Cancer* 2001, 84, 1252. [CrossRef] [PubMed]
98. Kataoka, K.; Togawa, H.; Harada, A.; Yasugi, K.; Matsumoto, T.; Katayose, S. Spontaneous formation of polyion complex micelles with narrow distribution from antisense oligonucleotide and cationic blockcopolymer in physiological saline. *Macromolecules* 1996, 29, 8556–8557. [CrossRef]
99. Vinogradov, S.V.; Bronich, T.K.; Kabanov, A.V. Self-Assembly of Polyamine—Poly (ethylene glycol) Copolymers with Phosphorothioate Oligonucleotides. *Bioconjugate Chem.* 1998, 9, 805–812. [CrossRef] [PubMed]

100. Schiffelers, R.M.; Ansari, A.; Xu, J.; Zhou, Q.; Tang, Q.; Storm, G.; Molema, G.; Lu, P.Y.; Scaria, P.V.; Woodle, M.C. Cancer siRNA therapy by tumor selective delivery with ligand-targeted sterically stabilized nanoparticle. *Nucl. Acids Res.* 2004, 32, e149. [CrossRef] [PubMed]
101. Kim, S.H.; Jeong, J.H.; Cho, K.C.; Kim, S.W.; Park, T.G. Target-specific gene silencing by siRNA plasmid DNA complexed with folate-modified poly (ethylenimine). *J. Control. Release* 2005, 104, 223–232. [CrossRef] [PubMed]
102. Harada, A.; Kataoka, K. Formation of polyion complex micelles in an aqueous milieu from a pair of oppositely-charged block copolymers with poly (ethylene glycol) segments. *Macromolecules* 1995, 28, 5294–5299. [CrossRef]
103. Kim, S.H.; Jeong, J.H.; Lee, S.H.; Kim, S.W.; Park, T.G. Local and systemic delivery of VEGF siRNA using polyelectrolyte complex micelles for effective treatment of cancer. *J. Control. Release* 2008, 129, 107–116. [CrossRef] [PubMed]
104. Joukov, V.; Kaipainen, A.; Jeltsch, M.; Pajusola, K.; Olofsson, B.; Kumar, V.; Eriksson, U.; Alitalo, K. Vascular endothelial growth factors VEGF-B and VEGF-C. *J. Cell. Physiol.* 1997, 173, 211–215. [CrossRef] *Pharmaceutics* 2018, 10, 65 31 of 44
105. Cohen, B.; Addadi, Y.; Sapoznik, S.; Meir, G.; Kalchenko, V.; Harmelin, A.; Ben-Dor, S.; Neeman, M.  
Transcriptional regulation of vascular endothelial growth factor C by oxidative and thermal stress is mediated by lens epithelium-derived growth factor/p75. *Neoplasia* 2009, 11, 921. [CrossRef] [PubMed]
106. Su, J.-L.; Yen, C.; Chen, P.; Chuang, S.; Hong, C.; Kuo, I.; Chen, H.; Hung, M.-C.; Kuo, M. The role of the VEGF-C/VEGFR-3 axis in cancer progression. *Br. J. Cancer* 2007, 96, 541–545. [CrossRef] [PubMed]
107. Hirakawa, S.; Brown, L.F.; Kodama, S.; Paavonen, K.; Alitalo, K.; Detmar, M. VEGF-C-induced lymphangiogenesis in sentinel lymph nodes promotes tumor metastasis to distant sites. *Blood* 2007, 109, 1010–1017. [CrossRef] [PubMed]
108. Jennbacken, K.; Vallbo, C.; Wang, W.; Damber, J.E. Expression of vascular endothelial growth factor C (VEGF-C) and VEGF receptor-3 in human prostate cancer is associated with regional lymph node metastasis. *Prostate* 2005, 65, 110–116. [CrossRef] [PubMed]



109. Jenny, B.; Harrison, J.; Baetens, D.; Tille, J.C.; Burkhardt, K.; Mottaz, H.; Kiss, J.Z.; Dietrich, P.Y.; De Tribolet, N.; Pizzolato, G. Expression and localization of VEGF-C and VEGFR-3 in glioblastomas and haemangioblastomas. *J. Pathol.* 2006, 209, 34–43. [CrossRef] [PubMed]
110. Huynh, H. AZD6244 (ARRY-142886) enhances the antitumor activity of rapamycin in mouse models of human hepatocellular carcinoma. *Cancer* 2010, 116, 1315–1325. [CrossRef] [PubMed]
111. Morelli, M.P.; Brown, A.M.; Pitts, T.M.; Tentler, J.J.; Ciardiello, F.; Ryan, A.; Jürgensmeier, J.M.; Eckhardt, S.G. Targeting vascular endothelial growth factor receptor-1 and-3 with cediranib (AZD2171): Effects on migration and invasion of gastrointestinal cancer cell lines. *Mol. Cancer Ther.* 2009, 8, 2546–2558. [CrossRef] [PubMed]
112. Svensson, S.; Jirström, K.; Rydén, L.; Roos, G.; Emdin, S.; Ostrowski, M.C.; Landberg, G. ERK phosphorylation is linked to VEGFR2 expression and Ets-2 phosphorylation in breast cancer and is associated with tamoxifen treatment resistance and small tumours with good prognosis. *Oncogene* 2005, 24, 4370–4379. [CrossRef] [PubMed]
113. Brand, S.; Dambacher, J.; Beigel, F.; Olszak, T.; Diebold, J.; Otte, J.-M.; Göke, B.; Eichhorst, S.T. CXCR4 and CXCL12 are inversely expressed in colorectal cancer cells and modulate cancer cell migration, invasion and MMP-9 activation. *Exp. Cell Res.* 2005, 310, 117–130. [CrossRef] [PubMed]
114. Peng, S.-B.; Peek, V.; Zhai, Y.; Paul, D.C.; Lou, Q.; Xia, X.; Eessalu, T.; Kohn, W.; Tang, S. Akt Activation, but not Extracellular Signal-Regulated Kinase Activation, Is Required for SDF-1 $\alpha$ /CXCR4-Mediated Migration of Epitheloid Carcinoma Cells. *Mol. Cancer Res.* 2005, 3, 227–236. [PubMed]
115. Fournier, E.; Birnbaum, D.; Borg, J.-P. Receptors for factors of the VEGF (vascular endothelial growth family). *Bull. Cancer* 1997, 84, 397–405. [PubMed]
116. Deckers, M.M.; Karperien, M.; van der Bent, C.; Yamashita, T.; Papapoulos, S.E.; Löwik, C.W. Expression of vascular endothelial growth factors and their receptors during osteoblast differentiation. *Endocrinology* 2000, 141, 1667–1674. [CrossRef] [PubMed]
117. Ge, Y.-L.; Zhang, X.; Zhang, J.-Y.; Hou, L.; Tian, R.-H. The mechanisms on apoptosis by inhibiting VEGF expression in human breast cancer cells. *Int. Immunopharmacol.* 2009, 9, 389–395. [CrossRef] [PubMed]
118. Kodama, M.; Kitadai, Y.; Tanaka, M.; Kuwai, T.; Tanaka, S.; Oue, N.; Yasui, W.; Chayama, K. Vascular endothelial growth factor C stimulates progression of human

gastric cancer via both autocrine and paracrine mechanisms. *Clin. Cancer Res.* 2008, 14, 7205–7214. [CrossRef] [PubMed]

119. Jüttner, S.; Wißmann, C.; Jöns, T.; Vieth, M.; Hertel, J.; Gretschel, S.; Schlag, P.M.; Kemmner, W.; Höcker, M. Vascular endothelial growth factor-D and its receptor VEGFR-3: Two novel independent prognostic markers in gastric adenocarcinoma. *J. Clin. Oncol.* 2006, 24, 228–240. [CrossRef] [PubMed]

120. Liu, Y.C.; Ma, W.H.; Ge, Y.L.; Xue, M.L.; Zhang, Z.; Zhang, J.Y.; Hou, L.; Mu, R.H. RNAi-mediated gene silencing of vascular endothelial growth factor C suppresses growth and induces apoptosis in mouse breast cancer in vitro and in vivo. *Oncol. Lett.* 2016, 12, 3896–3904. [CrossRef] [PubMed]

121. Feng, Y.; Hu, J.; Ma, J.; Feng, K.; Zhang, X.; Yang, S.; Wang, W.; Zhang, J.; Zhang, Y. RNAi-mediated silencing of VEGF-C inhibits non-small cell lung cancer progression by simultaneously down-regulating the CXCR4, CCR7, VEGFR-2 and VEGFR-3-dependent axes-induced ERK, p38 and AKT signalling pathways. *Eur. J. Cancer* 2011, 47, 2353–2363. [CrossRef] [PubMed]

122. Ellis, L.M. The role of neuropilins in cancer. *Mol. Cancer Ther.* 2006, 5, 1099–1107. [CrossRef] [PubMed]

123. Bielenberg, D.R.; Pettaway, C.A.; Takashima, S.; Klagsbrun, M. Neuropilins in neoplasms: Expression, regulation, and function. *Exp. Cell Res.* 2006, 312, 584–593. [CrossRef] [PubMed] *Pharmaceutics* 2018, 10, 65 32 of 44

124. Kärpänen, T.; Heckman, C.A.; Keskitalo, S.; Jeltsch, M.; Ollila, H.; Neufeld, G.; Tamagnone, L.; Alitalo, K. Functional interaction of VEGF-C and VEGF-D with neuropilin receptors. *FASEB J.* 2006, 20, 1462–1472. [CrossRef] [PubMed]

125. Gray, M.J.; Van Buren, G.; Dallas, N.A.; Xia, L.; Wang, X.; Yang, A.D.; Somcio, R.J.; Lin, Y.G.; Lim, S.; Fan, F. Therapeutic targeting of neuropilin-2 on colorectal carcinoma cells implanted in the murine liver. *J. Natl. Cancer Inst.* 2008, 100, 109–120. [CrossRef] [PubMed]

126. Ferrara, N.; Hillan, K.J.; Gerber, H.-P.; Novotny, W. Discovery and development of bevacizumab, an anti-VEGF antibody for treating cancer. *Nat. Rev. Drug Discov.* 2004, 3, 391–400. [CrossRef] [PubMed]

127. Elbashir, S.M.; Harborth, J.; Weber, K.; Tuschl, T. Analysis of gene function in somatic mammalian cells using small interfering RNAs. *Methods* 2002, 26, 199–213. [CrossRef]

128. Paddison, P.; Hannon, G. siRNAs and shRNAs: Skeleton keys to the human genome. *Curr. Opin. Mol. Ther.* 2003, 5, 217–224. [PubMed]
129. Carpenter, A.E.; Sabatini, D.M. Systematic genome-wide screens of gene function. *Nat. Rev. Genet.* 2004, 5, 11–22. [CrossRef] [PubMed]
130. Ganju, P.; Hall, J. Potential applications of siRNA for pain therapy. *Expert Opin. Biol. Ther.* 2004, 4, 531–542. [CrossRef] [PubMed]
131. Woodle, M.; Scaria, P.; Ganesh, S.; Subramanian, K.; Titmas, R.; Cheng, C.; Yang, J.; Pan, Y.; Weng, K.; Gu, C. Sterically stabilized polyplex: Ligand-mediated activity. *J. Control. Release* 2001, 74, 309–311. [CrossRef]
132. Langer, R. Drugs on target. *Science* 2001, 293, 58–59. [CrossRef] [PubMed]
133. Suh, W.; Han, S.-O.; Yu, L.; Kim, S.W. An angiogenic, endothelial-cell-targeted polymeric gene carrier. *Mol. Ther.* 2002, 6, 664–672. [CrossRef]
134. Verbaan, F.; Oussoren, C.; Snel, C.; Crommelin, D.; Hennink, W.; Storm, G. Steric stabilization of poly (2-(dimethylamino) ethyl methacrylate)-based polyplexes mediates prolonged circulation and tumor targeting in mice. *J. Gene Med.* 2004, 6, 64–75. [CrossRef] [PubMed]
135. Ogris, M.; Walker, G.; Blessing, T.; Kircheis, R.; Wolschek, M.; Wagner, E. Tumor-targeted gene therapy: Strategies for the preparation of ligand–polyethylene glycol–polyethylenimine/DNA complexes. *J. Control. Release* 2003, 91, 173–181. [CrossRef]
136. Wagner, E.; Kircheis, R.; Walker, G.F. Targeted nucleic acid delivery into tumors: New avenues for cancer therapy. *Biomed. Pharmacother.* 2004, 58, 152–161. [CrossRef] [PubMed]
137. Hart, S.L.; Knight, A.M.; Harbottle, R.P.; Mistry, A.; Hunger, H.; Cutler, D.F.; Williamson, R.; Coutelle, C. Cell binding and internalization by filamentous phage displaying a cyclic Arg-Gly-Asp-containing peptide. *J. Biol. Chem.* 1994, 269, 12468–12474. [PubMed]
138. Janssen, M.L.; Oyen, W.J.; Dijkgraaf, I.; Massuger, L.F.; Frielink, C.; Edwards, D.S.; Rajopadhye, M.; Boonstra, H.; Corstens, F.H.; Boerman, O.C. Tumor targeting with radiolabeled  $\alpha\text{v}\beta 3$  integrin binding peptides in a nude mouse model. *Cancer Res.* 2002, 62, 6146–6151. [PubMed]

139. Zitzmann, S.; Ehemann, V.; Schwab, M. Arginine-glycine-aspartic acid (RGD)-peptide binds to both tumor and tumor-endothelial cells in vivo. *Cancer Res.* 2002, 62, 5139–5143. [PubMed]
140. Voldborg, B.R.; Damstrup, L.; Spang-Thomsen, M.; Poulsen, H.S. Epidermal growth factor receptor (EGFR) and EGFR mutations, function and possible role in clinical trials. *Ann. Oncol.* 1997, 8, 1197–1206. [CrossRef] [PubMed]
141. Slamon, D.J.; Clark, G.M.; Wong, S.G.; Levin, W.J.; Ullrich, A.; McGuire, W.L. Human breast cancer: Correlation of relapse and survival with amplification of the HER-2/neu oncogene. *Science* 1987, 235, 177–182. [CrossRef] [PubMed]
142. Chowdhury, E. pH-sensitive nano-crystals of carbonate apatite for smart and cell-specific transgene delivery. *Expert Opin. Drug Deliv.* 2007, 4, 193–196. [CrossRef] [PubMed]
143. Tiash, S.; Kamaruzman, N.I.B.; Chowdhury, E.H. Carbonate apatite nanoparticles carry siRNA (s) targeting growth factor receptor genes EGFR1 and ErbB2 to regress mouse breast tumor. *Drug Deliv.* 2017, 24, 1721–1730. [CrossRef] [PubMed]
144. Xu, Y.; Fang, F.; Ludewig, G.; Iones, G.; Jones, D. A mutation found in the promoter region of the human survivin gene is correlated to overexpression of survivin in cancer cells. *DNA Cell Biol.* 2004, 23, 527–537. [CrossRef] [PubMed]
145. Wheatley, S.P.; McNeish, I.A. Survivin: A protein with dual roles in mitosis and apoptosis. *Int. Rev. Cytol.* 2005, 247, 35–88. [CrossRef] *Pharmaceutics* 2018, 10, 65 33 of 44
146. Altieri, D.C. Survivin, cancer networks and pathway-directed drug discovery. *Nat. Rev. Cancer* 2008, 8, 61–70. [CrossRef] [PubMed]
147. Hunter, A.M.; LaCasse, E.C.; Korneluk, R.G. The inhibitors of apoptosis (IAPs) as cancer targets. *Apoptosis* 2007, 12, 1543–1568. [CrossRef] [PubMed]
148. Schimmer, A.D. Inhibitor of apoptosis proteins: Translating basic knowledge into clinical practice. *Cancer Res.* 2004, 64, 7183–7190. [CrossRef] [PubMed]
149. Altieri, D.C. Targeted therapy by disabling crossroad signaling networks: The survivin paradigm. *Mol. Cancer Ther.* 2006, 5, 478–482. [CrossRef] [PubMed]
150. Fukuda, S.; Pelus, L.M. Survivin, a cancer target with an emerging role in normal adult tissues. *Mol. Cancer Ther.* 2006, 5, 1087–1098. [CrossRef] [PubMed]

151. Thomas, J.; Liu, T.; Cotter, M.A.; Florell, S.R.; Robinette, K.; Hanks, A.N.; Grossman, D. Melanocyte expression of survivin promotes development and metastasis of UV-induced melanoma in HGF-transgenic mice. *Cancer Res.* 2007, 67, 5172–5178. [CrossRef] [PubMed]
152. Mehrotra, S.; Languino, L.R.; Raskett, C.M.; Mercurio, A.M.; Dohi, T.; Altieri, D.C. IAP regulation of metastasis. *Cancer Cell* 2010, 17, 53–64. [CrossRef] [PubMed]
153. McKenzie, J.A.; Liu, T.; Goodson, A.; Grossman, D. Survivin enhances motility of melanoma cells by supporting Akt activation and  $\alpha 5$  integrin upregulation. *Cancer Res.* 2010, 194. [CrossRef]
154. Kawasaki, H.; Altieri, D.C.; Lu, C.-D.; Toyoda, M.; Tenjo, T.; Tanigawa, N. Inhibition of apoptosis by survivin predicts shorter survival rates in colorectal cancer. *Cancer Res.* 1998, 58, 5071–5074. [PubMed]
155. Tanaka, K.; Iwamoto, S.; Gon, G.; Nohara, T.; Iwamoto, M.; Tanigawa, N. Expression of survivin and its relationship to loss of apoptosis in breast carcinomas. *Clin. Cancer Res.* 2000, 6, 127–134. [PubMed]
156. Zaffaroni, N.; Pennati, M.; Colella, G.; Perego, P.; Supino, R.; Gatti, L.; Pilotti, S.; Zunino, F.; Daidone, M. Expression of the anti-apoptotic gene survivin correlates with taxol resistance in human ovarian cancer. *Cell. Mol. Life Sci.* 2002, 59, 1406–1412. [CrossRef] [PubMed]
157. Tran, J.; Master, Z.; Joanne, L.Y.; Rak, J.; Dumont, D.J.; Kerbel, R.S. A role for survivin in chemoresistance of endothelial cells mediated by VEGF. *Proc. Natl. Acad. Sci. USA* 2002, 99, 4349–4354. [CrossRef] [PubMed]
158. Cong, X.L.; Han, Z.C. Survivin and leukemia. *Int. J. Hematol.* 2004, 80, 232–238. [CrossRef] [PubMed]
159. Mao, S.; Sun, W.; Kissel, T. Chitosan-based formulations for delivery of DNA and siRNA. *Adv. Drug Deliv. Rev.* 2010, 62, 12–27. [CrossRef] [PubMed]
160. Park, S.; Jeong, E.J.; Lee, J.; Rhim, T.; Lee, S.K.; Lee, K.Y. Preparation and characterization of nonaarginine-modified chitosan nanoparticles for siRNA delivery. *Carbohydr. Polym.* 2013, 92, 57–62. [CrossRef] [PubMed]
161. Sharma, K.; Somavarapu, S.; Colombani, A.; Govind, N.; Taylor, K.M. Nebulised siRNA encapsulated crosslinked chitosan nanoparticles for pulmonary delivery. *Int. J. Pharm.* 2013, 455, 241–247. [CrossRef] [PubMed]

162. Lee, D.W.; Yun, K.-S.; Ban, H.-S.; Choe, W.; Lee, S.K.; Lee, K.Y. Preparation and characterization of chitosan/polyguluronate nanoparticles for siRNA delivery. *J. Control. Release* 2009, 139, 146–152. [CrossRef] [PubMed]
163. Gu, toaia, A.; Schuster, L.; Margutti, S.; Laufer, S.; Schlosshauer, B.; Krastev, R.; Stoll, D.; Hartmann, H. Fine-tuned PEGylation of chitosan to maintain optimal siRNA-nanoplex bioactivity. *Carbohydr. Polym.* 2016, 143, 25–34. [CrossRef] [PubMed]
164. Zheng, J.N.; Xie, H.G.; Yu, W.T.; Liu, X.D.; Xie, W.Y.; Zhu, J.; Ma, X.J. Chitosan-g-MPEG-modified alginate/chitosan hydrogel microcapsules: A quantitative study of the effect of polymer architecture on the resistance to protein adsorption. *Langmuir* 2010, 26, 17156–17164. [CrossRef] [PubMed]
165. Sun, P.; Huang, W.; Jin, M.; Wang, Q.; Fan, B.; Kang, L.; Gao, Z. Chitosan-based nanoparticles for survivin targeted siRNA delivery in breast tumor therapy and preventing its metastasis. *Int. J. Nanomed.* 2016, 11, 4931. [CrossRef] [PubMed]
166. Thomas, A.; Lins, L.; Divita, G.; Brasseur, R. Realistic modeling approaches of structure–function properties of CPPs in non-covalent complexes. *Biochim. Biophys. Acta Biomembr.* 2010, 1798, 2217–2222. [CrossRef] [PubMed]
167. Veiman, K.-L.; Künnapuu, K.; Lehto, T.; Kiisholts, K.; Pärn, K.; Langel, Ü.; Kurrikoff, K. PEG shielded MMP sensitive CPPs for efficient and tumor specific gene delivery in vivo. *J. Control. Release* 2015, 209, 238–247. [CrossRef] [PubMed] *Pharmaceutics* 2018, 10, 65 34 of 44
168. Bass, J. CPP magnetoresistance of magnetic multilayers: A critical review. *J. Magn. Magn. Mater.* 2016, 408, 244–320. [CrossRef]
169. Ronca, F.; Raggi, A. Structure-function relationships in mammalian histidine-proline-rich glycoprotein. *Biochimie* 2015, 118, 207–220. [CrossRef] [PubMed]
170. Chou, S.-T.; Hom, K.; Zhang, D.; Leng, Q.; Tricoli, L.J.; Hustedt, J.M.; Lee, A.; Shapiro, M.J.; Seog, J.; Kahn, J.D. Enhanced silencing and stabilization of siRNA polyplexes by histidine-mediated hydrogen bonds. *Biomaterials* 2014, 35, 846–855. [CrossRef] [PubMed]
171. Wen, Y.; Guo, Z.; Du, Z.; Fang, R.; Wu, H.; Zeng, X.; Wang, C.; Feng, M.; Pan, S. Serum tolerance and endosomal escape capacity of histidine-modified pDNA-loaded complexes based on polyamidoamine dendrimer derivatives. *Biomaterials* 2012, 33, 8111–8121. [CrossRef] [PubMed]

172. Liu, B.R.; Huang, Y.-W.; Winiarz, J.G.; Chiang, H.-J.; Lee, H.-J. Intracellular delivery of quantum dots mediated by a histidine-and arginine-rich HR9 cell-penetrating peptide through the direct membrane translocation mechanism. *Biomaterials* 2011, 32, 3520–3537. [CrossRef] [PubMed]
173. Moreira, C.; Oliveira, H.; Pires, L.R.; Simões, S.; Barbosa, M.A.; Pêgo, A.P. Improving chitosan-mediated gene transfer by the introduction of intracellular buffering moieties into the chitosan backbone. *Acta Biomater.* 2009, 5, 2995–3006. [CrossRef] [PubMed]
174. Corbet, C.; Ragelle, H.; Pourcelle, V.; Vanvarenberg, K.; Marchand-Brynaert, J.; Préat, V.; Feron, O. Delivery of siRNA targeting tumor metabolism using non-covalent PEGylated chitosan nanoparticles: Identification of an optimal combination of ligand structure, linker and grafting method. *J. Control. Release* 2016, 223, 53–63. [CrossRef] [PubMed]
175. Yang, F.; Huang, W.; Li, Y.; Liu, S.; Jin, M.; Wang, Y.; Jia, L.; Gao, Z. Anti-tumor effects in mice induced by survivin-targeted siRNA delivered through polysaccharide nanoparticles. *Biomaterials* 2013, 34, 5689–5699. [CrossRef] [PubMed]
176. Sun, P.; Huang, W.; Kang, L.; Jin, M.; Fan, B.; Jin, H.; Wang, Q.-M.; Gao, Z. siRNA-loaded poly (histidine-arginine) 6-modified chitosan nanoparticle with enhanced cell-penetrating and endosomal escape capacities for suppressing breast tumor metastasis. *Int. J. Nanomed.* 2017, 12, 3221. [CrossRef] [PubMed]
177. Nguyen, D.X.; Bos, P.D.; Massagué, J. Metastasis: From dissemination to organ-specific colonization. *Nat. Rev. Cancer* 2009, 9, 274–284. [CrossRef] [PubMed]
178. Zheng, Y.; Fernando, H.C. Surgical and nonresectional therapies for pulmonary metastasis. *Surg. Clin. N. Am.* 2010, 90, 1041–1051. [CrossRef] [PubMed]
179. Soengas, M.S.; Lowe, S.W. Apoptosis and melanoma chemoresistance. *Oncogene* 2003, 22, 3138–3151. [CrossRef] [PubMed]
180. Bolcato-Bellemin, A.-L.; Bonnet, M.-E.; Creusat, G.; Erbacher, P.; Behr, J.-P. Sticky overhangs enhance siRNA-mediated gene silencing. *Proc. Natl. Acad. Sci. USA* 2007, 104, 16050–16055. [CrossRef] [PubMed]
181. Keding, V.; Meulle, A.; Zounib, O.; Bonnet, M.-E.; Gossart, J.-B.; Benoit, E.; Messmer, M.; Shankaranarayanan, P.; Behr, J.-P.; Erbacher, P. Sticky siRNAs targeting survivin and cyclin B1 exert an antitumoral effect on melanoma subcutaneous xenografts and lung metastases. *BMC Cancer* 2013, 13, 338. [CrossRef] [PubMed]

182. Parker, B.; Sukumar, S. Distant metastasis in breast cancer: Molecular mechanisms and therapeutic targets. *Cancer Biol. Ther.* 2003, 2, 13–22. [CrossRef]
183. Matsumoto, A.; Cabral, H.; Sato, N.; Kataoka, K.; Miyahara, Y. Assessment of Tumor Metastasis by the Direct Determination of Cell-Membrane Sialic Acid Expression. *Angew. Chem. Int. Ed.* 2010, 49, 5494–5497. [CrossRef] [PubMed]
184. Büll, C.; Boltje, T.J.; van Dinther, E.A.; Peters, T.; de Graaf, A.M.; Leusen, J.H.; Kreutz, M.; Figdor, C.G.; den Brok, M.H.; Adema, G.J. Targeted delivery of a sialic acid-blocking glycomimetic to cancer cells inhibits metastatic spread. *ACS Nano* 2015, 9, 733–745. [CrossRef] [PubMed]
185. Fan, B.; Kang, L.; Chen, L.; Sun, P.; Jin, M.; Wang, Q.; Bae, Y.H.; Huang, W.; Gao, Z. Systemic siRNA delivery with a dual pH-responsive and tumor-targeted nanovector for inhibiting tumor growth and spontaneous metastasis in orthotopic murine model of breast carcinoma. *Theranostics* 2017, 7, 357. [CrossRef] [PubMed]
186. Morgan, D.O. Cyclin-dependent kinases: Engines, clocks, and microprocessors. *Ann. Rev. Cell Dev. Biol.* 1997, 13, 261–291. [CrossRef] [PubMed]
187. Krek, W.; Nigg, E. Differential phosphorylation of vertebrate p34cdc2 kinase at the G1/S and G2/M transitions of the cell cycle: Identification of major phosphorylation sites. *EMBO J.* 1991, 10, 305. [PubMed] *Pharmaceutics* 2018, 10, 65 35 of 44
188. Castedo, M.; Perfettini, J.; Roumier, T.; Kroemer, G. Cyclin-dependent kinase-1: Linking apoptosis to cell cycle and mitotic catastrophe. *Cell Death Differ.* 2002, 9, 1287. [CrossRef] [PubMed]
189. Jin, P.; Hardy, S.; Morgan, D.O. Nuclear localization of cyclin B1 controls mitotic entry after DNA damage. *J. Cell Biol.* 1998, 141, 875–885. [CrossRef] [PubMed]
190. Park, M.; Chae, H.-D.; Yun, J.; Jung, M.; Kim, Y.-S.; Kim, S.-H.; Han, M.H.; Shin, D.Y. Constitutive activation of cyclin B1-associated cdc2 kinase overrides p53-mediated G2-M arrest. *Cancer Res.* 2000, 60, 542–545. [PubMed]
191. Yin, X.-Y.; Grove, L.; Datta, N.S.; Katula, K.; Long, M.W.; Prochownik, E.V. Inverse regulation of cyclin B1 by c-Myc and p53 and induction of tetraploidy by cyclin B1 overexpression. *Cancer Res.* 2001, 61, 6487–6493. [PubMed]
192. Santana, C.; Ortega, E.; García-Carrancá, A. Oncogenic H-ras induces cyclin B1 expression in a p53-independent manner. *Mutat. Res. Fundam. Mol. Mech. Mutagen.* 2002, 508, 49–58. [CrossRef]



193. Sarafan-Vasseur, N.; Lamy, A.; Bourguignon, J.; Le Pessot, F.; Hieter, P.; Sesboue, R.; Bastard, C.; Frebourg, T.; Flaman, J.-M. Overexpression of B-type cyclins alters chromosomal segregation. *Oncogene* 2002, 21, 2051–2057. [CrossRef] [PubMed]
194. Dong, Y.; Sui, L.; Watanabe, Y.; Sugimoto, K.; Tokuda, M. Clinical relevance of cyclin B1 overexpression in laryngeal squamous cell carcinoma. *Cancer Lett.* 2002, 177, 13–19. [CrossRef]
195. Hassan, K.A.; Ang, K.K.; El-Naggar, A.K.; Story, M.D.; Lee, J.I.; Liu, D.; Hong, W.K.; Mao, L. Cyclin B1 overexpression and resistance to radiotherapy in head and neck squamous cell carcinoma. *Cancer Res.* 2002, 62, 6414–6417. [PubMed]
196. Takeno, S.; Noguchi, T.; Kikuchi, R.; Uchida, Y.; Yokoyama, S.; Müller, W. Prognostic value of cyclin B1 in patients with esophageal squamous cell carcinoma. *Cancer* 2002, 94, 2874–2881. [CrossRef] [PubMed]
197. Goga, A.; Yang, D.; Tward, A.D.; Morgan, D.O.; Bishop, J.M. Inhibition of CDK1 as a potential therapy for tumors over-expressing MYC. *Nat. Med.* 2007, 13, 820–827. [CrossRef] [PubMed]
198. Morris, M.C.; Gros, E.; Aldrian-Herrada, G.; Choob, M.; Archdeacon, J.; Heitz, F.; Divita, G. A non-covalent peptide-based carrier for in vivo delivery of DNA mimics. *Nucl. Acids Res.* 2007, 35, e49. [CrossRef] [PubMed]
199. Simeoni, F.; Morris, M.C.; Heitz, F.; Divita, G. Insight into the mechanism of the peptide-based gene delivery system MPG: Implications for delivery of siRNA into mammalian cells. *Nucl. Acids Res.* 2003, 31, 2717–2724. [CrossRef] [PubMed]
200. Morris, K.V.; Chan, S.W.-L.; Jacobsen, S.E.; Looney, D.J. Small interfering RNA-induced transcriptional gene silencing in human cells. *Science* 2004, 305, 1289–1292. [CrossRef] [PubMed]
201. Zeineddine, D.; Papadimou, E.; Chebli, K.; Gineste, M.; Liu, J.; Grey, C.; Thurig, S.; Behfar, A.; Wallace, V.A.; Skerjanc, I.S. Oct-3/4 dose dependently regulates specification of embryonic stem cells toward a cardiac lineage and early heart development. *Dev. Cell* 2006, 11, 535–546. [CrossRef] [PubMed]
202. Morris, M.C.; Depollier, J.; Mery, J.; Heitz, F.; Divita, G. A peptide carrier for the delivery of biologically active proteins into mammalian cells. *Nat. Biotechnol.* 2001, 19, 1173–1176. [CrossRef] [PubMed]

203. Crombez, L.; Morris, M.C.; Deshayes, S.; Heitz, F.; Divita, G. Peptide-based nanoparticle for ex vivo and in vivo drug delivery. *Curr. Pharm. Des.* 2008, 14, 3656–3665. [CrossRef] [PubMed]
204. Zorko, M.; Langel, Ü. Cell-penetrating peptides: Mechanism and kinetics of cargo delivery. *Adv. Drug Deliv. Rev.* 2005, 57, 529–545. [CrossRef] [PubMed]
205. Deshayes, S.; Morris, M.; Divita, G.; Heitz, F. Cell-penetrating peptides: Tools for intracellular delivery of therapeutics. *Cell. Mol. Life Sci.* 2005, 62, 1839–1849. [CrossRef] [PubMed]
206. Crombez, L.; Morris, M.C.; Dufort, S.; Aldrian-Herrada, G.; Nguyen, Q.; McMaster, G.; Coll, J.-L.; Heitz, F.; Divita, G. Targeting cyclin B1 through peptide-based delivery of siRNA prevents tumour growth. *Nucl. Acids Res.* 2009, 37, 4559–4569. [CrossRef] [PubMed]
207. Aznar, S.; Lacal, J.C. Rho signals to cell growth and apoptosis. *Cancer Lett.* 2001, 165, 1–10. [CrossRef]
208. Schmitz, A.A.; Govek, E.-E.; Böttner, B.; Van Aelst, L. Rho GTPases: Signaling, migration, and invasion. *Exp. Cell Res.* 2000, 261, 1–12. [CrossRef] [PubMed]
209. Fritz, G.; Just, I.; Kaina, B. Rho GTPases are over-expressed in human tumors. *Int. J. Cancer* 1999, 81, 682–687. [CrossRef]
210. Ridley, A.J. Rho GTPases and cell migration. *J. Cell Sci.* 2001, 114, 2713–2722. [PubMed]
211. Heasman, S.J.; Ridley, A.J. Mammalian Rho GTPases: New insights into their functions from in vivo studies. *Nat. Rev. Mol. Cell Biol.* 2008, 9, 690–701. [CrossRef] [PubMed] *Pharmaceutics* 2018, 10, 65 36 of 44
212. Lin, M.; DiVito, M.M.; Merajver, S.D.; Boyanapalli, M.; Van Golen, K.L. Regulation of pancreatic cancer cell migration and invasion by RhoC GTPase and caveolin-1. *Mol. Cancer* 2005, 4, 21. [CrossRef] [PubMed]
213. Whitehead, I.P.; Zohn, I.E.; Der, C.J. Rho GTPase-dependent transformation by G protein-coupled receptors. *Oncogene* 2001, 20, 1547. [CrossRef] [PubMed]
214. Gur, S.; Kadowitz, P.J.; Hellstrom, W.J. RhoA/Rho-kinase as a therapeutic target for the male urogenital tract. *J. Sex. Med.* 2011, 8, 675–687. [CrossRef] [PubMed]

215. Rathinam, R.; Berrier, A.; Alahari, S.K. Role of Rho GTPases and their regulators in cancer progression. *Front. Biosci.* 2011, 16, 2561–2571. [CrossRef]
216. Kwiatkowska, A.; Symons, M. Signaling determinants of glioma cell invasion. In *Glioma Signaling*; Springer: Berlin, Germany, 2013; pp. 121–141.
217. Oh, H.K.; Sin, J.-I.; Choi, J.; Park, S.H.; Lee, T.S.; Choi, Y.S. Overexpression of CD73 in epithelial ovarian carcinoma is associated with better prognosis, lower stage, better differentiation and lower regulatory T cell infiltration. *J. Gynecol. Oncol.* 2012, 23, 274–281. [CrossRef] [PubMed]
218. Denoyelle, C.; Albanese, P.; Uzan, G.; Hong, L.; Vannier, J.-P.; Soria, J.; Soria, C. Molecular mechanism of the anti-cancer activity of cerivastatin, an inhibitor of HMG-CoA reductase, on aggressive human breast cancer cells. *Cell. Signal.* 2003, 15, 327–338. [CrossRef]
219. Van Golen, K.L.; Wu, Z.-F.; Qiao, X.T.; Bao, L.W.; Merajver, S.D. RhoC GTPase, a novel transforming oncogene for human mammary epithelial cells that partially recapitulates the inflammatory breast cancer phenotype. *Cancer Res.* 2000, 60, 5832–5838. [PubMed]
220. Ma, L.; Teruya-Feldstein, J.; Weinberg, R.A. Tumour invasion and metastasis initiated by microRNA-10b in breast cancer. *Nature* 2007, 449, 682–688. [CrossRef] [PubMed]
221. Jemal, A.; Siegel, R.; Ward, E.; Murray, T.; Xu, J.; Thun, M.J. Cancer statistics, 2007. *CA Cancer J. Clin.* 2007, 57, 43–66. [CrossRef] [PubMed]
222. Jemal, A.; Siegel, R.; Ward, E.; Hao, Y.; Xu, J.; Murray, T.; Thun, M.J. Cancer statistics, 2008. *CA Cancer J. Clin.* 2008, 58, 71–96. [CrossRef] [PubMed]
223. Parkin, D.M.; Bray, F.; Ferlay, J.; Pisani, P. Global cancer statistics, 2002. *CA Cancer J. Clin.* 2005, 55, 74–108. [CrossRef] [PubMed]
224. Wilke, H.-J.; Van Cutsem, E. Current treatments and future perspectives in colorectal and gastric cancer. *Ann. Oncol.* 2003, 14, ii49–ii55. [CrossRef] [PubMed]
225. Wang, H.; Zhao, G.; Liu, X.; Sui, A.; Yang, K.; Yao, R.; Wang, Z.; Shi, Q. Silencing of RhoA and RhoC expression by RNA interference suppresses human colorectal carcinoma growth in vivo. *J. Exp. Clin. Cancer Res.* 2010, 29, 123. [CrossRef] [PubMed]

226. Bertrand, J.-R.; Pottier, M.; Vekris, A.; Opolon, P.; Maksimenko, A.; Malvy, C. Comparison of antisense oligonucleotides and siRNAs in cell culture and in vivo. *Biochem. Biophys. Res. Commun.* 2002, 296, 1000–1004. [CrossRef]
227. Pillé, J.-Y.; Denoyelle, C.; Varet, J.; Bertrand, J.-R.; Soria, J.; Opolon, P.; Lu, H.; Pritchard, L.-L.; Vannier, J.-P.; Malvy, C. Anti-RhoA and anti-RhoC siRNAs inhibit the proliferation and invasiveness of MDA-MB-231 breast cancer cells in vitro and in vivo. *Mol. Ther.* 2005, 11, 267–274. [CrossRef] [PubMed]
228. Pillé, J.-Y.; Li, H.; Blot, E.; Bertrand, J.-R.; Pritchard, L.-L.; Opolon, P.; Maksimenko, A.; Lu, H.; Vannier, J.-P.; Soria, J. Intravenous delivery of anti-RhoA small interfering RNA loaded in nanoparticles of chitosan in mice: Safety and efficacy in xenografted aggressive breast cancer. *Hum. Gene Ther.* 2006, 17, 1019–1026. [CrossRef] [PubMed]
229. Suwa, H.; Ohshio, G.; Imamura, T.; Watanabe, G.; Arii, S.; Imamura, M.; Narumiya, S.; Hiai, H.; Fukumoto, M. Overexpression of the RhoC gene correlates with progression of ductal adenocarcinoma of the pancreas. *Br. J. Cancer* 1998, 77, 147–152. [CrossRef] [PubMed]
230. Xie, S.; Zhu, M.; Lv, G.; Zhang, Q.; Wang, G. The role of RhoC in the proliferation and apoptosis of hepatocellular carcinoma cells. *Med. Oncol.* 2012, 29, 1802–1809. [CrossRef] [PubMed]
231. Robertson, F.M.; Bondy, M.; Yang, W.; Yamauchi, H.; Wiggins, S.; Kamrudin, S.; Krishnamurthy, S.; Le-Petross, H.; Bidaut, L.; Player, A.N. Inflammatory breast cancer: The disease, the biology, the treatment. *CA Cancer J. Clin.* 2010, 60, 351–375. [CrossRef] [PubMed]
232. Anderson, W.F.; Schairer, C.; Chen, B.E.; Hance, K.W.; Levine, P.H. Epidemiology of inflammatory breast cancer (IBC) 1. *Breast Dis.* 2006, 22, 9–23. [CrossRef] *Pharmaceutics* 2018, 10, 65 37 of 44
233. Van Golen, K.L.; Bao, L.W.; Pan, Q.; Miller, F.R.; Wu, Z.F.; Merajver, S.D. Mitogen activated protein kinase pathway is involved in RhoC GTPase induced motility, invasion and angiogenesis in inflammatory breast cancer. *Clin. Exp. Metastasis* 2002, 19, 301–311. [CrossRef] [PubMed]
234. Xu, X.-D.; Shen, H.-B.; Zhu, L.; Lu, J.-Q.; Zhang, L.; Luo, Z.-Y.; Wu, Y.-Q. Anti-rhoc sirnas inhibit the proliferation and invasiveness of breast cancer cells via modulating the Kai1, MMP9, and CXCR4 expression. *OncoTargets Ther.* 2017, 10, 1827. [CrossRef] [PubMed]

235. Kraus, C.; Liehr, T.; Hülsken, J.; Behrens, J.; Birchmeier, W.; Grzeschik, K.-H.; Ballhausen, W.G. Localization of the human  $\beta$ -catenin gene (CTNNB1) to 3p21: A region implicated in tumor development. *Genomics* 1994, 23, 272–274. [CrossRef] [PubMed]
236. MacDonald, B.T.; Tamai, K.; He, X. Wnt/ $\beta$ -catenin signaling: Components, mechanisms, and diseases. *Dev. Cell* 2009, 17, 9–26. [CrossRef] [PubMed]
237. Peifer, M.; Rauskolb, C.; Williams, M.; Riggleman, B.; Wieschaus, E. The segment polarity gene armadillo interacts with the wingless signaling pathway in both embryonic and adult pattern formation. *Development* 1991, 111, 1029–1043. [PubMed]
238. Noordermeer, J.; Klingensmith, J.; Perrimonl, N. Dishevelled and armadillo act in the Wingless signaling pathway in *Drosophila*. *Nature* 1994, 367, 80–83. [CrossRef] [PubMed]
239. Peifer, M.; Berg, S.; Reynolds, A.B. A repeating amino acid motif shared by proteins with diverse cellular roles. *Cell* 1994, 76, 789–791. [CrossRef]
240. Bilić, J.; Huang, Y.-L.; Davidson, G.; Zimmermann, T.; Cruciat, C.-M.; Bienz, M.; Niehrs, C. Wnt induces LRP6 signalosomes and promotes dishevelled-dependent LRP6 phosphorylation. *Science* 2007, 316, 1619–1622. [CrossRef] [PubMed]
241. Schwarz-Romond, T.; Fiedler, M.; Shibata, N.; Butler, P.J.G.; Kikuchi, A.; Higuchi, Y.; Bienz, M. The DIX domain of Dishevelled confers Wnt signaling by dynamic polymerization. *Nat. Struct. Mol. Biol.* 2007, 14, 484–492. [CrossRef] [PubMed]
242. Behrens, J.; von Kries, J.P.; Kühl, M.; Bruhn, L.; Wedlich, D.; Grosschedl, R.; Birchmeier, W. Functional interaction of  $\beta$ -catenin with the transcription factor LEF-1. *Nature* 1996, 382, 638–642. [CrossRef] [PubMed]
243. Molenaar, M.; van de Wetering, M.; Oosterwegel, M.; Peterson-Maduro, J.; Godsave, S.; Korinek, V.; Roose, J.; Destree, O.; Clevers, H. XTcf-3 transcription factor mediates  $\beta$ -catenin-induced axis formation in *Xenopus* embryos. *Cell* 1996, 86, 391–399. [CrossRef]
244. Grigoryan, T.; Wend, P.; Klaus, A.; Birchmeier, W. Deciphering the function of canonical Wnt signals in development and disease: Conditional loss-and gain-of-function mutations of  $\beta$ -catenin in mice. *Genes Dev.* 2008, 22, 2308–2341. [CrossRef] [PubMed]
245. Hajra, K.M.; Fearon, E.R. Cadherin and catenin alterations in human cancer. *Genes Chromosom. Cancer* 2002, 34, 255–268. [CrossRef] [PubMed]
246. Ilyas, M.; Tomlinson, I.; Rowan, A.; Pignatelli, M.; Bodmer, W.  $\beta$ -Catenin mutations in cell lines established from human colorectal cancers. *Proc. Natl. Acad. Sci. USA* 1997, 94, 10330–10334. [CrossRef] [PubMed]

247. Morin, P.J.; Sparks, A.B.; Korinek, V.; Barker, N.; Clevers, H.; Vogelstein, B.; Kinzler, K.W. Activation of  $\beta$ -catenin-Tcf signaling in colon cancer by mutations in  $\beta$ -catenin or APC. *Science* 1997, 275, 1787–1790. [CrossRef] [PubMed]
248. Polakis, P. Wnt signaling and cancer. *Genes Dev.* 2000, 14, 1837–1851. [CrossRef] [PubMed]
249. Sparks, A.B.; Morin, P.J.; Vogelstein, B.; Kinzler, K.W. Mutational analysis of the APC/ $\beta$ -catenin/Tcf pathway in colorectal cancer. *Cancer Res.* 1998, 58, 1130–1134. [PubMed]
250. Su, L.-K.; Vogelstein, B.; Kinzler, K.W. Association of the APC tumor suppressor protein with catenins. *Science* 1993, 262, 1734–1738. [CrossRef] [PubMed]
251. Korinek, V.; Barker, N.; Morin, P.J.; Van Wichen, D.; De Weger, R.; Kinzler, K.W.; Vogelstein, B.; Clevers, H. Constitutive transcriptional activation by a  $\beta$ -catenin-Tcf complex in APC<sup>-/-</sup> colon carcinoma. *Science* 1997, 275, 1784–1787. [CrossRef] [PubMed]
252. Bass, B.L. Double-stranded RNA as a template for gene silencing. *Cell* 2000, 101, 235–238. [CrossRef]
253. Verma, U.N.; Surabhi, R.M.; Schmaltieg, A.; Becerra, C.; Gaynor, R.B. Small interfering RNAs directed against  $\beta$ -catenin inhibit the in vitro and in vivo growth of colon cancer cells. *Clin. Cancer Res.* 2003, 9, 1291–1300. [PubMed] *Pharmaceutics* 2018, 10, 65 38 of 44
254. Barker, N.; Ridgway, R.A.; van Es, J.H.; van de Wetering, M.; Begthel, H.; van den Born, M.; Danenberg, E.; Clarke, A.R.; Sansom, O.J.; Clevers, H. Crypt stem cells as the cells-of-origin of intestinal cancer. *Nature* 2009, 457, 608–611. [CrossRef] [PubMed]
255. Barker, N.; Van Es, J.H.; Kuipers, J.; Kujala, P.; Van Den Born, M.; Cozijnsen, M.; Haegebarth, A.; Korving, J.; Begthel, H.; Peters, P.J. Identification of stem cells in small intestine and colon by marker gene *Lgr5*. *Nature* 2007, 449, 1003–1007. [CrossRef] [PubMed]
256. Rishi, A.K.; Zhang, L.; Yu, Y.; Jiang, Y.; Nautiyal, J.; Wali, A.; Fontana, J.A.; Levi, E.; Majumdar, A.P. Cell cycle-and apoptosis-regulatory protein-1 is involved in apoptosis signaling by epidermal growth factor receptor. *J. Biol. Chem.* 2006, 281, 13188–13198. [CrossRef] [PubMed]

257. Kim, J.H.; Yang, C.K.; Heo, K.; Roeder, R.G.; An, W.; Stallcup, M.R. CCAR1, a key regulator of mediator complex recruitment to nuclear receptor transcription complexes. *Mol. Cell* 2008, 31, 510–519. [CrossRef] [PubMed]
258. Ou, C.-Y.; Kim, J.H.; Yang, C.K.; Stallcup, M.R. Requirement of cell cycle and apoptosis regulator 1 for target gene activation by Wnt and  $\beta$ -catenin and for anchorage-independent growth of human colon carcinoma cells. *J. Biol. Chem.* 2009, 284, 20629–20637. [CrossRef] [PubMed]
259. Chang, T.-S.; Wei, K.-L.; Lu, C.-K.; Chen, Y.-H.; Cheng, Y.-T.; Tung, S.-Y.; Wu, C.-S.; Chiang, M.-K. Inhibition of CCAR1, a Coactivator of  $\beta$ -Catenin, Suppresses the Proliferation and Migration of Gastric Cancer Cells. *Int. J. Mol. Sci.* 2017, 18, 460. [CrossRef] [PubMed]
260. Amit, I.; Wides, R.; Yarden, Y. Evolvable signaling networks of receptor tyrosine kinases: Relevance of robustness to malignancy and to cancer therapy. *Mol. Syst. Biol.* 2007, 3, 151. [CrossRef] [PubMed]
261. Zelinski, D.P.; Zantek, N.D.; Stewart, J.C.; Irizarry, A.R.; Kinch, M.S. EphA2 overexpression causes tumorigenesis of mammary epithelial cells. *Cancer Res.* 2001, 61, 2301–2306. [PubMed]
262. Kullander, K.; Klein, R. Mechanisms and functions of Eph and ephrin signalling. *Nat. Rev. Mol. Cell Biol.* 2002, 3, 475–486. [CrossRef] [PubMed]
263. Hafner, C.; Schmitz, G.; Meyer, S.; Bataille, F.; Hau, P.; Langmann, T.; Dietmaier, W.; Landthaler, M.; Vogt, T. Differential gene expression of Eph receptors and ephrins in benign human tissues and cancers. *Clin. Chem.* 2004, 50, 490–499. [CrossRef] [PubMed]
264. Wang, L.-F.; Fokas, E.; Bieker, M.; Rose, F.; Rexin, P.; Zhu, Y.; Pagenstecher, A.; Engenhart-Cabillic, R.; An, H.-X. Increased expression of EphA2 correlates with adverse outcome in primary and recurrent glioblastoma multiforme patients. *Oncol. Rep.* 2008, 19, 151–156. [CrossRef] [PubMed]
265. Brannan, J.M.; Dong, W.; Prudkin, L.; Behrens, C.; Lotan, R.; Bekele, B.N.; Wistuba, I.; Johnson, F.M. Expression of the receptor tyrosine kinase EphA2 is increased in smokers and predicts poor survival in non-small cell lung cancer. *Clin. Cancer Res.* 2009, 15, 4423–4430. [CrossRef] [PubMed]
266. Cui, X.D.; Lee, M.J.; Yu, G.R.; Kim, I.H.; Yu, H.C.; Song, E.Y.; Kim, D.G. EFNA1 ligand and its receptor EphA2: Potential biomarkers for hepatocellular carcinoma. *Int. J. Cancer* 2010, 126, 940–949. [CrossRef] [PubMed]

267. Baeten, C.I.; Hillen, F.; Pauwels, P.; de Bruine, A.P.; Baeten, C.G. Prognostic role of vasculogenic mimicry in colorectal cancer. *Dis. Colon Rectum* 2009, 52, 2028–2035. [CrossRef] [PubMed]
268. Merritt, W.M.; Kamat, A.A.; Hwang, J.-Y.; Bottsford-Miller, J.; Lu, C.; Lin, Y.G.; Coffey, D.; Spannuth, W.A.; Nugent, E.; Han, L.Y. Clinical and biological impact of EphA2 overexpression and angiogenesis in endometrial cancer. *Cancer Biol. Ther.* 2010, 10, 1306–1314. [CrossRef] [PubMed]
269. Yuan, W.-J.; Ge, J.; Chen, Z.-K.; Wu, S.-B.; Shen, H.; Yang, P.; Hu, B.; Zhang, G.-W.; Chen, Z.-H. Over-expression of EphA2 and EphrinA-1 in human gastric adenocarcinoma and its prognostic value for postoperative patients. *Dig. Dis. Sci.* 2009, 54, 2410. [CrossRef] [PubMed]
270. Hirai, H.; Maru, Y.; Hagiwara, K.; Nishida, J.; Takaku, F. A novel putative tyrosine kinase receptor encoded by the eph gene. *Science* 1987, 238, 1717–1721. [CrossRef] [PubMed]
271. Thaker, P.H.; Deavers, M.; Celestino, J.; Thornton, A.; Fletcher, M.S.; Landen, C.N.; Kinch, M.S.; Kiener, P.A.; Sood, A.K. EphA2 expression is associated with aggressive features in ovarian carcinoma. *Clin. Cancer Res.* 2004, 10, 5145–5150. [CrossRef] [PubMed]
272. Zeng, G.; Hu, Z.; Kinch, M.S.; Pan, C.-X.; Flockhart, D.A.; Kao, C.; Gardner, T.A.; Zhang, S.; Li, L.; Baldrige, L.A. High-level expression of EphA2 receptor tyrosine kinase in prostatic intraepithelial neoplasia. *Am. J. Pathol.* 2003, 163, 2271–2276. [CrossRef] [PubMed]
- Pharmaceutics 2018, 10, 65 39 of 44
273. Wykosky, J.; Gibo, D.M.; Stanton, C.; Debinski, W. Interleukin-13 receptor  $\alpha 2$ , EphA2, and Fos-related antigen 1 as molecular denominators of high-grade astrocytomas and specific targets for combinatorial therapy. *Clin. Cancer Res.* 2008, 14, 199–208. [CrossRef] [PubMed]
274. Pandey, A.; Lazar, D.F.; Saltiel, A.R.; Dixit, V.M. Activation of the Eck receptor protein tyrosine kinase stimulates phosphatidylinositol 3-kinase activity. *J. Biol. Chem.* 1994, 269, 30154–30157. [PubMed]
275. Landen, C.N.; Chavez-Reyes, A.; Bucana, C.; Schmandt, R.; Deavers, M.T.; Lopez-Berestein, G.; Sood, A.K. Therapeutic EphA2 gene targeting in vivo using neutral liposomal small interfering RNA delivery. *Cancer Res.* 2005, 65, 6910–6918. [CrossRef] [PubMed]



276. Ayaki, M.; Komatsu, K.; Mukai, M.; Murata, K.; Kameyama, M.; Ishiguro, S.; Miyoshi, J.; Tatsuta, M.; Nakamura, H. Reduced expression of focal adhesion kinase in liver metastases compared with matched primary human colorectal adenocarcinomas. *Clin. Cancer Res.* 2001, 70, 3106–3112.
277. Cance, W.G.; Harris, J.E.; Iacocca, M.V.; Roche, E.; Yang, X.; Chang, J.; Simkins, S.; Xu, L. Immunohistochemical analyses of focal adhesion kinase expression in benign and malignant human breast and colon tissues: correlation with preinvasive and invasive phenotypes. *Clin. Cancer Res.* 2000, 6, 2417–2423. [PubMed]
278. Owens, L.V.; Xu, L.; Craven, R.J.; Dent, G.A.; Weiner, T.M.; Kornberg, L.; Liu, E.T.; Cance, W.G. Overexpression of the focal adhesion kinase (p125FAK) in invasive human tumors. *Cancer Res.* 1995, 55, 2752–2755. [PubMed]
279. Owens, L.V.; Xu, L.; Dent, G.A.; Yang, X.; Sturge, G.C.; Craven, R.J.; Cance, W.G. Focal adhesion kinase as a marker of invasive potential in differentiated human thyroid cancer. *Ann. Surg. Oncol.* 1996, 3, 100–105. [CrossRef] [PubMed]
280. Tremblay, L.; Hauck, W.; Aprikian, A.G.; Begin, L.R.; Chapdelaine, A.; Chevalier, S. Focal adhesion kinase (pp125FAK) expression, activation and association with paxillin and p50CSK in human metastatic prostate carcinoma. *Int. J. Cancer* 1996, 68, 164–171. [CrossRef]
281. Sood, A.K.; Coffin, J.E.; Schneider, G.B.; Fletcher, M.S.; DeYoung, B.R.; Gruman, L.M.; Gershenson, D.M.; Schaller, M.D.; Hendrix, M.J. Biological significance of focal adhesion kinase in ovarian cancer: role in migration and invasion. *Am. J. Pathol.* 2004, 165, 1087–1095. [CrossRef]
282. Ishizawar, R.; Parsons, S.J. c-Src and cooperating partners in human cancer. *Cancer Cell* 2004, 6, 209–214. [CrossRef] [PubMed]
283. Shahzad, M.M.; Lu, C.; Lee, J.-W.; Stone, R.L.; Mitra, R.; Mangala, L.S.; Lu, Y.; Baggerly, K.A.; Danes, C.G.; Nick, A.M. Dual targeting of EphA2 and FAK in ovarian carcinoma. *Cancer Biol. Ther.* 2009, 8, 1027–1034. [CrossRef] [PubMed]
284. Sulman, E.P.; Tang, X.X.; Allen, C.; Biegel, J.A.; Pleasure, D.E.; Brodeur, G.M.; Ikegaki, N. ECK, a HumanEPH-Related Gene, Maps to 1p36. 1, a Common Region of Alteration in Human Cancers. *Genomics* 1997, 40, 371–374. [CrossRef] [PubMed]
285. Yuan, W.; Chen, Z.; Wu, S.; Guo, J.; Ge, J.; Yang, P.; Huang, J. Silencing of EphA2 inhibits invasion of human gastric cancer SGC-7901 cells in vitro and in vivo. *Neoplasma* 2012, 59, 105–113. [CrossRef] [PubMed]

286. Higashiyama, M.; Doi, O.; Kodama, K.; Yokouchi, H.; Kasugai, T.; Ishiguro, S.; Takami, K.; Nakayama, T.; Nishisho, I. MDM2 gene amplification and expression in non-small-cell lung cancer: Immunohistochemical expression of its protein is a favourable prognostic marker in patients without p53 protein accumulation. *Br. J. Cancer* 1997, 75, 1302–1308. [CrossRef] [PubMed]
287. Graves, B.; Thompson, T.; Xia, M.; Janson, C.; Lukacs, C.; Deo, D.; Di Lello, P.; Fry, D.; Garvie, C.; Huang, K.-S. Activation of the p53 pathway by small-molecule-induced MDM2 and MDMX dimerization. *Proc. Natl. Acad. Sci. USA* 2012, 109, 11788–11793. [CrossRef] [PubMed]
288. Koster, R.; Timmer-Bosscha, H.; Bischoff, R.; Gietema, J.A.; de Jong, S. Disruption of the MDM2–p53 interaction strongly potentiates p53-dependent apoptosis in cisplatin-resistant human testicular carcinoma cells via the Fas/FasL pathway. *Cell Death Dis.* 2011, 2, e148. [CrossRef] [PubMed]
289. Yu, H.; Wagner, E. Bioresponsive polymers for nonviral gene delivery. *Curr. Opin. Mol. Ther.* 2009, 11, 165–178. [PubMed]
290. Yu, H.; Zou, Y.; Jiang, L.; Yin, Q.; He, X.; Chen, L.; Zhang, Z.; Gu, W.; Li, Y. Induction of apoptosis in non-small cell lung cancer by downregulation of MDM2 using pH-responsive PMPC-b-PDPA/siRNA complex nanoparticles. *Biomaterials* 2013, 34, 2738–2747. [CrossRef] [PubMed]
291. Li, S.-D.; Chono, S.; Huang, L. Efficient oncogene silencing and metastasis inhibition via systemic delivery of siRNA. *Mol. Ther.* 2008, 16, 942–946. [PubMed] *Pharmaceutics* 2018, 10, 65 40 of 44
292. Pollak, M. Insulin and insulin-like growth factor signalling in neoplasia. *Nat. Rev. Cancer* 2008, 8, 915–928. [CrossRef] [PubMed]
293. Beech, D.J.; Parekh, N.; Pang, Y. Insulin-like growth factor-I receptor antagonism results in increased cytotoxicity of breast cancer cells to doxorubicin and taxol. *Oncol. Rep.* 2001, 8, 325–329. [CrossRef] [PubMed]
294. Cantley, L.C.; Auger, K.R.; Carpenter, C.; Duckworth, B.; Graziani, A.; Kapeller, R.; Soltoff, S. Oncogenes and signal transduction. *Cell* 1991, 64, 281–302. [CrossRef]
295. Chernicky, C.L.; Yi, L.; Tan, H.; Gan, S.U.; Ilan, J. Treatment of human breast cancer cells with antisense RNA to the type I insulin-like growth factor receptor inhibits cell growth, suppresses tumorigenesis, alters the metastatic potential, and prolongs survival in vivo. *Cancer Gene Ther.* 2000, 7, 384. [CrossRef] [PubMed]

296. Wu, Y.; Tewari, M.; Cui, S.; Rubin, R. Activation of the insulin-like growth factor-I receptor inhibits tumor necrosis factor-induced cell death. *J. Cell. Physiol.* 1996, 168, 499–509. [CrossRef]
297. Baserga, R. The IGF-I receptor in cancer research. *Exp. Cell Res.* 1999, 253, 1–6. [CrossRef] [PubMed]
298. Lee, A.; Yee, D. Insulin-like growth factors and breast cancer. *Biomed. Pharmacother.* 1995, 49, 415–421. [CrossRef]
299. Iravani, S.; Zhang, H.Q.; Yuan, Z.Q.; Cheng, J.Q.; Karl, R.C.; Jove, R.; Coppola, D. Modification of insulin-like growth factor 1 receptor, c-Src, and Bcl-X L protein expression during the progression of barrett's neoplasia. *Hum. Pathol.* 2003, 34, 975–982. [CrossRef]
300. LeRoith, D.; Baserga, R.; Helman, L.; Roberts, C.T., Jr. Insulin-like growth factors and cancer. *Ann. Intern. Med.* 1995, 122, 54–59. [CrossRef] [PubMed]
301. Jemal, A.; Siegel, R.; Xu, J.; Ward, E. Cancer statistics, 2010. *CA Cancer J. Clin.* 2010, 60, 277–300. [CrossRef] [PubMed]
302. Gridelli, C. Targeted therapy developments in the treatment of non-small cell lung cancer: A promising but long and winding road. *Curr. Opin. Oncol.* 2008, 20, 145–147. [CrossRef] [PubMed]
303. Hansen, H.H. Treatment of advanced non-small cell lung cancer: Should include short courses of radiation, with palliation as the aim. *BMJ Br. Med. J.* 2002, 325, 452. [CrossRef]
304. Singh, P. Insulin-like growth factor system in growth, development and carcinogenesis. *J. Clin. Ligand Assay* 2000, 23, 214–232.
305. Dong, A.-Q.; Kong, M.-J.; Ma, Z.-Y.; Qian, J.-F.; Xu, X.-H. Down-regulation of IGF-IR using small, interfering, hairpin RNA (siRNA) inhibits growth of human lung cancer cell line A549 in vitro and in nude mice. *Cell Biol. Int.* 2007, 31, 500–507. [CrossRef] [PubMed]
306. Wang, C.; Ding, C.; Kong, M.; Dong, A.; Qian, J.; Jiang, D.; Shen, Z. Tumor-targeting magnetic lipoplex delivery of short hairpin RNA suppresses IGF-1R overexpression of lung adenocarcinoma A549 cells in vitro and in vivo. *Biochem. Biophys. Res. Commun.* 2011, 410, 537–542. [CrossRef] [PubMed]
307. Deveraux, Q.L.; Stennicke, H.R.; Salvesen, G.S.; Reed, J.C. Endogenous inhibitors of caspases. *J. Clin. Immunol.* 1999, 19, 388–398. [CrossRef] [PubMed]

308. Bergmann, A.; Yang, A.Y.-P.; Srivastava, M. Regulators of IAP function: Coming to grips with the grim reaper. *Curr. Opin. Cell Biol.* 2003, 15, 717–724. [CrossRef] [PubMed]
309. Yagihashi, A.; Asanuma, K.; Tsuji, N.; Torigoe, T.; Sato, N.; Hirata, K.; Watanabe, N. Detection of anti-livin antibody in gastrointestinal cancer patients. *Clin. Chem.* 2003, 49, 1206–1208. [CrossRef] [PubMed]
310. Ambrosini, G.; Adida, C.; Altieri, D.C. A novel anti-apoptosis gene, survivin, expressed in cancer and lymphoma. *Nat. Med.* 1997, 3, 917–921. [CrossRef] [PubMed]
311. Richter, B.W.; Duckett, C.S. The IAP proteins: Caspase inhibitors and beyond. *Sci. Signal.* 2000, 2000, pe1. [CrossRef] [PubMed]
312. Ashhab, Y.; Alian, A.; Polliack, A.; Panet, A.; Yehuda, D.B. Two splicing variants of a new inhibitor of apoptosis gene with different biological properties and tissue distribution pattern. *FEBS Lett.* 2001, 495, 56–60. [CrossRef]
313. Ka, H.; Hunt, J.S. Temporal and spatial patterns of expression of inhibitors of apoptosis in human placentas. *Am. J. Pathol.* 2003, 163, 413–422. [CrossRef]
314. Lv, J.; Chen, Z. Recent research about Livin in cancer. *Chin. J. Cancer Prev. Treat.* 2006, 13, 1347–1350.
315. Yagihashi, A.; Ohmura, T.; Asanuma, K.; Kobayashi, D.; Tsuji, N.; Torigoe, T.; Sato, N.; Hirata, K.; Watanabe, N. Detection of autoantibodies to survivin and livin in sera from patients with breast cancer. *Clin. Chim. Acta* 2005, 362, 125–130. [CrossRef] [PubMed]
- Pharmaceutics 2018, 10, 65 41 of 44
316. Hariu, H.; Hirohashi, Y.; Torigoe, T.; Asanuma, H.; Hariu, M.; Tamura, Y.; Aketa, K.; Nabeta, C.; Nakanishi, K.; Kamiguchi, K. Aberrant expression and potency as a cancer immunotherapy target of inhibitor of apoptosis protein family, Livin/ML-IAP in lung cancer. *Clin. Cancer Res.* 2005, 11, 1000–1009. [PubMed]
317. Jemal, A.; Bray, F.; Center, M.M.; Ferlay, J.; Ward, E.; Forman, D. Global cancer statistics. *CA Cancer J. Clin.* 2011, 61, 69–90. [CrossRef] [PubMed]
318. Siegel, R.L.; Miller, K.D.; Jemal, A. Cancer statistics, 2015. *CA Cancer J. Clin.* 2015, 65, 5–29. [CrossRef] [PubMed]
319. Bar-Eli, M. Role of AP-2 in tumor growth and metastasis of human melanoma. *Cancer Metastasis Rev.* 1999, 18, 377–385. [CrossRef] [PubMed]

320. Bar-Eli, M. Gene regulation in melanoma progression by the AP-2 transcription factor. *Pigment. Cell Melanoma Res.* 2001, 14, 78–85. [CrossRef]
321. Soutschek, J.; Akinc, A.; Bramlage, B.; Charisse, K.; Constien, R.; Donoghue, M.; Elbashir, S.; Geick, A.; Hadwiger, P.; Harborth, J. Therapeutic silencing of an endogenous gene by systemic administration of modified siRNAs. *Nature* 2004, 432, 173–178. [CrossRef] [PubMed]
322. Dykxhoorn, D.M.; Lieberman, J. The silent revolution: RNA interference as basic biology, research tool, and therapeutic. *Annu. Rev. Med.* 2005, 56, 401–423. [CrossRef] [PubMed]
323. Ryther, R.; Flynt, A.; Phillips, J.; Patton, J. siRNA therapeutics: Big potential from small RNAs. *Gene Ther.* 2005, 12, 5–11. [CrossRef] [PubMed]
324. Wang, H.; Yang, Y.; Wang, W.; Guan, B.; Xun, M.; Zhang, H.; Wang, Z.; Zhao, Y. Single-chain antibody–delivered Livin siRNA inhibits human malignant melanoma growth in vitro and in vivo. *Tumor Biol.* 2017, 39. [CrossRef] [PubMed]
325. Wang, R.; Lin, F.; Wang, X.; Gao, P.; Dong, K.; Zou, A.; Cheng, S.; Wei, S.; Zhang, H. Silencing Livin gene expression to inhibit proliferation and enhance chemosensitivity in tumor cells. *Cancer Gene Ther.* 2008, 15, 402–412. [CrossRef] [PubMed]
326. Call, K.M.; Glaser, T.; Ito, C.Y.; Buckler, A.J.; Pelletier, J.; Haber, D.A.; Rose, E.A.; Kral, A.; Yeger, H.; Lewis, W.H. Isolation and characterization of a zinc finger polypeptide gene at the human chromosome 11 Wilms' tumor locus. *Cell* 1990, 60, 509–520. [CrossRef]
327. Gessler, M.; Poustka, A.; Cavenee, W.; Neve, R.L.; Orkin, S.H.; Bruns, G.A. Homozygous deletion in Wilms tumours of a zinc-finger gene identified by chromosome jumping. *Nature* 1990, 343, 774. [CrossRef] [PubMed]
328. Sugiyama, H. Wilms' tumor gene WT1: Its oncogenic function and clinical application. *Int. J. Hematol.* 2001, 73, 177–187. [CrossRef] [PubMed]
329. Coppes, M.J.; Campbell, C.E.; Williams, B. The role of WT1 in Wilms tumorigenesis. *FASEB J.* 1993, 7, 886–895. [CrossRef] [PubMed]
330. Rauscher, F. The WT1 Wilms tumor gene product: A developmentally regulated transcription factor in the kidney that functions as a tumor suppressor. *FASEB J.* 1993, 7, 896–903. [CrossRef] [PubMed]

331. Haber, D.; Park, S.; Maheswaran, S.; Englert, C.; Re, G.; Hazen-Martin, D.; Sens, D.; Garvin, A. WT1-mediated growth suppression of Wilms' tumor cells expressing a WT1 splicing variant. *Science* 1993, 262, 2057–2059. [CrossRef] [PubMed]
332. Algar, E.M.; Kenney, M.T.; Simms, L.A.; Smith, S.I.; Kida, Y.; Smith, P.J. Homozygous intragenic deletion in the WT1 gene in a sporadic Wilms' tumour associated with high levels of expression of a truncated transcript. *Hum. Mutat.* 1995, 5, 221–227. [CrossRef] [PubMed]
333. Little, M.; Wells, C. A clinical overview of WT1 gene mutations. *Hum. Mutat.* 1997, 9, 209–225. [CrossRef]
334. Sugiyama, H. Cancer immunotherapy targeting Wilms' tumor gene WT1 product. *Expert Rev. Vaccines* 2005, 4, 503–512. [CrossRef] [PubMed]
335. Miwa, H.; Beran, M.; Saunders, G. Expression of the Wilms' tumor gene (WT1) in human leukemias. *Leukemia* 1992, 6, 405–409. [PubMed]
336. Moore, A.W.; McInnes, L.; Kreidberg, J.; Hastie, N.D.; Schedl, A. YAC complementation shows a requirement for Wt1 in the development of epicardium, adrenal gland and throughout nephrogenesis. *Development* 1999, 126, 1845–1857. [PubMed] *Pharmaceutics* 2018, 10, 65 42 of 44
337. Inoue, K.; Sugiyama, H.; Ogawa, H.; Nakagawa, M.; Yamagami, T.; Miwa, H.; Kita, K.; Hiraoka, A.; Masaoka, T.; Nasu, K. WT1 as a new prognostic factor and a new marker for the detection of minimal residual disease in acute leukemia. *Blood* 1994, 84, 3071–3079. [PubMed]
338. Oji, Y.; Miyoshi, S.; Maeda, H.; Hayashi, S.; Tamaki, H.; Nakatsuka, S.I.; Yao, M.; Takahashi, E.; Nakano, Y.; Hirabayashi, H. Overexpression of the Wilms' tumor gene WT1 in de novo lung cancers. *Int. J. Cancer* 2002, 100, 297–303. [CrossRef] [PubMed]
339. Loeb, D.M.; Evron, E.; Patel, C.B.; Sharma, P.M.; Niranjana, B.; Buluwela, L.; Weitzman, S.A.; Korz, D.; Sukumar, S. Wilms' tumor suppressor gene (WT1) is expressed in primary breast tumors despite tumor-specific promoter methylation. *Cancer Res.* 2001, 61, 921–925. [PubMed]
340. Miyoshi, Y.; Ando, A.; Egawa, C.; Taguchi, T.; Tamaki, Y.; Tamaki, H.; Sugiyama, H.; Noguchi, S. High expression of Wilms' tumor suppressor gene predicts poor prognosis in breast cancer patients. *Clin. Cancer Res.* 2002, 8, 1167–1171. [PubMed]

341. Oji, Y.; Suzuki, T.; Nakano, Y.; Maruno, M.; Nakatsuka, S.i.; Jomgeow, T.; Abeno, S.; Tatsumi, N.; Yokota, A.; Aoyagi, S. Overexpression of the Wilms' tumor gene WT1 in primary astrocytic tumors. *Cancer Sci.* 2004, 95, 822–827. [CrossRef] [PubMed]
342. Bowman, T.; Garcia, R.; Turkson, J.; Jove, R. STATs in oncogenesis. *Oncogene* 2000, 19, 2474. [CrossRef] [PubMed]
343. Bromberg, J. Stat proteins and oncogenesis. *J. Clin. Investig.* 2002, 109, 1139. [CrossRef] [PubMed]
344. Darnell, J.E. Validating Stat3 in cancer therapy. *Nat. Med.* 2005, 11, 595–596. [CrossRef] [PubMed]
345. Sinibaldi, D.; Wharton, W.; Turkson, J.; Bowman, T.; Pledger, W.J.; Jove, R. Induction of p21 WAF1/CIP1 and cyclin D1 expression by the Src oncoprotein in mouse fibroblasts: Role of activated STAT3 signaling. *Oncogene* 2000, 19, 5419–5427. [CrossRef] [PubMed]
346. Catlett-Falcone, R.; Dalton, W.S.; Jove, R. STAT proteins as novel targets for cancer therapy. *Curr. Opin. Oncol.* 1999, 11, 490. [CrossRef] [PubMed]
347. Thomas, A.; Hassan, R. Immunotherapies for non-small-cell lung cancer and mesothelioma. *Lancet Oncol.* 2012, 13, e301–e310. [CrossRef]
348. Xu, C.; Wu, C.; Xia, Y.; Zhong, Z.; Liu, X.; Xu, J.; Cui, F.; Chen, B.; Røe, O.D.; Li, A. WT1 promotes cell proliferation in non-small cell lung cancer cell lines through up-regulating cyclin D1 and p-pRb in vitro and in vivo. *PLoS ONE* 2013, 8, e68837. [CrossRef] [PubMed]
349. Derycke, A.S.; De Witte, P.A. Transferrin-mediated targeting of hypericin embedded in sterically stabilized PEG-liposomes. *Int. J. Oncol.* 2002, 20, 181–187. [CrossRef] [PubMed]
350. Stavridis, J.; Deliconstantinos, G.; Psallidopoulos, M.; Armenakas, N.; Hadjiminis, D.; Hadjiminis, J. Construction of transferrin-coated liposomes for in vivo transport of exogenous DNA to bone marrow erythroblasts in rabbits. *Exp. Cell Res.* 1986, 164, 568–572. [CrossRef]
351. Voinea, M.; Dragomir, E.; Manduteanu, I.; Simionescu, M. Binding and uptake of transferrin-bound liposomes targeted to transferrin receptors of endothelial cells. *Vasc. Pharmacol.* 2002, 39, 13–20. [CrossRef]

352. Kobayashi, T.; Ishida, T.; Okada, Y.; Ise, S.; Harashima, H.; Kiwada, H. Effect of transferrin receptor-targeted liposomal doxorubicin in P-glycoprotein-mediated drug resistant tumor cells. *Int. J. Pharm.* 2007, 329, 94–102. [CrossRef] [PubMed]
353. Saavedra-Alonso, S.; Zapata-Benavides, P.; Chavez-Escamilla, A.K.; Manilla-Muñoz, E.; Zamora-Avila, D.E.; Franco-Molina, M.A.; Rodriguez-Padilla, C. WT1 shRNA delivery using transferrin-conjugated PEG liposomes in an in vivo model of melanoma. *Exp. Ther. Med.* 2016, 12, 3778–3784. [CrossRef] [PubMed]
354. Hinitt, C.; Wood, J.; Lee, S.; Williams, A.; Howarth, J.; Glover, C.; Uney, J.; Hague, A. BAG-1 enhances cell–cell adhesion, reduces proliferation and induces chaperone-independent suppression of hepatocyte growth factor-induced epidermal keratinocyte migration. *Exp. Cell Res.* 2010, 316, 2042–2060. [CrossRef] [PubMed]
355. Liu, H.; Lu, S.; Gu, L.; Gao, Y.; Wang, T.; Zhao, J.; Rao, J.; Chen, J.; Hao, X.; Tang, S.-C. Modulation of BAG-1 expression alters the sensitivity of breast cancer cells to tamoxifen. *Cell. Physiol. Biochem.* 2014, 33, 365–374. [CrossRef] [PubMed]
356. Ozfiliz, P.; Arisan, E.D.; Coker-Gurkan, A.; Obakan, P.; Eralp, T.N.; Dinler-Doganay, G.; Palavan-Unsal, N. Bag-1L is a stress-withstand molecule prevents the downregulation of Mcl-1 and c-Raf under control of heat shock proteins in cisplatin treated HeLa cervix cancer cells. *Asian Pac. J. Cancer Prev.* 2014, 15, 4475–4482. [CrossRef] [PubMed]
- Pharmaceutics 2018, 10, 65 43 of 44
357. Torre, L.A.; Bray, F.; Siegel, R.L.; Ferlay, J.; Lortet-Tieulent, J.; Jemal, A. Global cancer statistics, 2012. *CA Cancer J. Clin.* 2015, 65, 87–108. [CrossRef] [PubMed]
358. El-Shami, K.; Oeffinger, K.C.; Erb, N.L.; Willis, A.; Bretsch, J.K.; Pratt-Chapman, M.L.; Cannady, R.S.; Wong, S.L.; Rose, J.; Barbour, A.L. American Cancer Society colorectal cancer survivorship care guidelines. *CA Cancer J. Clin.* 2015, 65, 427–455. [CrossRef] [PubMed]
359. Sun, N.; Meng, Q.; Tian, A. Expressions of the anti-apoptotic genes Bag-1 and Bcl-2 in colon cancer and their relationship. *Am. J. Surg.* 2010, 200, 341–345. [CrossRef] [PubMed]
360. Huang, W.; Zhou, G.; Ling, J.; Tian, A.; Sun, N. Silencing Bag-1 gene via magnetic gold nanoparticle-delivered siRNA plasmid for colorectal cancer therapy in vivo and in vitro. *Tumor Biol.* 2016, 37, 10365–10374. [CrossRef] [PubMed]



361. Zou, H.; McGarry, T.J.; Bernal, T.; Kirschner, M.W. Identification of a vertebrate sister-chromatid separation inhibitor involved in transformation and tumorigenesis. *Science* 1999, 285, 418–422. [CrossRef] [PubMed]
362. Jallepalli, P.V.; Waizenegger, I.C.; Bunz, F.; Langer, S.; Speicher, M.R.; Peters, J.-M.; Kinzler, K.W.; Vogelstein, B.; Lengauer, C. Securin is required for chromosomal stability in human cells. *Cell* 2001, 105, 445–457. [CrossRef]
363. Yu, R.; Lu, W.; Chen, J.; McCabe, C.J.; Melmed, S. Overexpressed pituitary tumor-transforming gene causes aneuploidy in live human cells. *Endocrinology* 2003, 144, 4991–4998. [CrossRef] [PubMed]
364. Christopoulou, L.; Moore, J.D.; Tyler-Smith, C. Over-expression of wild-type Securin leads to aneuploidy in human cells. *Cancer Lett.* 2003, 202, 213–218. [CrossRef]
365. Weaver, B.A.; Cleveland, D.W. Decoding the links between mitosis, cancer, and chemotherapy: The mitotic checkpoint, adaptation, and cell death. *Cancer Cell* 2005, 8, 7–12. [CrossRef] [PubMed]
366. Zhang, X.; Horwitz, G.A.; Heaney, A.P.; Nakashima, M.; Prezant, T.R.; Bronstein, M.D.; Melmed, S. Pituitary tumor transforming gene (PTTG) expression in pituitary adenomas. *J. Clin. Endocrinol. Metab.* 1999, 84, 761–767. [CrossRef] [PubMed]
367. Heaney, A.P.; Singson, R.; McCabe, C.J.; Nelson, V.; Nakashima, M.; Melmed, S. Expression of pituitary-tumour transforming gene in colorectal tumours. *Lancet* 2000, 355, 716–719. [CrossRef]
368. Puri, R.; Tousson, A.; Chen, L.; Kakar, S.S. Molecular cloning of pituitary tumor transforming gene 1 from ovarian tumors and its expression in tumors. *Cancer Lett.* 2001, 163, 131–139. [CrossRef]
369. Solbach, C.; Roller, M.; Fellbaum, C.; Nicoletti, M.; Kaufmann, M. PTTG mRNA expression in primary breast cancer: A prognostic marker for lymph node invasion and tumor recurrence. *Breast* 2004, 13, 80–81. [CrossRef] [PubMed]
370. Dominguez, A.; Ramos-Morales, F.; Romero, F.; Rios, R.M.; Dreyfus, F.; Tortolero, M.; Pintor-Toro, J.A. hpttg, a human homologue of rat pttg, is overexpressed in hematopoietic neoplasms. Evidence for a transcriptional activation function of hPTTG. *Oncogene* 1998, 17, 2187. [CrossRef] [PubMed]

371. Yu, R.; Melmed, S. Pituitary tumor transforming gene: An update. In *Molecular Pathology of the Pituitary*; Karger Publishers: Basel, Switzerland, 2004; Volume 32, pp. 175–185.
372. Thorgeirsson, S.S.; Grisham, J.W. Molecular pathogenesis of human hepatocellular carcinoma. *Nat. Genet.* 2002, 31, 339–346. [CrossRef] [PubMed]
373. Bruix, J.; Llovet, J.M. Prognostic prediction and treatment strategy in hepatocellular carcinoma. *Hepatology* 2002, 35, 519–524. [CrossRef] [PubMed]
374. Bernal, J.; Luna, R.; Espina, A. Human securin interacts with p53 and modulates p53-mediated transcriptional activity and apoptosis. *Nat. Genet.* 2002, 32, 306–311.
375. Jung, C.R.; Yoo, J.; Jang, Y.J.; Kim, S.; Chu, I.S.; Yeom, Y.I.; Choi, J.Y.; Im, D.S. Adenovirus-mediated transfer of siRNA against PTTG1 inhibits liver cancer cell growth in vitro and in vivo. *Hepatology* 2006, 43, 1042–1052. [CrossRef] [PubMed]
376. Frazier, W.A.; Gao, A.-G.; Dimitry, J.; Chung, J.; Brown, E.J.; Lindberg, F.P.; Linder, M.E. The thrombospondin receptor integrin-associated protein (CD47) functionally couples to heterotrimeric Gi. *J. Biol. Chem.* 1999, 274, 8554–8560. [CrossRef] [PubMed]
377. Oldenborg, P.-A.; Zheleznyak, A.; Fang, Y.-F.; Lagenaur, C.F.; Gresham, H.D.; Lindberg, F.P. Role of CD47 as a marker of self on red blood cells. *Science* 2000, 288, 2051–2054. [CrossRef] [PubMed]
378. Jaiswal, S.; Jamieson, C.H.; Pang, W.W.; Park, C.Y.; Chao, M.P.; Majeti, R.; Traver, D.; van Rooijen, N.; Weissman, I.L. CD47 is upregulated on circulating hematopoietic stem cells and leukemia cells to avoid phagocytosis. *Cell* 2009, 138, 271–285. [CrossRef] [PubMed] *Pharmaceutics* 2018, 10, 65 44 of 44
379. Majeti, R.; Chao, M.P.; Alizadeh, A.A.; Pang, W.W.; Jaiswal, S.; Gibbs, K.D.; van Rooijen, N.; Weissman, I.L. CD47 is an adverse prognostic factor and therapeutic antibody target on human acute myeloid leukemia stem cells. *Cell* 2009, 138, 286–299. [CrossRef] [PubMed]
380. Chan, K.S.; Espinosa, I.; Chao, M.; Wong, D.; Ailles, L.; Diehn, M.; Gill, H.; Presti, J.; Chang, H.Y.; van de Rijn, M. Identification, molecular characterization, clinical prognosis, and therapeutic targeting of human bladder tumor-initiating cells. *Proc. Natl. Acad. Sci. USA* 2009, 106, 14016–14021. [CrossRef] [PubMed]
381. Chao, M.P.; Alizadeh, A.A.; Tang, C.; Myklebust, J.H.; Varghese, B.; Gill, S.; Jan, M.; Cha, A.C.; Chan, C.K.; Tan, B.T. Anti-CD47 antibody synergizes with rituximab to

promote phagocytosis and eradicate non-Hodgkin lymphoma. *Cell* 2010, 142, 699–713. [CrossRef] [PubMed]

382. Wang, Y.; Xu, Z.; Guo, S.; Zhang, L.; Sharma, A.; Robertson, G.P.; Huang, L. Intravenous delivery of siRNA targeting CD47 effectively inhibits melanoma tumor growth and lung metastasis. *Mol. Ther.* 2013, 21, 1919–1929. [CrossRef] [PubMed]

## **Chapter 2**

**Research gap, Hypothesis, Objectives and Overview of Inorganic salt nanoparticles.**

## **2. Research gap, Hypothesis, Objectives and Overview of Inorganic salt nanoparticles.**

### **2.1. Research gap:**

The goal of nanomedicine is to develop efficient, targeted, biocompatible formulations for therapies and diagnosis of several complex and challenging diseases like cancer. The ability to understand the challenges and opportunities of cancer nanomedicine has gained the momentum quickly due to exploration of diverse nanotechnology. Inorganic nanoparticles hold great attention owing to their unique physicochemical properties, biocompatibility and improved pharmacokinetics properties compared to the organic counterpart. There are still severe limitations of inorganic NPs that hampered the systemic application for the treatment. The controllable and reproducible synthesis, scalable manufacturing, lower transfection rates, ineffective nuclear uptake, less tumor accumulation and late endosomal release of inorganic NPs warrant further research to make more closure to personalized medicine.

### **2.2. Hypothesis:**

Electrolytes and glucose might have significant roles in generating nano-size particles from reaction of two soluble salts. The developed nanoparticles would have the affinity towards nucleic acids, and subsequent surface modification with a hydrophilic polymer would make the nanoparticles more stable and biocompatible for efficient delivery of small interfering RNAs (siRNAs) both in vitro and in vivo.

### **2.3. Objectives:**

The main objective of my project is to establish the potential salt crystals with nano-size diameters having the capacity of adsorbing negatively charged siRNAs, effectively carrying them across the plasma membrane and finally leading to silencing of the target oncogenes gene(s) for induction of cytotoxicity in breast cancer cells. The steps of objective are given below:

01. The insoluble salt nanoparticles would be formed by mixing of two water soluble salts under the influence of glucose and electrolytes and subjected to surface modification for nanoparticle stabilization.
02. The formulated Strontium sulfite nanoparticles (SSNs) will be optimized based on their size, morphology, physic-chemical properties, affinity towards the negatively charged DNA/RNA, cellular endocytosis rate and intracellular dissolution for quick

release of the therapeutic molecules in cytosol and finally transfection efficacy in the context of gene knockdown of the target gene(s).

03. The bio distribution and toxicity analysis of NPs, and tumor regression study of NPs-siRNA complex will be carried out in a breast tumor mouse model.

#### **2.4. Overview of Inorganic salt nanoparticles:**

Inorganic nanoparticles hold great potential in the area of precision medicine particularly for treating cancer owing to their unique physicochemical properties, biocompatibility and improved pharmacokinetics properties compared to the organic counterpart. Maintenance of controlled particle size, homogenous distribution and morphology of inorganic nanoparticles are the vital facts for the development of ideal nanoparticles. Precipitation reaction is one of the attractive approaches in synthesizing nanoscale inorganic NPs owing to its simple operation, scale up mass production and easy experimental setup in terms of commercialization. It involves a reaction between two soluble salt reactants (cation and anion providing) in an aqueous solution to form an insoluble salt product via induction of super saturation. Generation of nanoparticles through nanoprecipitation method is quite easy, reproducible and able to produce in large scale with their controlled unique physicochemical properties. Nanoparticles prepared via precipitation method e.g. carbonate apatite, calcium carbonate ( $\text{CaCO}_3$ ), iron oxide ( $\text{Fe}_3\text{O}_4$ ), barium sulfate and zinc oxide ( $\text{ZnO}$ ) have shown promising results as drug and gene carriers. Alkaline earth metal strontium is a naturally found silvery metal which is a non-radioactive element and about 99% of the body strontium is found to be concentrated in the bones of human body. Strontium salts have a high boiling point of  $2,282^\circ$  Fahrenheit ( $1,250^\circ$  Celsius) and is soluble in water. it has been widely used as vitamin for bones(1, 2). Although strontium salts are considered rather stable chemicals that have a level of toxicity above that of calcium chloride, strontium attracted less attention compared to the other two divalent metals, calcium and magnesium. However, development of strontium ranelate in the treatment of osteoporosis increased the awareness of the biological role of strontium in human biology and pathology(3). Moreover, strontium substituted carbonate apatite nanoparticles exhibited promising results for the delivery of anticancer drugs methotrexate and cyclophosphamide(4). Strontium carbonate nanoparticles conjugated anticancer drug etoposide also exerted potent antitumor activity compared to free etoposide(5). The extensive and promising results of strontium salt as a drug carrier inspire us for further research on this new potential drug delivery carrier in cancer gene therapy. The positive domain of salt nanocrystals allows ionic interaction with siRNA, plasmid DNA and drugs for successfully carrying the payload to the target cell. The pH sensitive nature of inorganic salt NPs has added a new dimension to cancer gene therapy, offering rapid intracellular drug release from cargo via the early endosomal escape mechanisms (6-11). As proteins

in systemic circulation are charged, electrostatic interactions between them and nanoparticles may occur, in addition to local hydrophilic and hydrophobic patterns existing on the particle surface, resulting in the formation of “Protein Corona” which usually comprises opsonins and other proteins, and consequently removal of the particles by the reticuloendothelial system (RES). Adsorbed proteins, therefore, alter the parameters of nanoparticles, including hydrodynamic diameter and colloidal stability.

## References

1. Li ZH, Wu JM, Huang SJ, Guan J, Zhang XZ, editors. Strontium Hydroxyapatite Synthesis, Characterization and Cell Cytotoxicity. Advanced Materials Research; 2011: Trans Tech Publ.
2. Liu W, Wang T, Shen Y, Pan H, Peng S, Lu WW. Strontium incorporated coralline hydroxyapatite for engineering bone. ISRN Biomaterials. 2012;2013.
3. Li Z, Peng S, Pan H, Tang B, Lam RW, Lu WW. Microarchitecture and nanomechanical properties of trabecular bone after strontium administration in osteoporotic goats. Biological trace element research. 2012;145(1):39-46.
4. Tiash S, Othman I, Rosli R, Hoque Chowdhury E. Methotrexate-and cyclophosphamide-embedded pure and strontiumsubstituted carbonate apatite nanoparticles for augmentation of chemotherapeutic activities in breast cancer cells. Current drug delivery. 2014;11(2):214-22.
5. Qian W-Y, Sun D-M, Zhu R-R, Du X-L, Liu H, Wang S-L. pH-sensitive strontium carbonate nanoparticles as new anticancer vehicles for controlled etoposide release. International journal of nanomedicine. 2012;7:5781.
6. Li H, Du J, Liu J, Du X, Shen S, Zhu Y, et al. ACS Nano 2016, 10, 6753–6761. CrossRef| PubMed| CAS| Web of Science® Times Cited.12.
7. Li H-J, Du J-Z, Du X-J, Xu C-F, Sun C-Y, Wang H-X, et al. Stimuli-responsive clustered nanoparticles for improved tumor penetration and therapeutic efficacy. Proceedings of the National Academy of Sciences. 2016;113(15):4164-9.
8. Ju C, Mo R, Xue J, Zhang L, Zhao Z, Xue L, et al. Sequential intra-intercellular nanoparticle delivery system for deep tumor penetration. Angewandte Chemie International Edition. 2014;53(24):6253-8.
9. Du J-Z, Du X-J, Mao C-Q, Wang J. Tailor-made dual pH-sensitive polymer–doxorubicin nanoparticles for efficient anticancer drug delivery. Journal of the American Chemical Society. 2011;133(44):17560-3.
10. Miao L, Wang Y, Lin CM, Xiong Y, Chen N, Zhang L, et al. Nanoparticle modulation of the tumor microenvironment enhances therapeutic efficacy of cisplatin. Journal of Controlled Release. 2015;217:27-41.

11. Xu X, Saw PE, Tao W, Li Y, Ji X, Yu M, et al. Tumor Microenvironment-Responsive Multistaged Nanoplatfrom for Systemic RNAi and Cancer Therapy. Nano letters. 2017;17(7):4427-35.



## **Chapter 3**

### **Strontium Sulfite: A New pH-Responsive Inorganic Nanocarrier to Deliver Therapeutic siRNAs to Cancer Cells**

Work that is presented in this chapter is published in *Pharmaceutics* **2019**, *11*(2), 89 with minor adjustments in Figure/Table number to fit into the current thesis format. A snapshot of the research paper is included in page 97.



## Article

# Strontium Sulfite: A New pH-Responsive Inorganic Nanocarrier to Deliver Therapeutic siRNAs to Cancer Cells

Md. Emranul Karim <sup>1</sup>, Jayalaxmi Shetty <sup>1</sup>, Rowshan Ara Islam <sup>1</sup>, Ahsanul Kaiser <sup>1</sup>,  
Athirah Bakhtiar <sup>2</sup> and Ezharul Hoque Chowdhury <sup>1,\*</sup>

<sup>1</sup> Jeffrey Cheah School of Medicine and Health Sciences, Monash University Malaysia, Jalan Lagoon Selatan, Bandar Sunway, 47500 Petaling Jaya, Malaysia; karim604306@gmail.com (M.E.K.);

jayashetty21@gmail.com (J.S.); Rowshan.Islam@monash.edu (R.A.I.); ahsanul.kaiser@monash.edu (A.K.)

<sup>2</sup> Faculty of Pharmacy, Mahsa University, 2, Jalan SP 4/4, Bandar Saujana Putra, 42610 Jerjarom, Malaysia; athirahbakhtiar@gmail.com

\* Correspondence: md.ezharul.hoque@monash.edu; Tel.: +603-5514-4978; Fax: +603-5514-6323

Received: 16 November 2018; Accepted: 13 February 2019; Published: 20 February 2019



**Abstract:** Inorganic nanoparticles hold great potential in the area of precision medicine, particularly for treating cancer owing to their unique physicochemical properties, biocompatibility and improved pharmacokinetics properties compared to their organic counterparts. Here we introduce strontium sulfite nanoparticles as new pH-responsive inorganic nanocarriers for efficient transport of siRNAs into breast cancer cells. We employed the simplest nanoprecipitation method to generate the strontium sulfite nanoparticles (SSNs) and demonstrated the dramatic roles of NaCl and D-glucose in particle growth stabilization in order to produce even smaller nanosize particles (Na-Glc-SSN) with high affinity towards negatively charged siRNA, enabling it to efficiently enter the cancer cells. Moreover, the nanoparticles were found to be degraded with a small drop in pH, suggesting their potential capability to undergo rapid dissolution at endosomal pH so as to release the payload. While these particles were found to be nontoxic to the cells, they showed higher potency in facilitating cancer cell death through intracellular delivery and release of oncogene-specific siRNAs targeting *ros1* and *egfr1* mRNA transcripts, than the strontium sulfite particles prepared in absence of NaCl and D-glucose, as confirmed by growth inhibition assay. The mouse plasma binding analysis by Q-TOF LC-MS/MS demonstrated less protein binding to smaller particles of Na-Glc-SSNs. The biodistribution studies of the particles after 4 h of treatment showed Na-Glc-SSNs had less off-target distribution than SSNs, and after 24 h, all siRNAs were cleared from all major organs except the tumors. ROS1 siRNA with its potential therapeutic role in treating 4T1-induced breast tumor was selected for subsequent in vivo tumor regression study, revealing that ROS1 siRNA-loaded SSNs exerted more significant anti-tumor effects than Na-Glc-SSNs carrying the same siRNA following intravenous administration, without any systemic toxicity. Thus, strontium sulfite emerged as a powerful siRNA delivery tool with potential applications in cancer gene therapy.

**Keywords:** inorganic nanoparticles; tumor; strontium sulfite; pH-responsive drug delivery; siRNA; gene therapy; breast cancer

## 1. Introduction

Nanotechnology has contributed immensely to cancer gene therapy via introducing multiple nanocarriers to carry plasmid DNA, mRNA, siRNA, miRNA and anti-sense oligonucleotides (AONs) to the cytoplasm of targeted cancer cells [1]. Rigorous studies of cancer genetics have revealed that mutations in tumor suppressor genes and oncogenes are the key drivers for aberrant expression of

### **3. Strontium Sulfite: A New pH-Responsive Inorganic Nanocarrier to Deliver Therapeutic siRNAs to Cancer Cells**

#### **3.1. Introduction**

Nanotechnology has contributed immensely to cancer gene therapy via introducing multiple nanocarriers to carry plasmid DNA, mRNA, siRNA, miRNA and anti-sense oligonucleotides (AONs) to the cytoplasm of targeted cancer cells [1]. Rigorous studies of cancer genetics have revealed that mutations in tumor suppressor genes and oncogenes are the key drivers for aberrant expression of genes, leading to cancer [2]. As a RNA interference tool, siRNAs have been deployed successfully for silencing genes that regulate proliferation, survival and metastasis of cancer cells [3]. However, unmodified or naked siRNA is prone to nuclease degradation, phagocytic clearance, interactions with serum proteins and renal clearance [4]. Moreover, siRNA also copes with the abnormal tumor microenvironment (TME) including the dense extracellular matrix (ECM), and leaky and heterogeneous vessels which contribute to increased interstitial fluid pressure (IFP) [5–8]. To overcome this hurdle, naked siRNA potentially requires a vehicle to be successfully delivered into the target cancer cells. Compared to the viral counterparts, non-viral vectors comprising both organic and inorganic nanoparticles (NPs) are more attractive for clinical use due to their superior advantages in terms of safety, scalability and drug-loading capability [9–11]. Inorganic NPs of gold, carbonate apatite, quantum dots, iron oxide, mesoporous silica, and so on, represent a highly sophisticated platform for delivering siRNAs into the target cancer cells and provide greater advantages depending on the type of cancers. These include unique physico-chemical properties, high biocompatibility, improved pharmacokinetics and pharmacodynamics properties and active intracellular delivery in contrast to organic ones [12–15]. NPs-based drug delivery systems responsive to acidic pH, hypoxia and hyperthermia have added a new dimension to cancer gene therapy, offering enhanced diffusion, increased cellular uptake and rapid intracellular drug release from cargo via the early endosomal escape mechanisms [16–21]. The relatively lower pH of tumor extracellular compartments along with intracellular acidic endosomes has been capitalized to develop NPs that trigger release of drugs before or after entering the tumor cells [22,23]. Few pH-sensitive organic NPs like micelles [24,25], liposomes [26], chitosan-silica nanospheres [27] and polymeric nanoparticles [28] have been utilized in facilitating tumor-specific release of several anticancer drugs following delivery *in vivo*. Although organic NPs exert tumor inhibitory effects in mice, manufacturing difficulties, poor biocompatibility and poor drug loading capabilities limit their overall success rate. Recently inorganic pH-sensitive carbonate apatite NPs were shown to significantly and specifically carry both small molecular anticancer drugs and nucleic acids to cancer cells [29–33].

ROS1 which belongs to a family of receptor tyrosin kinases (RTKs) plays a vital role in growth and differentiation of normal cells, and in the development and progression of different cancers. The chromosomal rearrangement in a variety of cancers activates the ROS1 proto-oncogene, causing cellular transformation. The aberrant expression of ROS1 is implicated in a variety of cancers including lung cancer [34] and breast cancers [35]. On the other hand, epidermal growth factor receptor (EGFR), which belongs to another family of RTKs lies at the head of a complex transduction cascade, modulating cell proliferation, survival, adhesion, migration and differentiation. With extracellular ligand binding domain, EGFR protects cancer cells against apoptosis and helps promote invasion and angiogenesis [36]. While growth-factor-induced EGFR signaling is essential for many normal morphogenic processes and numerous additional cellular responses, the aberrant activity of the receptor family has been shown to play a key role in the development and growth of tumor cells. Epidermal growth factor (EGF)-like proteins and neuregulins stimulate cells to divide by activating members of the EGFR family, which consists of the EGFR itself and the receptors known as HER2–4. It has been reported that expression level of EGFR is relatively high in TNBC (triple-negative breast cancer) with gene amplification in approximately 25% cases of TNBC [37,38]. Thus, silencing overexpressed ROS1 and EGFR could be a promising modality for breast cancer treatment.

Here we introduce strontium sulfite NPs (SSNs), which have an electrostatic affinity towards siRNAs and the ability to efficiently carry them into breast cancer cells. Strontium, an alkaline earth metal was found to exert pharmacological effects against osteoporosis and was used for radiotherapy for bone cancer treatment. Strontium carbonate NPs were used previously to carry the anticancer drug, etoposide into human gastric cancer cells [39]. In this article, we present an easy, simple and scalable method for synthesis of both SSNs and siRNA-SSNs complexes and demonstrate the roles of NaCl and glucose in synthesis and stabilization of Na-Glc-SSNs with more uniform size. Synthesized SSNs were characterized and their siRNA loading capability, cellular internalization, and cytotoxicity against MCF-7 breast cancer cells were evaluated. Finally, the potential of these particles in intracellular delivery of *ros1*- and *egfr1*-specific siRNAs was investigated through assessment of cytotoxicity in breast cancer cells, biodistribution study and tumor regression in a synergetic mouse model of breast cancer.

## **3.2. Materials and Methods**

### *3.2.1. Materials*

Strontium chloride ( $\text{SrCl}_2$ ), sodium sulfite ( $\text{Na}_2\text{SO}_3$ ), NaCl, D-glucose and 4-(2-hydroxyethyl)-1-piperazineethanesulfonic acid (HEPES) were obtained from Sigma-Aldrich (St Louis, MO, USA). Dulbecco's modified eagle medium (DMEM), dimethyl sulfoxide (DMSO), thiazolyl blue tetrazolium bromide (MTT), and ethylene diamine

tetra acetic acid (EDTA) were purchased from Sigma-Aldrich (St. Louis, MO, USA). DMEM powder, fetal bovine serum (FBS), trypsin-ethylene diamine tetra acetate (trypsin-EDTA), and penicillin-streptomycin were from Gibco BRL (CA). All siRNAs used in this study were obtained from Qiagen (Hilden, Germany) and dissolved in RNase-free water provided by the company. MCF-7 cells were originally from ATCC (Manassas, VA, USA).

### *3.2.2. Cell Culture and Seeding*

Human breast cancer cell line, MCF-7 was cultured in a 25 cm<sup>2</sup> culture flask with complete DMEM (pH 7.4) supplemented with 10% heat-inactivated fetal bovine serum (FBS), 1% HEPES and 1% penicillin-streptomycin solution in a humidified atmosphere containing 5% CO<sub>2</sub> at 37 °C. The cells from the exponential growth phase were trypsinized and seeded at 50,000 cells per well into a 24-well plate.

### *3.2.3. Synthesis of SSNs and Na-Glc-SSNs*

SSNs and Na-Glc-SSNs were prepared by adding 1–5 µL of a cation providing salt, SrCl<sub>2</sub> (1 M) without or with 300 mM of NaCl and 200 mM of D-glucose into an anion providing salt, Na<sub>2</sub>SO<sub>3</sub> (1 M) and incubating at 37 °C for 30 min. Subsequently, 10% FBS supplemented DMEM (pH 7.5) medium was added to top up to 1 mL of final particle suspension. Spectrophotometric analysis was done at 320 nm wavelength to measure turbidity of SSNs, Na-SSNs (prepared in the presence of NaCl), Glc-SSNs (prepared in the presence of glucose) and Na-Glc-SSNs (prepared in the presence of both NaCl and glucose) by using UV 1800 Spectrophotometer, Shimadzu, Japan. Microscopic observations of Na-Glc-SSN nanoparticles were made by using an Olympus Microscope CKX41. All experiments were conducted at room temperature and the data was plotted into a graph with mean ± SD.

### *3.2.4. Particle Size, Zeta Potential Measurements and Observation of SSNs and Na-Glc-SSNs*

Size of the NPs was measured by using Zeta sizer (Nano ZS, Malvern, Worcestershire, UK) in different SrCl<sub>2</sub> concentrations with or without NaCl (300 mM) and glucose (200 mM). A refractive index (RI) of 1.325 was used to measure particle size and particle size distribution. The zeta potential of SSNs, Na-SSN, Glc-SSN and Na-Glc-SSN were also measured by using Zeta sizer (Nano ZS, Malvern, Worcestershire, UK). Zetasizer software 6.20 was employed to carry out the analysis of data and all samples were measured in triplicate. The data was plotted into a graph with mean ± SD.

### *3.2.5. Characterization of Particles by a Field Emission Scanning Electron Microscope (FE-SEM) and an Energy Dispersive X-ray (EDX) Analyzer*

The morphology of SSNs and Na-Glc-SSNs was observed by using FE-SEM. SSNs and Na-Glc-SSNs prepared by adding 60 mM of  $\text{SrCl}_2$ , with or without 300 mM of NaCl, 200 mM of D-glucose to 10 mM of  $\text{Na}_2\text{SO}_3$ . 3  $\mu\text{L}$  of particle suspension was then transferred to a glass slide for drying at  $37^\circ\text{C}$  for 1 hour. The dried sample was then placed onto a carbon tape-coated sample holder, followed by platinum sputtering of the dried samples with 30 mA sputter current at 2.30 tooling factor for 70 s and the sputtered particles were visualized at 5.00 kV using FE-SEM (Hitachi/SU8010, Tokyo, Japan) and analyzed for elemental composition by an EDX analyzer (X-max, 50 mm<sup>2</sup> HORIBA, JAPAN).

### *3.2.6. Characterization of NPs by Fourier Transform Infrared Spectroscopy (FT-IR) and X-Ray Diffraction (XRD)*

Na-Glc-SSNs and SSNs were prepared by addition of 60 mM of  $\text{SrCl}_2$ , with or without 300 mM of NaCl, 200 mM of D-glucose to 10 mM of  $\text{Na}_2\text{SO}_3$  and centrifuged at 3750 rpm for 30 min by using Allegra X-12 Centrifuge (Beckman Coulter, Fullerton, CA, USA), followed by removal of supernatant and re-centrifugation. Precipitated pellets were lyophilized by using a freeze dryer (Labconco, Kansas City, MO, USA). The spectrum of SSN and Na-Glc-SSN was observed by Varian FTIR using the Varian Resolution Pro 640 software (Agilent, Santa Clara, CA, USA) and XRD (inXitu, Mountain view, CA, USA).

### *3.2.7. Acid Dissolution Study of SSNs and Na-Glc-SSNs*

SSNs were prepared by mixing 60 mM of  $\text{SrCl}_2$  and 10 mM of  $\text{Na}_2\text{SO}_3$  and Na-Glc-SSNs were prepared by the addition of 60 mM of  $\text{SrCl}_2$ , 300 mM of NaCl, 200 mM of D-glucose and 10 mM of  $\text{Na}_2\text{SO}_3$ , followed by incubation for 30 min at  $37^\circ\text{C}$ . After the incubation, DMEM of different pHs was added to make the final volume 1 mL. The different pHs were adjusted by using 1 N HCl and the absorbance was measured at 320 nm wavelength by using a spectrophotometer. Experiments were done in triplicate and the data were plotted with mean  $\pm$  SD.

### *3.2.8. Assessment of siRNA Binding Affinity to Particles*

Different concentrations of AF 488 allstars negative siRNA were dissolved in 200  $\mu\text{L}$  of DMEM and fluorescence intensity was measured with a  $\lambda_{\text{ex}} = 490 \text{ nm}$  and  $\lambda_{\text{em}} = 535 \text{ nm}$  by using 2030 multilabel reader victor TM X5 (Perkin Elmer, MA, CA, USA). Data was analyzed by Perkin Elmer 2030 manager software. Each experiment was done in triplicate and a standard curve was obtained by plotting fluorescence intensity versus siRNA concentrations to calculate the amount of siRNA bound to the NPs. SSNs, Na-SSNs (prepared in the presence of NaCl), Glc-SSNs (prepared in the presence of Glucose) and Na-Glc-SSNs were prepared by addition of 60 mM of  $\text{SrCl}_2$ , 300 mM of NaCl, 200 mM of D-glucose to 10 mM of  $\text{Na}_2\text{SO}_3$  in presence of 10 nM of AF 488 siRNA and incubating for 30 min at  $37^\circ\text{C}$ . After the samples were centrifuged at 13,000 rpm for 15 min at  $4^\circ\text{C}$ ,

the supernatant was collected and fluorescence intensity measurement. The binding affinity of siRNA to differently formulated NPs was calculated by using the following formula:

$$\% \text{ of siRNA binding} = \frac{X_{\text{initial}} - X_{\text{free}}}{X_{\text{initial}}} \times 100\%$$

Where  $X_{\text{free}}$  is the concentrations of siRNA in the supernatant following centrifugation of NPs-siRNA, and  $X_{\text{initial}}$  denotes the total concentration of siRNA used in the experiment, which was 10 nM. The samples were prepared in duplicate and represented as mean  $\pm$  SD.

### 3.2.9. Cellular Uptake of siRNA-Loaded NPs

MCF-7 cells were seeded in a 24-well plate (50,000 cells/well), incubated overnight and treated with the NPs formulated with 10 nM of AF 488 siRNA for observing cellular uptake of NPs-siRNA complexes. SSNs, Na-SSNs, Glc-SSNs and Na-Glc-SSNs were prepared as described above, through incubation for 30 min at 37 °C. After 4 h and 12 h of incubation, the treated cells were washed with 5 mM of EDTA in PBS for dissolving extracellular particles and observed under a fluorescence microscope (Olympus DP73, Tokyo, Japan).

Additionally, treated cells after 4 and 12 h were washed with PBS, treated with 5 mM EDTA in PBS and lysed before fluorescence intensity of the lysate was measured in 2030 multilabel reader victor™ X5 (Perkin Elmer) attached with Perkin Elmer 2030 manager software using an excitation wavelength of 490 nm and an emission wavelength of 535 nm. Samples were blank corrected using untreated samples. The experiment was completed in duplicate and expressed as mean  $\pm$  SD.

### 3.2.10. Cell Viability Assay with MTT (3-(4,5-Dimethylthiazol-2-yl)-2,5-Diphenyltetrazolium Bromide)

Cytotoxicity of SSN, Na-SSN, Glc-SSN and Na-Glc-SSN in MCF-7 cells was assessed by MTT assay.  $5 \times 10^4$  cells were seeded in a 24-well plate in triplicate. On the following day, the cells were incubated with SSNs, Na-SSNs, Glc-SSNs and NA-Glc-SSNs for 48 h and MTT assay was conducted. Briefly, 50  $\mu$ L of MTT (5 mg/mL in PBS) was added to each well and incubated for 4 h. After dissolving the resulting formazan products with 300  $\mu$ L of DMSO (dimethyl sulfoxide), the absorbance was analyzed on a microplate reader (microplate spectrophotometer, Biorad, Hercules, CA, USA) at 595 nm wavelength with reference to 630 nm.

Cytotoxic effects of SSNs- and Na-Glc-SSNs-bound EGFR and ROS1 siRNAs in MCF-7 cells were also assessed by MTT assay. The siRNAs-loaded SSNs and Na-Glc-SSNs were prepared by adding 60 mM of  $\text{SrCl}_2$ , without or with 300 mM of NaCl and 200 mM of D-glucose to 10mM of  $\text{Na}_2\text{SO}_3$  and 1 nM of the respective siRNA and incubating for 30 min

at 37 °C. The particle suspension was finally topped up to 1 mL with 10% FBS-containing DMEM (pH 7.5).  $5 \times 10^4$  cells were seeded in a 24-well plate. On the following day, the cells were treated with SSNs, SSNs-EGFR siRNA, SSN-ROS1, Na-Glc-SSN, Na-Glc-SSN-EGFR and Na-Glc-SSN-ROS1, followed by incubation for 48 h, and finally, cytotoxicity was measured. Briefly, 50  $\mu$ L of MTT (5 mg/mL in PBS) was added to each well prior to incubation of the plate for 4 h. After dissolving the resulting formazan crystals with 300  $\mu$ L of DMSO (dimethyl sulfoxide), the absorbance was analyzed on a microplate reader (microplate spectrophotometer, Biorad, Hercules, CA, USA) at 595 nm wavelength with reference to 630 nm. The percent of metabolically active cells (CV) was calculated for treated samples using the following equation:

$$\% \text{ cell viability} = \frac{\text{Absorbance of treated sample}}{\text{Absorbance of control}} \times 100\%$$

All the experiments were done in triplicate and the data was plotted as % of cell viability with mean  $\pm$  SD.

### 3.2.11. *In-Solution Digestion of SSN and Na-Glc-SSN Protein Corona for Mass Spectrometric Analysis*

SSNs and Na-Glc-SSNs were prepared by adding 60 mM of  $\text{SrCl}_2$ , with or without 300 mM of NaCl, 200 mM of D-glucose to 10mM of  $\text{Na}_2\text{SO}_3$  and incubating for 30 min at 37 °C, and subjected to additional incubation with mouse plasma (10%) for 15 min at 37 °C. After centrifugation of the particle suspensions at 13,000 RPM for 15 min, the supernatants were discarded, and the pellets were washed in Milli Q water, followed by centrifugation and removal of the supernatants. The pellets were dissolved with 100  $\mu$ L of 50 mM EDTA in  $\text{H}_2\text{O}$ . 25  $\mu$ L of 100 mM ammonium bicarbonate solution, 25  $\mu$ L tetrafluoroethylene (TFE) denaturing agent and 1  $\mu$ L of 200 mM dithiothreitol (DTT) solution were added to the protein mixture (released from pellets), followed by vortexing and heating under a heating block at 60 °C for 1 h. After adding 4  $\mu$ L of 200 mM iodoacetamide (IAM) and briefly vortexing, the protein mixture (representing protein corona) was incubated in the dark at room temperature for 1 h. 1  $\mu$ L of 200 mM DTT solution was added to the protein mixture which was then incubated in the dark at room temperature for 1 h. Afterwards, the treated protein mixture was incubated at room temperature in presence of 100  $\mu$ L ammonium bicarbonate solution (100 mM) and MS Grade 25  $\mu$ L of Trypsin (1  $\mu$ g/mL) at 37 °C for 4 to 18 h. Finally, 1 $\mu$ L formic acid was added to stop the reaction, and the samples were subjected to speed vacuum overnight prior to analysis by Q-TOF LC-MS/MS.

### 3.2.12. *Sample Preparation for Mass Spectrometry-Based Proteomics*

10  $\mu$ L of formic acid (0.1%) in water was added to dissolve dry peptide digest. Samples were then sonicated in ultrasonic water bath for 10 min, while maintaining room



temperature using ice. Samples were centrifuged (14,000× g, 5 min) and 5 µL of supernatant was placed in MS tube before being directly transferred on LC-QTOF auto-sampler for analysis.

### *3.2.13. High Efficiency Nanoflow Liquid Chromatography Electrospray-Ionization Coupled with Mass Spectrometry*

The peptides digested were loaded into an Agilent Poroshell 300 Å pore C18 columns (Agilent, Santa Clara, CA, USA) using 0.1% formic acid mobile phase to equilibrate the column. The peptides were eluted from the column with 90% acetonitrile in 0.1% formic acid (solution B), using the gradients of 5% solution B over 0–30 min and 75% solution B over 30–39 min. Quadrupole-time of flight (Q-TOF) polarity was set at positive with capillary and fragmented voltage being set at 1750 V and 360 V, respectively, and 5 L/min of gas flow with a temperature of 325 °C. The peptide spectrum was analyzed in auto MS mode ranging from 110–3000 m/z for MS scan and 50–3000 m/z for MS/MS scan. Acquisition rates were 2 (spectra/s) for MS and 4 (spectra/s) for MS/MS. The spectrum was then analyzed with Agilent MassHunter (Agilent Technologies, Santa Clara, CA, USA) data acquisition software and then PEAKS 8.0 software (Bioinformatics Solutions Inc., Waterloo, ON, Canada).

### *3.2.14. Protein Identification and Quantification by Automated De Novo Sequencing (PEAKS Studio 8.0)*

Protein identification was performed by integrating a database search (SwissProt.Mus\_musculus) with de novo sequencing, for the homology search using PEAKS Studio 8.0 (Bioinformatics Solution Inc., Waterloo, ON, Canada). Carbamidomethylation was set as the fixed modification with maximum mixed cleavages at 3. Parent mass and fragment mass error tolerance were both set 0.1 Da with monoisotopic mass as the precursor mass search type. Trypsin was selected as the enzyme for digestion. False discovery rate (FDR) of 1% and unique peptides ≥1 were used for filtering out inaccurate proteins. A-10lgP score of greater than 20 indicates that detected proteins are relatively high in confidence as it targets very few decoy matches above that threshold. Relative differential changes of proteins commonly found in different complex protein samples of SSNs were quantified using PEAKS Q protein quantification software. Label free quantification method is based on the relative intensities of peptide ion peak features detected in multiple samples. Feature detection is performed separately on each sample with more overlapped features, by using the EM (expectation-maximization) algorithm. The features of the same peptide from different samples are reliably aligned together using a high-performance retention time alignment algorithm. The groups are color-coded to be used in the heat map summary to distinguish the groups between two NPs and the intensity of a quantifiable peptide. The significance

of a peptide is denoted by its  $-10\text{LogP}$  score. The cut off value was set at 20 which is equivalent to a P-value of 0.01. Heat Map displays the protein groups that passed the filters for quantitative analysis. The relative protein abundance is represented as a heat map of the representative proteins of each protein group. The representative proteins are clustered if they exhibit a similar expression trend across the samples. The hierarchical clustering is generated using a neighbor-joining algorithm with a Euclidean distance similarity measurement of the  $\log_2$  ratios of the abundance of each sample relative to the average abundance.

### *3.2.15. In Vivo Biodistribution Study of SSNs and Na-Glc-SSNs*

For biodistribution study, female Balb/c mice (6–8 weeks old) of 20–25 gm of body weights were obtained from the School of Medicine and Health Science Animal Facility, Monash University. The mice were maintained in 12:12 light: dark conditions and provided with *ab libitum* and water. All the experiments were done in accordance with the protocol approved by MONASH Animal Ethics Committee (MARF/2016/126). Approximately  $1 \times 10^5$  4T1 cells (in 180  $\mu\text{L}$  PBS) were injected subcutaneously on the mammary pad of mice (considered as day 1) and the mice were checked regularly for the outgrowth of tumor by touching the area of injection by index finger. The tumor bearing mice were administered with fluorescent AF-488 labeled neg. siRNA (75 mM) either in free or NPs-bound form through tail vein injection when the tumor volume reached 79  $\text{mm}^3$ . Mice were sacrificed humanely by cervical dislocation after 4 or 24 h of the administration. Afterwards, the heart, liver, kidney, spleen, lung, brain and tumor were collected and washed twice in chilled PBS, followed by addition of 500  $\mu\text{L}$  lysis buffer per 500 mg of tissue mass. Tissues were lysed using a mechanical homogenizer with four strokes intermittently while maintaining the samples on ice till a completely homogenized solution was obtained. The solutions of tissue lysates were centrifuged for 25 min at 4 °C with 8000 rpm. 200  $\mu\text{L}$  of the supernatant was added to each well of a 96-well opti-plate (Nunc) for measuring fluorescence intensity of AF-488 labeled siRNA with 2030 multilabel reader vitor<sup>TM</sup> X5 (Perkin Elmer) attached with Perkin Elmer 2030 manager software using  $\lambda_{\text{ex}} = 490 \text{ nm}$  and  $\lambda_{\text{em}} = 535 \text{ nm}$ . Data were represented as mean  $\pm$  SEM of fluorescence intensity/500 mg of tissue mass after the values were blank-corrected using an untreated group of mice for each tissue.

### *3.2.16. 4T1-Induced Mouse Model of Breast Cancer and Anti-Tumor Activity of siRNA-Loaded NPs*

Female Balb/c mice (6–8 weeks old) with body weights of 20–25 gm (obtained from the School of Medicine and Health Science Animal Facility, Monash University) were maintained in 12:12 light:dark conditions and provided with *ab libitum* and water. All the experiments were done in accordance with the protocol approved by MONASH

Animal Ethics Committee (MARF/2016/126). Approximately  $1 \times 10^5$  4T1 cells (in 100  $\mu$ L PBS) were injected subcutaneously on the mammary pad. When the volume of the growing tumor reached an average of 39 mm<sup>3</sup> at around Day 9–10, mice were grouped randomly with 4 mice per group and treated intravenously (tail-vein) at the right or left caudal vein, while the second dose was administered 3 days after the 1st dose. The length and width of tumor outgrowth were estimated using the Vernier caliper in mm scale over the period of 24 days, with the data subsequently presented as mean  $\pm$  SEM of the tumor volumes of each group. The volume of the tumor was calculated based on the following formula:

$$\text{Tumor Volume (mm}^3\text{)} = \frac{1}{2} (\text{length} \times \text{width}^2).$$

### 3.2.17. Statistical Analysis

Statistical analysis was done by using SPSS version 23 (Armonk, NY, USA). LSD post hoc test for one way ANOVA and independent-samples *t*-test were used for analyzing in vitro and in vivo data and comparing the significant difference. Data were considered statistically significant when  $*p < 0.05$  and very significant when  $**p < 0.001$ .

## 3.3. Results and Discussion

### 3.3.1. Generation of SSNs and Evaluating Effects of NaCl and Glucose on Regulation of Particle Growth

SSNs were synthesized by mixing different concentrations of SrCl<sub>2</sub> (20–100 mM) and 10 mM of Na<sub>2</sub>SO<sub>3</sub> and incubating at 37 °C for 30 min, followed by addition of 10% FBS-supplemented DMEM (pH 7.5) to make the final volume to 1 mL. The particles were characterized by UV-VIS spectrophotometer and optical image analysis. The increment of reactant concentration leads to higher rates of particle formation, and consequential self-aggregation to form bigger size particles. Since DMEM contains high concentrations of NaCl and glucose, it is necessary to identify their roles in particle growth and stabilization of particle size. Particles with diameters ranging from 20 to 200 nm are supposed to have excellent tumor accumulation capacity and higher circulation time [40–43]. To investigate the effects of NaCl and glucose on SSNs formation, we added 300 mM of NaCl and 200 mM of glucose to form Na-SSNs, Glc-SSNs and Na-Glc-SSNs. As shown in Figure 1A, particle formation was enhanced with increasing Sr<sup>2+</sup> concentration, as represented by high turbidity. However, when we added 300 mM of NaCl to form Na-SSN particles, a significant drop in turbidity was observed for all Sr<sup>2+</sup> concentrations. This could be achieved by minimizing charges via temporary ionic interaction between the SrSO<sub>3</sub> and NaCl, thereby slowing down the rate of reaction for particle formation. On the other hand, addition of D-glucose also significantly decreased the growth of particles as demonstrated by lower turbidity in Figure 1A, suggesting that glucose could shield the particles, impeding the interactions between the particles for subsequent growth.

However, addition of NaCl and glucose to form Na-Glc-SSNs demonstrated lower turbidity in comparison to either Na-SSNs or Glc-SSNs, indicating that the combination of NaCl and glucose could effectively reduce and stabilize particle growth by controlling particle aggregation. Optical microscopic visualization of Na-Glc-SSNs following incubation at 37 °C for 1h in a 24-well plate showed an increasing number of aggregated particles with increasing  $\text{Sr}^{2+}$  concentrations (Figure 1B), in parallel with the increase in absorbance (Figure 1A).

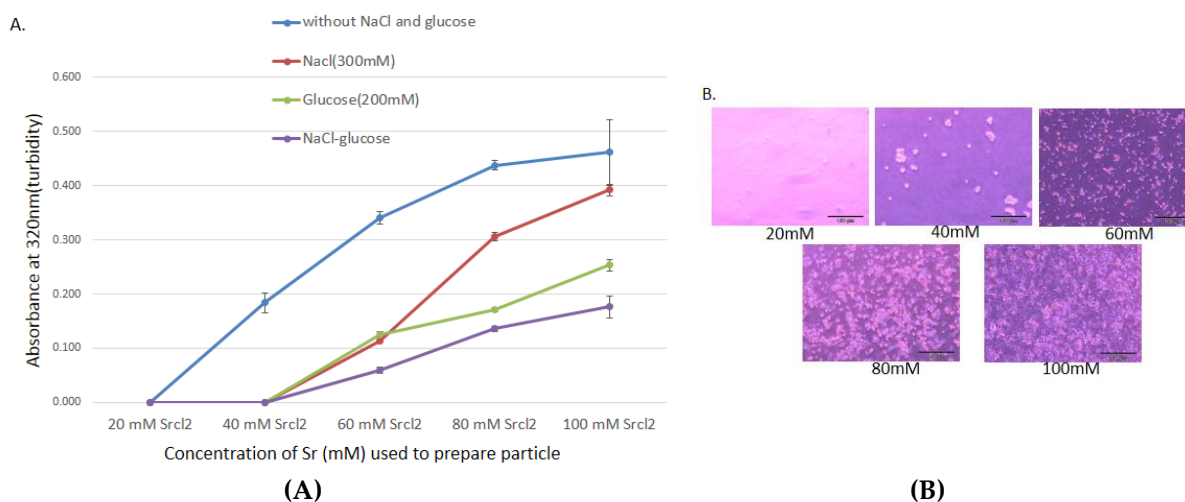
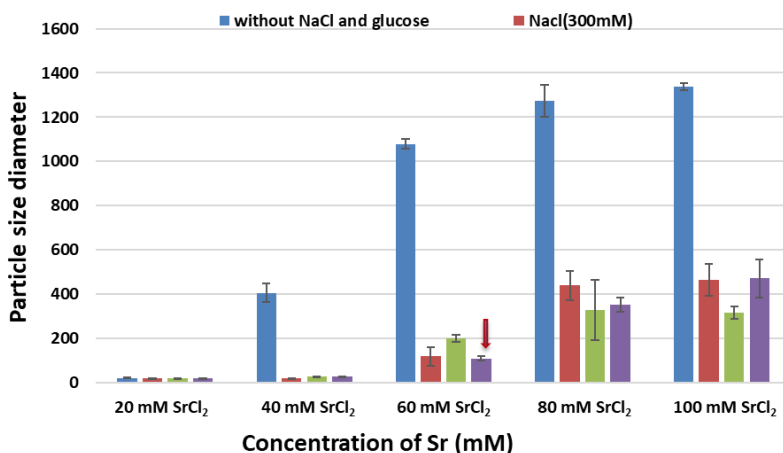


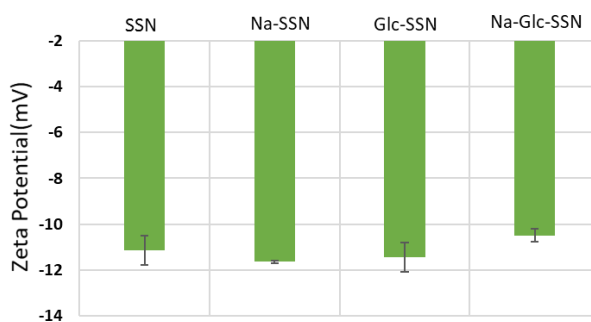
**Figure 1. (A).** Turbidity and optical microscopic analysis of differently formulated NPs. A. Turbidity (absorbance at 320 nm) of the particles formed without and with NaCl and/or glucose. Particles were formed by addition of 1–5  $\mu\text{L}$  of (1M)  $\text{SrCl}_2$  to 0.5  $\mu\text{L}$  of (1M)  $\text{Na}_2\text{SO}_3$  in 50  $\mu\text{L}$  aqueous solution with or without inclusion of 25  $\mu\text{L}$  of NaCl (0.5 M) and/or 10  $\mu\text{L}$  of D-glucose (1M), and incubation for 30 minutes at 37 °C. Subsequently, serum-supplemented DMEM media was added to achieve 1 mL particle suspension. Absorbance at 320 nm wavelength was measured for all generated NPs using a spectrophotometer. (B). Microscopic observation of Na-Glc-SSNs prepared at different  $\text{Sr}^{2+}$  concentrations, and images were captured at 10X resolution.

Since particle diameter is crucial in regulating pharmacokinetics and tumor targeting of particle-loaded therapeutics, we measured the average particle size by Zetasizer and investigated the effects of NaCl and glucose in the stabilization of particle diameter. As shown in Figure 2, the average size of SSNs without NaCl and glucose ranged from 20 nm to 1.3  $\mu\text{m}$ , with a trend of forming larger particle with increasing  $\text{Sr}^{2+}$  concentrations, while addition of NaCl and glucose to the reaction mixture reduced the particle sizes of SSNs (i.e. Na-Glc-SSNs), which varied from 20 nm to 463 nm depending on the concentration of  $\text{SrCl}_2$  in a similar trend as in the turbidity study (Figure 2A). The surface charge of NPs is crucial for stability in systemic circulation, cellular uptake and successful delivery of drug into the target tumor cytoplasm. The zeta potential of SSNs, Na-SSNs and Glc-SSNs were almost same and remained in the range of -10.7 mV to -11.9 mV,

whereas incorporation of NaCl and glucose into the SSNs slightly reduced the zeta potential ( $-10.5$ ). The combination of NaCl and glucose reduced the size and stabilized the growth of Na-Glc-SSN more significantly than SSNs formed without NaCl and glucose. We propose that NaCl prevents particle aggregation by temporary binding with  $\text{SrSO}_3$  particles through its cations ( $\text{Na}^+$ ) and anions ( $\text{Cl}^-$ ) (Figure 3A), whereas glucose may be partitioned between the particles, thereby producing less aggregated and small sized particles (Figure 3B).



(A)



(B)

**Figure 2.** Size (A) and zeta potential (B) of different strontium sulfite nanoparticles with or without NaCl and glucose. Strontium sulfite nanoparticles were prepared by adding 60 mM of  $\text{SrCl}_2$ , 300 mM of NaCl, 200 mM of glucose and fixed amount of  $\text{Na}_2\text{SO}_3$ .

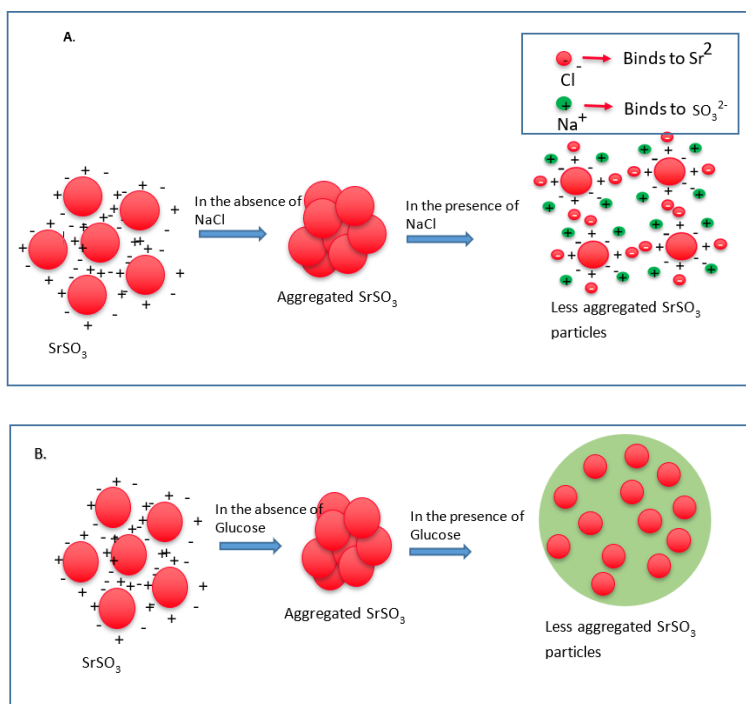
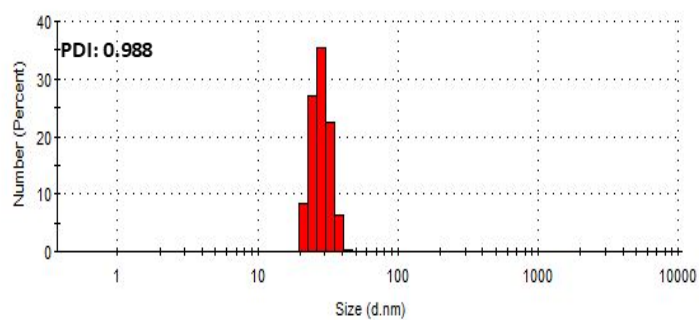


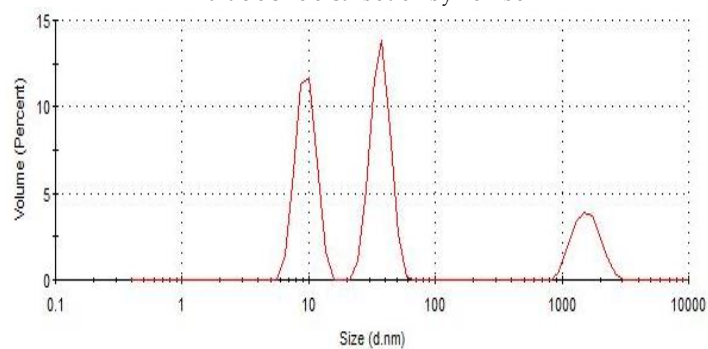
**Figure 3.** Schematic representation of effects of NaCl and glucose in stabilization of  $\text{SrSO}_3$  particles. A.  $\text{SrSO}_3$  particles stick to each other to form aggregates, while NaCl slows down the particle formation by temporally binding with  $\text{Sr}^{2+}$  and  $\text{SO}_3^{2-}$ . B. Without D-glucose,  $\text{SrSO}_3$  particles bind to each other forming large particles, but glucose lies between the particles and forms a shield to prevent particle-particle agglomeration.

### 3.3.2. Characterization of SSNs and Na-Glc-SSNs by Zeta Sizer

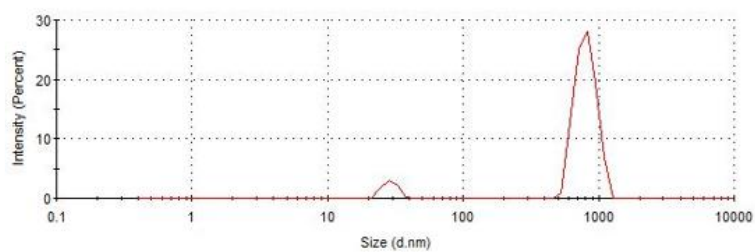
Zeta Sizer was used to investigate the particle size distribution of SSNs and Na-Glc-SSNs. The PDI (poly dispersing index) value was measured to know the dispersion homogeneity of the particles. As shown in Figure 4A, the PDI value of SSN particles was 0.988, indicating the heterogenous distribution of SSNs. Particle size distribution by number and volume also demonstrated variably sized particles. On the other hand, Na-Glc-SSNs particles formed with 60 mM of  $\text{SrCl}_2$  and 10 mM of  $\text{Na}_2\text{SO}_3$  in the presence of 300 mM of NaCl and 200 mM of glucose showed a PDI value of 0.290 (Figure 4B). The lower PDI value of Na-Glc-SSNs indicates that particle has less tendency to agglomerate and form smaller and uniformly distributed particles. Preclinical studies showed that the particles within a diameter range of 100–150 nm are able to access the liver and tumor tissues after IV administration [44]. As shown in Figure 4(B), relatively small size particles in Na-Glc-SSNs constitute the majority of the particles, suggesting that siRNA-Na-Glc-SSN complexes would have favourable pharmacokinetics and greater ability to penetrate into target cells via endocytosis more efficiently than SSN-siRNA complex.



Particle size distribution by number



Particle size distribution by volume



Particle size distribution by intensity

(A)

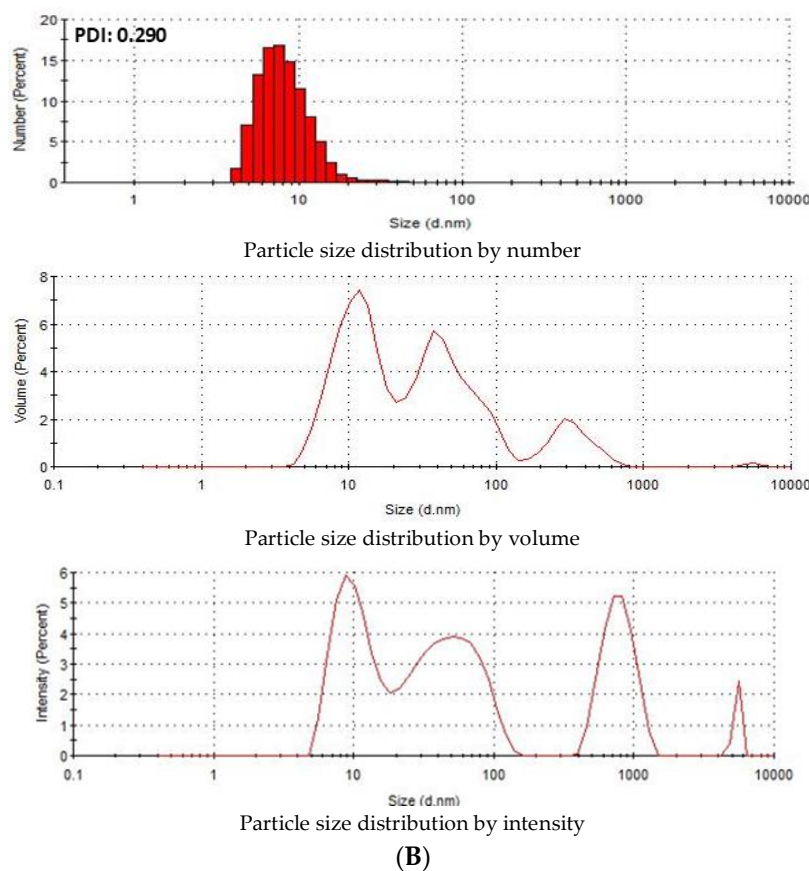
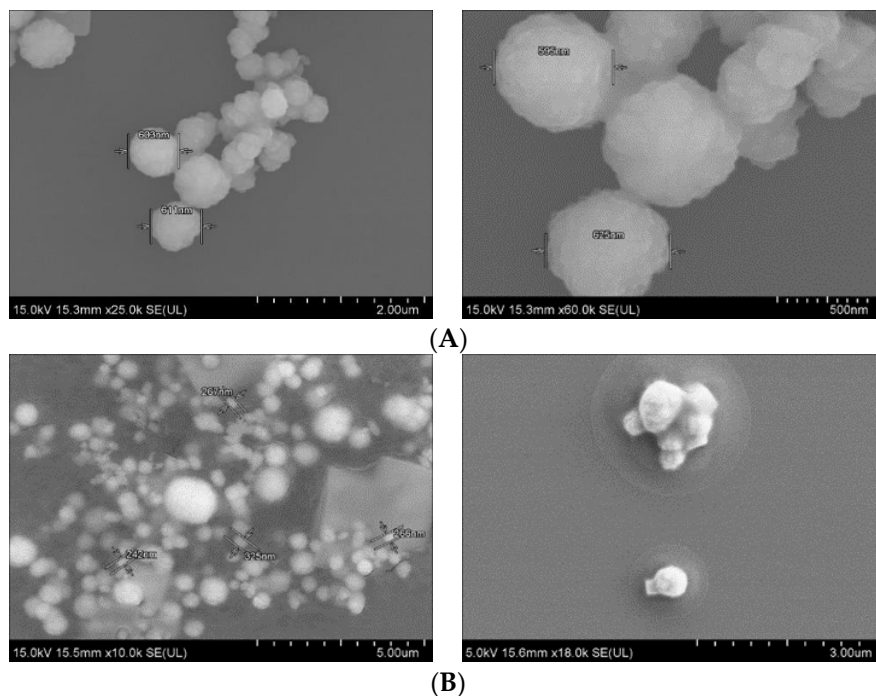


**Figure 4.** Particle size distribution of (A). SSNs and (B). Na-Glc-SSNs. SSNs and Na-Glc-SSNs were prepared by adding 60mM of  $\text{SrCl}_2$ , 300 mM of NaCl, 200 mM of glucose and 10 mM of  $\text{Na}_2\text{SO}_3$ .

### 3.3.3. Characterization of Differently Formulated Particles by FE-SEM

Field-emission scanning electron microscopy was used to observe the morphology and actual size of the particles. As shown in Figure 5(A), SSNs displayed a spherical shape with rough surface. The average diameter of the particles was in the range of 595–625nm, suggesting formation of the large particle size due to self-aggregation. On the other hand, Na-Glc-SSNs showed relatively more particles of a spherical shape with relatively smaller size distribution (242–267nm) (Figure 5(B)). The smaller particle size could be due to the effects of NaCl in stabilizing the particles by slowing down the reaction and D-glucose that lies between the particles in preventing self-aggregation. The smaller and rough surfaced SSNs were expected to demonstrate better drug binding ability as well as less protein binding affinity in systemic circulation.

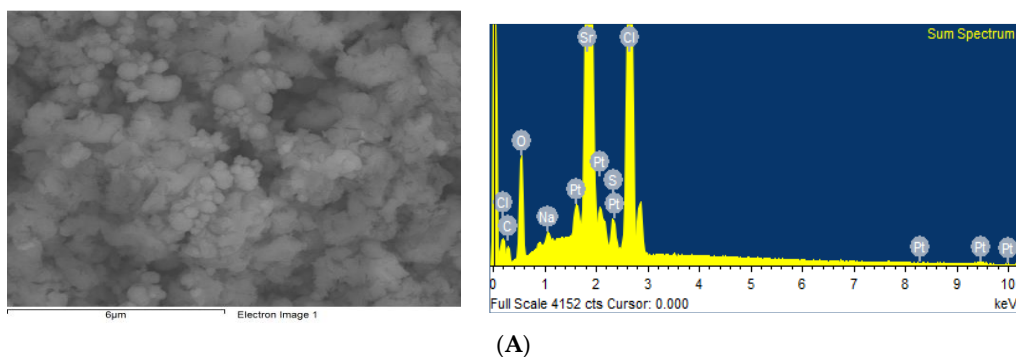


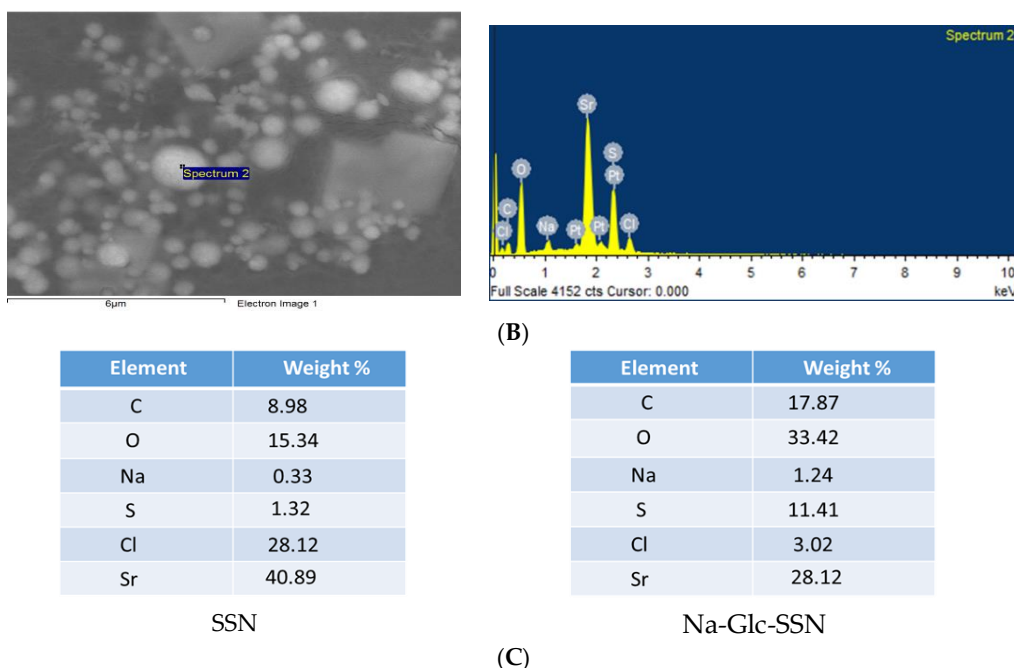


**Figure 5.** FE-SEM images of nanoparticles. (A). micrographs of SSNs at 2  $\mu\text{m}$  and 500 nm scale, (B). Micrographs of Na-Glc-SSNs at 5  $\mu\text{m}$  and 3  $\mu\text{m}$  scale.

### 3.3.4. Elemental Analysis of Nanoparticles by EDX

The EDX spectrum showed strong peaks of strontium around 2 KeV for both SSNs and Na-Glc-SSNs (Figure 6), confirming strontium as a major constituent. In addition, sulfur, oxygen and chlorine also showed peaks for both NPs with small amount of sodium, carbon, oxygen and platinum. The signals for sulfur and oxygen might originate from the sulfite group of the particles. Glucose and NaCl used in the fabrication of Na-Glc-SSNs contributed to the signals for carbon, oxygen, sodium and chloride. The other signals might come from platinum sputtering of the dried samples.

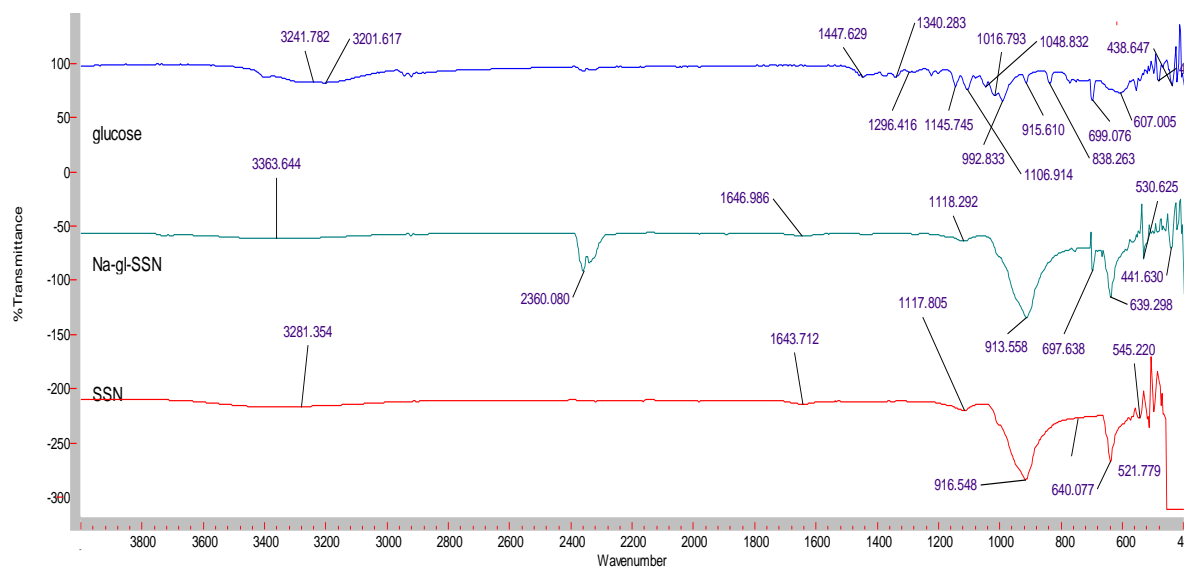




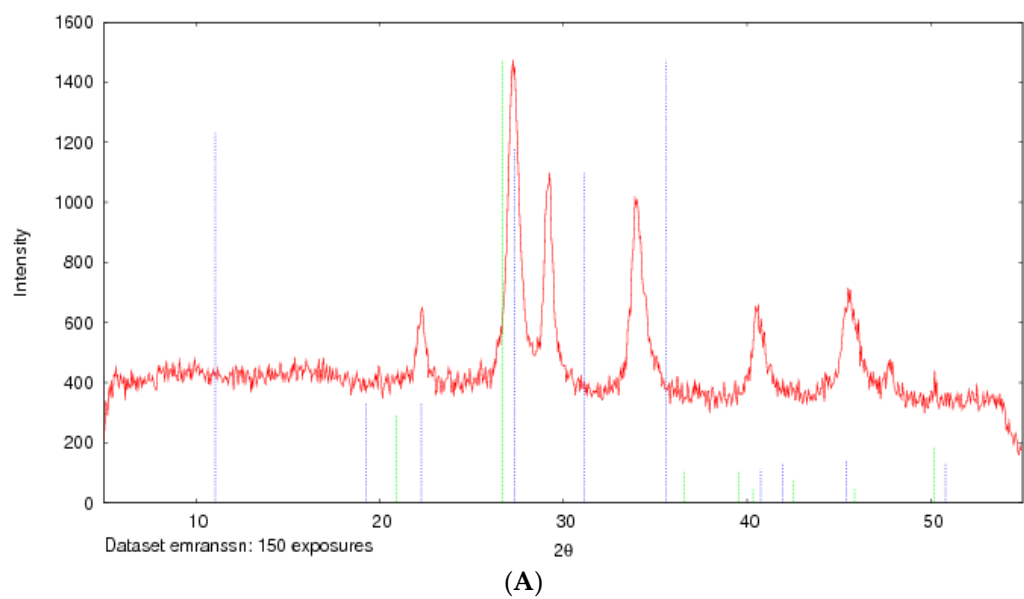
**Figure 6.** EDX analysis of nanoparticles. EDX spectrum of SSNs (A) and Na-Glc-SSNs (B) nanoparticle (C). Element weight percent of SSNs and Na-Glc-SSNs.

### 3.3.5. Characterization of SSNs and Na-Glc-SSNs by FT-IR and XRD

The formation of strontium sulfite was confirmed via FT-IR, which involves the vibration of molecules targeted via the infrared spectroscopy on the lyophilized SSNs and Na-Glc-SSNs. The FT-IR spectra of glucose, SSNs and Na-Glc-SSNs were obtained. The spectra of SSNs displayed two strong peaks at  $916\text{ cm}^{-1}$ ,  $640\text{ cm}^{-1}$  and  $521\text{ cm}^{-1}$ , which are the characteristic peaks of  $\text{SO}_3^{2-}$  (Figure 7). On the other hand, the similar peaks for  $\text{SO}_3^{2-}$  in Na-Glc-SSNs were noted at around  $913\text{ cm}^{-1}$ ,  $631\text{ cm}^{-1}$  and  $530\text{ cm}^{-1}$  with a small shift, which is probably due to the presence of strontium, NaCl and glucose. Moreover, the overall vibration pattern that is characteristic of  $\text{SrSO}_3$  strongly suggests that  $\text{SrSO}_3$  was successfully formed. The XRD peak profiles of SSNs and Na-Glc-SSN crystals were similar to the standard peak profile of  $\text{SrSO}_3$  (Figure 8). In addition, the peak broadening of the material could be indicative of its lower degree of crystallinity, an important factor determining particle dissolution rate.



**Figure 7.** FTIR spectra for free glucose, SSNs (formed using 60 mM of  $\text{SrCl}_2$  and 10 mM of  $\text{Na}_2\text{SO}_3$ ) and Na-Glc-SSNs (formed by adding 60 mM of  $\text{SrCl}_2$ , 300 mM of  $\text{NaCl}$ , 200 mM of glucose and 10 mM of  $\text{Na}_2\text{SO}_3$ ).



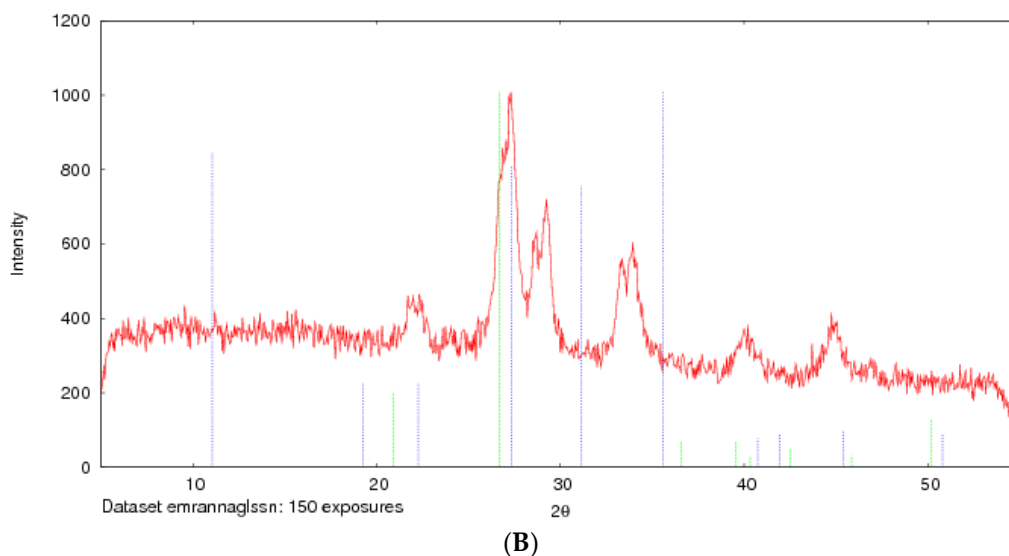


**Figure 8.** XRD patterns of SSNs (formed with 60 mM of  $\text{SrCl}_2$  and 10 mM  $\text{Na}_2\text{SO}_3$ , (A) and Na-Glc-SSNs (formed with 60 mM of  $\text{SrCl}_2$ , 300 mM of  $\text{NaCl}$ , 200 mM of glucose and 10 mM of  $\text{Na}_2\text{SO}_3$ ) (B).

### 3.3.6. Acid Dissolution Profiles of SSNs and Na-Glc-SSNs

The success of nanoparticles-mediated siRNA therapy depends on the efficient release of siRNA from the carrier in order to silence the target mRNA in cytoplasm. NPs/siRNA complex after being internalized into the cell via endocytosis should escape from endosomes as well as avoid lysosomal degradation. Particles that can be dissolved in acidic endosomes are able to release the payload from the NPs. Particle dissolution could also lead to accumulation of ions ( $\text{Ca}^{2+}$ ,  $\text{PO}_4^{3-}$  and  $\text{CO}_3^{2-}$ ) with eventual development of osmotic pressure across the endosomal membrane, which might result in endosomal breakdown and release of the therapeutics in cytosol. As shown in Figure 9, the absorbance of both SSNs and Na-Glc-SSNs was decreased sharply with a decrease in pH and at pH 6, the particle were fully degraded with an absorbance value below 0.1 nm. The result suggests that SSNs and Na-Glc-SSNs were unstable and degraded in the acidic pH, thus indicating that the particles would be dissolved in the acidic environment of endosomes to facilitate early release of siRNA.

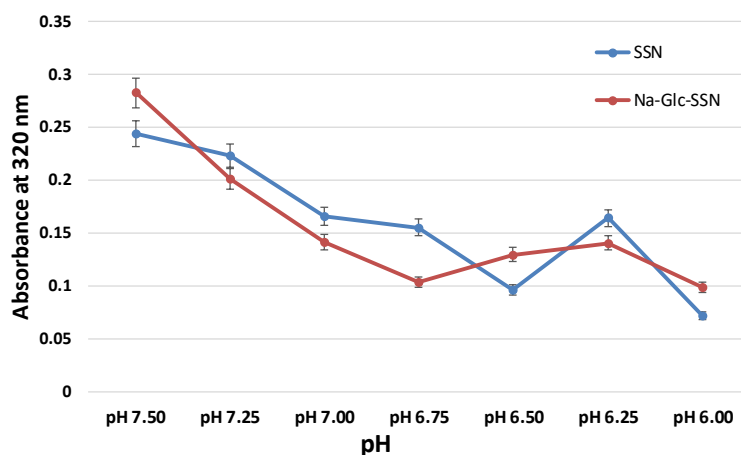


**Figure 9.** Acid dissolution profiles of SSNs, prepared by adding  $\text{SrCl}_2$  (60 mM) and  $\text{Na}_2\text{SO}_3$  (10 mM) and Na-Glc-SSNs, prepared by adding 60 mM of  $\text{SrCl}_2$ , 300 mM of NaCl, 200 mM of glucose and 10 mM of  $\text{Na}_2\text{SO}_3$ , in a 50  $\mu\text{L}$  of an aqueous solution.

### 3.3.7. Assessment of Binding Affinity of siRNA to SSNs and Na-Glc-SSNs

The binding affinity of siRNA towards nanoparticles is vital to prevent its nuclease-mediated siRNA degradation and dissociation from the particles after being exposed to blood components. siRNA, which is negatively charged due to its phosphate backbone was expected to interact with strontium sulfite nanoparticles owing to their positively charged  $\text{Sr}^{2+}$ -rich domains. As shown in Figure 10, SSNs, Na-SSNs, Glc-SSNs and Na-Glc-SSNs demonstrated significant binding affinity (ranging from 91% to 94%) towards the siRNA, suggesting that the potential ability of the nanoparticles in carrying siRNAs into cancer cells by preventing nuclease-mediated degradation and enhancing cellular uptake via endocytosis.

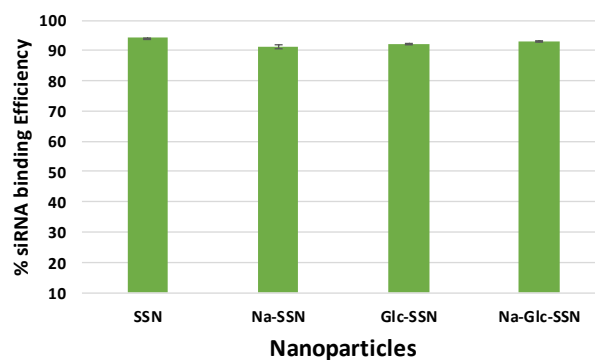


**Figure 10.** Binding efficiency of negative siRNA with differently formulated strontium sulfite particles formed by mixing  $\text{SrCl}_2$  (60 mM) and  $\text{Na}_2\text{SO}_3$  (10 mM) along with 10 nM AF488 negative siRNA in the presence or absence of NaCl (300 mM) and glucose (200 mM).

### *3.3.8. Cellular Uptake of Fluorescence-Labeled siRNA Carried by Differently Formulated Strontium Sulfite Nanoparticles*

Cellular uptake of siRNA, one of the most critical steps in regulating overall silencing efficacy is predominantly influenced by siRNA binding affinity for nanoparticles and size of the particles. The small particles are expected to have more cellular internalization in comparison to larger ones. MCF-7 cells were treated with differently formulated strontium sulfite nanoparticles for 4 h prior to removal of extracellular particles with EDTA and subsequent observation by a fluorescence microscope. After 4 h of treatment, as shown in Figure 11(A), untreated cells and cells treated with free siRNA did not show any fluorescence signals. On the other hand, cells treated with all different forms of strontium sulfite particles revealed significant fluorescence signal. However, after 12 h of treatment, cells treated with SSNs coupled siRNA gave more significant fluorescence signal as demonstrated in Figure 11(B), suggesting their efficient internalization into the breast cancer cells in extended time. The fluorescence intensity of Na-Glc-SSNs at 4 h was much higher than that of free siRNA and SSNs, as shown in Figure 12(A).

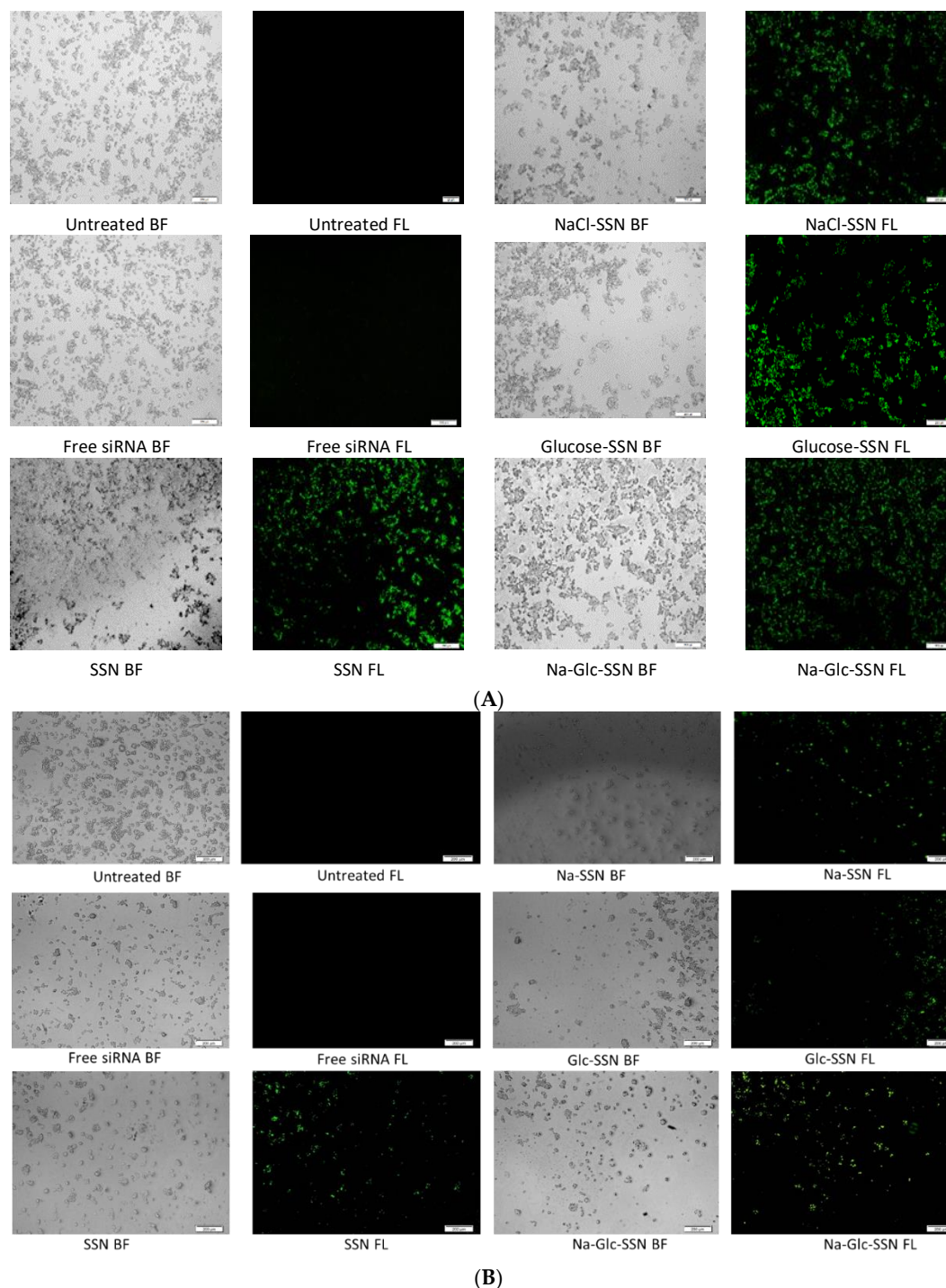


**Figure 11.** Cellular uptake of strontium sulfite particles with bound fluorescence-labeled siRNA. MCF-7 cells were treated with media (untreated), free siRNA and different strontium sulfite particles. SSNs, NaCl-SSNs, Glc-SSNs and Na-Glc-SSNs with loaded siRNA were formed by adding  $\text{SrCl}_2$  (60 mM),  $\text{Na}_2\text{SO}_3$  (10 mM) and 10 nM of AF488 negative siRNA in presence or absence of NaCl (300 mM) and/or glucose (200 mM) at (A) 4 h of treatment and (B) 12 h of treatment.

On the other hand, the fluorescence intensity of Na-Glc-SSNs at 12 h were increased over an extended period of time (Figure 12(B)). The SSNs which were prepared in the absence of NaCl and glucose, with a much bigger size than the others, seemed to mainly adhere to the cell membrane rather than going into the cells, indicating that particle size dramatically influences the cellular uptake process.

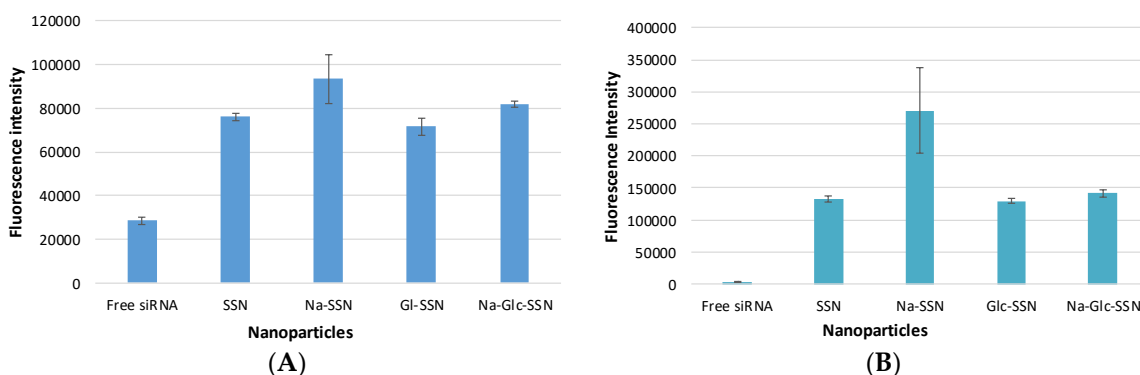


**Figure 12.** Fluorescence intensity of cell lysates. MCF-7 cells were treated with free siRNA, and NPs-siRNA formed with 60 mM of  $\text{SrCl}_2$  and 10 nM AF-488 negative control siRNA. After (A) 4 h and (B) 12 h, fluorescence intensity of cell lysates was measured. Values are representative of duplicate samples.

### 3.3.9. Cell Viability Assessment with MTT Assay

The biocompatibility of strontium sulfite nanoparticles and the extent of toxicity were assayed through MTT colorimetric assay. As shown in Figure 13, the viability of differently fabricated strontium sulfite particles was approximately 80% compared to the untreated cells, indicating that the nanoparticles are apparently biocompatible. Around 20% of cell deaths could be due to sedimentation of too many particles on the cell surface in a culture system.



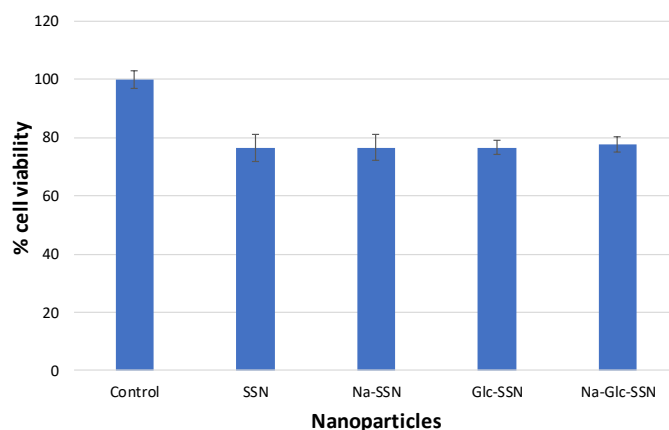


**Figure 13.** Cell viability assessment of different strontium sulfite particles formed with or without NaCl and D-glucose. MCF-7 cells were seeded and treated with SSNs (60mM SrCl<sub>2</sub> and 10 mM of Na<sub>2</sub>SO<sub>3</sub>, Na-SSN(60 mM SrCl<sub>2</sub>, 10 mM of Na<sub>2</sub>SO<sub>3</sub> and 300 mM of NaCl), Glc-SSN (60 mM SrCl<sub>2</sub>, 10 mM of Na<sub>2</sub>SO<sub>3</sub> and 200 mM of D-glucose) and Na-Glc-SSN (60 mM SrCl<sub>2</sub>, 10 mM of Na<sub>2</sub>SO<sub>3</sub>, 300 mM of NaCl and 200 mM of D-glucose).

### 3.3.10. Intracellular Delivery of EGFR and ROS1 siRNA Using SSNs and Na-Glc-SSNs

To investigate the efficiency of strontium sulfite as a nanocarrier to transport siRNA into the target tumor, we selected siRNAs to silence EGFR and ROS1 genes, which are essential in proliferating cancer cells. Epidermal growth factor (EGF) stimulates cells to divide by activating members of the EGF receptor (EGFR) family which are the members of receptor tyrosine kinases that modulate cell proliferation, survival, adhesion, migration and differentiation. Although growth-factor-induced EGFR signaling is essential for many normal morphogenic processes and cellular responses, the aberrant expression of EGFR genes in different tumor cells has been noted [45]. The product of proto-oncogene ROS1 is another member of receptor tyrosine kinases (RTKs) that regulates the initiation and progression of various types of cancers. Several chromosomal rearrangements and aberrant expression of ROS1 gene were found in acute lymphoplastic leukemia, ovarian cancer, malignant gliomas, non-small cell lung cancer and breast cancer cells [30,46–50]. Silencing of EGFR or ROS1 gene expression could be a potential treatment modality for breast cancer through suppressing cancer aggressiveness. As shown in Figure 14, while SSNs with loaded EGFR or ROS1 siRNA did not show statistically significant toxicity in comparison to SSNs treatment, Na-Glc-SSNs with the same siRNAs showed significant cytotoxicity in MCF-7 cells in comparison to Na-Glc-SSNs treatment. The high variations in viability of the cells treated with SSNs could be due to their inconsistent, strong associating with cell membrane. On the other hand, Na-Glc-SSNs, which are quite small in size showed a promising outcome following delivery of the therapeutic siRNAs.

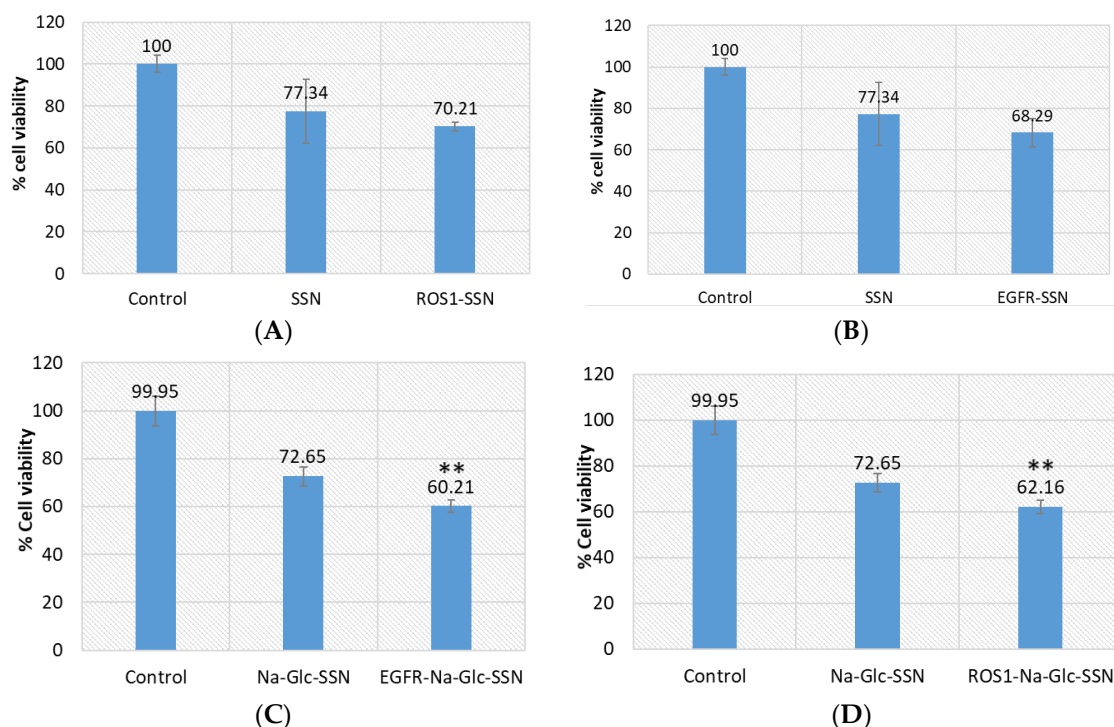


**Figure 14.** Cell viability assay following exposure of MCF-7 cells to SSNs and Na-Glc-SSNs with loaded ROS1 or EGFR siRNA. Cells were treated with particles alone and siRNA-loaded particles. SSNs and Na-Glc-SSNs were prepared by adding 60 mM SrCl<sub>2</sub>, without and with 300 mM of NaCl and 200 mM of D-glucose into 10 mM of Na<sub>2</sub>SO<sub>3</sub>. 1 nM of siRNA was used for fabrication of siRNA-loaded particles. Values are represented as % of cell viability in comparison to control for triplicate samples. (A). SSNs with loaded siRNA against ROS1. (B). SSNs with loaded siRNA against EGFR. (C). Na-Glc-SSNs with loaded siRNA against ROS1. (D). Na-Glc-SSNs with loaded siRNA against EGFR. Values were very significant (\*\*) at *p* value 0.001 to 0.01 compared to NPs treatment.

### 3.3.11. Analysis of Protein Corona Formed onto SSNs and Na-Glc-SSNs

The interactions between the proteins present in the serum and the surface of SSNs were analyzed by LC-MS/MS Q-TOP. The in-solution digestion of the protein corona formed around SSNs and Na-Glc-SSNs was carried out to detect the peptides. The peptides derived from de novo sequencing were identified as exact or homologous peptides using the Mus\_musculus database (SwissProt). The protein corona profile was characterized with the help of unique peptide, molecular weight, coverage % for peptides and significance (−10lgp). Detected proteins were listed along with their functions in Tables 1 and 2 for SSNs and Na-Glc-SSNs. Protein classification based on their biological functions was plotted in a pie chart (Figure 15).

As shown in Figure 15, SSNs prepared without NaCl and glucose possessed affinity for different types of proteins including structural proteins (different keratins, Nup205), transport proteins (albumin, oligomeric Golgi complex subunit 7), and enzymes (protein

kinases, endonucleases, glutamine synthetase), whereas SSNs prepared in the presence of glucose and NaCl showed affinity for more selective proteins, such as structural proteins (keratins) and enzymes (helicase), which could be due to the effects of Na<sup>+</sup> and Cl<sup>-</sup> ions in interfering in the weak ionic interactions of proteins with the particles. Serum albumin, the most abundant protein in the blood and a dysopsonin were detected in SSNs.

**Table 1.** Proteins bound with SSNs in the presence of 10% of mice plasma.

Protein Classes	Identified Proteins	-10lgP	Coverage	Mass	Function
Transport proteins	Albumin 1	156.86	31	68,693	chaperone binding, DNA binding, fatty acid binding, identical protein binding, oxygen binding, pyridoxal phosphate binding and toxic substance binding
Enzymes	Glutamine synthetase	38.65	4	42,019	glutamine biosynthetic process
Structural proteins	Keratin 16	32.67	1	51,606	structural constituent of cytoskeleton
Structural proteins	Keratin 16	32.67	1	51,693	structural molecule activity
Structural proteins	Keratin intermediate filament 16b	32.67	1	51,966	structural molecule activity
Structural proteins	Keratin intermediate filament 16a	32.67	1	52,053	structural molecule activity
Structural proteins	Uncharacterized protein	24.55	2	33,882	structural molecule activity
Structural proteins	Keratin 24 variant 2	24.55	2	40,994	structural molecule activity
Structural proteins	Keratin 19	24.55	2	44,542	protein-containing complex binding, structural constituent of muscle
Structural proteins	Keratin, type I cuticular Ha2	24.55	2	51,153	structural molecule activity
Structural proteins	Keratin 15, isoform CRA_a	24.55	2	49,494	scaffold protein binding, structural molecule activity
Structural proteins	Keratin, type I cytoskeletal 10	24.55	1	57,041	protein heterodimerization activity, structural constituent of epidermis
Structural proteins	Nup205	23.83	1	69,494	structural constituent of nuclear pore
Transport Proteins	Conserved oligomeric Golgi complex subunit 7	23.83	1	80,582	intracellular protein transport

Transport Proteins	Conserved oligomeric Golgi complex subunit 7	23.83	1	86,075	intracellular protein transport
Enzymes	Ercc5 protein	22.76	1	86,901	endonuclease activity, single-stranded DNA binding
Enzymes	Nek1 protein	21.82	2	48,636	ATP binding, protein serine/threonine kinase activity
Enzymes	Nek1 protein	21.82	1	133,856	ATP binding, protein kinase activity
Enzymes	Nek1 protein	21.82	1	139,659	ATP binding, protein kinase activity
Enzymes	MKIAA1901 protein	21.82	1	139,947	ATP binding, protein kinase activity
Enzymes	Nek1 protein	21.82	1	144,269	ATP binding, protein kinase activity
others	WD repeat-containing protein 81	21.82	1	211,931	mitochondrion organization

**Table 2.** Proteins bound with Na-Glc-SSNs in the presence of 10% of mice plasma.

Protein classes	Identified proteins	-10lgP	Coverage (%)	Mass	Functions
Structural proteins	Keratin, type I cytoskeletal 10	127.77	22	57,041	Protein heterodimerization activity, structural constituent of epidermis.
Structural proteins	Keratin, type II cytoskeletal 6B	112.44	9	59,526	structural molecule activity
Structural proteins	Krt6b protein	112.44	9	60,191	structural molecule activity
Structural proteins	Krt6b protein	112.44	9	60,273	structural molecule activity
Structural proteins	Keratin 77	106.07	6	61,302	structural molecule activity
Structural proteins	Keratin 77	106.07	6	61,359	structural molecule activity
Structural proteins	Keratin Kb40	69.48	2	85,239	structural molecule activity
Structural proteins	Keratin 78	69.48	1	112,265	structural molecule activity
Structural proteins	Type II cytokeratin Kb40	69.03	3	47,619	structural molecule activity
Structural proteins	Krt78 protein	63.78	3	54,765	structural molecule activity
Structural proteins	Krt78 protein	63.78	3	56,780	structural molecule activity
Structural proteins	Krt78 protein	63.78	3	54,774	structural molecule activity

Structural proteins	Keratin 15, isoform CRA_a	68.25	4	49,494	scaffold protein binding, structural molecule activity
Structural proteins	Uncharacterized protein	47.85	2	58,266	structural molecule activity
Structural proteins	Uncharacterized protein	47.85	2	58,240	structural molecule activity
Structural proteins	Keratin 90	47.85	2	58,224	structural molecule activity
Structural proteins	Krt2 protein	42.78	1	70,923	structural molecule activity
Enzymes	Eif4a1	29.17	3	33,069	ATP binding, ATP-dependent RNA helicase activity, translation initiation factor activity
Enzymes	Eukaryotic initiation factor 4A-II	29.17	3	36,166	ATP binding, ATP-dependent RNA helicase activity, translation initiation factor activity
Enzymes	Eukaryotic initiation factor 4A-II	29.17	2	41,290	ATP binding, ATP-dependent RNA helicase activity, translation initiation factor activity
Enzymes	Eif4a1	29.17	2	41,491	ATP binding, ATP-dependent RNA helicase activity, translation initiation factor activity
Enzymes	Eif4a1 protein	29.17	2	46,023	ATP binding, ATP-dependent RNA helicase activity, translation initiation factor activity
Enzymes	Eif4a1	29.17	2	46,184	ATP binding, ATP-dependent RNA helicase activity, translation initiation factor activity
Enzymes	Eif4a1	29.17	2	46,140	ATP binding, ATP-dependent RNA helicase activity, translation initiation factor activity
Enzymes	Eif4a1	29.17	2	46,154	ATP binding, ATP-dependent RNA helicase activity, translation initiation factor activity
Enzymes	Eukaryotic translation initiation factor 4A2	29.17	2	46,402	ATP binding, ATP-dependent RNA helicase activity, translation initiation factor activity

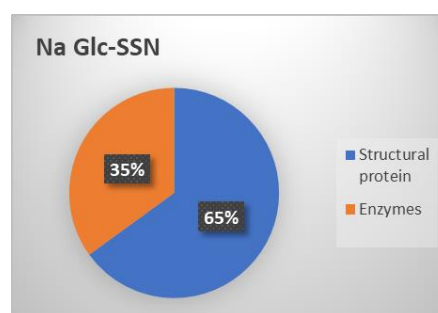
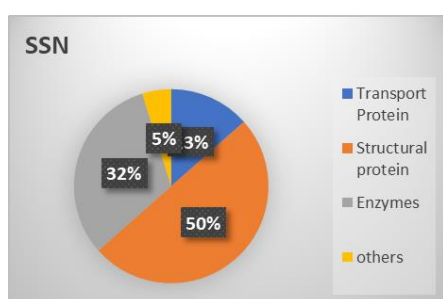


**Figure 15.** Protein corona profiling after 30 min incubation of SSNs (**left**), and Na-Glc-SSNs (**right**) with 10% of mice plasma. The detected proteins were classified based on their biological functions.

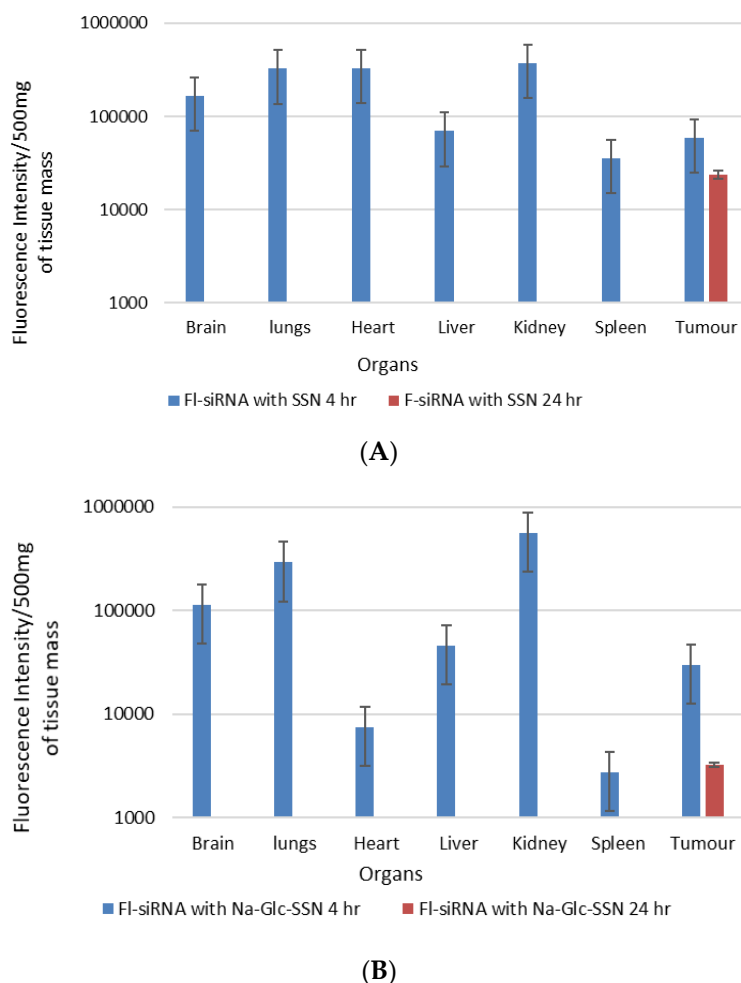
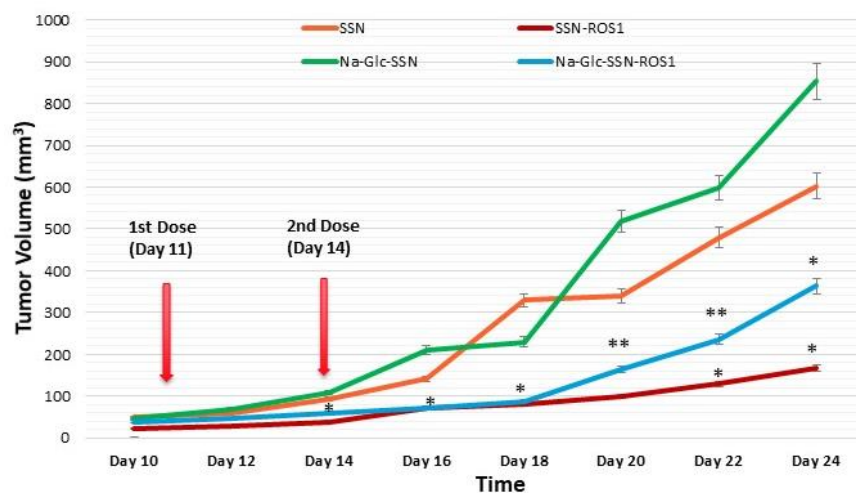


**Figure 16.** In vivo biodistribution of AF-488-labelled siRNA in nude mice bearing a xenografted 4T1 tumor 4 h and 24 h after intravenous injection of siRNA-loaded nanoparticles; (A). SSNs and (B). Na-Glc-SSNs. Each bar represents the mean  $\pm$  SEM based on three mice per groups in all cases.

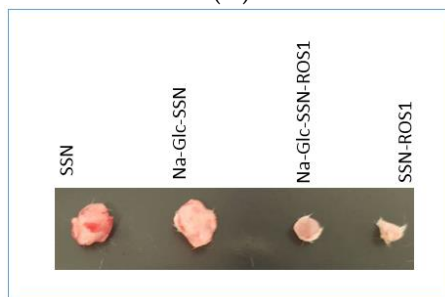
### 3.3.12. In Vivo Biodistribution Study of SSNs and Na-Glc-SSNs

The biodistribution and tumor accumulation of siRNA was investigated upon intravenous injection of AF-488-siRNA-complexed nanoparticles into mice bearing a subcutaneous 4T1 tumor. After 4 h of the treatment, major organs and tumor were collected and fluorescence intensity was measured. We observed significant differences in the biodistribution and tumor accumulation of the siRNA electrostatically associated with SSNs and Na-Glc-SSNs, as shown in Figure 16. The SSNs were significantly accumulated in RES organs (liver, spleen), brain, respiratory systems, heart and urinary systems. On the contrary, accumulation of Na-Glc-SSNs was lesser in major organs than that of SSNs except kidneys, which showed higher fluorescence signals, which could be explained by the notion that smaller particle size distribution of the former led to accelerated renal clearance. This might be reversed by increasing the hydrodynamic

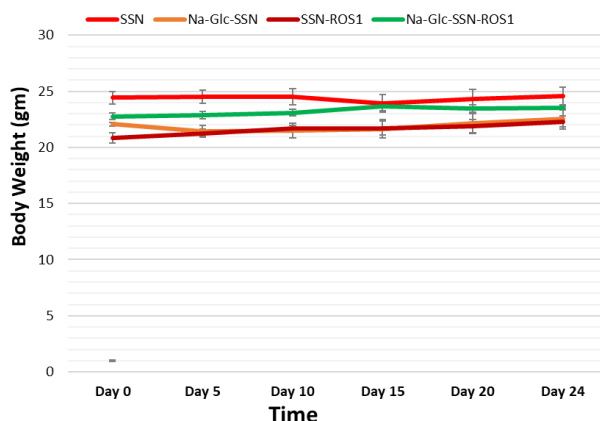
diameter via coating Na-Glc-SSNs with a highly polymer like PEG, etc. After 24 h of the treatment, both nanoparticles were completely eliminated from the body (Figure 16). The tumor accumulation of nanoparticles depends on their physicochemical properties to cross the TME. The EPR effects and vascular pore cut off size ranging from 200 nm to 1.2  $\mu$ m of tumors allow the nanoparticles to accumulate in the tumor region more efficiently [51]. We found that the SSNs and Na-Glc-SSNs facilitated significant tumor accumulation of the loaded siRNA after 4 h of the treatment and remained after 24 h of the treatment. Interestingly, there was a noticeable siRNA accumulation in the brain at 4 h, followed by complete removal after 24 h.



(A)



(B)



(C)

Figure 17. Effects of intravenously administered nanoparticles and siRNA-loaded nanoparticles on tumor regression. (A), Images of excised tumors at day 20 (B) and total body weight (C) in a 4T1 tumor bearing mice. 4T1 cells were inoculated subcutaneously on the mammary pad of mice. Tumor-bearing mice were treated intravenously through tail vein injection with 50  $\mu$ L of either nanoparticles or siRNA-loaded nanoparticles, formed by the addition of 60 mM  $\text{SrCl}_2$ , 300mM of NaCl, and 200 mm of D-glucose to 10 mM of  $\text{Na}_2\text{SO}_3$  in the absence and presence of 50 nM of ROS1 siRNA, respectively, when the tumor volume reached approximately 39  $\text{mm}^3$ . Four mice per group were used and data were represented as mean  $\pm$  SEM of tumor volume. Values were very significant (\*\*) at  $p$  value 0.001 to 0.01 and significant (\*) at  $p$  value 0.01 to 0.05 as compared to the control group.

### 3.3.13. *In Vivo* Anti-Tumor Effect of ROS1 siRNA-Loaded SSNs and Na-Glc-SSNs

A 4T1-induced murine breast cancer model was used to investigate the effect of SSNs and Na-Glc-SSNs carrying ROS1 siRNA on tumor regression. 50  $\mu$ L volumes of SSNs-ROS1 and Na-Glc-SSNs-ROS1 prepared with 60 mM  $\text{SrCl}_2$ , 10 mM of  $\text{Na}_2\text{SO}_3$  and 50 nM of ROS1 siRNA in the absence and presence of 300 mM of NaCl and 200 mm of D-glucose, respectively, were administered twice within an interval of 3 days through the tail vein, after the tumour volume reached 39  $\text{mm}^3$ . The results of the tumor growth curve (Figure 17-A) show that tumors, following intravenous injections of SSNs and Na-Glc-SSNs, prepared under the same conditions except addition of siRNA, grew quickly almost in the same pattern. In contrast, the tumor growth of the mice treated with SSNs-ROS1 or Na-Glc-SSNs-ROS1 exhibited a relatively slower rate and smaller tumor volumes at the end, suggesting that both SSNs-ROS1 and Na-Glc-SSN-ROS1 effectively reduced the tumor growth in vivo. However, the tumor growth inhibition rate for SSNs-ROS1 was more prominent than Na-Glc-SSN-ROS1 at the later stage, which could be explained by higher renal clearance and lesser tumor accumulation of the latter. None of the two different particle types showed any obvious influence on mouse body weight (Figure 17-C), which suggests that siRNA-loaded particles do not have any detrimental systemic toxicity in mice. The notable anti-tumor effects of SSNs and Na-Glc-SSNs carrying ROS1 siRNA indicates that strontium sulfite particles could protect the loaded siRNA against



nuclease attack, confer favourable pharmacokinetics, induce no noticeable systemic cytotoxicity, promote excellent tumor uptake and cytosolic release of the siRNA.

Since tumor extracellular environment is acidic, dissolution of the pH-sensitive particles could not be ruled out, with the consequence of siRNA release from the particles before their internalization into the target cells. We assume that under that acidic environment, particles could be dissolved either partially or completely, depending on the number of particles accumulated there. If the particles are partially dissolved, siRNAs released thereby might enter the target tumor cells by passive diffusion, which is rather inefficient considering the size of siRNA and the electrostatic repulsion between the negatively charged phosphate backbone of siRNA and the cell membrane, which is also negatively charged due to the presence of sulfate-carrying proteoglycans while the intact particles with electrostatically associated siRNA would enter via endocytosis resulting in particle dissolution under endosomal acidic pH and siRNA release from endosomes to cytosol. On the other hand, if the particles are fully dissolved in the extracellular compartment, the released siRNA would enter the tumor cells exclusively via passive diffusion with the consequence of poor therapeutic outcome. Since we have observed robust anti-tumor effect, we presume that the particles were partially dissolved or remained resistant to degradation under the mildly acidic environment.

### 3.4. Conclusion

SSNs and Na-Glc-SSNs synthesized via a simple precipitation method emerge as pH-sensitive smart carriers for effectively delivering therapeutic siRNAs to the tumor. We found significant roles of NaCl and D-glucose in stabilizing the strontium sulfite particles with a more uniform particle size of 220nm. The low pH-triggered dissolution of strontium sulfite apparently helps in the efficient release of the siRNA in early endosomes, which is critical for silencing the target mRNA in cytosol. We have also found a significant effect of SSNs coupled siRNA in reducing tumor both in vitro and in vivo without any apparent toxicity. To our knowledge, this is the first successful report revealing that strontium sulfite nanoparticles are highly promising siRNA delivery vehicles to facilitate target oncogene knockdown and promote efficient tumor regression. Our findings therefore emphasize the need to perform further studies with strontium sulfite for tumor-targeted delivery of therapeutics in preclinical cancer models for potential translation into clinics in the future.

### References

1. Wong, J.K.; Mohseni, R.; Hamidieh, A.A.; MacLaren, R.E.; Habib, N.; Seifalian, A.M. Will nanotechnology bring new hope for gene delivery? *Trends Biotechnol.* **2017**, *35*, 434–451.

2. Karim, E.; Rosli, R.; H Chowdhury, E. Systemic delivery of nanoformulations of anti-cancer drugs with therapeutic potency in animal models of cancer. *Curr. Cancer Ther. Rev.* **2016**, *12*, 204–220.
3. Babu, A.; Muralidharan, R.; Amreddy, N.; Mehta, M.; Munshi, A.; Ramesh, R. Nanoparticles for sirna-based gene silencing in tumor therapy. *IEEE Trans. Nanobiosci.* **2016**, *15*, 849–863.
4. Karim, M.E.; Tha, K.K.; Othman, I.; Borhan Uddin, M.; Chowdhury, E.H. Therapeutic potency of nanoformulations of sirnas and shrnas in animal models of cancers. *Pharmaceutics* **2018**, *10*, 65.
5. Mitchell, M.J.; Jain, R.K.; Langer, R. Engineering and physical sciences in oncology: Challenges and opportunities. *Nat. Rev. Cancer* **2017**, *17*, 659.
6. Lu, P.; Weaver, V.M.; Werb, Z. The extracellular matrix: A dynamic niche in cancer progression. *J. Cell Biol.* **2012**, *196*, 395–406.
7. Jain, R.K. Normalizing tumor microenvironment to treat cancer: Bench to bedside to biomarkers. *J. Clin. Oncol.* **2013**, *31*, 2205–2218.
8. Hanahan, D.; Coussens, L.M. Accessories to the crime: Functions of cells recruited to the tumor microenvironment. *Cancer Cell* **2012**, *21*, 309–322.
9. Sun, N.-f.; Liu, Z.-a.; Huang, W.-b.; Tian, A.-l.; Hu, S.-y. The research of nanoparticles as gene vector for tumor gene therapy. *Crit. Rev. Oncol./Hematol.* **2014**, *89*, 352–357.
10. Zhou, Z.; Liu, X.; Zhu, D.; Wang, Y.; Zhang, Z.; Zhou, X.; Qiu, N.; Chen, X.; Shen, Y. Nonviral cancer gene therapy: Delivery cascade and vector nanoproperty integration. *Adv. Drug Deliv. Rev.* **2017**, *115*, 115–154.
11. Mintzer, M.A.; Simanek, E.E. Nonviral vectors for gene delivery. *Chem. Rev.* **2008**, *109*, 259–302.
12. Loh, X.J.; Lee, T.-C.; Dou, Q.; Deen, G.R. Utilising inorganic nanocarriers for gene delivery. *Biomater. Sci.* **2016**, *4*, 70–86.
13. Mozar, F.S.; Chowdhury, E.H. Surface-modification of carbonate apatite nanoparticles enhances delivery and cytotoxicity of gemcitabine and anastrozole in breast cancer cells. *Pharmaceutics* **2017**, *9*, 21.
14. Murakami, T.; Tsuchida, K. Recent advances in inorganic nanoparticle-based drug delivery systems. *Mini Rev. Med. Chem.* **2008**, *8*, 175–183.
15. Huang, H.-C.; Barua, S.; Sharma, G.; Dey, S.K.; Rege, K. Inorganic nanoparticles for cancer imaging and therapy. *J. Control. Release* **2011**, *155*, 344–357.
16. Li, H.; Du, J.; Liu, J.; Du, X.; Shen, S.; Zhu, Y.; Wang, X.; Ye, X.; Nie, S.; Wang, J. Smart Superstructures with Ultrahigh pH-Sensitivity for Targeting Acidic Tumor Microenvironment: Instantaneous Size Switching and Improved Tumor Penetration. *Acs Nano* **2016**, *10*, 6753–6761.
17. Li, H.-J.; Du, J.-Z.; Du, X.-J.; Xu, C.-F.; Sun, C.-Y.; Wang, H.-X.; Cao, Z.-T.; Yang, X.-Z.; Zhu, Y.-H.; Nie, S. Stimuli-responsive clustered nanoparticles for improved tumor penetration and therapeutic efficacy. *Proceed. Nat. Acad. Sci.* **2016**, *113*, 4164–4169.

18. Ju, C.; Mo, R.; Xue, J.; Zhang, L.; Zhao, Z.; Xue, L.; Ping, Q.; Zhang, C. Sequential intra-intercellular nanoparticle delivery system for deep tumor penetration. *Angew. Chem. Int. Ed.* **2014**, *53*, 6253–6258.
19. Du, J.-Z.; Du, X.-J.; Mao, C.-Q.; Wang, J. Tailor-made dual ph-sensitive polymer–doxorubicin nanoparticles for efficient anticancer drug delivery. *J. Am. Chem. Society* **2011**, *133*, 17560–17563.
20. Miao, L.; Wang, Y.; Lin, C.M.; Xiong, Y.; Chen, N.; Zhang, L.; Kim, W.Y.; Huang, L. Nanoparticle modulation of the tumor microenvironment enhances therapeutic efficacy of cisplatin. *J. Control. Release* **2015**, *217*, 27–41.
21. Xu, X.; Saw, P.E.; Tao, W.; Li, Y.; Ji, X.; Yu, M.; Mahmoudi, M.; Rasmussen, J.; Ayyash, D.; Zhou, Y. Tumor microenvironment-responsive multistaged nanoplatform for systemic rna and cancer therapy. *Nano Letters* **2017**, *17*, 4427–4435.
22. Helmlinger, G.; Sckell, A.; Dellian, M.; Forbes, N.S.; Jain, R.K. Acid production in glycolysis-impaired tumors provides new insights into tumor metabolism. *Clin. Cancer Res.* **2002**, *8*, 1284–1291.
23. Wojtkowiak, J.W.; Verduzco, D.; Schramm, K.J.; Gillies, R.J. Drug resistance and cellular adaptation to tumor acidic PH microenvironment. *Mo. Pharm.* **2011**, *8*, 2032–2038.
24. Yang, X.; Grailer, J.J.; Pilla, S.; Steeber, D.A.; Gong, S. Tumor-targeting, ph-responsive, and stable unimolecular micelles as drug nanocarriers for targeted cancer therapy. *Bioconjug. Chem.* **2010**, *21*, 496–504.
25. Bae, Y.; Jang, W.-D.; Nishiyama, N.; Fukushima, S.; Kataoka, K. Multifunctional polymeric micelles with folate-mediated cancer cell targeting and PH-triggered drug releasing properties for active intracellular drug delivery. *Mol. BioSyst.* **2005**, *1*, 242–250.
26. Kim, I.-Y.; Kang, Y.-S.; Lee, D.S.; Park, H.-J.; Choi, E.-K.; Oh, Y.-K.; Son, H.-J.; Kim, J.-S. Antitumor activity of egfr targeted ph-sensitive immunoliposomes encapsulating gemcitabine in a549 xenograft nude mice. *J. Control. Release* **2009**, *140*, 55–60.
27. Deng, Z.; Zhen, Z.; Hu, X.; Wu, S.; Xu, Z.; Chu, P.K. Hollow chitosan–silica nanospheres as ph-sensitive targeted delivery carriers in breast cancer therapy. *Biomaterials* **2011**, *32*, 4976–4986.
28. Shen, M.; Huang, Y.; Han, L.; Qin, J.; Fang, X.; Wang, J.; Yang, V.C. Multifunctional drug delivery system for targeting tumor and its acidic microenvironment. *J. Control. Release* **2012**, *161*, 884–892.
29. Chowdhury, E.H. Ph-responsive magnesium-and carbonate-substituted apatite nano-crystals for efficient and cell-targeted delivery of transgenes. *Open J. Genet.* **2013**, *3*, 38.
30. Chua, M.; Tiash, S.; Fatemian, T.; Noordin, M.; Keng, C.; Chowdhury, E. Carbonate apatite-facilitated intracellular delivery of c-ros1 small interfering rna sensitises mcf-7 breast cancer cells to cisplatin and paclitaxel. *OA Cancer* **2013**, *1*.

31. Tada, S.; Chowdhury, E.H.; Cho, C.-S.; Akaike, T. Ph-sensitive carbonate apatite as an intracellular protein transporter. *Biomaterials* **2010**, *31*, 1453–1459.
32. Tiash, S.; Kamaruzman, N.I.B.; Chowdhury, E.H. Carbonate apatite nanoparticles carry sirna (s) targeting growth factor receptor genes egfr1 and erbb2 to regress mouse breast tumor. *Drug Deliv.* **2017**, *24*, 1721–1730.
33. Uddin, M.B.; Balaravi Pillai, B.; Tha, K.K.; Ashaie, M.; Karim, M.E.; Chowdhury, E.H. Carbonate apatite nanoparticles-facilitated intracellular delivery of sirna (s) targeting calcium ion channels efficiently kills breast cancer cells. *Toxics* **2018**, *6*, 34.
34. Shaw, A.T.; Ou, S.-H.I.; Bang, Y.-J.; Camidge, D.R.; Solomon, B.J.; Salgia, R.; Riely, G.J.; Varella-Garcia, M.; Shapiro, G.I.; Costa, D.B. Crizotinib in ros1-rearranged non-small-cell lung cancer. *New Engl. J. Med.* **2014**, *371*, 1963–1971.
35. Eom, M.; Lkhagvadorj, S.; Oh, S.S.; Han, A.; Park, K.H. Ros1 expression in invasive ductal carcinoma of the breast related to proliferation activity. *Yonsei Med. J.* **2013**, *54*, 650–657.
36. Eccles, S.A. The epidermal growth factor receptor/erb-b/her family in normal and malignant breast biology. *Int. J. Dev. Biol.* **2011**, *55*, 685–696.
37. Bhargava, R.; Gerald, W.L.; Li, A.R.; Pan, Q.; Lal, P.; Ladanyi, M.; Chen, B. Egfr gene amplification in breast cancer: Correlation with epidermal growth factor receptor mrna and protein expression and her-2 status and absence of egfr-activating mutations. *Mod. Pathol.* **2005**, *18*, 1027.
38. Weber, F.; Fukino, K.; Sawada, T.; Williams, N.; Sweet, K.; Brena, R.; Plass, C.; Caldes, T.; Mutter, G.; Villalona-Calero, M. Variability in organ-specific egfr mutational spectra in tumour epithelium and stroma may be the biological basis for differential responses to tyrosine kinase inhibitors. *Br. J. Cancer* **2005**, *92*, 1922.
39. Qian, W.-Y.; Sun, D.-M.; Zhu, R.-R.; Du, X.-L.; Liu, H.; Wang, S.-L. Ph-sensitive strontium carbonate nanoparticles as new anticancer vehicles for controlled etoposide release. *Int. J. Nanomed.* **2012**, *7*, 5781.
40. Miele, E.; Spinelli, G.P.; Miele, E.; Di Fabrizio, E.; Ferretti, E.; Tomao, S.; Gulino, A. Nanoparticle-based delivery of small interfering rna: Challenges for cancer therapy. *Int. J. Nanomed.* **2012**, *7*, 3637.
41. Wisse, E.; Jacobs, F.; Topal, B.; Frederik, P.; De Geest, B. The size of endothelial fenestrae in human liver sinusoids: Implications for hepatocyte-directed gene transfer. *Gene Ther.* **2008**, *15*, 1193.
42. Aird, W.C. Phenotypic heterogeneity of the endothelium: I. Structure, function, and mechanisms. *Circ. Res.* **2007**, *100*, 158–173.
43. Kanasty, R.; Dorkin, J.R.; Vegas, A.; Anderson, D. Delivery materials for sirna therapeutics. *Nat. Mater.* **2013**, *12*, 967.
44. Davis, M.E.; Shin, D.M. Nanoparticle therapeutics: An emerging treatment modality for cancer. *Nat. Rev. Drug Discov.* **2008**, *7*, 771.

45. Yarden, Y. The egfr family and its ligands in human cancer: Signalling mechanisms and therapeutic opportunities. *Eur. J. Cancer* **2001**, 37, 3–8.
46. Tiash, S.; Chua, M.J.; Chowdhury, E.H. Knockdown of ros1 gene sensitizes breast tumor growth to doxorubicin in a syngeneic mouse model. *Int. J. Oncol.* **2016**, 48, 2359–2366.
47. Trent, J.M.; Rosenfeld, S.B.; Meyskens, F.L. Chromosome 6q involvement in human malignant melanoma. *Cancer Genet. Cytogenet.* **1983**, 9, 177–180.
48. Watkins, D.; Dion, F.; Poisson, M.; Delattre, J.-Y.; Rouleau, G.A. Analysis of oncogene expression in primary human gliomas: Evidence for increased expression of the ros oncogene. *Cancer Genet. Cytogenet.* **1994**, 72, 130–136.
49. Rikova, K.; Guo, A.; Zeng, Q.; Possemato, A.; Yu, J.; Haack, H.; Nardone, J.; Lee, K.; Reeves, C.; Li, Y. Global survey of phosphotyrosine signaling identifies oncogenic kinases in lung cancer. *Cell* **2007**, 131, 1190–1203.
50. Eom, M.; Han, A.; Yi, S.Y.; Shin, J.J.; Cui, Y.; Park, K.H. Rheb expression in fibroadenomas of the breast. *Pathol. Int.* **2008**, 58, 226–232.
51. Hashizume, H.; Baluk, P.; Morikawa, S.; McLean, J.W.; Thurston, G.; Roberge, S.; Jain, R.K.; McDonald, D.M. Openings between defective endothelial cells explain tumor vessel leakiness. *Am. J. Pathol.* **2000**, 156, 1363–1380.



## Chapter 4

### **PEGylated Strontium sulfite for improving antitumor efficacy of EGFR siRNA against the breast cancer cell.**

Work that is presented in this chapter is submitted in *Molecular Therapy* with minor adjustments in Figure/Table number to fit into the current thesis format. A snapshot of the submitted proof is included in page 134.

<b>Manuscript #</b>	MTJ-19-3907
<b>Current Revision #</b>	0
<b>Submission Date</b>	27-Apr-2019 04:18:29
<b>Current Stage</b>	Under Consideration
<b>Title</b>	PEGylated Strontium sulfite for improving antitumor efficacy of EGFR siRNA against the breast cancer cell.
<b>Running Title</b>	PEG-SSN-EGFR for improving antitumor efficacy.
<b>Manuscript Type</b>	Original Article
<b>Special Section</b>	N/A
<b>Corresponding Author</b>	Ezharul Chowdhury (md.ezharul.hoque@monash.edu) (Monash University)
<b>Contributing Author</b>	Md karim
<b>Abstract</b>	Inorganic NPs based siRNA delivery possess great potential for improving stability of siRNA and tumor directed delivery. pH sensitive Strontium sulfite NPs(SSNs) have been proven to be an effective delivery vehicles for siRNAs due to their excellent anticancer efficacy. However uneven distribution of SSNs contributed to siRNA deposition in major organs caused unwanted effects and less accumulation of siRNA in tumor site. To date, here we report, for the first time, surface modifications of SSNs with PEG for enhancing blood circulation time and drug accumulation in tumor region to maximize the anti-tumor efficacy of SSNs. The modified SSNs showed reduced particle size, higher siRNA encapsulation efficiency and stability in blood plasma. Subsequently, grafting of PEG on the surface of SSNs conjugated EGFR facilitate their uptake in cancer cells and undergone dissociation of SSNs at early endosomal stage. The in vivo tumor regression study exerted significant tumor inhibitory effects of PEG-SSNs coupled EGFR than unmodified SSNs. Moreover, a safety evaluation of PEG-SSNs performed both in vitro and in vivo exerting no toxicity. These our PEG-SSNs could be a stable, safe and promising siRNA nanovehicle for improvising antitumor efficacy along with favorable pharmacokinetics profile.
<b>Deputy Editor</b>	Not Assigned
<b>Keywords</b>	Inorganic NPs,, SSNs, PEG, siRNA,, serum stability, EGFR, Gene therapy, Breast cancer.
<b>Conflict of Interest Statement</b>	There is <b>NO</b> conflict of interest to disclose.
<b>Clinical Trial</b>	No
<b>Society Member</b>	No

## Manuscript Items

1. Author Cover Letter [PDF \(154KB\)](#) 
2. Article File [PDF \(1962KB\)](#) 

## **4. PEGylated Strontium sulfite for improving antitumor efficacy of EGFR siRNA against the breast cancer cell.**

### **4.1. Introduction:**

The biotechnology revolution has brought RNAi (RNA interference) for being harnessed with great potential to treat the cancer at genetic level. RNAi therapeutics are very efficient in selectively silencing the overexpressed genes responsible for development of cancer. But the naked siRNA suffers from systemic instability (1) due to nuclease degradation, phagocytosis and rapid renal clearance (2-4). To date a lot of viral and non-viral vectors have been deployed to carry the siRNA into the cytoplasm of target cancer cell by providing the stealth effect against biological barriers. Recently, inorganic NPs have been evolved rapidly and widely investigated especially in cancer gene therapy, diagnosis and imaging. The unique physicochemical properties such as size, shape, electrical and optical properties, and elasticity, reasonable manufacturing cost compared with organic NPs, flexibility, ease of functionalization, improved solubility and biocompatibility of inorganic NPs made them more reliable for cancer management (5, 6). Cationic NPs interact with negatively charged siRNA owing to their phosphate backbone, thus facilitating efficient cellular internalization. Several groups have reported inorganic salt based NPs for the delivery of genes and siRNAs in breast cancer (7, 8). In our previous study, we have reported strontium sulfite nanoparticles (SSNs) for the delivery of siRNA into breast tumor, showing significant anti-tumor effects (9). Despite the enormous progress and vigorous research on cancer nanomedicine, several challenges and shortcomings have been identified that limit the successful translation into clinical setting. As the inorganic NPs contain charge in their surface, after reaching into the biological circulation they are prone to interactions with serum proteins that adsorb onto the surface of NPs, being readily taken up by macrophages of reticuloendothelial system (RES) (10, 11). In pharmaceutical point of view, premature degradation before reaching to target site caused sub-therapeutic action of the drug. Moreover, the small sized NPs offer large surface area for adsorbing blood proteins that leads to uneven distribution and causes unwanted effects into the body (12-14). So it is necessary to minimize unwanted clearance and wide distribution of NPs for maximizing therapeutic efficacy and targetability, and reducing off-target effects.

EGFR (epidermal growth factor receptor) is the member of receptor tyrosine kinase, ErbB/HER family that forms homo and hetero dynamic receptors and modulate cancer cell proliferation, cellular adhesion and motility, apoptosis, progression and migration by activating signal transduction pathways (15-18). In breast cancer, EGFR



overexpression has been reported for all types of breast cancers, particularly for triple negative breast cancer (TNBC) and inflammatory breast cancer (IBC) (9, 19, 20). The overexpression of EGFRs in breast cancer, their aggressive behaviors and poor clinical outcomes make them ideal targets for cancer gene therapy. Silencing of EGFR via using anti-EGFR siRNA could be an efficient strategy for cancer management.

Polyethylene glycol (PEG), a water soluble, non-ionic and biocompatible coating material is widely used for extending the blood circulation time of drug-loaded NPs and thus enhancing the therapeutic efficacy (21-25). PEGylation of NPs reduced their interactions with serum proteins and eventually their opsonization and phagocytosis. However, it also offers several additional advantages like reduction in glomerular filtration rate by increasing hydrophilicity, protection from enzymatic degradation and lowering the neutralizing antibody formation in blood (26, 27).

In our previous study, we successfully synthesized SSNs and used them to efficaciously carry siRNA into tumor cells with significant reduction in tumor volume in a murine breast cancer model (9). To make the system more effective for systemic administration, we modified the surface of SSNs via biotin PEG for improving their blood circulation time, minimizing off target distribution and augmenting tumor accumulation. We have found particle size reduction capacity of Biotin PEG association resulted in a reduction in size of the hybrid particle by reducing particle aggregation. With the confirmation of size, size distribution and elemental analysis of PEG-SSNs, we assumed that small sized PEG-SSNs would protect the siRNA from biological instability and increase accumulation of intended tumor site through EPR effect. The stability of NPs in plasma and other media was evaluated to see the fate after reaching systemic circulation. We also examined the binding affinity of PEG-SSNs to siRNA and their capability to carry siRNA into the tumor cell and silence the overexpressed EGFR gene with anti-EGFR siRNA in human and murine breast cancer cell lines. The pharmacodynamics of SSNs and PEG-SSNs along with anti-EGFR siRNA were examined in breast tumor-bearing mice model. Moreover, the biocompatibility of PEG-SSNs was tested in blood.

## **4.2. Materials and methods:**

### *4.2.1. Materials:*

Strontium chloride ( $\text{SrCl}_2$ ), sodium sulfite ( $\text{Na}_2\text{SO}_3$ ) and 4-(2-hydroxyethyl)-1-piperazineethanesulfonic acid (HEPES) were obtained from Sigma-Aldrich (St Louis, MO, USA). Dulbecco's modified eagle medium (DMEM), dimethyl sulphoxide (DMSO), thiazolyl blue tetrazolium bromide (MTT), and ethylene diamine tetra acetic acid (EDTA)

were purchased from Sigma-Aldrich (St. Louis, MO, USA). DMEM powder, fetal bovine serum (FBS), trypsin-ethylene diamine tetra acetate (trypsin-EDTA), and penicillin-streptomycin were from Gibco BRL (CA). Poly(ethylene glycol) 2-aminoethyl ether biotin were purchased from Sigma Aldrich (St. Louis, MO, USA). All siRNAs used in this study were obtained from Qiagen (Hilden, Germany) and dissolved in RNase-free water provided by the company. MCF-7 cells were originally from ATCC (Manassas, VA, USA).

#### *4.2.2. Synthesis of SSNs and PEG-SSNs:*

SSNs were prepared by mixing 40 mM of  $\text{SrCl}_2$  and 10 mM of  $\text{Na}_2\text{SO}_3$  in 50  $\mu\text{l}$  of aqueous solution, followed by incubation at 37°C for 30 min and topped up with DMEM media (pH7.5) to make the final volume to 1 ml. For preparing PEG-SSNs, 40 mM of  $\text{SrCl}_2$  and 10 mM of  $\text{Na}_2\text{SO}_3$  were mixed in 50  $\mu\text{l}$  of aqueous solution, incubated for 30 min at 37°C. After incubation different concentration (1, 5, 10, 15  $\mu\text{l}$ ) of biotin PEG (1  $\mu\text{M}$ ) were added and incubate for 10 min at 37°C for 30 min.

#### *4.2.3. Turbidity and Optical images of PEG-SSNs:*

SSNs and PEG-SSNs were prepared as mentioned above. Spectrophotometric analysis was done at 320 nm wavelength to measure absorbance (turbidity) of SSNs and PEG-SSNs at different concentration (1, 5, 10, 15  $\mu\text{l}$ ) by using a Jasco UV-VIS spectrophotometer (Ocklahoma city, OK, USA). Microscopic observations of formed PEG-SSNs nanoparticles were done by using an Olympus Microscope CKX41 in bright field 10X magnification. All experiments were measured in triplicates and conducted at room temperature and the data was plotted into a graph with mean  $\pm$  SD.

#### *4.2.4. Characterizations of PEG-SSNs:*

SSNs and PEG-SSNs were prepared by mixing of 40 mM of  $\text{SrCl}_2$  and 10 mM of  $\text{Na}_2\text{SO}_3$  in 50  $\mu\text{l}$  of aqueous solution, followed by incubation at 37°C for 30 min and finally added 1  $\mu\text{l}$  of Biotin PEG(1  $\mu\text{M}$ ) and incubated for 10min. The particle size, surface charge, particle size distribution and PDI value were measured by Malvern nano zeta sizer (Worcestershire, UK) and accompanying software. All sample were measured in triplicates and plotted into a graph with mean  $\pm$  SD.

#### *4.2.5. Energy Dispersive X-ray (EDX) assay of PEG-SSNs:*

The elemental composition of SSNs and PEG-SSNs was calculated by using EDX. SSNs and PEG-SSNs were prepared by adding 40 mM of  $\text{SrCl}_2$ , 10mM of  $\text{Na}_2\text{SO}_3$  and 1  $\mu\text{L}$  of biotin PEG. The particles then centrifuged at 13000 rpm for 15 minutes and 3  $\mu\text{L}$  of particle suspension was then transferred to a glass slide for drying at 37°C for 1 hour. The

dried sample was then placed onto a carbon tape-coated sample holder, followed by platinum sputtering of the dried samples with 30 mA sputter current at 2.30 tooling factor for 40 s and the sputtered particles were visualized at 5.00 kV using FE-SEM (Hitachi/SU8010, Tokyo, Japan) and analyzed for elemental composition by an EDX analyzer (X-maX, 50mm<sup>2</sup> HORIBA, JAPAN).

#### 4.2.6. Stability of PEG-SSNs in mice plasma:

The stability and size distribution pattern were assessed by using dynamic light scattering instruments, Malvern nano zeta sizer (Worcestershire, UK). To collect the plasma, fresh blood from female balb/c were collected into Heparin containing centrifuge tubes and centrifuged at 1000 rcf for 10 min at 4<sup>0</sup>c. The supernatant was collected and further centrifuged for 15 min at 2000 rcf and 4<sup>0</sup>c for separating plasma and blood cell. PEG-SSNs were prepared by using 40 mM of SrCl<sub>2</sub>, 10mM of Na<sub>2</sub>SO<sub>3</sub> and 1 μL of biotin PEG and dispersed in deionized water, DMEM cell culture medium and mice plasma (10% in PBS) and subjected to DLS measurement.

#### 4.2.7. siRNA encapsulation efficiency of PEG-SSNs:

To estimate the siRNA binding affinity of PEG-SSNs, different concentrations (0, 2, 4, 6, 8, 10 nM) of AF 488 allstars negative siRNA were dissolved in 200 μL of DMEM and fluorescence intensity was measured with a  $\lambda_{\text{exc}} = 490 \text{ nm}$  and  $\lambda_{\text{em}} = 535 \text{ nm}$  by using 2030 multilabel reader victor TM X5 (Perkin Elmer, MA, CA, USA). Data was analyzed by Perkin Elmer 2030 manager software. Each sample was measured in triplicate and a standard curve was obtained by plotting fluorescence intensity versus siRNA concentrations to calculate the amount of siRNA bound to the NPs. SSNs and PEG-SSNs were prepared by adding 40 mM of SrCl<sub>2</sub>, 10 mM of Na<sub>2</sub>SO<sub>3</sub> and 1 μL of biotin PEG in presence of 10 nM of AF 488 siRNA to make NPs-siRNA complex. After the samples were centrifuged at 13,000 rpm for 15 min at 4 °C, the pellet was collected and fluorescence intensity measurement. The binding affinity of siRNA to differently formulated NPs was calculated by using the following formula:

$$\% \text{ of siRNA binding} = \frac{X_{\text{initial}} - X_{\text{free}}}{X_{\text{initial}}} \times 100\%$$

Where  $X_{\text{free}}$  is the concentrations of siRNA in the supernatant following centrifugation of NPs-siRNA, and  $X_{\text{initial}}$  denotes the total concentration of siRNA used in the experiment, which was 10 nM. The samples were prepared in triplicate and represented as mean  $\pm$  SD.

#### 4.2.8. Cytotoxicity and hemolysis assay of PEG-SSNs:

For hemolysis study, fresh blood was collected from female blab/c mice and centrifuged at 2000 rpm for 10 min at 4°C for separating Red Blood Cells (RBCs) from blood. The collected RBCs then washed with PBS three times and diluted with 20% (v/v) of PBS. The PEG-SSNs were prepared by the addition of 40 mM of SrCl<sub>2</sub>, 10 mM of Na<sub>2</sub>SO<sub>3</sub> and 1 µL of biotin PEG and added to RBCs solution prior to incubation at 37 °C for 60 min. After incubation, the samples were centrifuged for 5 min at 4000 rpm and the supernatant were analyzed by UV-VIS spectrophotometer at absorbance value of 541nm. Deionized water and PBS were taken as positive and negative control. The hemolysis percentage of PEG-SSNs were calculated by using following equation:

$$\% \text{ of Hemolysis} = \frac{Abs_{\text{sample}} - Abs_{\text{Neg}}}{Abs_{\text{Pos}} - Abs_{\text{Neg}}}$$

In case of cytotoxicity study, approximately 50,000 of MCF-7 cells (Human breast cancer cells) were seeded on 24-well plate and incubated overnight. The next day cells were treated with SSNs and PEG-SSNs and incubated in 37 °C and 5% CO<sub>2</sub> for 48 h. MTT assay was conducted by adding 50 µL of MTT (5 mg/mL in PBS) solution into each well and incubated for 4 h. 300 µL of DMSO (dimethyl sulfoxide) was added to dissolve resulted formazan and the absorbance was analyzed on a microplate reader (microplate spectrophotometer, Biorad, Hercules, CA, USA) at 595 nm wavelength with reference to 630 nm.

#### 4.2.9. In vitro cytotoxicity assay of SSNs and PEG-SSNs coupled EGFR siRNA by MTT:

Human breast cancer cell line (MCF-7) and Mouse breast cancer cell line (4T1) were cultured in DMEM supplemented with 10% FBS, 1% penicillin/streptomycin at 37 °C in a humidified 5% CO<sub>2</sub> chamber and approximately 50,000 cells/well were seeded in 24 well plate. After the overnight incubation the cells were treated with SSNs, PEG-SSNs, SSNs-EGFR and PEG-SSNs-EGFR and incubated for 48 h. SSNs were prepared by adding 40 mM of SrCl<sub>2</sub>, 10 mM of Na<sub>2</sub>SO<sub>3</sub> and 1 µL of biotin PEG added to make PEG-SSNs. 1 nM of EGFR siRNA was added to SSNs and PEG-SSNs for making SSNs-EGFR and PEG-SSNs-EGFR complex for treatment and media treats as untreated. After 48 h of incubation, MTT assay was done for calculating cytotoxicity. 50 µL of MTT (5 mg/mL in PBS) solution were added into each well and incubated for 4 h and added of 300 µL of DMSO (dimethyl sulfoxide) before analyzing the absorbance on a microplate reader (microplate spectrophotometer, Biorad, Hercules, CA, USA) at 595 nm wavelength with reference to 630 nm. The percent of metabolically active cells (CV) was calculated for treated samples using the following equation:

$$\% \text{ cell viability} = \frac{\text{Absorbance of treated sample}}{\text{Absorbance of control}} \times 100\%$$

All the experiments were done in triplicate and the data was plotted as % of cell viability with mean  $\pm$  SD.

#### *4.2.10. Tumor induction in mice:*

Female nude Balb/c mice of 6–8 weeks old with body weights of 20–25 gm were obtained from the School of Medicine and Health Science Animal Facility, Monash University and maintained in 12:12 light: dark conditions and provided with *ab libitum* and water. All the experiments were done in accordance with the protocol approved by MONASH Animal Ethics Committee (MARF/2016/126). Approximately  $1 \times 10^5$  of 4T1 cells were suspended in 100  $\mu$ L PBS and injected subcutaneously on the mammary pad of mice.

#### *4.2.11. In vivo antitumor efficacy of EGFR siRNA-loaded SSNs and PEG-SSNs:*

After tumor reached an average volume of  $\sim 22 \text{ mm}^3$  at around Day 10-11, tumor bearing mice were injected with free SSNs, free PEG-SSNs, EGFR-SSNs (50nM of EGFR siRNA) and EGFR-PEG-SSNs (50nM of EGFR siRNA) intravenously (tail-vein) at the right or left caudal vein, while the second dose was administered 3 days after the 1st dose. Each group of treatment contained 4 mice. The length and width of tumor outgrowth were measured at certain period of time interval using the Vernier caliper in mm scale over the period of 24 days. The data subsequently presented as mean  $\pm$  SEM of the tumor volumes of each group. The volume of the tumor was calculated based on the following formula:

$$\text{Tumor Volume (mm}^3\text{)} = \frac{1}{2} (\text{length} \times \text{width}^2).$$

The gross body weight was also measured throughout the experiment and monitored carefully. After 24 days of treatment, the mice were sacrificed humanly by cervical dislocation.

#### *4.2.12. Blood chemistry and histology (H&E) study:*

The blood was collected from the mice treated with PEG-SSNs-EGFR (treatment) and without any treatment (control) at the end of experiment (day 26) for biochemical analysis to calculate the levels of alkaline phosphatase (ALP), aspartate aminotransferase (AST), alanine aminotransferase (ALT), amylase (Amy) and creatinine (Cr) in serum samples of mice for both control (untreated) and treatment group. For histopathology analysis, collected major organs including heart, liver, spleen, kidney and lung from both control

and treatment group were fixed at day 26. The fixed organs were then processed for haematoxylin and eosin (H&E) staining and images were taken for analysis.

#### 4.2.13. Statistical analysis:

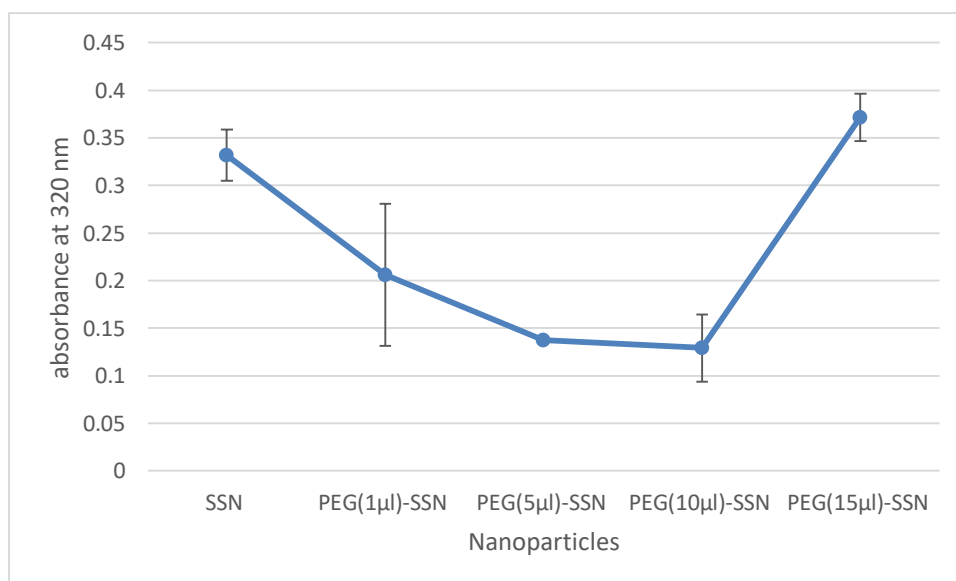
Statistical analysis was done by using GraphPad software (San Diego, CA, USA) to calculate p values. A t-test was applied for analyzing in vitro and in vivo data and comparing the significant difference. Data were considered statistically significant when  $*p < 0.05$  and very significant when  $**p < 0.001$ .

### 4.3. Results:

#### 4.3.1. Turbidity and optical images of PEG-SSNs:

In order to confirm the PEG-SSNs formation, we measured the turbidity by measuring absorbance at 320nm. SSNs were prepared by mixing 40 mM of  $\text{SrCl}_2$  and 10 mM of  $\text{Na}_2\text{SO}_3$  in 50  $\mu\text{l}$  of aqueous solution, followed by incubation at 37°C for 30 min. Then different concentrations (1  $\mu\text{l}$ , 5  $\mu\text{l}$ , 10  $\mu\text{l}$  and 15  $\mu\text{l}$  of 1  $\mu\text{M}$ ) of Biotin PEG were added and incubated for 10 min at 37°C and topped up with DMEM media (pH7.5) to make the final volume to 1 ml. The turbidity was then measured by using UV-VIS spectrophotometer. As shown in the figure 1(A), the SSNs without PEG showed higher turbidity, while the addition of PEG reduced the turbidity of SSNs significantly at 1  $\mu\text{l}$ , 5  $\mu\text{l}$  and 10  $\mu\text{l}$  except at 15  $\mu\text{l}$  of PEG concentration. This was probably due to the hindrance of particle-particle agglomeration and less particle formation as a result of coating with biotinylated PEG. To observe the NPs formation, optical images of SSNs with or without PEG were taken 20 min after the synthesis of SSNs by using different concentration of PEG (figure 1(B)). PEGylated SSNs exerted the uniform distribution of particle for 1, 5 and 10  $\mu\text{l}$  concentration except for 15  $\mu\text{l}$ . For 1 and 5  $\mu\text{l}$  PEG less aggregated and smaller particles were visible in compare to free SSNs.

A.



B.

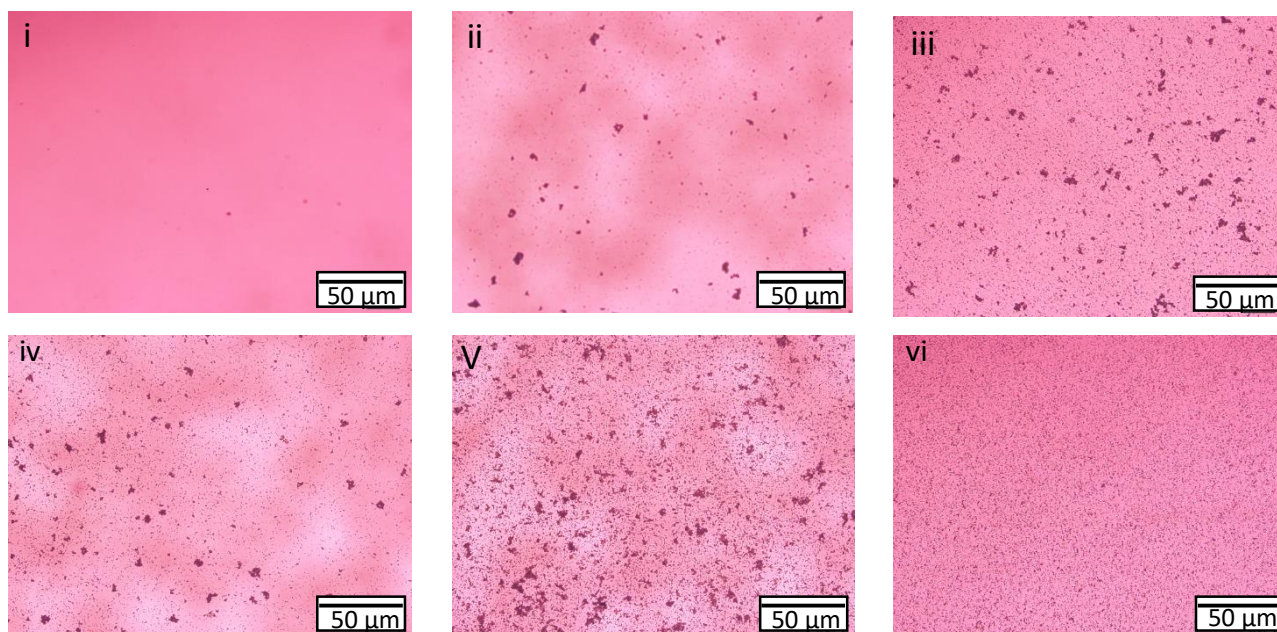


Figure 1: (A) Turbidity of SSNs with or without biotin PEG (1 $\mu$ M) at different concentrations (1 $\mu$ l, 5 $\mu$ l, 10 $\mu$ l and 15 $\mu$ l) at 320nm of absorbance. (B) Optical images of SSNs with or without PEG-(i) media only,(ii)SSNs formulated by 40mM of SrCl<sub>2</sub> and 10 mM of Na<sub>2</sub>SO<sub>3</sub>,(iii) PEG-SSNs formulated with 40mM of SrCl<sub>2</sub> and 10 mM of Na<sub>2</sub>SO<sub>3</sub> and coated with 1 $\mu$ l of Biotin PEG,(iv) PEG-SSNs formulated with 40mM of SrCl<sub>2</sub> and 10 mM of Na<sub>2</sub>SO<sub>3</sub> and coated with 5 $\mu$ l of Biotin PEG,(v) PEG-SSNs formulated with 40mM of SrCl<sub>2</sub> and 10 mM of Na<sub>2</sub>SO<sub>3</sub> and coated with 10 $\mu$ l of Biotin PEG,(vi) PEG-SSNs formulated with 40mM of SrCl<sub>2</sub> and 10 mM of Na<sub>2</sub>SO<sub>3</sub> and coated with 15 $\mu$ l of Biotin PEG.

#### 4.3.2. Size and Zeta potential of free SSN and PEG-SSNs:

Particles size and net charge on their surfaces of nanoparticles are the two main vital factors for determining the fate of NPs both in vitro and in vivo. The rate of bio distribution, tumor accumulation and the clearance of NPs may vary with particles size and charge (28-30). As detected by DLS, the size of the SSNs prepared by mixing of 40mM of SrCl<sub>2</sub> and 10 mM of Na<sub>2</sub>SO<sub>3</sub> without PEG showed a mean particle size of 2096.33 nm and a negative zeta potential of -11.95mV (figure 2). On the other hand, the average diameter of PEGylated SSNs were showed significant decrement pattern at different concentration of biotin PEG. The size of different concentration of PEG-SSN (1 $\mu$ l, 5 $\mu$ l, 10 $\mu$ l and 15 $\mu$ l) were ranging from 689-832 nm and the negative zeta potential gets lower

from -9.345 to -7.25mV, indicating the adsorption of the PEG on the surface of SSNs (figure 2).

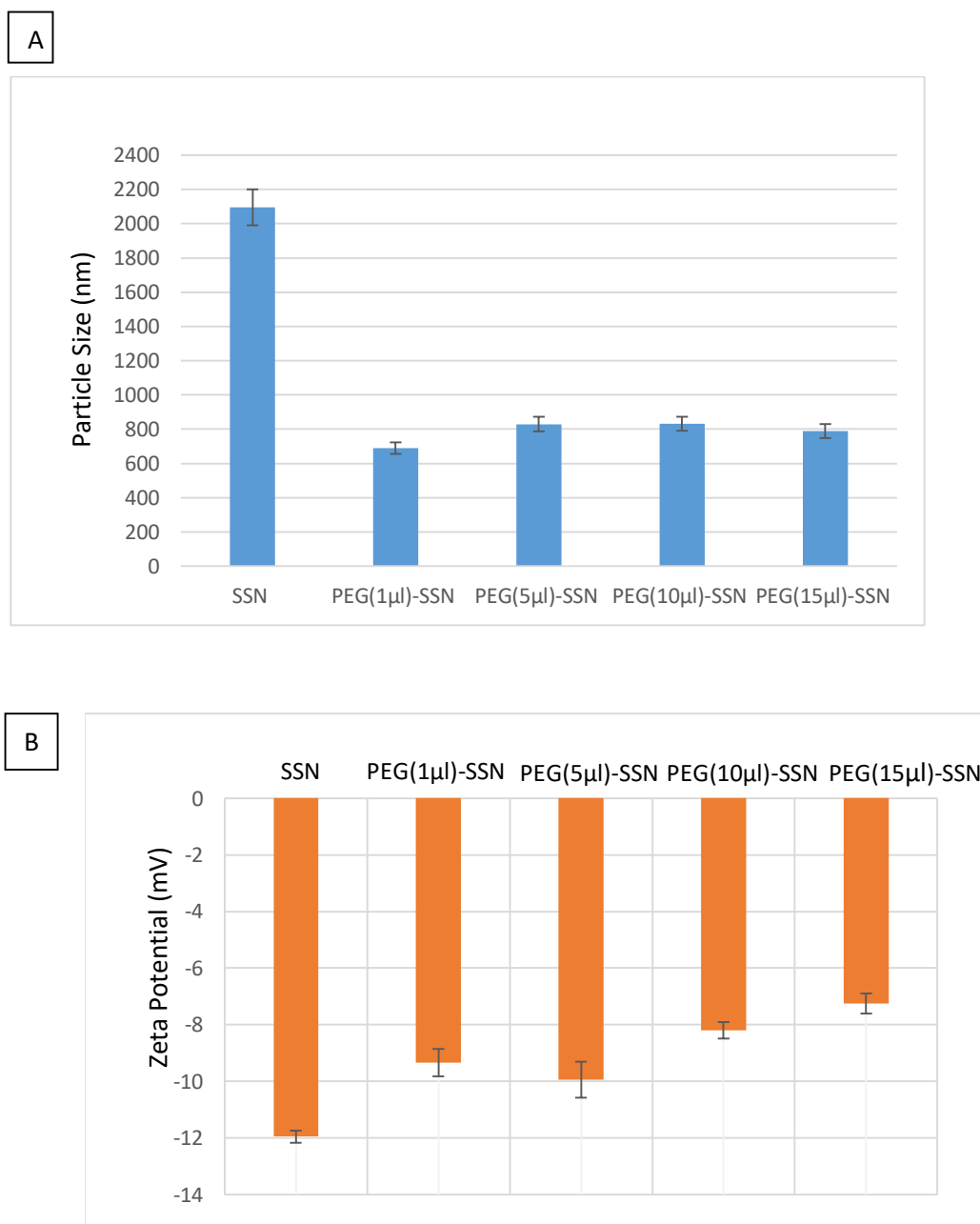


Figure 2: Sizes and zeta potential of SSNs with or without PEG. (A) Size of SSNs with or without Biotin PEG (1μM) at different concentration (1μl, 5μl, 10μl and 15μl). (B) Zeta potential of SSNs with different concentration (1μl, 5μl, 10μl and 15μl) of Biotin PEG.



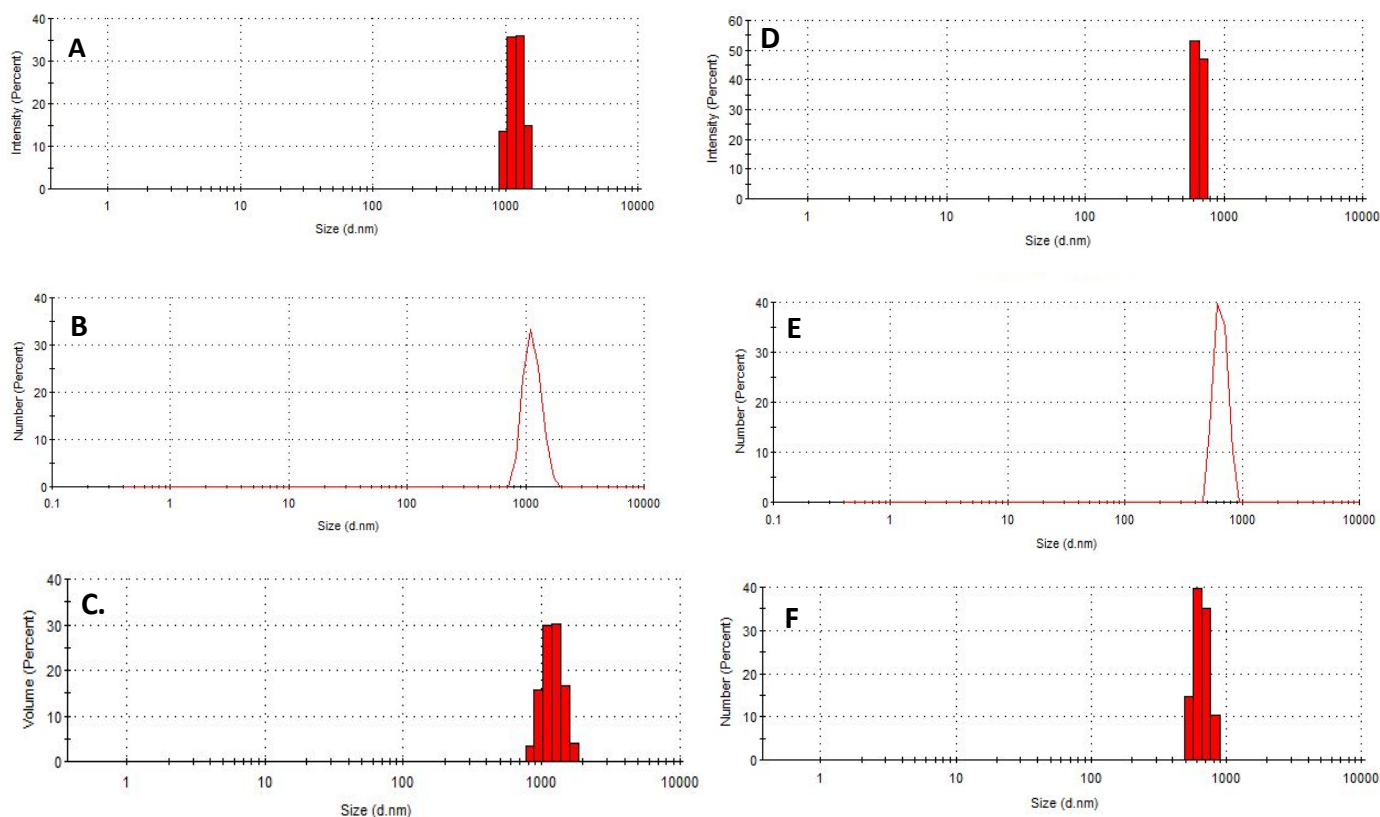


Figure 3: Particle size distribution by Intensity, Number and Volume of SSNs and PEG-SSNs by Zetasizer. SSNs and PEG-SSNs were prepared by mixing of 40 mM of  $\text{SrCl}_2$  and 10 mM of  $\text{Na}_2\text{SO}_3$  in 50  $\mu\text{l}$  of aqueous solution, followed by incubation at 37°C for 30 min and finally added 1  $\mu\text{l}$  of Biotin PEG (1  $\mu\text{M}$ ) to make PEG-SSNs.

#### 4.3.3. Characterization of SSNs and PEG-SSNs by Dynamic Light Scattering (DLS):

Size distribution of particles by intensity, number and volume and PDI value were evaluated by DLS technique which determines the distribution of particles and PDI based on intensity having a limitations of signal domination of larger NPs than smaller particles and interference from light adsorbing species (31). SSNs particles exerted large sized particle distribution for intensity, number and volume with a PDI value of 0.319 while modification of SSNs by using 1  $\mu\text{l}$  of Biotin PEG resulted smaller particle sized distribution with a PDI value of 0.869 as shown in the figure (3).

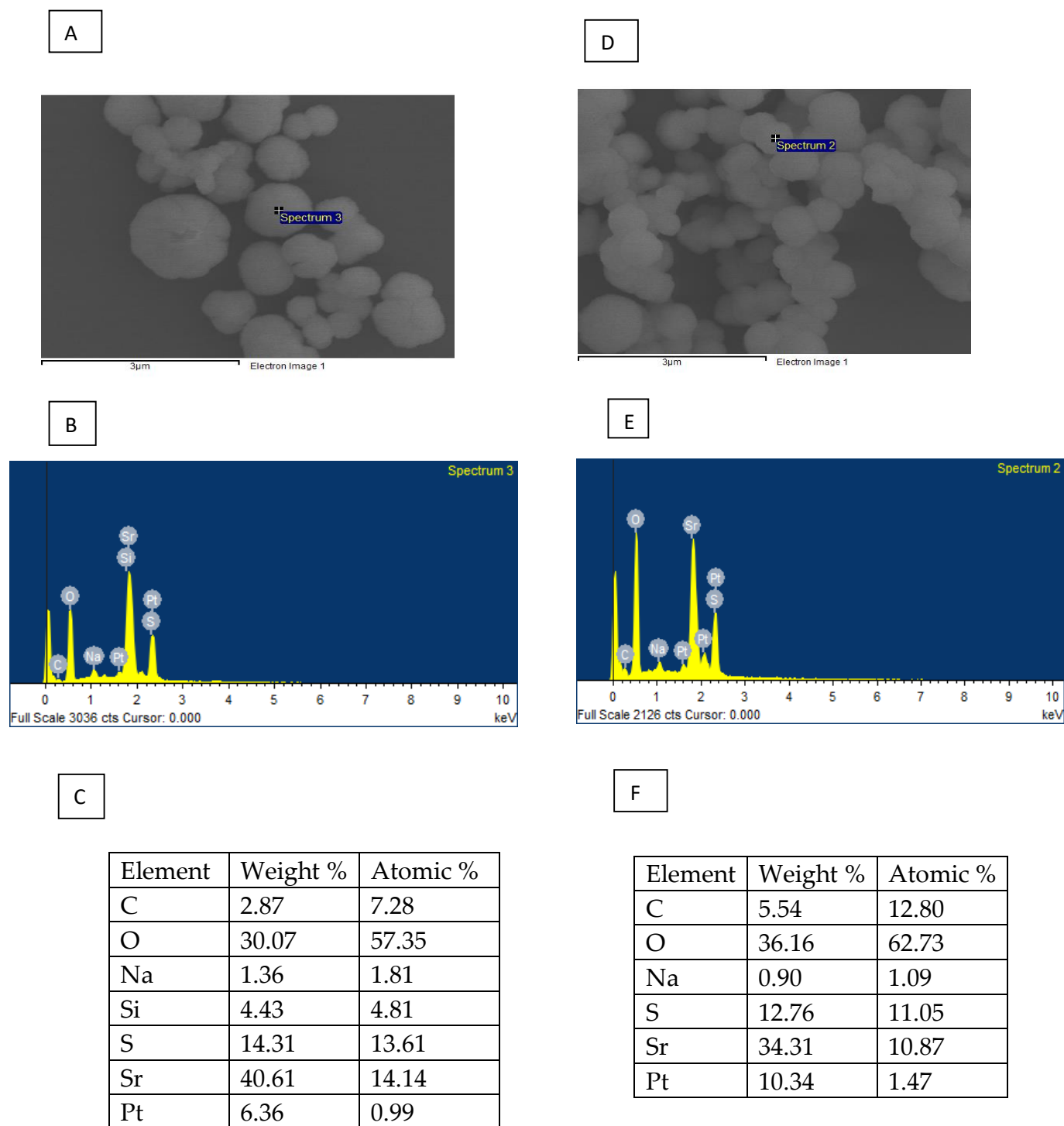


Figure 4: Elemental analysis of PEG-SSNs by EDX, PEG-SSNs were prepared by adding 40 mM of  $\text{SrCl}_2$  and 10 mM of  $\text{Na}_2\text{SO}_3$  in 50  $\mu\text{l}$  of aqueous solution and finally added 1  $\mu\text{l}$  of Biotin PEG (1  $\mu\text{M}$ ). (A, B) EDX spectrum of SSNs, (C) weight and atomic percentage of SSNs, (D, E) EDX spectrum of PEG-SSNs, (F) Weight and atomic percentage of PEG-SSNs.

#### 4.3.4. Elemental analysis of PEG-SSNs by EDX:

In order to analyze the elemental composition of SSNs and PEGylated SSNs, 40 mM of  $\text{SrCl}_2$  and 10 mM of  $\text{Na}_2\text{SO}_3$  in 50  $\mu\text{l}$  of aqueous solution, followed by incubation at 37°C for 30 min and finally added 1  $\mu\text{l}$  of Biotin PEG (1  $\mu\text{M}$ ) were subjected to EDX analysis for confirming formation of SSNs and surface modified SSNs. According to the EDX results as shown in the figure (4), Sr, O and S contained higher percentage of total element and PEGylated SSNs also contained higher ratio of Sr, O and S. Biotin PEG modified SSNs contained more percentage of Oxygen than unmodified one. Traces of Si, C and Pt were found for both SSNs due to usage of carbon sputtering and sample glass holder.

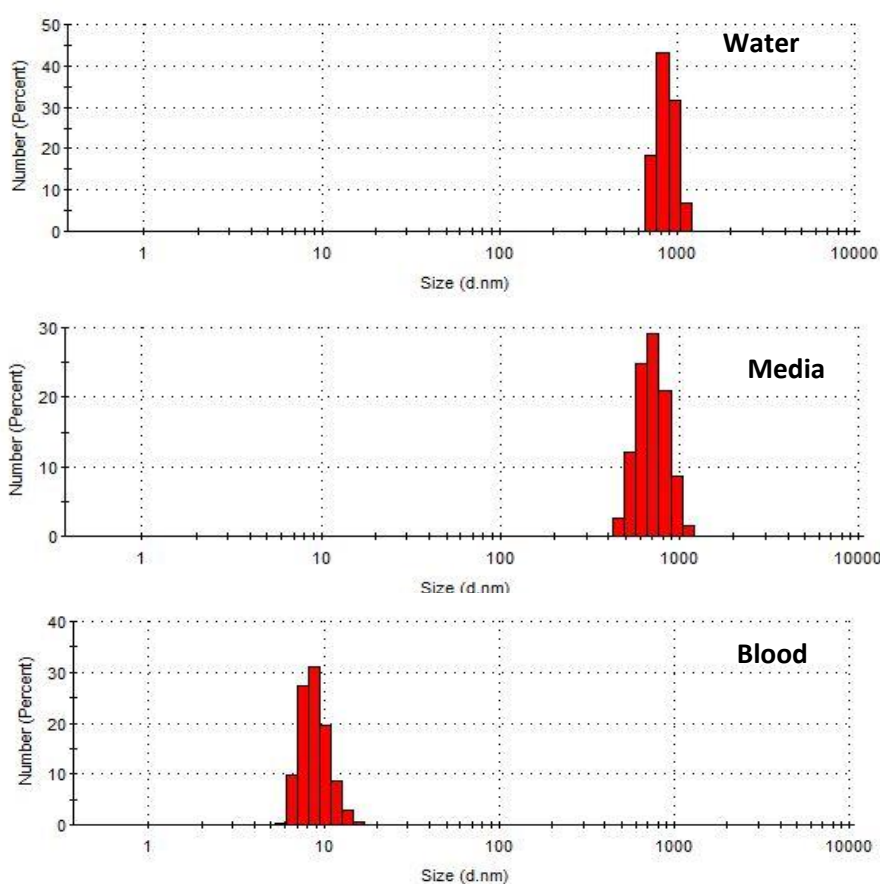


Figure 5: Particle size distribution analysis of PEG-SSNs in water, DMEM culture medium and the blood obtained from mice by dynamic light scattering (DLS). PEG-SSNs were synthesized by the addition of 40 mM of  $\text{SrCl}_2$  and 10 mM of  $\text{Na}_2\text{SO}_3$  in 50  $\mu\text{l}$  of aqueous solution and finally 1  $\mu\text{l}$  of Biotin PEG (1  $\mu\text{M}$ ).

#### 4.3.5. Stability of PEG-SSNs in mice plasma by DLS:

The stability of PEG-SSNs in blood were determined by using DLS. PEG-SSNs were prepared by using 40 mM of  $\text{SrCl}_2$  and 10 mM of  $\text{Na}_2\text{SO}_3$  in 50  $\mu\text{l}$  of aqueous solution, followed by incubation at 37°C for 30 min and finally added 1  $\mu\text{l}$  of Biotin PEG (1  $\mu\text{M}$ ) before topped up with DMEM media (950  $\mu\text{l}$ ), water (950  $\mu\text{l}$ ) and plasma of mouse blood (10% in PBS). As shown in the figure (5), PEGylated SSNs in DMEM media and deionized water exerted same particle size distribution pattern and stability with a PDI value of 0.659. On the other hand, in mice blood the particle were getting smaller, small sized distribution have been found that may be due to coating of blood proteins on the surface of PEG-SSNs.

#### 4.3.6. siRNA encapsulation efficiency of PEG-SSNs:

Binding of negatively charged siRNA with Nanoparticles is the main prerequisite for carrying the siRNA into target cytoplasm of cancer cells. Efficient binding interaction of siRNA and NPs ensures the better cellular uptake, release and pharmacological action. SSNs and siRNA complexes were prepared by adding 40 mM of  $\text{SrCl}_2$ , 10 mM of  $\text{Na}_2\text{SO}_3$  and 10 nm of AF-488 fluorescence siRNA.

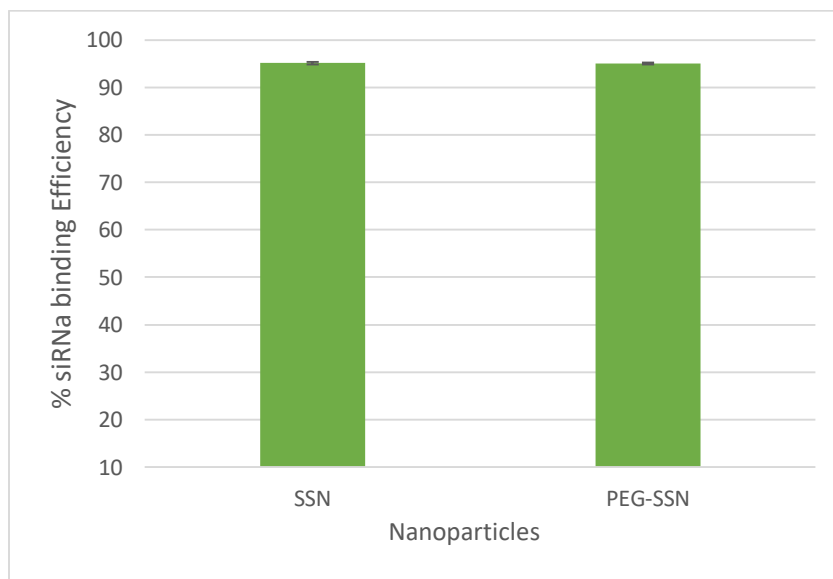


Figure 6: % siRNA binding efficiency of PEG-SSNs encapsulated AF-488 siRNA. PEG-siRNA-SSNs were prepared by mixing of mixing 40 mM of  $\text{SrCl}_2$ , 10 mM of  $\text{Na}_2\text{SO}_3$  and 10 nm of AF-488 fluorescence siRNA in 50  $\mu\text{l}$  of aqueous solution, followed by incubation at 37°C for 30 min. After incubation, 1  $\mu\text{l}$  of biotin PEG were added and incubated for 10 min to prepare PEG-siRNA-SSNs complex.

The standard curve was plotted by siRNA concentration versus the peak area and siRNA encapsulation efficiency were calculated. As shown in the figure (6), SSNs showed 95% of binding efficiency whereas SSNs coated with Biotin PEG also showed 95% of binding efficiency, indicated that PEG coating didn't interfere the siRNA binding.

#### *4.3.7. Cytotoxicity and hemolysis assay:*

The hematological biocompatibility of SSNs and PEG-SSNs was evaluated by using hemolytic experiment in vitro. The hemolysis percentage of SSNs and PEGylated SSNs were found very low (only 1%) and the positive control gave 100% rupture of RBC (figure 7.A.). The biocompatibility of SSNs and PEG-SSNs was evaluated in MCF-7 cells via MTT assay to assess the cytotoxicity of NPs. In figure 7(B), SSNs and PEG-SSNs demonstrated cell viability of 80% and 73%.

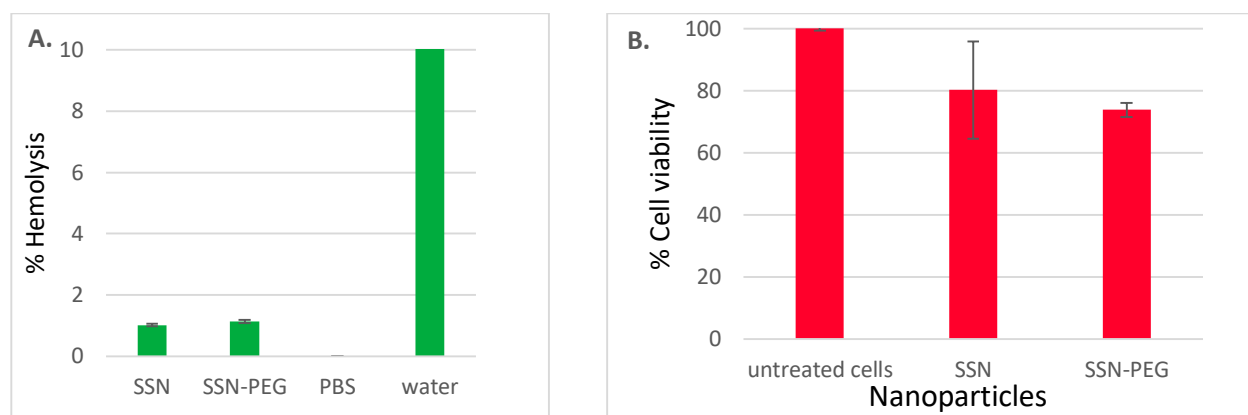


Figure 7: (A) Hemolysis percentage of RBCs incubated with SSNs with or without PEG, (B) cell viability of SSN and PEG-SSNs in MCF-7 cells. Cells were treated with media (untreated), SSNs and PEG-SSNs formed with 40 mM of  $\text{SrCl}_2$ , 10 mM of  $\text{Na}_2\text{SO}_3$  and 1  $\mu\text{l}$  of biotin PEG. Data were represented as mean  $\pm$  SD for triplicate samples.

#### 4.3.8. *In vitro* antitumor activity assay of EGFR siRNA coupled SSNs and PEG-SSNs:

EGFR and their activated signaling molecules have remarkable roles in the development and progression of human breast cancer cell and reported to be overexpressed in TNBC (triple-negative breast cancer)(9, 32, 33). Overexpression of EGFR induces cellular proliferation as well as plays a vital role in the pathology of breast cancer. We hypothesized that silencing of growth factor receptors expression by using anti-sense siRNA might reduce aggressiveness of cancer cells and beneficial for exerting antitumor activity. To investigate the *in vitro* anticancer efficacy, SSNs and PEG-SSNs coupled with siRNA to silence the overexpressed EGFR was evaluated in MCF-7 (human breast cancer cell line) and 4T1 (murine mammary adenocarcinoma cell line) by MTT assay. We first seeded  $5 \times 10^4$  of MCF-7 and 4T1 cells in a 24-well plate. On the following day, the cells were treated with SSNs, SSNs-EGFR siRNA, PEG-SSNs and PEG-SSN-EGFR siRNA, followed by incubation for 48 h, and finally, cytotoxicity was measured. As shown in the figure 8(A), In MCF-7 cell line, the viability of free SSNs and PEG-SSNs were 85% and 89% whereas EGFR coupled SSNs and PEG-SSNs showed the cytotoxicity of 8% and 17% compared to free Nanoparticles. This data clearly indicates that, SSNs and PEG-SSNs carried the siRNA efficiently into the breast tumor cell and inhibit the growth of tumor cell by silencing EGFR gene expression. PEGylated SSNs provided more cytotoxic effects than unmodified SSNs which would be due to their more cellular internalization of small sized PEG-SSNs. For 4T1 cell line, the average viability of SSNs and PEG-SSNs were 85% and 77% respectively as shown in the figure 8(B). The cytotoxicity of siRNA targeted to

EGFR gene coupled SSNs and PEG-SSNs were found to be 19% and 4 % after 48 hour of treatment.

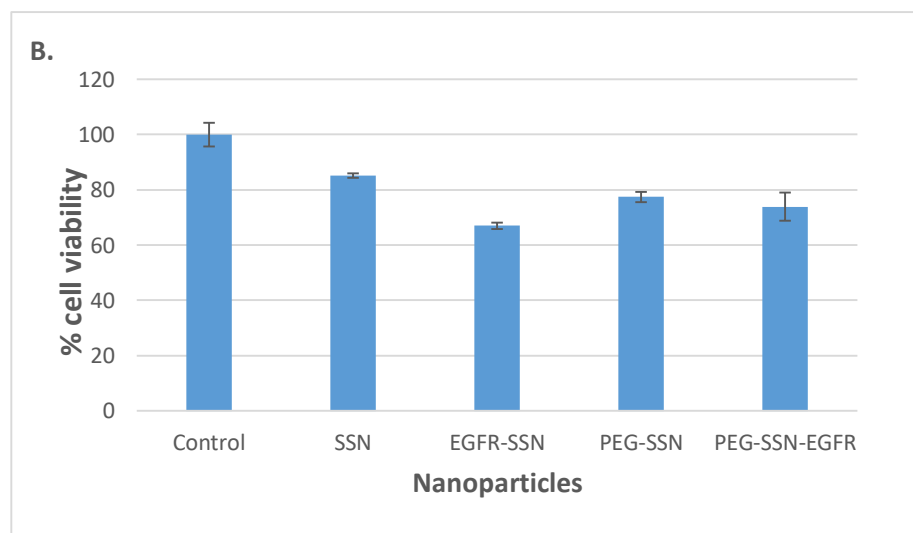
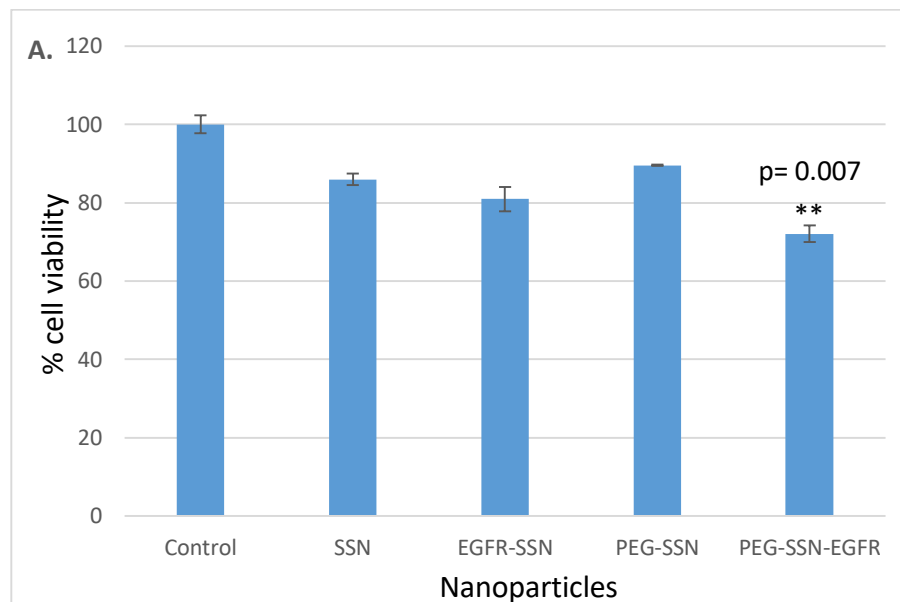
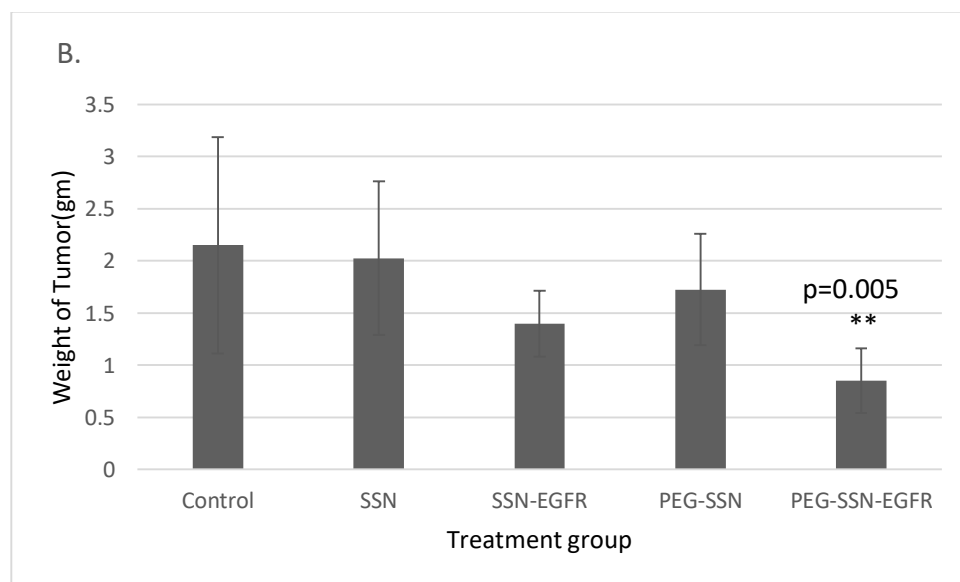
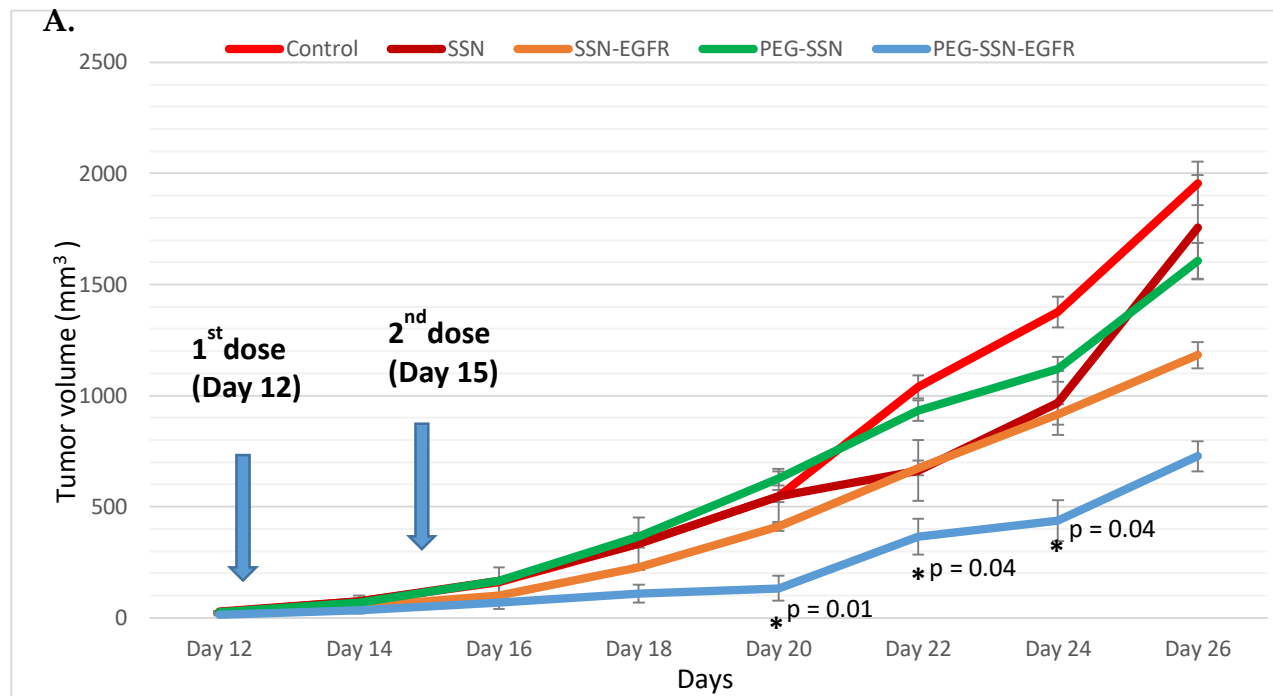


Figure 8: Cytotoxicity assay of SSNs and PEG-SSNs loaded EGFR siRNA in MCF-7(A) and 4T1 (B) cell line. % of Cell viability assessment of free SSNs and PEG-SSNs, SSNs-EGFR and PEG-SSN-EGFR in MCF-7 cell after 48 h of treatment. SSNs, PEG-SSNs conjugated EGFR were prepared by adding 40 mM of  $\text{SrCl}_2$ , 10 mM of  $\text{Na}_2\text{SO}_3$  and 1 nm of EGFR siRNA and 1  $\mu\text{l}$  of biotin PEG for making PEG-SSN-EGFR. Values were very significant (\*\*) at  $p$  value 0.001 to 0.01 and significant (\*) at  $p$  value 0.01 to 0.05 as compared to the PEG-SSN group.





C.

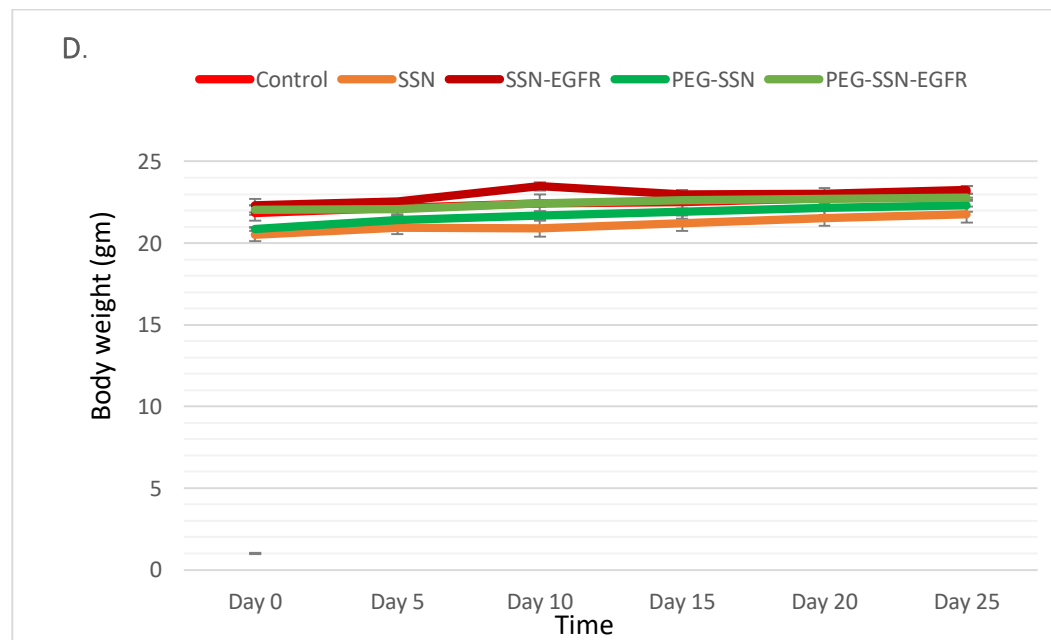
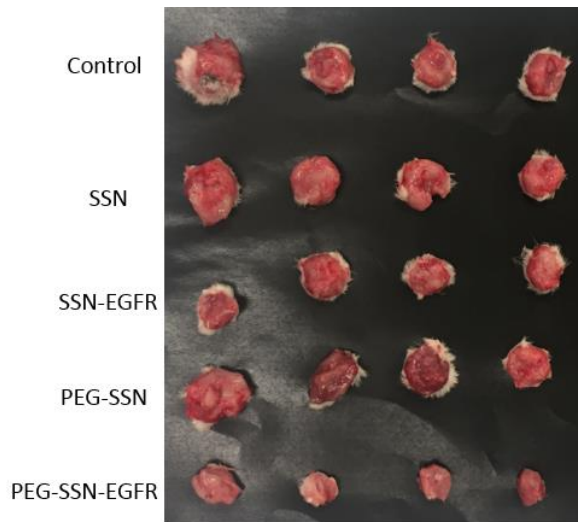


Figure 9: Tumor growth inhibition effects of PEG-SSNs coupled with EGFR siRNA in murine 4T1 subcutaneous tumor model (A). Tumor growth curves for five different groups treated with control (untreated), SSN, SSN-EGFR (50nM), PEG-SSN and PEG-SSN-EGFR (50nM). (B) weight of tumors collected at the end of experiment. (C) images of excised tumors at day 26. (D) Body weights of mice. Each group of treatment contained 4 mice and error bars are based on standard error of mean. Values for PEG-SSN-EGFR were very significant (\*\*) at  $p$  value 0.001 to 0.01 and significant (\*) at  $p$  value 0.01 to 0.05 as compared to the PEG-SSN group.

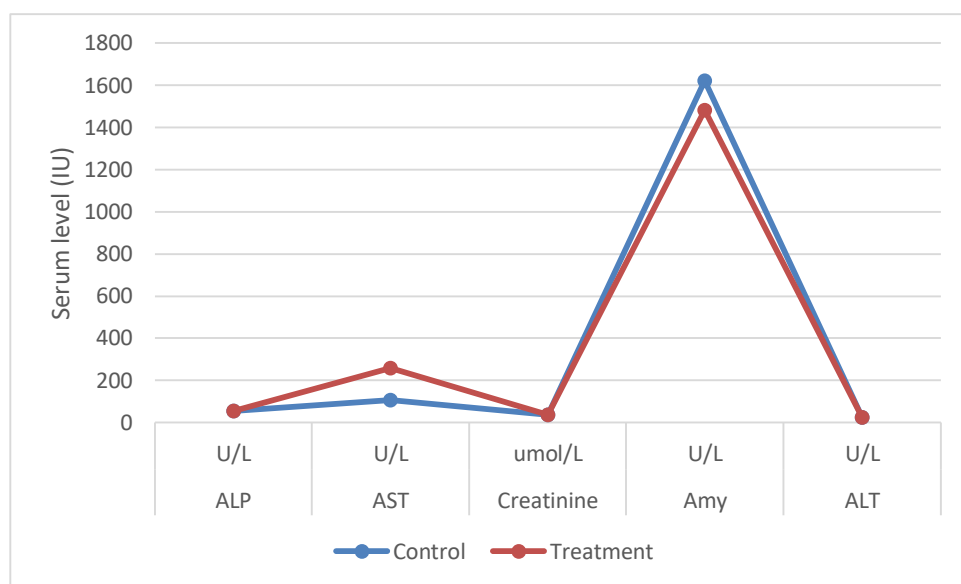
#### *4.3.9. Tumor regression study of PEG-SSNs conjugated EGFR siRNA in mouse model:*

The tumor regression study was carried out in pre-established 4T1 tumor induced female balb/c mice in accordance with the protocol approved by MONASH Animal Ethics Committee (MARF/2016/126). In order to investigate the anti-tumor effects of SSNs particles, tumor bearing mice were treated with SSNs, PEG-SSNs, SSN-EGFR (50nM of EGFR siRNA) and PEG-SSN-EGFR (50nM of EGFR siRNA) through tail vein. The mice without any treatment remained as untreated (control) group. Tumor volume were measured for a period of 26<sup>th</sup> days of treatment at a certain time interval. As shown in the tumor growth curve (figure 09), the tumor volume for untreated group was 1956.15 mm<sup>3</sup> and the growing rate was quicker than other group of mice. Only SSNs and PEG-SSNs were also showed large tumor volume around 1606-1756 mm<sup>3</sup> with an increasing growing trend after 26<sup>th</sup> days of treatment. SSNs conjugated with EGFR exerted modest lower tumor growth trend than other three groups and tumor volume was recorded to 1182.80 mm<sup>3</sup>. However, PEGylated SSNs along with anti-EGFR siRNA gave slower tumor growth rate and significant tumor reduction effects (tumor volume 726.46 mm<sup>3</sup>) in comparison to control and free NPs treating group. The mice receiving PEG-SSN-EGFR showed significant antitumor effects (almost 60% reduction of tumor volume) in compare to control group. The tumors were excised after 26 days of treatment and it was found that average tumor weight of group of mice treated with PEG-SSN-EGFR had smallest tumor weight in compare to control and free NPs group. Additionally, body weight of mice were found to be same for all group both treated and untreated throughout the whole experiment.

#### *4.3.10. Blood Chemistry and Histology (H&E) study:*

To measure the systemic toxicity of mice treated with control and treatment, collected blood and major organs were subjected to blood chemistry analysis and histology assay after 26 days of intravenous administration. As shown in the figure 10(A), the levels of blood chemistry were normal for both control and treatment group except for the AST and amylase. On the other hand, we didn't notice any significant changes in the histology of major organs of mice treated with EGFR coupled PEG-SSNs as presented in the figure 10(B).

A.



B.

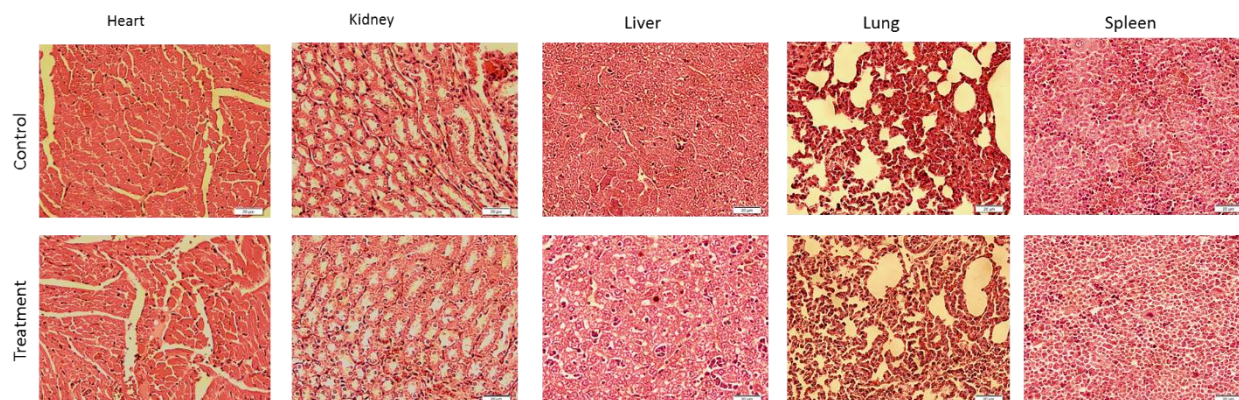


Figure 10: (A) Blood chemistry analysis of control and treated mice after 26 days of treatment. (B) Histopathology images of H&E stained major organs collected from control (untreated) and treatment group on day 26. All images were taken at scale bar 20  $\mu$ m.

#### 4.4. Discussion:

Although inorganic NPs are advantageous in terms of drug loading capability, unique physicochemical properties and biocompatibility, their instability in the systemic circulation and off target bio-distribution still remain major challenge (34-36). Previously

we reported SSNs as inorganic nanocarriers for the delivery of siRNA into cancer cells(9). SSNs nanoparticles showed non-specific distribution and less tumor accumulation of siRNA after intravenous administration. We have modified SSNs with biotin PEG to increase circulation half-life, reduce off target distribution and increase tumor accumulation of siRNA. SSNs without modification had high absorbance value reflecting the formation of more clustered particles and large sized particles. On the other hand, PEGylation of SSNs showed decreasing trends of absorbance at different concentrations of PEG except 15 $\mu$ l (figure 1.A.). This is probably due to surface coating of SSNs by hydrophilic PEG which prevents the particle-particle aggregation and perhaps formed small sized particles. The microscopic observation of SSNs also revealed that particles aggregates were less in PEGylated SSNs in compare to free SSNs. The size and zeta potential of SSNs and PEG-SSNs were measured by DLS method. For in vitro studies, cellular internalization of NPs depends on the size and surface charge of NPs and it was found that smaller and positively charged NPs had more cellular uptake (37-40). In case of In vivo experiments, blood protein-NPs interaction, recognitions by RES, extravasation from blood to tumor tissues, clearance by kidneys were affected by the size and surface charge of the NPs(4, 29). The size of the unmodified SSNs were found to be large (figure 2) and the size distribution pattern were in more than 1000 nm range whereas PEGylated SSNs gave small sized particles and particle size distribution below 1000 nm similar to absorbance value. Biotin PEG may be bound with Sr ions and hinder the particle agglomeration resulted small sized and uniformly distributed particles. Moreover, the zeta potential of PEGylated SSNs were decrease to more electropositive than free SSNs, indicating the adsorption of PEG on the surface of the SSNs. The overall small sized and negatively charged PEG-SSNs would prevent the interaction with negatively charged blood proteins and increase the tumor accumulation (41, 42).

Next we examined the elemental composition of formed SSNs and PEG-SSNs by using EDX analysis. Both modified and unmodified SSNs gave higher concentration of Sr<sup>++</sup>, S and O, reflecting the formation of SSNs successfully. Additionally, PEG coated SSNs gave more percentage of Carbon and Oxygen than free SSNs which is from PEG chain (figure 4). The stability of PEG-SSNs after entering into the systemic circulation are very important and crucial for the stability of PEG-SSNs in biological solutions. The particle size distribution and PDI value of PEG-SSNs were remain same in water and Media whereas the PDI value were same in blood plasma and the size distribution pattern shifted to small sized particles. This is due to coated of the PEG-SSNs by the proteins present in the mice plasma (figure 5). We observed a significant binding efficiency of SSNs and PEG-SSNs with siRNA and more interestingly PEGylation didn't hamper the

binding of siRNA. We can assume that modified SSNs would bind with siRNA for carrying them into the target cytoplasm of cancer cells and also ensured the remarkable drug loading capability of modified SSNs. The biocompatibility of SSNs and PEG-SSNs were evaluated by both hemolytic activity and cytotoxicity. It was found that the modified SSNs had no toxic effects in blood cells as well as in normal cells, indicating PEG-SSNs are suitable nanocarriers for the delivery of siRNA and gene into the body. As we have got small particle size, smaller sized particle distribution and higher affinity towards the siRNA, we assumed that PEG-SSNs will efficiently carry the siRNA into the breast cancer cell through endocytosis pathways. After entering into the cell, pH sensitive PEG-SSNs would pull the ions, increase osmotic pressure resulted swelling and burst out of siRNA from endosomal membrane at the early stage of endosome. The early release of siRNA from endosome are expected to give quick response in silencing EGFR siRNA, induce apoptosis and anticancer effects. We have found higher cytotoxicity of PEG-SSNs coupled EGFR than unmodified one for both MCF-7 and 4T1 cell lines. The smaller size PEG-SSN probably regulates more cellular uptake than the free SSNs and degrades the PEG-SSN-EGFR complex in the acidic environment of early endosomal stage, released the EGFR siRNA into the cytoplasm and prevents the tumorigenesis by silencing overexpressed EGFR gene.

Finally, surface modified SSNs with electrostatically associated EGFR siRNA were tested in 4T1 tumor-bearing mice for evaluating anticancer effects. PEG-SSN-EGFR complex showed significant reduction in tumor volume compared to the control group, which could be attributed to extended biological stability of NPs, more tumor accumulation, improved cellular internalization and fast release of the siRNA inside cell to silence the target gene. Free siRNA without any carrier is prone to systemic degradation by nucleases and rapid clearance by kidneys. SSNs without any surface modification could be attacked by hundreds of proteins present in the blood, leading to macrophage recognition, off target distribution and finally less tumor accumulation of siRNA. PEGylation of SSNs caused reduced particle size, improved the blood circulation time, reduced off target effects and accelerated the tumor accumulation of siRNA by preventing the opsonization of SSNs. The unchanged body weight of mice treating with control, free SSNs and siRNA coupled SSNs indicate the null systemic toxicity of NPs and NP-siRNA complexes in the mouse model. There were no remarkable changes in the blood biochemical parameters in both control and treated mice. In addition, no noticeable damages or changes in the histology of major organs collected from both control and treatment group were observable, indicating higher safety profile of PEG-SSN nanoparticles for carrying siRNA into target tumor.

#### 4.5. Conclusion:

PEGylation of NPs is the most widely used approach for enhancing the stability and tumor targetability of NPs. In this work, we have successfully coated the surface of the SSNs with biotin PEG through non-covalent (electrostatic) interactions. Surface modification of SSNs with PEG made the surface charge of SSNs more electropositive and reduced the particle size significantly by stopping the particle-particle aggregation. These PEG-SSNs with desired small size promoted high siRNA loading efficiency. More importantly, PEGylated SSNs led to prolonged circulation time, augmented tumor uptake, and superior therapeutic outcome in terms of anti-tumor activity. In consideration of the above facts, PEG-SSNs have merged as a promising tool for tumor-targeted delivery of siRNAs, genes and small molecule drugs for cancer management in near future.

#### References

1. Zhao G, Long L, Zhang L, Peng M, Cui T, Wen X, et al. Smart pH-sensitive nanoassemblies with cleavable PEGylation for tumor targeted drug delivery. *Scientific reports*. 2017;7(1):3383.
2. Karim M, Tha K, Othman I, Borhan Uddin M, Chowdhury E. Therapeutic potency of nanoformulations of siRNAs and shRNAs in animal models of cancers. *Pharmaceutics*. 2018;10(2):65.
3. Pecot CV, Calin GA, Coleman RL, Lopez-Berestein G, Sood AK. RNA interference in the clinic: challenges and future directions. *Nature Reviews Cancer*. 2011;11(1):59.
4. Alexis F, Pridgen E, Molnar LK, Farokhzad OC. Factors affecting the clearance and biodistribution of polymeric nanoparticles. *Molecular pharmaceutics*. 2008;5(4):505-15.
5. Riley M, Vermerris W. Recent advances in nanomaterials for gene delivery—a review. *Nanomaterials*. 2017;7(5):94.
6. Erathodiyil N, Ying JY. Functionalization of inorganic nanoparticles for bioimaging applications. *Accounts of chemical research*. 2011;44(10):925-35.
7. Kunnath A, Tiash S, Fatemian T, Morshed M, Mohamed S, Chowdhury E. Intracellular delivery of ERBB2 siRNA and p53 gene synergistically inhibits the growth of established tumour in an immunocompetent mouse. *J Cancer Sci Ther*. 2014;6:99-104.
8. Tiash S, Chua MJ, Chowdhury EH. Knockdown of ROS1 gene sensitizes breast tumor growth to doxorubicin in a syngeneic mouse model. *International journal of oncology*. 2016;48(6):2359-66.

9. Karim M, Shetty J, Islam RA, Kaiser A, Bakhtiar A, Chowdhury EH. Strontium Sulfite: A New pH-Responsive Inorganic Nanocarrier to Deliver Therapeutic siRNAs to Cancer Cells. *Pharmaceutics*. 2019;11(2):89.
10. Albanese A, Tang PS, Chan WC. The effect of nanoparticle size, shape, and surface chemistry on biological systems. *Annual review of biomedical engineering*. 2012;14:1-16.
11. Walkey CD, Olsen JB, Guo H, Emili A, Chan WC. Nanoparticle size and surface chemistry determine serum protein adsorption and macrophage uptake. *Journal of the American Chemical Society*. 2012;134(4):2139-47.
12. Lynch I, Dawson KA. Protein-nanoparticle interactions. *Nano today*. 2008;3(1-2):40-7.
13. Cedervall T, Lynch I, Foy M, Berggård T, Donnelly SC, Cagney G, et al. Detailed identification of plasma proteins adsorbed on copolymer nanoparticles. *Angewandte Chemie International Edition*. 2007;46(30):5754-6.
14. Cedervall T, Lynch I, Lindman S, Berggård T, Thulin E, Nilsson H, et al. Understanding the nanoparticle–protein corona using methods to quantify exchange rates and affinities of proteins for nanoparticles. *Proceedings of the National Academy of Sciences*. 2007;104(7):2050-5.
15. Ali R, Wendt MK. The paradoxical functions of EGFR during breast cancer progression. *Signal transduction and targeted therapy*. 2017;2:16042.
16. Cohen S, Fava RA, Sawyer ST. Purification and characterization of epidermal growth factor receptor/protein kinase from normal mouse liver. *Proceedings of the National Academy of Sciences*. 1982;79(20):6237-41.
17. Yarden Y, Sliwkowski MX. Untangling the ErbB signalling network. *Nature reviews Molecular cell biology*. 2001;2(2):127.
18. Tiash S, Kamaruzman NIB, Chowdhury EH. Carbonate apatite nanoparticles carry siRNA (s) targeting growth factor receptor genes egfr1 and erbb2 to regress mouse breast tumor. *Drug delivery*. 2017;24(1):1721-30.
19. Masuda H, Zhang D, Bartholomeusz C, Doihara H, Hortobagyi GN, Ueno NT. Role of epidermal growth factor receptor in breast cancer. *Breast cancer research and treatment*. 2012;136(2):331-45.
20. Burness ML, Grushko TA, Olopade OI. Epidermal growth factor receptor in triple-negative and basal-like breast cancer: promising clinical target or only a marker? *The Cancer Journal*. 2010;16(1):23-32.
21. Guo S, Huang L. Nanoparticles escaping RES and endosome: challenges for siRNA delivery for cancer therapy. *Journal of Nanomaterials*. 2011;2011:11.
22. Suk JS, Xu Q, Kim N, Hanes J, Ensign LM. PEGylation as a strategy for improving nanoparticle-based drug and gene delivery. *Advanced drug delivery reviews*. 2016;99:28-51.

23. Kolate A, Baradia D, Patil S, Vhora I, Kore G, Misra A. PEG—a versatile conjugating ligand for drugs and drug delivery systems. *Journal of controlled release*. 2014;192:67-81.
24. Nehate C, Jain S, Saneja A, Khare V, Alam N, Dhar Dubey R, et al. Paclitaxel formulations: challenges and novel delivery options. *Current drug delivery*. 2014;11(6):666-86.
25. Cosco D, Bulotta A, Ventura M, Celia C, Calimeri T, Perri G, et al. In vivo activity of gemcitabine-loaded PEGylated small unilamellar liposomes against pancreatic cancer. *Cancer chemotherapy and pharmacology*. 2009;64(5):1009-20.
26. Caliceti P, Veronese FM. Pharmacokinetic and biodistribution properties of poly (ethylene glycol)–protein conjugates. *Advanced drug delivery reviews*. 2003;55(10):1261-77.
27. Mishra P, Nayak B, Dey R. PEGylation in anti-cancer therapy: An overview. *asian journal of pharmaceutical sciences*. 2016;11(3):337-48.
28. E Grottgau B, Cai X, Wang J, Yang X, Lin Y. Polymeric nanoparticles for a drug delivery system. *Current drug metabolism*. 2013;14(8):840-6.
29. He C, Hu Y, Yin L, Tang C, Yin C. Effects of particle size and surface charge on cellular uptake and biodistribution of polymeric nanoparticles. *Biomaterials*. 2010;31(13):3657-66.
30. Wang J, Byrne JD, Napier ME, DeSimone JM. More effective nanomedicines through particle design. *Small*. 2011;7(14):1919-31.
31. Shang L, Nienhaus K, Nienhaus GU. Engineered nanoparticles interacting with cells: size matters. *Journal of nanobiotechnology*. 2014;12(1):5.
32. Knowlden JM, Hutcheson IR, Jones HE, Madden T, Gee JM, Harper ME, et al. Elevated levels of epidermal growth factor receptor/c-erbB2 heterodimers mediate an autocrine growth regulatory pathway in tamoxifen-resistant MCF-7 cells. *Endocrinology*. 2003;144(3):1032-44.
33. Garcia R, Franklin RA, McCubrey JA. Cell death of MCF-7 human breast cancer cells induced by EGFR activation in the absence of other growth factors. *Cell cycle (Georgetown, Tex)*. 2006;5(16):1840-6.
34. Anselmo AC, Mitragotri S. A review of clinical translation of inorganic nanoparticles. *The AAPS journal*. 2015;17(5):1041-54.
35. Senapati S, Mahanta AK, Kumar S, Maiti P. Controlled drug delivery vehicles for cancer treatment and their performance. *Signal transduction and targeted therapy*. 2018;3(1):7.
36. Shi J, Kantoff PW, Wooster R, Farokhzad OC. Cancer nanomedicine: progress, challenges and opportunities. *Nature Reviews Cancer*. 2017;17(1):20.
37. Dash BC, Réthoré G, Monaghan M, Fitzgerald K, Gallagher W, Pandit A. The influence of size and charge of chitosan/polyglutamic acid hollow spheres on cellular internalization, viability and blood compatibility. *Biomaterials*. 2010;31(32):8188-97.



38. Conner SD, Schmid SL. Regulated portals of entry into the cell. *Nature*. 2003;422(6927):37.
39. Zhao F, Zhao Y, Liu Y, Chang X, Chen C, Zhao Y. Cellular uptake, intracellular trafficking, and cytotoxicity of nanomaterials. *Small*. 2011;7(10):1322-37.
40. Bhattacharjee S, Ershov D, Fytianos K, van der Gucht J, Alink GM, Rietjens IM, et al. Cytotoxicity and cellular uptake of tri-block copolymer nanoparticles with different size and surface characteristics. *Particle and fibre toxicology*. 2012;9(1):11.
41. Chen K, Xu J, Luft JC, Tian S, Raval JS, DeSimone JM. Design of asymmetric particles containing a charged interior and a neutral surface charge: comparative study on in vivo circulation of polyelectrolyte microgels. *Journal of the American Chemical Society*. 2014;136(28):9947-52.
42. Gao P, Zhang X, Wang H, Zhang Q, Li H, Li Y, et al. Biocompatible and colloidally stabilized mPEG-PE/calcium phosphate hybrid nanoparticles loaded with siRNAs targeting tumors. *Oncotarget*. 2016;7(3):2855.

\*

## Chapter 5

### **Effects of PEGylated SSNs on protein corona formation and off-target distribution of siRNA.**

Work that is presented in this chapter is submitted in *Biochemical and Biophysical Research Communications* with minor adjustments in Figure/Table number to fit into the current thesis format. A snapshot of the submitted proof is included in page 162.

---

## Biochemical and Biophysical Research Communications: Submission Confirmation

1 message

**BBRC (ELS)** <eesserver@eesmail.elsevier.com>  
Reply-To: "BBRC (ELS)" <bbr@elsevier.com>  
To: md.ezharul.hoque@monash.edu  
Cc: karim604306@gmail.com

Sun, Apr 28, 2019 at 1:00 PM

\*\*\* Automated email sent by the system \*\*\*

Title: Effects of PEGylated SSNs on protein corona formation and off-target distribution of siRNA.  
Corresponding Author: Dr. Ezharul Hoque Chowdhury  
Authors: Md E Karim, Bachelor of Pharmacy;  
Short communication/Full length article

Dear Dr. Chowdhury,

This is to confirm that the above-mentioned manuscript has been received for consideration in Biochemical and Biophysical Research Communications. If you have the same submission kept incomplete in your profile or your co-author's profile, please remove it.

You will be able to check on the progress of your manuscript by logging on to the Elsevier Editorial System for Biochemical and Biophysical Research Communications as an author:

<https://ees.elsevier.com/bbr/>

Your username is: md.ezharul.hoque@monash.edu

If you need to retrieve password details, please go to: [http://ees.elsevier.com/BBRC/automail\\_query.asp](http://ees.elsevier.com/BBRC/automail_query.asp)

Your paper will be given a manuscript number shortly and you will soon receive an e-mail with this number for your reference.

Thank you for submitting your manuscript to Biochemical and Biophysical Research Communications. Should you have any questions, please feel free to contact our office.

Email: [bbr@elsevier.com](mailto:bbr@elsevier.com)

For further assistance, please visit our customer support site at <http://help.elsevier.com/app/answers/list/p/7923> Here you can search for solutions on a range of topics, find answers to frequently asked questions and learn more about EES via interactive tutorials. You will also find our 24/7 support contact details should you need any further assistance from one of our customer support representatives.

## **5. Effects of PEGylated SSNs on protein corona formation and off-target distribution of siRNA.**

### **5.1. Introduction:**

The use of nanotherapeutics has revolutionized the field of cancer as it shows promising success in drug and gene delivery, imaging and diagnosis (1-5). Recently nanoparticle-based RNAi therapy for cancer has drawn much attention owing to the unique physicochemical properties, improved circulation time and reduced toxicity of RNA-based therapeutics (6, 7). Considering the number of nano-sized products approved and investigated in clinical trials, nanomedicine will lead future cancer diagnosis and management arena. The rapid advancement in cancer nanomedicine introduces several challenges that need to be addressed for safer human exposure. Most of the NPs that are administered intravenously accumulate in target tumor cell after the extravasation from the blood through the EPR effects of leaky tumor vasculature (8-10). However during travelling from the site of administration to the site of action, NPs have to face a number of physiological obstacles, like interactions with extracellular components, resulting in instability in biological fluid and non-specific bio-distribution and thus causing unwanted side effects. Briefly, when NPs enter into blood circulation, thousands of proteins from biological environment like blood and extracellular matrix (ECM) are sequestered with NPs surface owing to their smaller particle size, large surface to volume ratio and surface charge (11, 12). The Interactions between NPs and proteins form a crown or layer around the surface called “protein corona” (PC), transforming NPs into a new biological entity “NPs-PC” complex (11, 13-15). The newly formed NPs-PC complex alters the physicochemical properties of NPs, determining the pharmacokinetics and pharmacodynamics parameters of the latter (12, 16, 17).

Depending on the physicochemical properties and exposure time of NPs for exchanging proteins, protein corona (PC) may be hard corona or soft corona. Hard corona comprises the high affinity proteins that form irreversible and tight layer on the surface of NPs and can be exchangeable in many hours. On the other hand, soft corona consists of the low affinity proteins, forming reversible and cleavable layer on the interface of NPs and being exchangeable rapidly within minutes or seconds (14, 18, 19). The NPs-PC complex contains hundreds of different proteins, with the most abundant identified proteins being apolipoproteins, adhesion mediators, signaling and transport proteins, immunoglobulin (IgG) complement compound and coagulation factors (20, 21). Among them complement and IgG proteins play a vital role in opsonization of NPs and the opsonized NPs are readily taken by macrophages including dendritic cells and blood monocytes present in

the liver, spleen and lymph nodes (17, 22), consequently, triggering the opsonin-mediated macrophage clearance, non-specific bio distribution, rapid clearance and formation of thrombosis, and declining therapeutic efficiency of drug-loaded NPs. Conversely, serum albumin and apolipoprotein known as dysopsonins which are also found in protein corona prevent the opsonin-mediated macrophage clearance and increase the stability of NPs in the biological fluid (3, 23, 24).

Surface modification would be a potential approach to avoid opsonization and systemic instability of NPs for improved therapeutic action as well as to reduce side effects. PEGylation is the most acceptable way to mask opsonin effects, improve solubility by increasing hydrophilicity, reduce the protein binding site, inhibit the macrophage uptake and extend the half-life in blood. PEG increases steric distance between the NPs and proteins, thereby reducing protein adsorption (25-28). Moreover, PEG modifies the size and flexibility of NPs reducing the renal filtration, and influences the extravasation by forming softer NPs.

Modifications of SSNs with biotin PEG would modulate protein adsorption, bioavailability and tumor targetability of SSNs. Our earlier study showed improved therapeutic efficiency of biotin PEG-SSNs carrying oncogene-specific siRNAs both in vitro and in vivo. In this study, we have successfully synthesized PEG-SSNs with desirable size and modified surface for successfully delivering the siRNA to the target tumor cell. We have analyzed the proteins entrapped onto the surface of SSNs and PEG-SSNs by using triple quadrupole liquid chromatography mass spectroscopy (QQQ LC/MS). We have also measured the distribution of fluorescence-labeled siRNA in different major organs and tumor for both SSNs and PEG-SSNs at certain time interval. This study thus provides insights in correlating pharmacokinetics of NPs with the constituents of protein corona formed onto NPs.

## **5.2. Materials and methods:**

### *5.2.1. Materials:*

Strontium chloride ( $\text{SrCl}_2$ ), sodium sulfite ( $\text{Na}_2\text{SO}_3$ ) and 4-(2-hydroxyethyl)-1-piperazineethanesulfonic acid (HEPES) were obtained from Sigma-Aldrich (St Louis, MO, USA). Dulbecco's modified eagle medium (DMEM), dimethyl sulfoxide (DMSO), thiazolyl blue tetrazolium bromide (MTT), and ethylene diamine tetra acetic acid (EDTA) were purchased from Sigma-Aldrich (St. Louis, MO, USA). DMEM powder, fetal bovine serum (FBS), trypsin-ethylene diamine tetra acetate (trypsin-EDTA), and penicillin-streptomycin were from Gibco BRL (CA). Poly (ethylene glycol) 2-aminoethyl ether biotin

were purchased from Sigma Aldrich (St. Louis, MO, USA). All siRNAs used in this study were obtained from Qiagen (Hilden, Germany) and dissolved in RNase-free water provided by the company.

#### *5.2.2. Synthesis of PEG-SSNs:*

Strontium sulfite NPs were prepared by mixing 40 mM of  $\text{SrCl}_2$  and 10 mM of  $\text{Na}_2\text{SO}_3$  in 50  $\mu\text{l}$  of aqueous solution, followed by incubation at 37°C for 30 min. 1  $\mu\text{l}$  of biotin PEG (1  $\mu\text{M}$ ) was added to the particles in the solution which was subsequently incubated for 10 min at 37°C and topped up with DMEM media (pH7.5) to make the final volume to 1 ml. On the other hand, SSNs were prepared by adding 40 mM of  $\text{SrCl}_2$  and 10 mM of  $\text{Na}_2\text{SO}_3$  in 50  $\mu\text{l}$  of aqueous solution, followed by incubation at 37°C for 30 min.

#### *5.2.3. Field Emission Scanning Electron Microscope (FE-SEM) of PEG-SSNs:*

The actual size, surface and shape of SSNs and PEG-SSNs was observed by using FE-SEM. PEG-SSNs and SSNs prepared by mixing 40 mM of  $\text{SrCl}_2$ , 10mM of  $\text{Na}_2\text{SO}_3$  and 1  $\mu\text{l}$  of biotin PEG (1  $\mu\text{M}$ ) and SSNs were prepared without PEG by using same amount of  $\text{SrCl}_2$  and  $\text{Na}_2\text{SO}_3$ . The synthesized particles were then centrifuged at 13,000 rpm for 15 min. The resulting pellet was suspended in 500  $\mu\text{L}$  of water. 3  $\mu\text{L}$  of particle suspension was then transferred to a glass slide for drying at 37°C for 1 hour. The dried sample was placed onto a carbon tape-coated sample holder, followed by platinum sputtering of the dried samples with 30 mA sputter current at 2.30 tooling factor for 40 s and the sputtered particles were visualized at 5.00 kV using FE-SEM (Hitachi/SU8010, Tokyo, Japan).

#### *5.2.4. In-Solution Digestion of SSNs and PEG-SSNs Protein Corona for Mass Spectrometric Analysis*

SSNs and PEG-SSNs were prepared by adding 40 mM of  $\text{SrCl}_2$  to 10mM of  $\text{Na}_2\text{SO}_3$  and incubated for 30 min at 37 °C, and for PEG-SSNs, 40 mM of  $\text{SrCl}_2$  to 10mM of  $\text{Na}_2\text{SO}_3$ , incubated for 30 min at 37 °C, 1  $\mu\text{l}$  of biotin PEG (1  $\mu\text{M}$ ) were added prior to incubated for 10 min at 37 °C. The synthesized SSNs and PEG-SSNs were subjected to additional incubation with mouse plasma (10%) for 15 min at 37 °C. After centrifugation of the particle suspensions at 13,000 RPM for 15 min, the supernatants were discarded, and the pellets were washed in Milli Q water, followed by centrifugation and removal of the supernatants. The pellets were dissolved with 100  $\mu\text{L}$  of 50 mM EDTA in  $\text{H}_2\text{O}$ . 25  $\mu\text{L}$  of 100 mM ammonium bicarbonate solution, 25  $\mu\text{L}$  tetrafluoroethylene (TFE) denaturing agent and 1  $\mu\text{L}$  of 200 mM dithiothreitol (DTT) solution were added to the protein mixture (released from pellets), followed by vortexing and heating under a heating block at 60 °C for 1 h. After adding 4  $\mu\text{L}$  of 200 mM iodoacetamide (IAM) and briefly vortexing,

the protein mixture (representing protein corona) was incubated in the dark at room temperature for 1 h. 1  $\mu$ L of 200 mM DTT solution was added to the protein mixture which was then incubated in the dark at room temperature for 1 h. Afterwards, the treated protein mixture was incubated at room temperature in presence of 100  $\mu$ L ammonium bicarbonate solution (100 mM) and MS Grade 25  $\mu$ L of Trypsin (1  $\mu$ g/mL) at 37 °C for 4 to 18 h. Finally, 1  $\mu$ L formic acid was added to stop the reaction, and the samples were subjected to speed vacuum overnight prior to analysis by Q-TOF LC-MS/MS.

#### *5.2.5. Sample Preparation for Mass Spectrometry-Based Proteomics:*

10  $\mu$ L of formic acid (0.1%) in water was added to dissolve dry peptide digest. Samples were then sonicated in ultrasonic water bath for 10 min, while maintaining low temperature using ice. Samples were centrifuged (14,000 $\times$  g, 5 min) and 5  $\mu$ L of supernatant was placed in MS tube before being directly transferred on LC-QTOF auto-sampler for analysis.

#### *5.2.6. High Efficiency Nanoflow Liquid Chromatography Electrospray-Ionization Coupled with Mass Spectrometry*

The peptides digested were loaded into an Agilent Poroshell 300 Å pore C18 columns (Agilent, Santa Clara, CA, USA) using 0.1% formic acid mobile phase to equilibrate the column. The peptides were eluted from the column with 90% acetonitrile in 0.1% formic acid (solution B), using the gradients of 5% solution B over 0–30 min and 75% solution B over 30–39 min. Quadrupole-time of flight (Q-TOF) polarity was set at positive with capillary and fragmented voltage being set at 1750 V and 360 V, respectively, and 5 L/min of gas flow with a temperature of 325 °C. The peptide spectrum was analyzed in auto MS mode ranging from 110–3000 m/z for MS scan and 50–3000 m/z for MS/MS scan. Acquisition rates were 2 (spectra/s) for MS and 4 (spectra/s) for MS/MS. The spectrum was then analyzed with Agilent MassHunter (Agilent Technologies, Santa Clara, CA, USA) data acquisition software and then PEAKS 8.5 software (Bioinformatics Solutions Inc., Waterloo, ON, Canada).

#### *5.2.7. Protein Identification and Quantification by Automated De Novo Sequencing (PEAKS Studio 8.5)*

Protein identification was performed by integrating a database search (SwissProt.Mus\_musculus) with de novo sequencing, for the homology search using PEAKS Studio 8.5 (Bioinformatics Solution Inc., Waterloo, ON, Canada). Carbamidomethylation was set as the fixed modification with maximum mixed cleavages at 3. Parent mass and fragment mass error tolerance were both set 0.1 Da with monoisotopic mass as the precursor mass search type. Trypsin was selected as the enzyme for digestion. False discovery rate (FDR) of 1% and unique peptides  $\geq 1$  were used

for filtering out inaccurate proteins. A-10lgP score of greater than 20 indicates that detected proteins are relatively high in confidence as it targets very few decoy matches above that threshold. Relative differential changes of proteins commonly found in different complex protein samples of SSNs and PEG-SSNs were quantified using PEAKS Q protein quantification software. Label free quantification method is based on the relative intensities of peptide ion peak features detected in multiple samples. Feature detection is performed separately on each sample with more overlapped features, by using the EM (expectation-maximization) algorithm. The features of the same peptide from different samples are reliably aligned together using a high-performance retention time alignment algorithm. The groups are color-coded to be used in the heat map summary to distinguish the groups between two NPs and the intensity of a quantifiable peptide. The significance of a peptide is denoted by its  $-10\log P$  score. The cut off value was set at 20 which is equivalent to a P-value of 0.01. Heat Map displays the protein groups that passed the filters for quantitative analysis. The relative protein abundance is represented as a heat map of the representative proteins of each protein group. The representative proteins are clustered if they exhibit a similar expression trend across the samples. The hierarchical clustering is generated using a neighbor-joining algorithm with a Euclidean distance similarity measurement of the  $\log_2$  ratios of the abundance of each sample relative to the average abundance.

#### *5.2.8. Biodistribution study of siRNA-carrying SSNs and PEG-SSNs complexes:*

For biodistribution study, 7–8 weeks old of female Balb/c mice of 21–25 gm of body weights were obtained from the School of Medicine and Health Science Animal Facility, Monash University. The mice were maintained in 12:12 light: dark conditions and provided with *ad libitum* and water. All the experiments were done in accordance with the protocol approved by MONASH Animal Ethics Committee (MARF/2016/126). Approximately  $1 \times 10^5$  4T1 cells (in 180  $\mu\text{L}$  PBS) were injected subcutaneously on the mammary pad of mice (considered as day 1) and the mice were checked regularly for the outgrowth of tumor by touching the area of injection by index finger. When the tumor volume reached  $75 \text{ mm}^3$  at day 11 of injection, the tumor bearing mice were treated with SSNs and PEG-SSNs (both 1 & 10  $\mu\text{L}$  of biotin PEG) complexed with fluorescent AF-488 labeled neg. siRNA (75 mM) through tail vein injection. Mice were sacrificed humanely by cervical dislocation after 4 or 24 h of the administration. Afterwards, the heart, liver, kidney, spleen, lung, brain and tumor were collected and washed twice in chilled PBS, followed by addition of 500  $\mu\text{L}$  lysis buffer per 500 mg of tissue mass. Tissues were lysed using a mechanical homogenizer with four strokes intermittently while maintaining the samples on ice till a completely homogenized solution was obtained. The solutions of tissue lysates were centrifuged for 25 min at  $4^\circ\text{C}$  with 8000 rpm. 200  $\mu\text{L}$  of the supernatant



was added to each well of a 96-well opti-plate (Nunc) for measuring fluorescence intensity of AF-488 labeled siRNA with 2030 multilabel reader vitor TM X5 (Perkin Elmer) attached with Perkin Elmer 2030 manager software using  $\lambda_{ex} = 490$  nm and  $\lambda_{em} = 535$  nm. Data were represented as mean  $\pm$  SEM of fluorescence intensity/500 mg of tissue mass after the values were blank-corrected using an untreated group of mice for each tissue.

### **5.3. Results:**

#### *5.3.1. FESEM of SSNs and PEG-SSNs:*

The morphology of modified and unmodified SSNs were evaluated by FE-SEM. SSNs were prepared by mixing of 40 mM of  $\text{SrCl}_2$  and 10 mM of  $\text{Na}_2\text{SO}_3$  in 50  $\mu\text{l}$  of aqueous solution, followed by incubation at 37°C for 30 min. 1  $\mu\text{l}$  of biotin PEG was added to the pre-formed SSNs to make PEG-SSNs. The generated SSNs and PEG-SSNs were centrifuged at 13,000 rpm for 15 min and the resultant pellets were subjected to FE-SEM after being resuspended in water. The shape of SSNs was almost spherical with spiky surface for SSNs (Figure 1: A.B.C), and for PEG-SSNs (Figure 1: D.E.F) the shape remained the same with a reduction of spiky surface due to entrapment of PEG chain on the surface. The size of the SSNs was found to be within a range of 1.28-1.67  $\mu\text{m}$ , whereas for PEG-SSNs the size range was reduced significantly to 384-516 nm. The above results indicate that PEG has a vital role in reducing the complex size by adsorbing onto the particle surface and preventing particle-particle aggregation. The smaller particles with reduced spiky nature of the surface of PEG-SSNs might play beneficial roles in inhibiting opsonization and macrophage uptake and, improving half-life in systemic circulation.

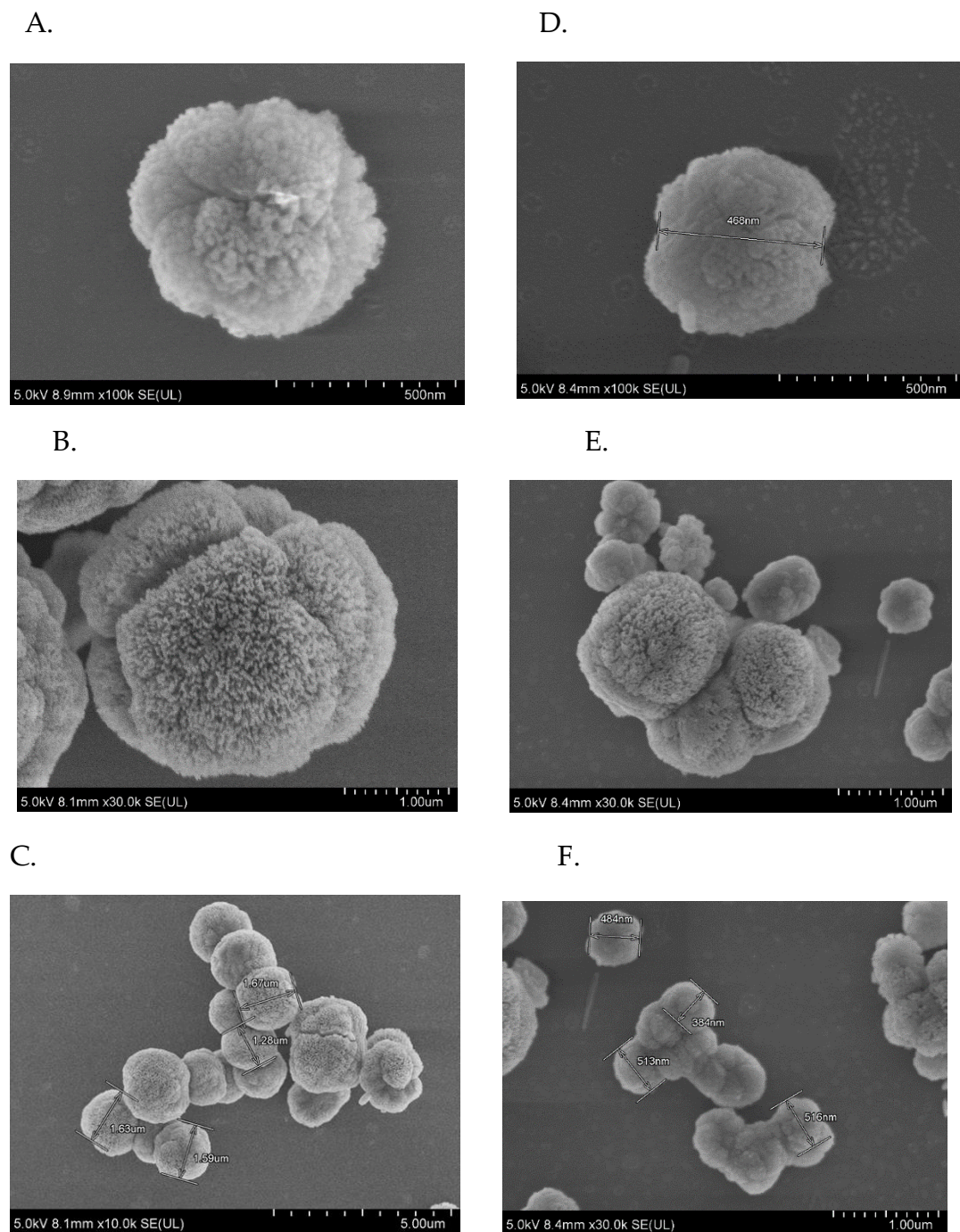


Figure 1: FE-SEM images of SSNs and PEG-SSNs, prprepared by adding 40 mM of  $\text{SrCl}_2$  and 10 mM of  $\text{Na}_2\text{SO}_3$  in 50 $\mu\text{l}$  of aqueous solution and 1  $\mu\text{l}$  of biotin PEG. Images denoated by A, B and C represent unmodified SSNs, while those indicated by D, E and F represent PEGylated SSNs observed at 5.0 KV.

### 5.3.2. Protein corona profiling of SSNs and PEG-SSNs by LC-MS/MS:

The protein corona formed on the surface of SSNs and PEG-SSNs was analyzed by using LC-MS/MS. The peptides derived from de novo sequencing were identified as exact or homologous peptides using Mus\_musculus database (SwissProt). Protein corona profile was characterized with the help of unique peptide, molecular weight, coverage % for peptides and significance (-10lgp). Detected proteins were listed along with their functions in table 1 and 2 for SSNs, and PEG-SSNs. Protein classification based on their biological functions was plotted in pie chart.

As shown in the figure 2, SSNs prepared without PEG show affinity for different types of proteins including structural proteins (different keratins, Nup205), transport proteins (albumin, oligomeric Golgi complex subunit 7), and enzymes (protein kinases, endonucleases, glutamine synthetase). On the other hand, PEGylated particles show affinity towards structural proteins (keratins) and transport proteins (albumin). Serum albumin, the most abundant proteins in the blood and a dysopsonin, was detected in both SSNs and PEG-SSNs. Binding to the dysopsonin proteins would provide the stealth effects of SSNs and PEG-SSNs and enable escaping from the interactions with opsonin protein, thus reducing phagocytic uptake. Moreover, SSNs were found to more highly interact with several proteins and enzymes than modified SSNs.

Protein classes	Identified proteins	-10lgP	Coverage	Mass	Function
Transport proteins	Albumin 1	156.86	31	68693	chaperone binding, DNA binding, fatty acid binding, identical protein binding, oxygen binding, pyridoxal phosphate binding and toxic substance binding
Enzymes	Glutamine synthetase	38.65	4	42019	glutamine biosynthetic process
Structural proteins	Keratin 16	32.67	1	51606	structural constituent of cytoskeleton
Structural proteins	Keratin 16	32.67	1	51693	structural molecule activity
Structural proteins	Keratin intermediate filament 16b	32.67	1	51966	structural molecule activity
Structural proteins	Keratin intermediate filament 16a	32.67	1	52053	structural molecule activity

Structural proteins	Uncharacterized protein	24.55	2	33882	structural molecule activity
Structural proteins	Keratin 24 variant 2	24.55	2	40994	structural molecule activity
Structural proteins	Keratin 19	24.55	2	44542	protein-containing complex binding, structural constituent of muscle
Structural proteins	Keratin, type I cuticular Ha2	24.55	2	51153	structural molecule activity
Structural proteins	Keratin 15, isoform CRA_a	24.55	2	49494	scaffold protein binding, structural molecule activity
Structural proteins	Keratin, type I cytoskeletal 10	24.55	1	57041	protein heterodimerization activity, structural constituent of epidermis
Structural proteins	Nup205	23.83	1	69494	structural constituent of nuclear pore
Transport Proteins	Conserved oligomeric Golgi complex subunit 7	23.83	1	80582	intracellular protein transport
Transport Proteins	Conserved oligomeric Golgi complex subunit 7	23.83	1	86075	intracellular protein transport
Enzymes	Ercc5 protein	22.76	1	86901	endonuclease activity, single-stranded DNA binding
Enzymes	Nek1 protein	21.82	2	48636	ATP binding, protein serine/threonine kinase activity
Enzymes	Nek1 protein	21.82	1	133856	ATP binding, protein kinase activity
Enzymes	Nek1 protein	21.82	1	139659	ATP binding, protein kinase activity
Enzymes	MKIAA1901 protein	21.82	1	139947	ATP binding, protein kinase activity
Enzymes	Nek1 protein	21.82	1	144269	ATP binding, protein kinase activity
others	WD repeat-containing protein 81	21.82	1	211931	mitochondrion organization

Table 1: Proteins found with SSNs following incubation with 10% of mice plasma. Proteins name, molecular mass and biological functions were obtained from Uniprot database.

Protein classes	Identified protein	-10lgP	Coverage (%)	Mass	Function
Structural proteins	Keratin, type I cytoskeletal 10	160.85	39	57041	Protein heterodimerization activity, structural constituent of epidermis.
Structural proteins	Keratin 77	134.13	15	61359	structural molecule activity
Structural proteins	Keratin 77	134.13	15	61302	structural molecule activity
Transport proteins	Albumin 1	131.44	16	68693	chaperone binding, DNA binding, fatty acid binding, identical protein binding, oxygen binding, pyridoxal phosphate binding and toxic substance binding
Structural proteins	Keratin, type II cytoskeletal 6B	126.58	11	59526	structural molecule activity
Structural proteins	Krt6b protein	126.58	11	60191	structural molecule activity
Structural proteins	Krt6b protein	126.58	11	60273	structural molecule activity
Structural proteins	Keratin 5	112.68	12	61767	scaffold protein binding, structural molecule activity
Structural proteins	Krt2 protein	99.11	11	70923	structural molecule activity
Structural proteins	Keratin 15, isoform CRA_a	95.8	10	49494	scaffold protein binding, structural molecule activity
Structural proteins	Keratin Kb40	92.26	2	85239	structural molecule activity
Structural proteins	Keratin 78	92.26	1	112265	structural molecule activity
Structural proteins	Krt78 protein	92.26	3	54765	structural molecule activity
Structural proteins	Krt78 protein	92.26	3	54774	structural molecule activity
Structural proteins	Krt78 protein	92.26	3	56780	structural molecule activity
Structural proteins	Type II cytokeratin Kb40	92.26	3	47619	structural molecule activity
Structural proteins	Uncharacterized protein	81.33	5	58266	structural molecule activity
Structural proteins	Uncharacterized protein	81.33	5	58240	structural molecule activity
Structural proteins	Keratin 90	81.33	5	58224	structural molecule activity
Structural proteins	Keratin 16	69	5	51606	structural molecule activity

Structural proteins	Keratin 16	69	5	51693	structural molecule activity
Structural proteins	Keratin intermediate filament 16b	69	5	51966	structural molecule activity
Structural proteins	Keratin intermediate filament 16a	69	5	52053	structural molecule activity

Table 2: Protein that are found for PEG-SSNs with 10% of mice plasma. Proteins name, molecular mass and biological functions were obtained from Uniprot database.

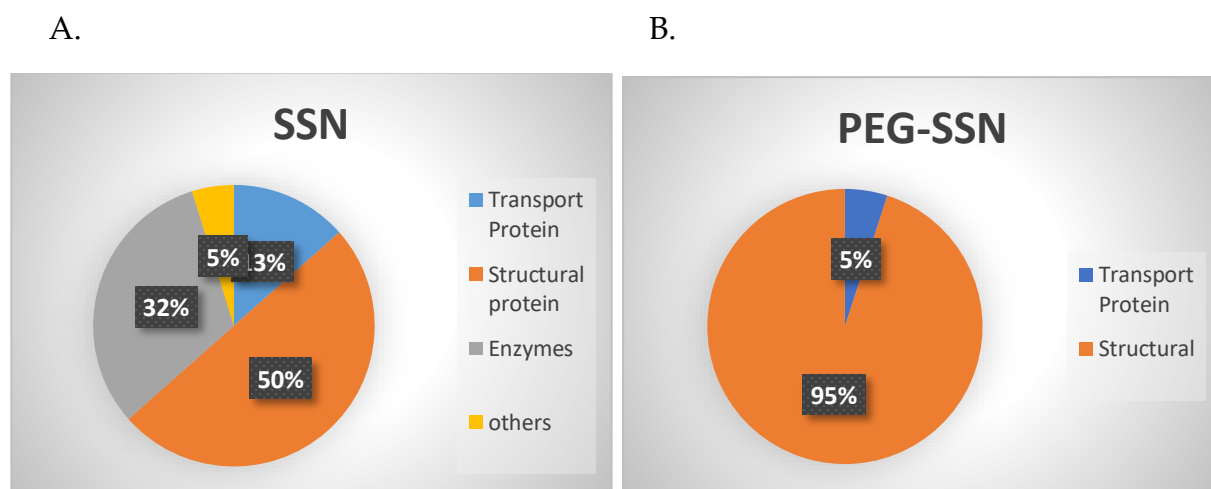


Figure 02: Protein corona composition of SSNs (A) and PEG-SSNs (B) with 10% mice plasma. SSNs were prepared by mixing 40 mM of  $\text{SrCl}_2$  and 10 mM of  $\text{Na}_2\text{SO}_3$  in 50  $\mu\text{l}$  of aqueous solution, and 1  $\mu\text{l}$  of biotin PEG was added to form PEG-SSNs. 10% of mice plasma was added and incubated for 30 min, prior to identification of bound proteins.

### 5.3.3. Bio-distribution of SSNs and PEG-SSNs:

SSNs and PEG-SSNs were couple with fluorescence siRNA and subjected to bio distribution study for investigating the pharmacokinetics parameters. Breast tumor bearing mice were intravenously treated with AF 488 siRNA-SSNs and PEG-SSNs complex and after 4 and 24 hours major organs and tumor were collected, harvested, homogenized and measured for the fluorescence intensity. We have used two concentrations of PEG (1 and 10  $\mu\text{L}$  of 1  $\mu\text{M}$ ) for observing and comparing the effects of concentration of PEG on bio-distribution at two time points, 4 hour and 24 hour. SSNs without any modification at 4 hour showed significant accumulation in the brain and RES organ, spleen with a minimal tumor accumulation and after 24 hours fluorescence signals were found to be increased in tumor along with brain and spleen (Figure 3). On the other

hand, coating of SSNs with 1 $\mu$ L of biotin PEG resulted in higher accumulation in tumor than free SSNs after 4 hour of treatment. Moreover, higher uptake by the kidney and brain were also found, indicating the effects of smaller size particles on clearance by kidney. Interestingly at 24 hours of time point, remarkable tumor accumulation was found for PEG-SSNs made by using 1 $\mu$ L of biotin PEG as shown in the Fig. 3. The siRNA from the brain was completely eliminated that might reduce the neurotoxicity. At higher concentration of PEG 10 $\mu$ L), no fluorescence signals was detected in any major organs and tumor.

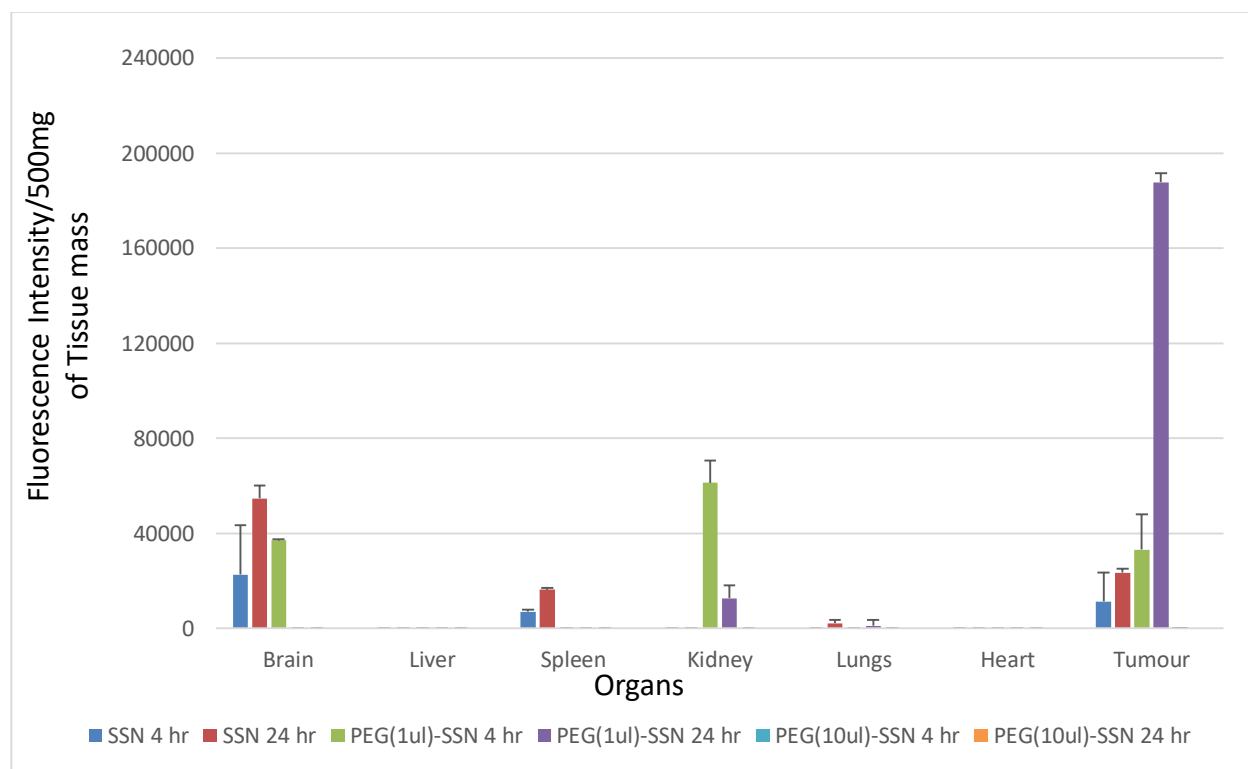


Figure 3: Organ distribution of siRNA complexed with SSNs and PEG-SSNs (1 & 10  $\mu$ l of biotin PEG) after 4 hour and 24 hour of treatment into female balb/c mice. Each group contained 4 mice and data were represented as mean  $\pm$  SEM.

#### 5.4. Discussion:

We characterized the PEG-SSNs and SSNs by using FE-SEM to check the morphology and also investigate the effects of PEGylation on size, shape and surface of SSNs and PEG-SSNs. Previous study revealed that carbonate apatite NPs coated with biotin PEG reduced the particle size significantly (29). We further proved for the first time that modifications of SSNs with biotin PEG reduced the particle size significantly. The biotin moiety in PEG contains protonable amine groups which allowed PEG to interact with cationic domains ( $\text{Sr}^{++}$ ) of SSNs. The attachment of PEG on the surface of SSNs prevents

particle-particle aggregation, thereby reducing the particle size as shown in Fig. 1. PEGylated NPs demonstrated enhanced half-lives, reduced off target distribution and increased anticancer effects compared to the free NPs (30, 31). We hypothesized that PEGylated SSNs would confer better pharmacokinetics and pharmacodynamics parameters due to their smaller particle size and different surface properties compared to free SSNs.

When NPs enter into the biological fluids after IV administration, they are exposed to interact with thousands of blood proteins owing to their high surface energy (12-14). In particular, plasma proteins bind or adsorb with the exogenous NPs to form biological coating on the surface of NPs called protein corona. This NPs-protein complex gives a new biological identity which modulates biodistribution, therapeutic effects, pathophysiological effects and toxicity of NPs (32-34). The opsonized NPs might undergo opsonin-triggered phagocytosis and accumulation in RES organs like Liver and spleen, which resulted in the off target distribution and reduced tumor accumulation. There are some important factors that affect the NP-plasma proteins interaction like physicochemical properties of NPs, exposure time and abundance of plasma proteins. It was found that hydrophobic and charged particles have a higher tendency to form protein corona than hydrophilic and neutral charged particles(17, 35). Therefore, it is necessary to inhibit such unforeseen biological effects for avoiding unwanted biological effects and rapid clearance of NPs. However, NPs coated with PEG could protect the NPs from protein recognition and interaction through stealth effects which are highly dependent on PEG length and density (36, 37). In this present work, we have demonstrated the successful application of the biotin PEG to prevent opsonization for optimizing SSNs based siRNA delivery. As shown in the Table 1, bare SSNs showed affinity towards different type of proteins specially protein corona forming proteins. Interaction with different types of proteins led to uneven distribution, shorter half-lives in biological system, rapid clearance from the body and more importantly less antitumor efficacy due to reduction of siRNA accumulation in target tumor site. The cationic domain of SSNs ( $\text{Sr}^{2+}$ ) interacts electrostatically with negatively charged proteins available in mice blood plasma, which reduces their stability in blood. On the other hand, PEGylated SSNs bound less amount of opsonin forming proteins as shown in the Table 2. The PEG coating of SSNs hindered the adsorption of different type of proteins on the surface of SSNs due to reduction of surface charge. The less interaction with opsonin proteins leads to higher stability in plasma while improving the antitumor efficacy. The PEG-SSNs also showed affinity towards albumin, the dysopsonin proteins that skip the PEG-SSNs from macrophage recognition and increase circulation time. Although both



SSNs and PEG-SSNs have the affinity towards the dysopsonin proteins, PEG-SSNs showed less protein binding than uncoated SSNs.

Next we checked the organ distribution of SSNs and PEG-SSNs in mice to find out the correlation between the protein corona formation and biodistribution as well as the effects of PEGylation. PEGylation is widely used coating technique to enhance drug stability of nanoparticles for efficient drug delivery system. The main objectives of NPs based gene delivery is to protect the nucleic acids from biological degradation, extended circulation time, reduced non-specific distribution and improved delivery to the target cytoplasm of tumor cell. Figure (3) represent the amount of siRNA uptaken by various organs and tumor after 4 and 24 hour of treatment. Unmodified SSNs after 4 and 24 hours of treatment was found to be accumulated in brain and RES organ i.e. spleen due to protein corona triggered accumulation and more interestingly bypass the liver. On the other hand, PEGylation of SSNs reduced the opsonization and bypass the accumulation in RES organs Liver and spleen. Binding with dysopsonin proteins caused escape of SSNs from opsonin-mediated macrophage uptake and increased tumor accumulation as shown in the (figure 03). Comparing with unmodified SSNs showed remarkable tumor accumulation after 24 hours of treatment, indicating PEG-SSNs are able to deliver siRNA specifically to the target tumor cell with augmented cytotoxicity and less unwanted effects in other major organs. Another important factors that affect the biodistribution of siRNA are the size of particles. Smaller sized PEGylated particles are diffuse more readily and reduced the tumor volume significantly (29, 38). Hydrophilic materials PEG reduced the particle size of SSNs ranging 384-516 nm and being hydrophilic readily excreted through kidneys as shown in the figure. The pore cutoff sizes of tumor vasculature ranging from 200nm to 1.2 $\mu$ m(39) which allows the PEG-SSNs-siRNA complex transported into tumor cells via EPR effects and are released into the cytoplasm of cancer cell through pH dependent release mechanism at early endosomal stage and silence the target gene. At last, we have demonstrated that PEGylation of SSNs reduce opsonization, reduce the macrophage mediated phagocytosis, increase biological stability and improves tumor accumulation which will ultimately give significant anti-cancer effects.

## 5.5. Conclusion:

Electrostatic interactions of SSNs with biotin PEG introduced a very simple, scalable method to synthesize PEG-SSNs that increases the tumor targetability and reduces off-target effects. PEG hindered the protein adsorption of SSNs particles which is the key determinant for the biological fate of nanoparticles. In our study, we have found that immobilization of biotin PEG on SSNs led to less protein adsorption on the surface of

SSNs, more stability in biological fluid, reduced off target distribution, less macrophage uptake, reduced toxicity and finally augmented tumor accumulation of siRNA in a breast cancer mouse model. Although dysopsonin proteins protect the NPs from rapid clearance, binding percentage of blood proteins still make sense for the opsonization mediated NPs clearance. PEG-SSNs could be a versatile and effective strategy to limit the protein adsorption for optimizing the PEG-SSNs based siRNA delivery system, providing more depth insights for the rational design of nanomedicine for safer human applications.

## References

1. Choi CL, Alivisatos AP. From artificial atoms to nanocrystal molecules: Preparation and properties of more complex nanostructures. *Annual Review of Physical Chemistry*. 2010;61:369-89.
2. Xia D, Ku Z, Lee S, Brueck S. Nanostructures and functional materials fabricated by interferometric lithography. *Advanced materials*. 2011;23(2):147-79.
3. Walkey CD, Olsen JB, Guo H, Emili A, Chan WC. Nanoparticle size and surface chemistry determine serum protein adsorption and macrophage uptake. *Journal of the American Chemical Society*. 2012;134(4):2139-47.
4. Guo P. RNA nanotechnology: engineering, assembly and applications in detection, gene delivery and therapy. *Journal of nanoscience and nanotechnology*. 2005;5(12):1964-82.
5. Shi J, Votruba AR, Farokhzad OC, Langer R. Nanotechnology in drug delivery and tissue engineering: from discovery to applications. *Nano letters*. 2010;10(9):3223-30.
6. Karim M, Tha K, Othman I, Borhan Uddin M, Chowdhury E. Therapeutic potency of nanoformulations of siRNAs and shRNAs in animal models of cancers. *Pharmaceutics*. 2018;10(2):65.
7. Molinaro R, Wolfram J, Federico C, Cilurzo F, Di Marzio L, Ventura CA, et al. Polyethylenimine and chitosan carriers for the delivery of RNA interference effectors. *Expert opinion on drug delivery*. 2013;10(12):1653-68.
8. Matsumura Y, Maeda H. A new concept for macromolecular therapeutics in cancer chemotherapy: mechanism of tumoritropic accumulation of proteins and the antitumor agent smancs. *Cancer research*. 1986;46(12 Part 1):6387-92.
9. Bertrand N, Wu J, Xu X, Kamaly N, Farokhzad OC. Cancer nanotechnology: the impact of passive and active targeting in the era of modern cancer biology. *Advanced drug delivery reviews*. 2014;66:2-25.
10. Maeda H. Toward a full understanding of the EPR effect in primary and metastatic tumors as well as issues related to its heterogeneity. *Advanced drug delivery reviews*. 2015;91:3-6.

11. Cedervall T, Lynch I, Lindman S, Berggård T, Thulin E, Nilsson H, et al. Understanding the nanoparticle–protein corona using methods to quantify exchange rates and affinities of proteins for nanoparticles. *Proceedings of the National Academy of Sciences*. 2007;104(7):2050-5.
12. Monopoli MP, Åberg C, Salvati A, Dawson KA. Biomolecular coronas provide the biological identity of nanosized materials. *Nature nanotechnology*. 2012;7(12):779.
13. Nel AE, Mädler L, Velegol D, Xia T, Hoek EM, Somasundaran P, et al. Understanding biophysicochemical interactions at the nano–bio interface. *Nature materials*. 2009;8(7):543.
14. Corbo C, Molinaro R, Parodi A, Toledano Furman NE, Salvatore F, Tasciotti E. The impact of nanoparticle protein corona on cytotoxicity, immunotoxicity and target drug delivery. *Nanomedicine*. 2016;11(1):81-100.
15. Corbo C, Molinaro R, Tabatabaei M, Farokhzad OC, Mahmoudi M. Personalized protein corona on nanoparticles and its clinical implications. *Biomaterials science*. 2017;5(3):378-87.
16. Westmeier D, Chen C, Stauber RH, Docter D. The bio-corona and its impact on nanomaterial toxicity. *European Journal of Nanomedicine*. 2015;7(3):153-68.
17. Mahmoudi M, Lynch I, Ejtehadi MR, Monopoli MP, Bombelli FB, Laurent S. Protein– nanoparticle interactions: opportunities and challenges. *Chemical reviews*. 2011;111(9):5610-37.
18. Milani S, Baldelli Bombelli F, Pitek AS, Dawson KA, Rädler J. Reversible versus irreversible binding of transferrin to polystyrene nanoparticles: soft and hard corona. *ACS nano*. 2012;6(3):2532-41.
19. Dell'Orco D, Lundqvist M, Oslakovic C, Cedervall T, Linse S. Modeling the time evolution of the nanoparticle-protein corona in a body fluid. *PLoS One*. 2010;5(6):e10949.
20. Walkey CD, Chan WC. Understanding and controlling the interaction of nanomaterials with proteins in a physiological environment. *Chemical Society Reviews*. 2012;41(7):2780-99.
21. Aggarwal P, Hall JB, McLeland CB, Dobrovolskaia MA, McNeil SE. Nanoparticle interaction with plasma proteins as it relates to particle biodistribution, biocompatibility and therapeutic efficacy. *Advanced drug delivery reviews*. 2009;61(6):428-37.
22. Ruh H, Kühl B, Brenner-Weiss G, Hopf C, Diabaté S, Weiss C. Identification of serum proteins bound to industrial nanomaterials. *Toxicology letters*. 2012;208(1):41-50.
23. Ritz S, Schöttler S, Kotman N, Baier G, Musyanovych A, Kuharev Jr, et al. Protein corona of nanoparticles: distinct proteins regulate the cellular uptake. *Biomacromolecules*. 2015;16(4):1311-21.
24. Ogawara K-i, Furumoto K, Nagayama S, Minato K, Higaki K, Kai T, et al. Pre-coating with serum albumin reduces receptor-mediated hepatic disposition of polystyrene nanosphere: implications for rational design of nanoparticles. *Journal of controlled release*. 2004;100(3):451-5.

25. Pasut G, Paolino D, Celia C, Mero A, Joseph AS, Wolfram J, et al. Polyethylene glycol (PEG)-dendron phospholipids as innovative constructs for the preparation of super stealth liposomes for anticancer therapy. *Journal of Controlled Release*. 2015;199:106-13.
26. Vonarbourg A, Passirani C, Saulnier P, Benoit J-P. Parameters influencing the stealthiness of colloidal drug delivery systems. *Biomaterials*. 2006;27(24):4356-73.
27. Satulovsky J, Carignano M, Szleifer I. Kinetic and thermodynamic control of protein adsorption. *Proceedings of the National Academy of Sciences*. 2000;97(16):9037-41.
28. Niidome T, Yamagata M, Okamoto Y, Akiyama Y, Takahashi H, Kawano T, et al. PEG-modified gold nanorods with a stealth character for in vivo applications. *Journal of Controlled Release*. 2006;114(3):343-7.
29. Mozar F, Chowdhury E. Surface-modification of carbonate apatite nanoparticles enhances delivery and cytotoxicity of gemcitabine and anastrozole in breast cancer cells. *Pharmaceutics*. 2017;9(2):21.
30. Avgoustakis K, Beletsi A, Panagi Z, Klepetsanis P, Livaniou E, Evangelatos G, et al. Effect of copolymer composition on the physicochemical characteristics, in vitro stability, and biodistribution of PLGA-mPEG nanoparticles. *International journal of pharmaceutics*. 2003;259(1-2):115-27.
31. Perry JL, Reuter KG, Kai MP, Herlihy KP, Jones SW, Luft JC, et al. PEGylated PRINT nanoparticles: the impact of PEG density on protein binding, macrophage association, biodistribution, and pharmacokinetics. *Nano letters*. 2012;12(10):5304-10.
32. Van Hong Nguyen B-JL. Protein corona: a new approach for nanomedicine design. *International journal of nanomedicine*. 2017;12:3137.
33. Dobrovolskaia MA, Germolec DR, Weaver JL. Evaluation of nanoparticle immunotoxicity. *Nature nanotechnology*. 2009;4(7):411.
34. Salvati A, Pitek AS, Monopoli MP, Prapainop K, Bombelli FB, Hristov DR, et al. Transferrin-functionalized nanoparticles lose their targeting capabilities when a biomolecule corona adsorbs on the surface. *Nature nanotechnology*. 2013;8(2):137.
35. Lindman S, Lynch I, Thulin E, Nilsson H, Dawson KA, Linse S. Systematic investigation of the thermodynamics of HSA adsorption to N-iso-propylacrylamide/N-tert-butylacrylamide copolymer nanoparticles. Effects of particle size and hydrophobicity. *Nano letters*. 2007;7(4):914-20.
36. Mozar FS, Chowdhury EH. PEGylation of carbonate apatite nanoparticles prevents opsonin binding and enhances tumor accumulation of gemcitabine. *Journal of pharmaceutical sciences*. 2018;107(9):2497-508.
37. Hinerfeld D, Innamorati D, Pirro J, Tam SW. Serum/plasma depletion with chicken immunoglobulin Y antibodies for proteomic analysis from multiple mammalian species. *Journal of biomolecular techniques: JBT*. 2004;15(3):184.

38. Wang Y, Fan W, Dai X, Katragadda U, Mckinley D, Teng Q, et al. Enhanced tumor delivery of gemcitabine via PEG-DSPE/TPGS mixed micelles. *Molecular pharmaceutics*. 2014;11(4):1140-50.
39. Hobbs SK, Monsky WL, Yuan F, Roberts WG, Griffith L, Torchilin VP, et al. Regulation of transport pathways in tumor vessels: role of tumor type and microenvironment. *Proceedings of the National Academy of Sciences*. 1998;95(8):4607-12.

## **Chapter 6**

### **Conclusion and Future directions**

## 6. Conclusion and future directions:

### 6.1. Conclusion:

In summary, we have synthesized SSNs by using simple and one step method from inorganic salts along with desired physicochemical properties. The method is scalable for mass production. The several characterization methods assured the successful formation of SSNs in nano-size scale. We have demonstrated the effects of glucose and electrolytes (NaCl) in optimization and stabilization of SSNs and more importantly in significant particle size reduction capacity. The reduced and stabilized Na-Glc-SSN (SSNs fabricated with NaCl and glucose) didn't interfere siRNA binding and cellular uptake of siRNA coupled Na-Glc-SSNs. The pH dependent dissolution of SSNs with or without NaCl and glucose facilitated rapid release of siRNA from SSNs at the acidic endosomal environment of the tumor cell. The Na-Glc-SSNs coupled with ROS-1 siRNA improved the cytotoxic effects in breast cancer cell lines owing to their smaller particle size in comparison to SSNs without NaCl and Glucose which influence the cellular uptake of Na-Glc-SSNs. The pharmacokinetics study of SSNs with or without NaCl and glucose showed less off target distribution and tumor accumulation of siRNA after 4 and 24 hours, indicating the lesser systemic side effects. The number of proteins adsorbed on the surface of NPs was also reduced significantly in Na-Glc-SSNs compared to SSNs. The in vivo tumor regression study of SSNs with or without NaCl and glucose carrying ROS-1 siRNA conferred significant anti-tumor effects without any systemic cytotoxicity.

Furthermore, surface modification of SSNs with biotin PEG led to stabilized and small sized particles along with altered surface properties. We have found a profound effect of PEG in reducing particle size by stopping particle-particle agglomeration. The experimental results of PEGylated SSNs from different characterization methods, stability testing and binding affinity towards the siRNA revealed that surface modified SSNs retained significant serum stability without hampering the binding capacity. The modified SSNs coupled with EGFR siRNA exerted more cytotoxicity in both human and animal breast cancer cell lines compared to free SSNs. The LCMS and pharmacokinetics studies demonstrated that PEGylated SSNs could prevent the protein binding (opsonization) in systemic circulation, extend the circulation half-life of siRNA and reduce off target distribution, thus improving tumor accumulation. Thus PEG-SSNs-EGFR complexes induced anti-tumor efficacy in breast tumor-bearing mice without inducing any histological changes in the major organs and biochemistry level at the given dosing level and regimen. In conclusion, the results of this work suggest that the developed SSNs, Na-Glc-SSNs and PEG-SSNs are very efficient tools for carrying siRNAs into the target tumor cell and thus present a promising strategy for treating breast cancer with high clinical outcome.

## **6.2. Future directions:**

Our findings therefore emphasize the need to perform further studies with strontium sulfite for tumor-targeted delivery of therapeutics including genes and drugs in preclinical cancer models for potential translation into clinics in the future. The additional pre-clinical studies on NPs elimination and safety evaluation would pave the way to evaluate their potency in human trials. Moreover, strontium sulfite-based carrier could be explored to deliver genes, siRNA and drugs in several other cancer models like liver, colorectal and prostate cancers for maximizing antitumor efficacy.

**THE END**